# THE LINK BETWEEN METABOLIC STRESS AND ELECTRICAL FAILURE IN A MODEL OF VENTRICULAR FIBRILLATION INDUCED SUDDEN CARDIAC ARREST

by

Tyson G. Taylor

A dissertation submitted to the faculty of
The University of Utah
in partial fulfillment of the requirements for the degree of

Doctor of Philosophy

Department of Bioengineering

The University of Utah

August 2014

**The University of Utah Graduate School**

**STATEMENT OF DISSERTATION APPROVAL**

The dissertation of **Tyson G. Taylor**

has been approved by the following supervisory committee members:

| | | |
|---|---|---|
| **Alexey V. Zaitsev** | , Chair | **May 29, 2014** Date Approved |
| **Vladimir Hlady** | , Member | **May 29, 2014** Date Approved |
| **Robert MacLeod** | , Member | **June 13, 2014** Date Approved |
| **Michael Sanguinetti** | , Member | **May 29, 2014** Date Approved |
| **Mark Warren** | , Member | **May 29, 2014** Date Approved |

and by **Patrick Tresco** , Chair/Dean of

the Department/College/School of **Bioengineering**

and by David B. Kieda, Dean of The Graduate School.

ABSTRACT

Sudden cardiac arrest (SCA) is a leading killer in the United States. A large number of patients experience SCA outside of hospitals where there is an inherent delay in treatment due to slow first response times. In the out-of-hospital setting, ventricular fibrillation (VF)-induced SCA (VF-SCA) is the most common context in which the event manifests. VF leads to chaotic electrical and hence contractile function of the heart resulting in loss of cardiac output causing ischemia. Left untreated, electrical activity rapidly deteriorates, culminating in complete electrical failure or asystole. Survival rates for patients found in asystole are a mere 1%: asystole is a death sentence. Despite the high event and death rates of VF-SCA, little is known concerning the mechanisms of electrical failure. This dissertation represents the first concerted effort to understand the pathophysiology of electrical failure. The work contained herein can be divided into three projects. These projects were conducted in whole animal and isolated whole heart models of VF-SCA. The first is a detailed examination of the complex patterns of electrical failure in VF-SCA. I found a highly complex pattern of electrical failure spanning the intra- and interchamber heterogeneities in three-dimensions. Second, I investigated the contributions of two canonical yet untested theories of electrical failure during VF-SCA: hyperkalemia and ATP-sensitive potassium channel ($K_{ATP}$) opening. I reached the surprising conclusion that neither hyperkalemia nor $K_{ATP}$ opening—individually or combined—can explain the pattern of electrical failure in VF-SCA. Third, I investigated the effect of increasing metabolic demand on electrical failure during VF-SCA through increased β-adrenergic stimulation and excitation rate. The findings point toward a necessity to reexamine current resuscitation protocols. Specifically, the use of epinephrine (an α- and β-adrenergic agonist) may promote electrical failure during treatment of VF-SCA leading to increased mortality.

To Bridget, Archer, & Aiden

CONTENTS

ACKNOWLEDGEMENTS

I am greatly indebted to my advisor, Dr. Alexey Zaitsev for the excellent scientific mentorship I have received during my doctoral training. Alexey's hands on approach to teaching, patience, and direct critical feedback have given me a healthy skepticism of my own findings along with the confidence to expound and justify my thoughts. Without his mentorship I would not be the independent thinker I am today. I also want to thank Alexey for one of the most enjoyable work environments I have experienced. I want to give thanks to all the members of the Zaitsev lab, Alicja Booth, Vivek Garg, Katie Sciuto, and Junko Warren all of whom are trusted colleagues and friends. I particularly want to thank Paul Venable for the countless hours of joint research and conversations about life through which we have become close friends and colleagues. I would like to thank the staff here at CVRTI who played key roles in making my tenure here a success. Jayne Davis and Nancy Allen made possible the animal preparations. Bruce Steadman, Dennis King, and Wilson Lobaina lent me their expertise and skills to create experimental setups. Phil Ershler and Marshall Scott made sure data acquisition and analysis were possible. Jerry Jenkins and Mike Heidinger always made sure the supplies I needed arrived on time. Alicia Geeseman and Tonnya Baxter for their insights into academic funding. I am grateful to the Nora Eccles Treadwell Foundation for making such a collaborative and friendly environment possible here at CVRTI. I would also like to thank my committee members. Dr. Vladimir Hlady, Dr. Rob MacLeod, Dr. Mike Sanguinetti, and Dr. Mark Warren for their insights and advice in developing my dissertation and career. I especially want to thank Mark for teaching me many electrophysiology techniques including the Langendorff setup and optical mapping without which this dissertation would not exist. Most importantly, I want to thank Bridget, my best friend and wife, for the love and support she's given me throughout my seemingly endless years of schooling. Thank you for giving me a reason to excel.

# CHAPTER 1

# BACKGROUND

## 1.1 Ventricular Fibrillation Induced Sudden Cardiac Arrest

Sudden cardiac arrest (SCA) is a leading killer with the number of victims totaling over 300,000 per annum in the U.S. alone [1-4] and accounts for 50% of deaths due to cardiovascular disease [5]. The defining feature of SCA is the loss of cardiac output that results in global ischemia. There are two primary pathways in which loss of cardiac output occurs. One, a progressive decrease in heart rate leading to electromechanical dissociation, eventual total electrical silence (asystole), and death. This pathway is called a bradyarrhythmia. The second pathway, is the induction of ventricular fibrillation (VF) via a triggering event. VF is characterized by chaotic electrical activity which leads to disorganized myocardial contraction (often described as a bag of worms) resulting in loss of cardiac output and ischemia. Left untreated, VF-induced SCA (VF-SCA) leads to a progressive deterioration of electrical activity culminating in asystole and death.

Although sudden cardiac death affects a diverse population—young, old, sick and healthy—a majority of cases occur in patients with no prior history of heart disease but who manifest risk factors highly predictive of SCA: such as, hyperlipidemia, hypertension, as well as age, lifestyle, and history of smoking [1, 6, 7]. Because these conditions tend to be chronic and patients do not require hospitalization, approximately 80% of patients experience SCA outside of hospitals (OHSCA) [5]. Indeed, the SCA patients with no prior history of cardiovascular disease represent the majority of sudden death cases. Furthermore, while bradyarrhythmias are common in patients with prior heart disease, VF-SCA is the most common mode of OHSCA [1, 2, 8-10].

In the out-of-hospital setting, the onset of SCA is sudden and treatment must occur immediately to be effective. Indeed, defibrillation immediately following VF onset has an approximately 90% success rate [11] with an accompanying high survival rate [12]. If treatment is delayed following onset of VF-SCA, survival probability plummets to approximately 60% in the 1st minute decreasing an additional 5% each minute [13] reaching an overall survival rate of 5% to 20% [5, 14, 15]. If patients are unlucky enough to be found in asystole, survival probability is an even more dismal, less than 1%. [15, 16] Thus the primary problem in treating OHSCA is the time delay between onset and arrival of emergency medical services (EMS). EMS arrival time can vary greatly by location but even in highly efficient systems can take several minutes leading to the low survival probability of OHSCA patients overall [17-21]. In order to improve survival rates in OHSCA two approaches can be pursued: 1) decreasing the time to first response and 2) extending the time window for viable resuscitation.

For decades various methods for decreasing time to first intervention have been pursued. Prior to 1960 the treatment for OHSCA was open chest cardiac massage after EMS had brought the patient to the hospital. Cardiac massage was rarely attempted and even more rarely successful [22, 23]. In 1956, Paul Zoll performed the first successful external defibrillation on man [24, 25], making possible the treatment of VF. Years later the external cardiac defibillator was miniaturized enough to allow EMS to carry them into the field. Although the portable defibrillator significantly shortened time to first intervention, the time delay from OHSCA onset to initial shock was still relatively long. Around the same time (1960) protocols for effective cardiopulmonary resusciation (CPR) were developed by a group at Johns Hopkins Hospital which were shown to significantly improve survival compared to previous methods which were largely ineffective [26, 27]. The usage of CPR was quickly spread to the public and has served as both a bridge to EMS arrival, a core component of hospital treatment, and the frontline of SCA treatment [5, 28]. In recent years, the invention and implementation of the automatic external defibrillator (AED) has allowed administration of defibrillatory shocks by the lay public, further decreasing time to first response [11, 17, 29]. Today, AED placement is ubiquitous in most public venues, work places, and are even available for the private home.

In parallel to efforts to decrease time to first response, substantial work has been done to

extend the window for viable resuscitation. The most notable outcome of this effort was the development of the Advanced Cardiac Life Support (ACLS) guidelines [28] which outlines the optimal process, based on current evidence, for resuscitation. These guidelines provide the framework in which resuscitation is performed by medical professionals and is constantly updated based on extensive research into optimizing parameters such as CPR compression rate and depth, defibrillation energy and waveform, as well as additional interventions such as therapeutic hypothermia [30-35].

Although efforts to both decrease time to first response and extend time of viable resuscitation have resulted in substantially improved survival outcomes from SCA compared to the days in which open chest cardiac massage was the standard of care, survival rates are still unacceptably low [5, 14, 15]. One potential reason for this is the increased prevalence of patients found in asystole in recent years [36-39]. Combined with the fact that first response time has remained similar or decreased at the same time, this observation points to a change in the time course of OHSCA in the general population. Unfortunately, very little is known concerning the mechanisms of electrical decline and failure. Efforts to-date in treating VF induced OHSCA have focused on optimizing parameters for current treatments despite the fact that some of these interventions may have no beneficial effect or even be harmful.

For example, therapeutic hypothermia reentered the spotlight as a promising therapeutic approach following the observation that an OHSCA victim found in extreme hypothermia survived three hours of cardiac arrest [40]. While a large amount of resources have been spent on optimizing the parameters and developing devices for therapeutic hypothermia, little work has been done to understand the mechanism of protection additionally treatment is accompanied by significant risk. Specifically, a recent study published in the New England Journal of Medicine calls into question the beneficial effects of mild therapeutic hypothermia [41]. Another example can be seen in current ACLS guidelines, which assume return of spontaneous circulation (ROSC) as a primary endpoint indicative of beneficial outcome and catecholamine administration as a means to achieve this goal [28]. Yet, evidence exists that improved ROSC may not be an accurate predictor of long-term survival; specifically in the case of epinephrine treatment [42-44]. Literature suggests additional considerations must be made. Lacking are the mechanistic insights

to understand why survival probability decreases so rapidly in OHSCA and why different interventions improve survival probability. If mechanistic insights could be gained, targeted therapeutic strategies could be developed to address shortcomings in current treatments or target the beneficial mechanisms of current therapeutic strategies while avoiding the detrimental side effects.

This dissertation is one step in the effort to develop a mechanism based treatment and focuses on a narrow, but highly important facet of OHSCA: namely, the mechanism of electrical failure post initiation of OHSCA in the context of VF and accompanying ischemia, or VF-SCA. The difficulty of a mechanistic approach is the complexity of the task and time required to develop a treatment. Understanding the entire pathophysiology of OHSCA is complex and multifaceted even when only the heart is considered separately from the rest of the organism. Thus, these efforts should be made in parallel to improving current treatment paradigms which provide short-term small improvements in survival rates. The goal of this dissertation was to first scrutinize the currently accepted, yet previously untested paradigm for the mechanism of electrical failure in VF-SCA and second, to develop an updated theory for the mechanisms of electrical failure.

Prior to the work presented in this dissertation, studies concerning electrical failure in VF-SCA have been limited to characterization of the process of electrical decline and neither the mechanisms giving rise to heterogeneous electrical decline nor asystole were well understood. Indeed, the state of knowledge consisted of the observation that left untreated, VF-SCA manifested as an increasingly heterogeneous decline in transmural electrical activity leading to eventual asystole [45-52]. It is thought that the development of electrical heterogeneities contributes to reduced defibrillation success through formation of reentrant pathways, and reinitiation of VF on reperfusion leading to a positive feedback loop in which VF becomes more and more difficult to treat as time elapses, culminating in asystole and death. One study directly implicated the anatomical distribution of Purkinje fibers in the development of the transmural component of heterogeneous electrical decline. The study found that ablating the Purkinje system, which is limited to the endocardium in canine hearts, resulted in loss of transmural heterogeneities in electrical activity [50]. Further evidence for the role of the Purkinje system in the transmural heterogeneities during LDVF can be seen by comparing porcine and canine hearts.

While Purkinje fibers are limited to the endocardium in canine hearts, porcine hearts have Purkinje fibers throughout the myocardial wall. As Tabereaux et al. predicted, porcine hearts do not develop a transmural electrical gradient during VF-SCA. Nevertheless, electrical deterioration occurs, defibrillation becomes progressively more difficult, and VF-SCA culminates in asystole [45-50]. Thus, the localization of Purkinje fibers appears to modulate the pattern of electrical decline but have little to do with the mechanism of electrical failure. A pertinent question is, why the endocardial localization of Purkinje fibers result in a transmural gradient. If indeed Purkinje fibers are the source of activity during VF-SCA why does electrical propagation initiated on the endocardium not reach the epicardium in canine hearts?

The key to understanding the primary mechanisms of electrical failure lie in the changes that occur as an acute response to VF-SCA and the resultant metabolic challenge. In other words, one must understand how the heart adjusts to the lack of oxygen, nutrients, and waste removal. In the acute setting of OHSCA where death occurs within minutes it is unlikely that changes in gene and protein expression play primary roles since such changes are typically measured in hours [53]. It is far more likely that ion channel permeabilities along with ionic and metabolic imbalance—which can respond to changes in the time frame of minutes, seconds, or even milliseconds—play major roles. To develop a valid hypothesis, it is critical to understand how electrical activity in the heart is generated at the single cell level and scale up to the whole heart and how this electrical activity is affected by conditions present during VF-SCA.

## 1.2 Electrical Activity in the Heart

### 1.2.1 Cellular Electrophysiology

At a fundamental level, cell excitability can be understood by a few key concepts: 1) electrochemical gradients, 2) gating of sarcolemmal permeability to ions, and 3) energy metabolism for system maintenance. Figure 1.1 shows a schematic diagram for major contributors to each of these components in the cardiac myocyte. The ion concentrations inside and outside the cell are listed to right of the diagram (values obtained from Luo & Rudy 1991 [54]). Major ion channels for $K^+$ (red) $Na^+$ (blue) and $Ca^{++}$ (green) are shown along with major pumps and

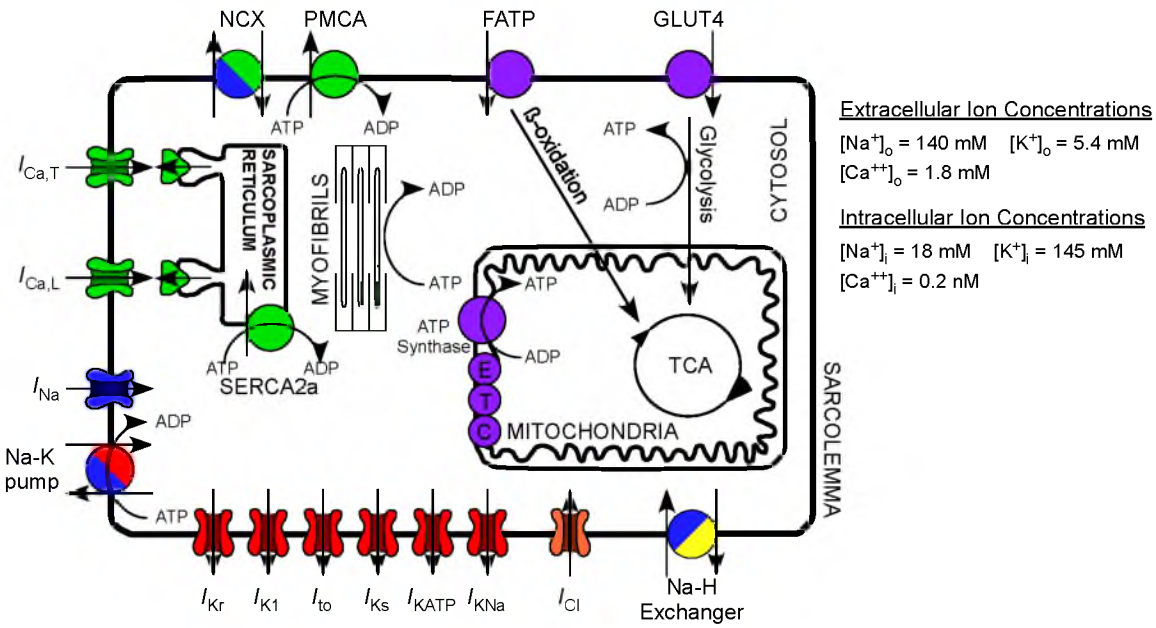


**Figure 1.1**: Schematic diagram of a cardiac myocyte. Typical extracellular ion concentrations are listed to the right. Green indicates $Ca^{++}$ handeling components, blue $Na^{+}$, red $K^{+}$, and orange Cl-. Purple indicates major components of metabolism. Cellular compartments are separated by black and labeled accordingly. These components can be catagorized broadly into three functions for the maintenance of electrical excitability: 1) The electrochemical gradient listed to the right. 2) Gating of sarcolemmal permeability, predominantly regulated by ion channels. 3) System maintenance through energy production and expenditure via pumps and metabolic pathways.

exchangers. The primary metabolic pathways for energy production (i.e., glycolysis, β-oxidation, and Krebs cycle) along with proteins involved in metabolite trafficking, the electron transport chain, and the $F_0$-$F_1$ ATP synthase (purple). The black lines indicate lipid bilayers separating compartments in the myocyte; namely the cytosol, sarcoplasmic reticulum (SR), and mitochondria. The myofibrils are responsible for contraction and are the major consumers of energy. The following subsections describe in some detail the conceptual framework by which these components drive electrical activity in the heart.

### 1.2.1.1 Electrochemical Gradients

The cell membrane acts as a nonconductive barrier preventing free flow of ions. The balance of ions in the intra- and extracellular spaces determine the electrochemical gradient and provides the driving force necessary for ion movement through pore forming proteins. Steady-state membrane potential ($V_m$), or sarcolemmal potential can be calculated using the Nernst

equation given the sarcolemma is permeable to only a single ion.

$$V_m = \frac{RT}{zF} \ln\left(\frac{[C]_o}{[C]_i}\right) \quad (1)$$

where R is the universal gas constant, T is the temperature in degrees Kelvin, z is the ion valence, and $[C]_o$ and $[C]_i$ are the ion concentrations outside and inside the cell, respectively. This is called the Nernst potential, also referred to as the reversal potential, for the specific ion and indicates the potential at which ion influx and efflux are in equilibrium. When the sarcolemma is permeable to additional ions the Goldman-Hodgkin-Katz equation (GHK) is used, instead, to determine the steady state $V_m$.

$$V_m = \frac{RT}{F} \ln\left(\frac{\sum_i^N P_{C_i}^+ \left[C_i^+\right]_o + \sum_j^N P_{A_j}^- \left[A_j^-\right]_i}{\sum_i^N P_{C_i}^+ \left[C_i^+\right]_i + \sum_j^N P_{A_j}^- \left[A_j^-\right]_o}\right) \quad (2)$$

where $P_{Ci}^+$ and $P_{Aj}^-$ are the permeabilities of cations and anions, respectively, and $[C]_i$ and $[C]_o$ indicate the concentrations of ions inside and outside the cell, respectively. It can easily be seen that as permeability to all but one ion approaches zero the equation is simplified to the Nernst equation. Also apparent is the possibility to hyper polarize or depolarize $V_m$ without altering the electrochemical gradients—given at least two ions have reversal potentials that are separated—which is critical for allowing rapid $V_m$ transition between the Nernst potentials for differing ions during electrical activity. For example, if initially the sarcolemma is permeable only to potassium ions ($K^+$) $V_m$ becomes the reversal potential for $K^+$ (approximately -90 mV for myocytes). If permeability to sodium ($Na^+$) suddenly increases $V_m$ rapidly approaches the reversal potential for $Na^+$ (approximately 55 mV) reaching a $V_m$ dependent on the ratios of $K^+$ and $Na^+$ permeability. The caveat being the GHK equation represents steady state $V_m$ since membrane capacitance is not considered. Conceptually it can be thought of as the larger the permeability to an ion relative to other ion permeabilities the closer the $V_m$ to that ion's reversal potential.

1.2.1.2 Sarcolemmal Permeability to Ions

Hodgkin and Huxley proved that the major component of electrical excitability in neurons was rapidly changing ion permeability which was later shown to be regulated by ion channels. The permeability of these ion channels to their respective ions can be very complex [55-61]. In the simplest conceptual framework ion channels can be thought to exist in three states, open, closed, or inactivated. Occupancy of each state can be a function time, $V_m$, and ligand binding. Hodgkin and Huxley showed that the current through the membrane in the whole cell could be described as a function of both time and $V_m$ as follows:

$$I = C_m \frac{dV_m}{dt} + g_{Na} m^3 h (V_m - V_{Na}) + g_K n^4 (V_m - V_K) + g_l (V_m - V_l) \quad (3)$$

$$\frac{dL}{dt} = \alpha_L (1 - L) - \beta_L L \quad (4)$$

$$\alpha_L = \frac{L_\infty}{\tau_L} \quad (5)$$

$$\beta_L = \frac{(1 - L_\infty)}{\tau_L} \quad (6)$$

where $I$ is current per unit area, $C_m$ is the membrane capacitance, $g_L$ is the maximal conductance for each ion given L has a value between 0 and 1 and represents the proportion of channels in the activated ($m$ for the $Na^+$ channels in equation 3 and $n$ for the $K^+$ channel in equation 3) or inactivated ($h$ for the $Na^+$ channel in equation 3) state, $L_\infty$ are steady state values for m, n and h at voltage $V_m$ with time constant $\tau_L$, and $\alpha_L$ and $\beta_L$ are the rate constants for activation and deactivation, respectively. To obtain a better conceptual understanding of the behavior of, for example, the $Na^+$, channel various parameters can be characterized experimentally through voltage clamp techniques and fitted to the equations above. As an example see Zhang et al. who showed the behavior of the cardiac $Na^+$ channel (Nav1.5) [62]. Mathematical descriptions can be developed for any ion channel and through these types of visualizations one can begin to understand the behavior of ion channels in excitable cells. It is important to note that while ion

transporters and pumps can also produce currents that are relatively small in comparison to ion channel currents; their major roles are the maintenance of the electrochemical gradient and hence the driving force.

1.2.1.3 Energy Metabolism

Electrochemical gradients and ion channel gating is sufficient to produce action potentials (APs), yet even with the relatively small number of ions required to produce the necessary current for each AP, there would be eventual rundown of the system during which the electrochemical gradient gradually diminishes if pumps were inactive. Thus, cardiomyocytes utilize energy through pumps, transporters, and exchangers to maintain electrochemical gradients to prevent system rundown. Energy can be obtained from the electrochemical gradient, as in the case of the $Na^+$-$Ca^{++}$ exchanger (NCX) where the driving force of $Na^+$ is utilized to extrude $Ca^{++}$ from the cell. On the other hand, pumps typically utilize hydrolysis of intracellular ATP for energy as in the case of the $Na^+$-$K^+$ pump extruding $Na^+$ and importing $K^+$ against their gradients. Thus, through energy utilization the electrochemical gradients for each ion is maintained, preventing systemic rundown, and making repeated, sustained, electrical activity possible.

ATP production in myocytes occurs from two sources as seen in Figure 1.1: glycolysis and aerobic respiration (β-oxidation does not independently produce ATP). Glycolysis produces a relatively small amount of ATP from free glucose or glucose derived from cellular glycogen stores. Aerobic respiration, on the other hand, produces a much larger quantity of ATP from pyruvate obtained through glycolysis or acytyl-co-A through β-oxidation. The key point is that aerobic respiration (36 ATP/glucose) is much more efficient than glycolysis (2 ATP/glucose) at producing energy but aerobic respiration requires oxygen ($O_2$) [63, 64] which is absent during VF-SCA. Furthermore, ATP can also act as a ligand regulating ion channel function creating further implications for direct effects of metabolism on electrical activity (see Section 1.3.3).

1.2.1.4 The Cardiac Action Potential

Combining the conceptual framework of the GHK equation and Hodgkin and Huxley's ion channel gating framework provides a mathematical understanding for the rise of APs. By rapid transition of membrane permeability to different ions over time, the $V_m$ rapidly shifts towards the Nernst potential of one ion and then another: the consequence is the generation of a finely tuned electrical signal that can be used for cellular communication or controlling cellular function. Energy production and utilization plays a key role in maintaining this system allowing ongoing electrical activity without systemic rundown.

In the heart, the basic cardiac action potential (AP) takes the form seen in Figure 1.2. The shape is determined primarily by the currents illustrated, which can be divided into inward currents (Figure 1.2 above) and outward currents (Figure 1.2 below). Inward currents—or source currents—are mostly $Na^+$ and calcium ($Ca^{++}$) currents and depolarize the cell. Outward currents—or sink currents—are mostly $K^+$ currents and polarize the cell. The balance of source and sink currents determine $V_m$ at each time point and hence electrical excitability of the cell. In general, a differing combination of currents is active during each phase of the cardiac AP indicated by the numbers 0 through 4 (center panel Figure 1.2). At rest the $V_m$ of the cardiomyocyte is established by currents through the inward rectifier $K^+$ channel ($I_{K1}$), hence the resting membrane potential ($V_{rest}$) is established near the $K^+$ reversal potential (-90 mV). As the cell depolarizes the open probability of $Na^+$ channels is increased leading to a positive feedback loop with large inward current and rapid depolarization of the membrane (phase 0) approaching the reversal potential of $Na^+$. Due to the rapid inactivation of the $Na^+$ current ($I_{Na}$) and the subsequent activation of the transient outward $K^+$ current ($I_{to}$) the downward notch at the top of phase 1 is produced. The activation of L-type $Ca^{++}$ current ($I_{CaL}$) combined with the activation of the rapid component of the outward $K^+$ current ($I_{Kr}$) produces phase 2, or the plateau phase, where the $V_m$ reaches somewhere between the $Ca^{++}$ and $K^+$ reversal potentials. As $I_{CaL}$ inactivates and $I_{Kr}$ and the slow component of the outward $K^+$ current ($I_{Ks}$) activates, leading to the repolarization phase, or phase 3, moving $V_m$ back to phase 4 or rest [65].

The shape of the cardiac AP is important for two primary reasons. First, the relatively long plateau phase allows the sustained entry of $Ca^{++}$ that activates intracellular $Ca^{++}$ release

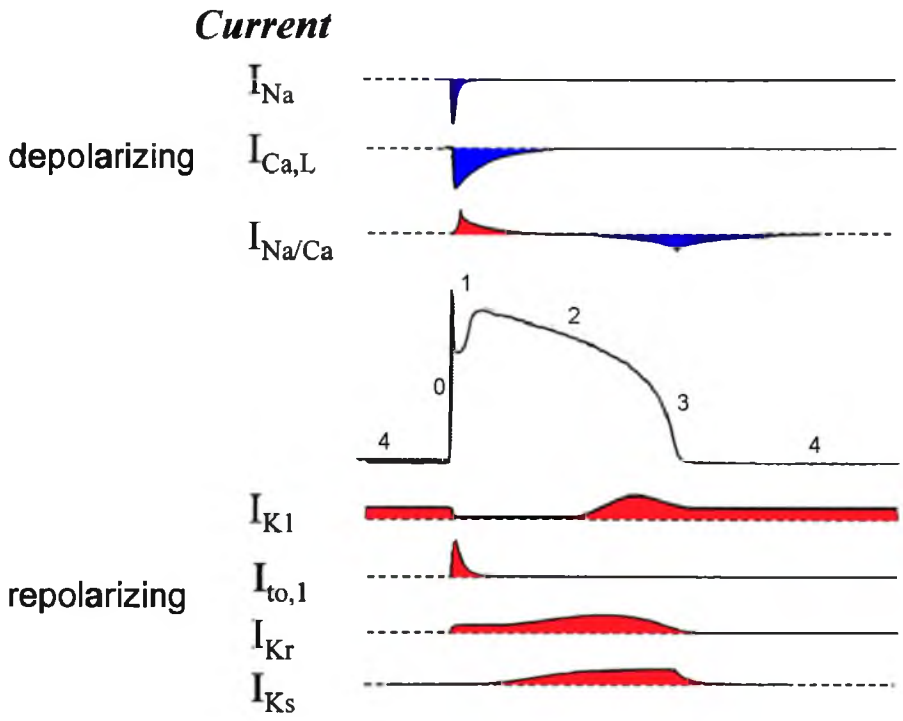


**Figure 1.2**: The cardiac action potential and its primary components. Above in blue, source currents flow into the cell depolarizing the membrane. Center, the cardiac action potential with each of the four phases labeled. Below in red, sink currents flow out of the cell polarizing the membrane. The balance of source and sink currents determines cell excitability and the shape of the action potential.

from the SR leading to activation of the actin-myocin filaments (see Figure 1.1) and is thus essential for proper contractile activity of the heart [66]. Second, the long AP duration (APD) serves to increase the refractory period by delaying the timing of $Na^+$ channel recovery from the inactivated to closed state. The prolonged refractory period reduces the propensity for reentrant arrhythmias by increasing the duration of electrical wavefronts preventing the propagating wave from reexciting tissue prematurely [66]. An alternate conceptualization is that a longer wavefront necessitates a longer path length for formation of reentry. The idea of reentrant arrhythmias is discussed in more detail in the following section.

### 1.2.3 Cardiac Arrhythmogenesis

Both $Ca^{++}$ signaling and refractory period are thought to play important roles in generating cardiac arrhythmias. The classical concept for arrhythmogenesis requires the presence

of a proarrhythmic trigger and substrate. This concept is illustrated in Figure 1.3 where the substrate is defined as a region of tissue with sufficient path length around a region of unidirectional electrical block (upper right) [66-68]. The region of block can be either functional or anatomical but must allow the electrical wavefront to anchor and rotate around the blocked area and reenter the original site. The path length for this reentrant wave must be sufficient so that the reentering wave does not encounter refractory tissue and annihilate. Path length can be modulated through the physical size of the circuit but can also be affected by refractory period and conduction velocity [66-68]. While anatomical block results from mechanisms such as scar tissue formation and ischemic myocardium, currents which generate early-after or delayed-after depolarizations (EADs and DADs, respectively, Figure 1.3 bottom row) are thought to be a common trigger for arrhythmias [66-68] by presumably resulting in regions of ectopic activity, complex wave interactions, and arrhythmias. Despite this theoretical framework exactly how VF is triggered in hearts is still unproven. VF causes loss of organized contraction, leading to ischemia with its accompanying lack of $O_2$ delivery and waste removal. The resulting is a lack of energy to prevent system rundown that can directly modulate electrical function (as discussed in

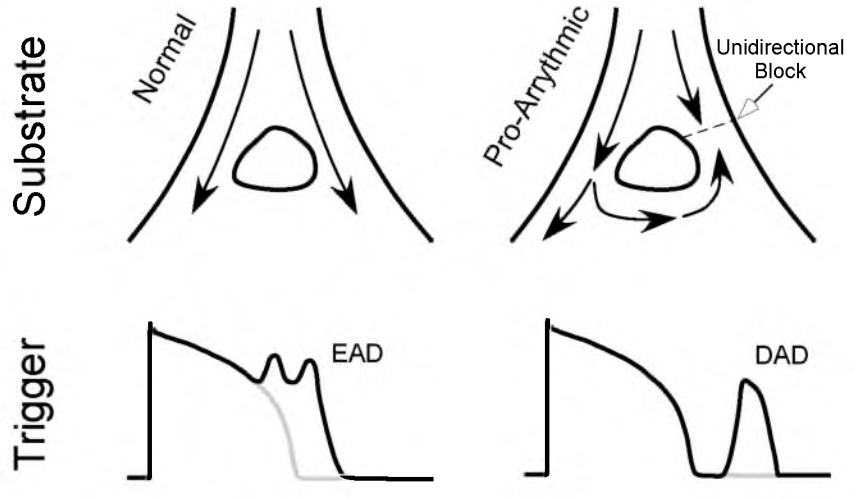


**Figure 1.3**: An illustration of the primary components leading to VF based on current theory. Top row: illustrates the need for a proarrythmic substrate in triggering reentrant arrhythmias. The top left indicates normal conduction around an anatomical feature. The top right shows the formation of a reentrant pathway due to the presence of an area of unidirection block. The path length must be sufficient that the wavefront does not collide with the wave tail and annihilate. Lower row: diagrams of EADs and DADs that are thought to be $Ca^{++}$ mediated triggers of arrhythmias. Current theory points to a need for both proarrythimc substrate and trigger for the formation of reentrant arrythimas such as VF.

1.3.3). Given the framework discussed above, I started with the premise of metabolic challenge Section 1.3.3). Therefore, I started with the premise of metabolic challenge as a consequence of VF-SCA and developed a hypothesis for electrical failure due to changes in electrochemical gradients and ion channel function.

## 1.3 Theoretical Mechanisms of Electrical Failure

Principles of electrically excitable cells points to the balance of source and sink currents as determinants of electrical failure. Figure 1.2 illustrated the major currents that make up the cardiac action potential that can be divided into either inward (source) currents or outward (sink currents). The net current determines whether an AP fires. For the purposes of electrical failure at the cellular level one can specifically focus on the AP upstroke since the presence of the upstroke determines whether the cell is excitable. This concept can be extended to the tissue level where the presence or lack (conduction block) of AP propagation to neighboring cells is determined by the source currents flowing from excited cells to neighboring cells at rest and the sink currents present in those same cells.

### 1.3.1 Reduced Source Current–Hyperkalemia

By examining phase 0 (see Figure 1.2) of the AP one can begin to understand potential causes for inexcitability. As previously stated, the resting potential is determined by the GHK equation (equation 2). At rest under normal conditions, $Na^+$ and $Ca^{++}$ conductances are very low which allows the GHK equation to be simplified to the Nernst equation (Equation 1) (Figure 1.4 top left) for $K^+$ leading to a $V_{rest}$ of approximately -88 mV. At this state almost all $Na_+$ channels are available for recruitment in AP firing (Figure 1.4 top center). Thus a well-polarized $V_{rest}$ results in robust AP firing (Figure 1.4 top right).

During ischemia $[K^+]_o$ accumulates [69, 70] leading to a reduction in source currents. Under the assumption that $Na^+$ and $Ca^{++}$ conductances remain approximately zero, this $[K^+]_o$ accumulation leads to depolarization of the $V_{rest}$ (Figure 1.4 lower left) which in turn leads to inactivation of a large proportion of $Na^+$ channels and reduced availability of $I_{Na}$ (Figure 1.4 lower

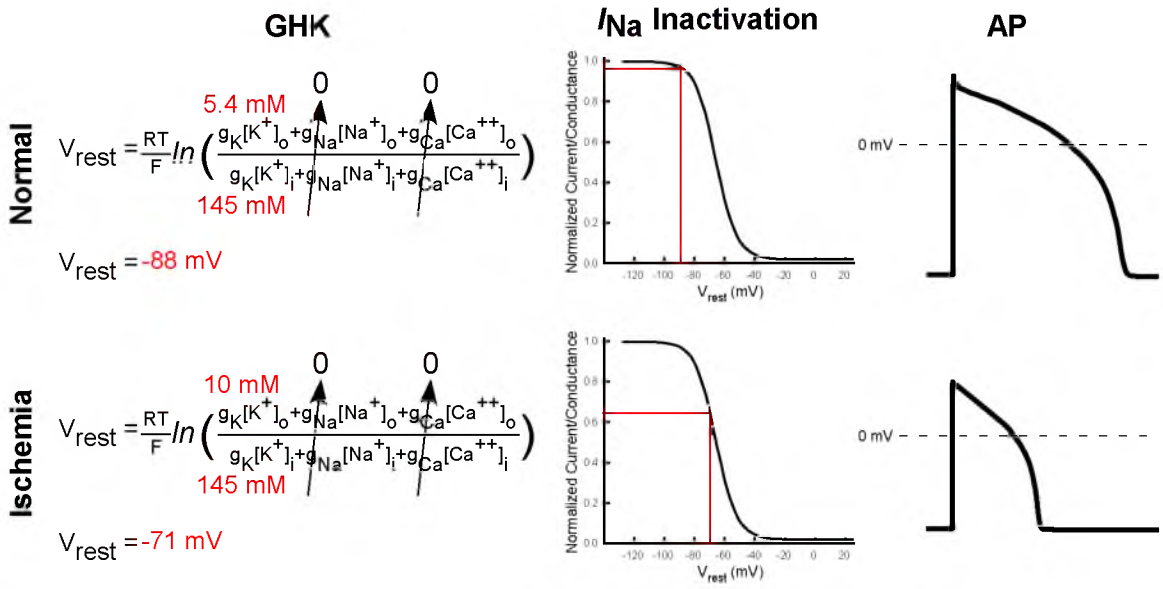


**Figure 1.4**: The effects of hyperkalemia on AP firing. Left column: the GHK equation determines steady state $V_m$. At rest $Na^+$ and $Ca^{++}$ conductances are low meaning, $V_{rest}$ will be determined by the Nernst potential of $K^+$. Center column: the effect of $V_{rest}$ $I_{Na}$ availability. Right column: the resulting AP. Upper row: under normal conditions $[K^+]_o$ is low leading to a well polarized $V_{rest}$, large $Na^+$ channel availability, and rhobust AP firing. During ischemia $[K^+]_o$ accumulates depolarizing Vrest, reducing $Na^+$ channel availability, and less robust AP firing. With sufficient $[K^+]_o$ accumulation $Na^+$ channel availability can be reduced sufficiently to cause electrical failure.

center) and reduced AP amplitude (Figure 1.4 lower right). If the $I_{Na}$ current is reduced sufficiently APs cannot fire at all. Thus, during ischemia there is reduced source current through increasing inactivation of $I_{Na}$. Furthermore, hyperkalemia may contribute to heterogeneous electrical decline and failure through either heterogeneous $[K^+]_o$ accumulation or due to heterogeneous $Na^+$ channel expression or function throughout the heart. Cordeiro et al. showed heterogeneous $Na^+$ channel function between the ENDO and EPI [71]. Specifically, it was shown that during ischemia although $I_{Na}$ density was not significantly different between ENDO and EPI, EPI cells displayed a more negative half-inactivation voltage suggesting reduced $I_{Na}$ availability on the EPI.

### 1.3.2 Ischemia Activated Potassium Channels

In addition to decreased source current, sink current is thought to increase during ischemia through the activation of ischemia activated $K^+$ channels. Of particular interest for the

past few decades has been the ATP-sensitive $K^+$ channel ($K_{ATP}$) [72]. $K_{ATP}$ channels in the ventricular sarcolemma form an octomeric structure comprised of four Kir6.2 pore forming subunits and four SUR2A regulatory subunits (see Figure 1.5A). $K_{ATP}$ current ($I_{KATP}$) provides a direct link between metabolism and electrical activity since it is blocked by normal levels of $[ATP]_i$ and activated by high intracellular ADP concentration ($[ADP]_i$) (Figure 1.5A). In addition, $K_{ATP}$ expression and/or function has been shown to be heterogeneous throughout the heart (left vs. right ventricle, ENDO vs. EPI) [69, 70]. Another potential mechanism for increased sink current during VF-SCA is the $Na^+$-sensitive $K^+$ channel ($K_{Na}$). The molecular identity of $K_{Na}$ was determined a decade ago [73]. Thus far it has been shown that in the rabbit ventricles there is functional expression of $K_{Na}$ in the form of tetrameric Slo2.1 (Figure 1.5B). $K_{Na}$ presents an especially attractive possibility for increased sink current during VF-SCA since it creates a rate dependent increase in sink current: as activation rate increases intracellular $Na^+$ concentration ($[Na^+]_i$) increases resulting in more $K_{Na}$ current ($I_{KNa}$) [74, 75]. Indeed, $K_{Na}$ opening should affect electrical activity in much the same way as $K_{ATP}$ opening except that the effects would be greater at higher rates of excitation. In addition, evidence suggests that $K_{Na}$ can also sense $[ATP]_i$ potentially creating a direct link to metabolism as well [74, 75] although more recent evidence points to lack of ATP sensitivity of $I_{KNa}$ [76]. Furthermore, both $I_{KATP}$ and $I_{KNa}$ activation could substantially increase sink during ischemia due to their relatively large conductance (80 pS and 180 pS, respectively) [77, 78]. With their large conductances and the lack of voltage and time sensitive gating, the result is a large increase in sink current during the AP (i.e., $I_{KATP}$ and $I_{KNa}$ are proportional to the difference between $V_m$ and $E_k$).

### 1.3.3 Source-Sink Mismatch

The result of hyperkalemia and ischemia activated $K^+$ channel opening is the combination of decreased source current and increased sink current. Such imbalance of source and sink currents—called source-sink mismatch—increases propensity for conduction block and electrical failure. Figure 1.6 shows schematically how source-sink mismatch translates from the single cell to tissue in a one-dimensional tissue consisting of four cardiomyocytes. For electrical conduction

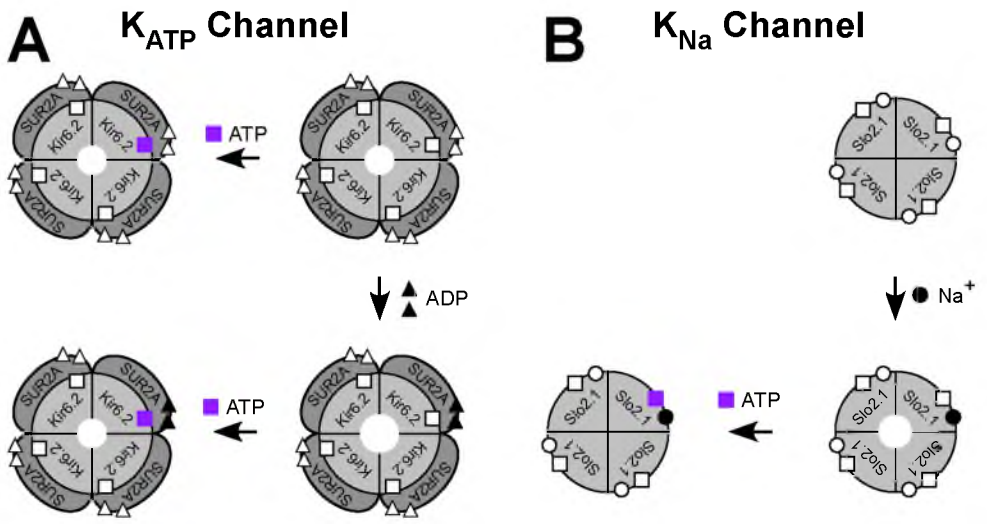


**Figure 1.5**: Schematic representation of $K_{ATP}$ and $K_{Na}$ channel gating. Both $K_{ATP}$ and $K_{Na}$ are ligand gated and lack voltage and time sensitive gating. Furthermore, their large conductances and ATP sensitivity make them ideal candidates for linking metabolic stress with electrical failure. **A.** $K_{ATP}$ is an octomeric structure of four Kir6.2 pore forming subunits and four SUR2A regulatory subunits. Kir6.2 has a binding site for ATP that prevents pore opening. In the absence of ATP binding ADP can activate KATP; nevertheless, ATP binding even in the presence of ADP binding leads to loss of conductance. **B.** $K_{Na}$ is activated by $[Na^+]_i$ which is thought to be increased during ischemia. During VF-SCA there is likely $[Na^+]_i$ accumulation due to increased AP firing rate leading to a potential rate dependent increase in ischemic sink current.

to occur the AP firing in the first cell must be transmitted to each neighboring cell by depolarizing the neighboring cell's $V_m$ above threshold (indicated by the dashed lines). Under normal conditions (Figure 1.6 top pannel) source currents (indicated in blue) and sink currents (indicated in red) are in proper balance allowing the membrane potential of the first cell to reach threshold resulting in AP firing which creates electrotonic source currents that depolarize the neighboring cell sufficiently so it also reaches threshold and fires an AP. If there is a substantial decrease in source currents (Figure 1.6 second panel), as during ischemia through hyperkalemia and inactivation of $I_{Na}$, the electrotonic source current to neighboring cells can be insufficient to depolarize $V_m$ to threshold resulting in conduction block. If instead, there is a substantial increase in sink current (Figure 1.6 third panel), as during ischemia through activation of $I_{KATP}$ or $I_{KNa}$, the electrotonic source current from the first cell is counteracted by the increased sink preventing $V_m$ from depolarizing to threshold and thus resulting in conduction block. During ischemia both decreased source and increased sink are present, greatly increasing source-sink mismatch and propensity for conduction block (Figure 1.6 lower panel).

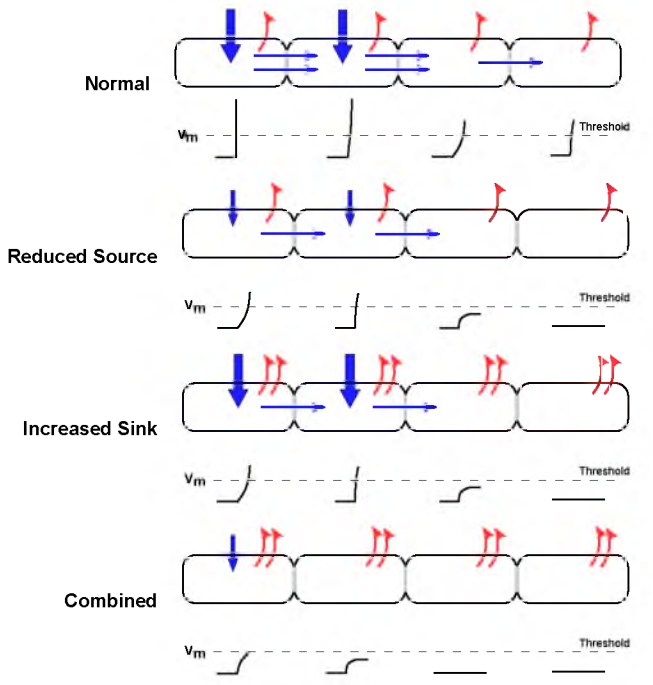


**Figure 1.6**: Conceptual framework of source-sink mismatch in tissue. A figure of four myocytes forming a one dimensional tissue under various conditions of source-sink mismatch. Blue arrows indicate source currents, red arrows indicate sink currents, dashed lines indicate the threshold to which $V_m$ must depolarized for AP firing to occur. The first panel shows normal conditions where the balance between source and sink allows neighboring cells to depolarize to threshold leading to AP propagation. The second panel indicates the consequences of reduced source current through mechanisms such as hyperkalemia leading to insufficient depolarization of neighboring cells resulting in conduction block. The third panel illustrates the result of increased sink current through mechanisms such as $K_{ATP}$ or $K_{Na}$ activation which counteracts electrotonic source currents preventing depolarization to threshold and AP firing in neighboring cells. The fourth panel shows the combination of both decreased source and increased sink—as during ischemia—leading to large source-sink mismatch and conduction failure.

Shaw and Rudy investigated precisely this idea *in silico* by modeling the relationship between $[K^+]_o$ and conduction velocity (CV) [79]. Their results indicate that gradually increasing $[K^+]_o$ leads first to a range of $[K^+]_o$ where CV is supernormal then falling off rapidly reaching conduction block at a $[K^+]_o$ of approximately 14 to 15 mM. In addition, they modeled what occurs if there is extreme depletion of intracellular $[ATP]_i$, much lower than bulk tissue $[ATP]_i$ depletion measured during ischemia [80]; nevertheless, these low $[ATP]_i$ may exist locally near the sarcolemma as suggested by Lamp and Weiss [81]. In effect, the model simulated the consequence of combined hyperkalemia and extreme $I_{KATP}$ activation or large source-sink mismatch. The model predicted a left shift in the $[K^+]_o$ necessary to cause conduction block, shifting the blocking $[K^+]_o$ from 15 mM to approximately 10 mM. Shaw and Rudy concluded that

hyperkalemia is the major factor determining conduction block while $I_{KATP}$ activation plays a relatively small role. Contrary to Shaw and Rudy's conclusion about the small role of $I_{KATP}$, several studies suggest that under ischemia combined with pharmacological mitochondrial stress through the use of a protonophore which depolarized the mitochondrial membrane potential—aggravating mitochondrial stress during ischemia—conduction block and arrhythmias arise through the activation of $I_{KATP}$ without the presence of hyperkalemia [82-85]. This phenomenon has been called "metabolic sink block" and this mechanism is a key factor in conduction failure. Both the proposed mechanisms for electrical failure (i.e., hyperkalemia and $K_{ATP}$ opening) are the products of simulations. Together, the findings above are inconclusive about what causes electrical failure during ischemia, although they do provide a starting point.

### 1.3.4 Rate and β-Adrenergic Stimulation

The theories for electrical failure discussed above were developed in the general context of myocardial ischemia. Yet there are two factors present during VF-SCA that may accelerate electrical failure compared to ischemia alone. First, it is well known that VF leads to exceedingly high excitation rate reaching around 10 Hz without ischemia in canine hearts (see Chapter 3 for examples). In fact, high rate is an intrinsic characteristic of VF. Second, VF-SCA results in exposure to a high degree of β-adrenergic stimulation (β-AS) which is a consequence of endogenous catecholamine release, from adrenal glands and nerve endings in the myocardium, during ischemia—approximately 7-fold for norepinephrine during ischemia; furthermore, during procedures mimicking life saving resuscitation there is an approximately 100-fold increase in interstitial fluid catecholamine levels [86]. In addition, during clinical resuscitation ACLS guidelines recommend administration of epinephrine every 3-5 minutes [28]. Thus, especially in patients, the exposure to increased β-AS occurs from two routs. In addition, β-AS has a tendency to accelerate the frequency of VF further increasing excitation rate [87]. Figure 1.7 shows a schematic diagram of the complex potential consequences of increased excitation rate and β-AS leading to increased source-sink mismatch and hence electrical failure during VF-SCA.

The concept in Figure 1.7 is that increased rate or β-AS leads to both increased metabolic

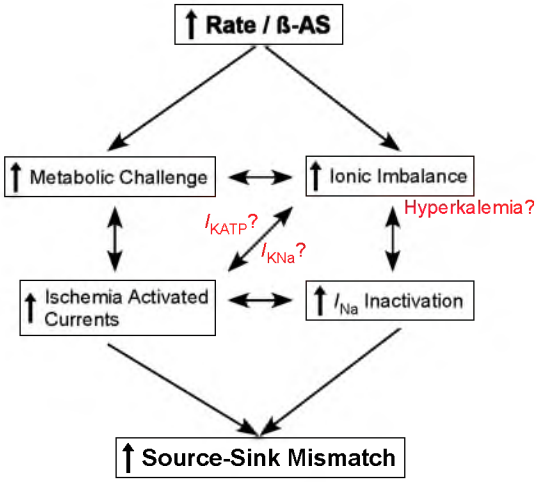


**Figure 1.7**: Conceptual implications for the potentially detrimental effects of high excitation rate and β-AS present during VF-SCA. Increased rate and β-AS can lead to increased ionic imbalance and metabolic challenge. This in turn leads to increased $I_{Na}$ inactivation and inschemia activated currents leading to source-sink mismatch and hence electrical failure. Each of these exacerbated changes may be linked through various mechanisms such as $K_{ATP}$ and $K_{Na}$ activation. This figure serves to illustrate the complex interactions likely present and emphasizes the likelihood of the multifactorial nature of electrical failure in VF-SCA.

challenge and ionic imbalance that are themselves linked. For example, rate could modulate $[Na^+]_i$ imbalance since the integral of $I_{Na}$ over time (i.e., the quantity of $Na^+$ ion influx) would increase. This in return could lead to greater energy expenditure by the $Na^+$-$K^+$ ATPase. As a consequence source current would be reduced through decreased $Na^+$ driving force and sink could be increased through activation of $I_{KNa}$ promoting source-sink mismatch and electrical failure. As another example, β-AS leads to greater $Ca^{++}$ cycling which requires greater energy expenditure leading to intracellular $Ca^{++}$ ($[Ca^{++}]_i$) accumulation. Elevated diastolic $[Ca^{++}]_i$, in turn, could lead to increased mitochondrial challenge through mitochondrial permeability transition [88] promoting activation of $I_{KATP}$ again promoting source-sink mismatch and electrical failure. While Figure 1.7 is speculative, some hints exist in literature for the detrimental role of both high excitation rate and β-AS. First, Blake et al. showed that the deviation of the estimated $K^+$ reversal potential ($E_K$) from $V_{rest}$ in a regionally ischemic dog heart was modulated by rate and extracellular $Ca^{++}$ [89]. Such a deviation in $V_{rest}$ and $E_K$ would point to the emergence of a depolarizing current during ischemia that exacerbates source-sink mismatch and hence electrical failure (see Section 7.3.1 for a detailed discussion). Second, retrospective clinical studies show a

potentially detrimental role of epinephrine treatment despite the increased occurrence of ROSC during resuscitation. Specifically, there are indications of reduced long-term survival to hospital discharge as a consequence of epinephrine treatment [42-44]. Third, the use of a β-adrenergic receptor antagonist, esmolol, in open-chest canine models of VF-SCA also point toward the detrimental role of β-AS in electrical failure by reducing the number of defibrillatory shocks necessary to achieve ROSC [86]. Thus, the literature points towards detrimental roles of high rate excitation and β-AS. Nevertheless, there has been no systematic examination of the independent and potentially synergistic roles of high rate excitation and β-AS in electrical failure nor is there insight into the mechanism of action during VF-SCA. In addition, my findings not only point to the detrimental roles of high rate excitation and β-AS in electrical failure but also in the promotion of ischemic arrhythmogenesis suggesting the critical role of abnormal impulse propagation rather than abnormal impulse formation (see Section 6.4.5 for details).

# CHAPTER 2

# OVERVIEW OF THE DISSERTATION

## 2.1 Motivation

The work in this dissertation was motivated by the desire to contribute meaningful advances in the understanding of electrical failure during VF-SCA. If a mechanism causing or even contributing to electrical failure could be identified such knowledge could impact interventions for clinical trials in resuscitation. Moreover, if electrical failure can be delayed through such interventions, perhaps survival rates can be improved; after all, survival rates for patients in asystole are much lower than those with some rhythm (See Section 1.1). The goal became to first understand the pathophysiology of VF-SCA. Based on the background discussed in Chapter 1, specific aims were developed to test each of the mechanisms discussed above using the isolated Langendorff perfused heart. The plan was to first determine the contribution of each mechanism to electrical failure during VF-SCA independently and second, to test the synergy that may exist between multiple factors. You will see through this dissertation that neither of the factors previously thought to cause electrical failure (hyperkalemia nor $I_{KATP}$) are—independent or combined—sufficient to explain the pattern of electrical failure seen during VF-SCA. Furthermore, additional hypotheses were tested involving $I_{KNa}$, excitation rate, and β-AS, which shed light on electrical failure but leave unanswered the additional mechanisms of electrical failure. In conclusion, I propose hypotheses to account for the missing mechanisms of electrical failure and the future work necessary to realize the goal for a clinical intervention.

## 2.2 Projects

Below are concise descriptions of the four projects reported (Chapters 3 through 6) in this dissertation along with the original hypotheses on which the projects were based.

For project 1 I aimed to determine the transmural distribution of $[K^+]_o$ during VF-SCA and assess its role in the distribution of VF rate and asystole during VF-SCA. I hypothesized that $[K^+]_o$ would rise to higher levels in the subepicardium than in the subendocardium, reflecting transmural differences in ischemia-induced potassium efflux. I assessed the contribution of hyperkalemia to the heterogeneous electrical depression and inexcitability during VF-SCA by comparing the relationship between $[K^+]_o$ and VF rate (VFR) during normoxemic VF and ischemic VF.

For project 2 I aimed to assess the role of $K_{ATP}$ in electrical depression and asystole during VF-SCA. I hypothesized that the opening of $K_{ATP}$ channels during VF-SCA contributes to heterogeneous electrical depression and asystole during VF-SCA (in accordance with the "sink block" mechanism) [82]. Hence, blockade of $K_{ATP}$ would postpone electrical depression and asystole during VF-SCA. Moreover, pharmacological $K_{ATP}$ activation in combination with hyperkalemia and normoxemic VF would not reproduce the pattern of electrical depression observed during VF-SCA.

For project 3 I sought to Assess the role of $K_{Na}$ in electrical depression and asystole during VF-SCA. I hypothesized that $K_{Na}$ blockade would delay heterogeneous electrical depression and asystole during VF-SCA (or rapid pacing and ischemia) similar to the outcome of $K_{ATP}$ blockade. Moreover, the effects of $K_{Na}$ blockade would diminish at slower pacing rates.

For project 4 I aimed to determine the roles of high excitation rate and β-adrenergic stimulation in electrical depression and asystole during VF-SCA. I hypotheseized that both high excitation rate and β-AS independently promote electrical depression and asystole. Furthermore, the detrimental effects of high rate and β-AS would be additive in that combined they would further accelerate electrical failure. Moreover, the detrimental effect would be mediated by $I_{KNa}$ and $I_{KATP}$.

## 2.3 Approach

### 2.3.1 Overall Strategy

Initially, it was necessary to establish the phenomenology of electrical failure in VFSCA. To achieve this I determined the time course and pattern of electrical deterioration and failure in open-chest and isolated Langendorff perfused canine heart models to establish a baseline for VF-SCA. Thereafter, the overall strategy for investigating the mechanisms of electrical failure in VF-SCA was 2-fold: 1) I investigated the role of each hypothesized mechanism independently during ischemia with VF or rapid pacing using an isolated heart model (Figure 2.1 above solid line); and 2) I manipulated multiple factors simultaneously in a normally oxygenated langendorff perfused heart in an attempt to reproduce the characteristic electrical decline observed during VF-SCA (Figure 2.1 below solid line).

In Strategy 1 (Ischemic model), isolated hearts were exposed to global ischemic episodes lasting between 10 and 30 minutes by stopping the perfusion pump. $[K^+]_o$ was monitored and ion channels were pharmacologically modulated. The goal of Strategy 1 was to determine the contribution of each factor to electrical decline during ischemia in the presence of VF or rapid

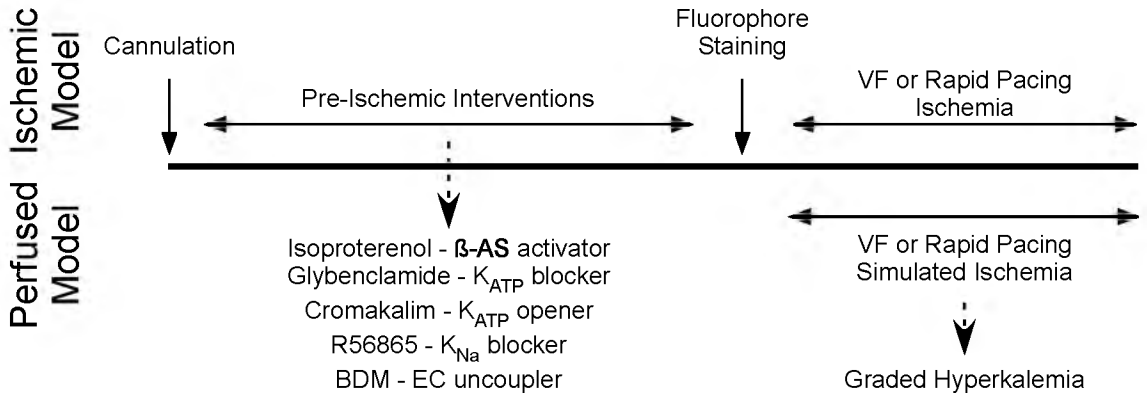


**Figure 2.1**: The two overall strategies used for projects in this dissertation (ischemic model and perfused model). The solid line indicates the time course of an experiment following cannulation till the end of VF-SCA. Above the solid line is illustrated the ischemic model where following interventions common to both models VF-SCA was simulated using a combination of VF or rapid pacing with ischemia. Below the solid line is illustrated the time course for the perfused model. Where VF-SCA was simulated using a VF or rapid pacing with graded hyperkalemia instead of ischemia. In each model various interventions were performed which are listed below the dashed arrow under preischemic interventions.

pacing. In Strategy 2 (Perfused model), isolated hearts were perfused with normal oxygenated solution while either in VF or under rapid pacing. Then perfusate composition was manipulated (i.e., $K^+$ concentration or pharmacological interventions). The goal of Strategy 2 was to determine the mechanism, or combination of mechanisms, that best reproduced the characteristic electrical deterioration observed during the baseline study of VF-SCA (described in Chapter 3).

### 2.3.2 Experimental Setup

Hearts were obtained from pound dogs, purpose bread dogs, and New Zealand white rabbits of both sexes. Dogs weighed between 15 to 25 kg while rabbits weighed 1.75 ± 0.25 kg. The canine setup was designed for recirculation of a relatively small volume of blood (~700 mL) and the rabbit setup was designed for continuous perfusion with fresh Tyrode solution. In both setups gas composition and pH was controlled through a hollow fiber membrane oxygenator. Hearts were isolated through midline sternotomy and rapidly excised, placed in cold osmotically balanced saline, and rapidly cannulated. Perfusion was maintained at 140 ~ 200 mL/min for canine hearts and 30 mL/min for rabbit hearts. Hearts were placed in either a superfusion or vapor chamber for temperature maintenance during ischemia. Temperature was maintained at 37 ± 1 °C for both perfusion and superfusion.

### 2.3.3 Optical Mapping

Figure 2.2A shows a schematic diagram of the multichannel optical mapping setup developed for the work contained in this dissertation. The setup consists of red, green, and blue laser light sources with a holographic diffuser for beam expansion and smoothing (i.e., flattened Gaussian distribution of beam intensity), a multiband dichroic mirror for separation of excitation light from emission, an emission splitting dichroic mirror for separation of multiple emission spectra, band-pass or long-pass filters for isolation of the emission signal, and two CCD cameras for detection of the signals. The system has been used successfully with five fluorophores (Di-4 ANEPPS, RH237, Rhod-2, TMRM, DCF) but was designed to accommodate additional fluorophores. For the work in this dissertation data collected only from Di-4 ANEPPS is shown

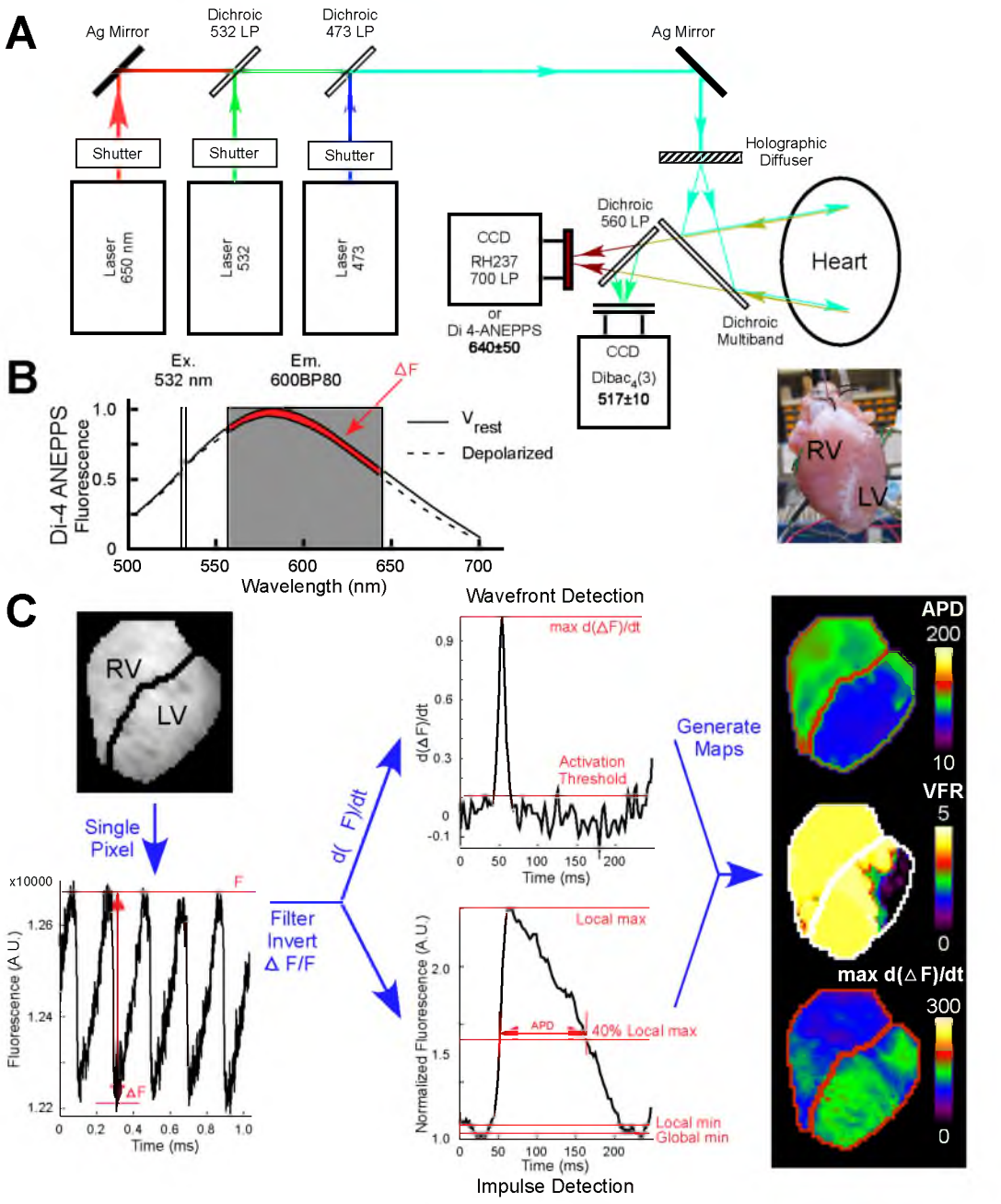


**Figure 2.2**: Optical mapping setup and analysis. **A**. Layout of components in optical mapping setup. Illustrates the simplicity and flexibility of the design that allows acquisition of fluorescence from a wide range of fluorophores and dual mapping capabilities. **B**. Di-4 ANEPPS fluorescence as a function of wavelength. The green vertical bar is the laser light, the gray box indicates the range of the bandpass filter in which light is collected. The solid line indicates the emission spectra at $V_{rest}$ and the dashed line the emission at depolarized states. The difference in integral under the two curves gives the AP signal ΔF. **C.** Analysis work flow for optical data. A fluorescence move obtained from the surface of the heart is analyzed one pixel at a time. Each pixel is filtered in space and time, inverted, and normalized by background fluorescence F. Two separate algorithms were used to detect various parameters, a wavefront detection algorithm and an impulse detection algorithm. From the results of these two algorithms maps of various parameters were generated. Most notably, APD, VF rate (VFR), and max dΔF/dt maps.

with the detailed information concerning the optics used contained in the methods section of each relevant chapter. Di-4 ANEPPS (Pyridinium, 4-(2-(6-(dibutylamino)-2-naphthalenyl)ethenyl)-1-(3-sulfopropyl)-hydroxide is a zwitterion with a large hydrophobic region that binds to the cell membrane and changes excitation and emission wavelengths as it undergoes a conformational change in response to an electric field (Figure 2.2B). The change in emission wavelength of Di-4 ANEPPS is recorded as a dimming in acquired fluorescence ($\Delta F$, Figure 2.2C lower left) due to the reduced photon flux through the bandpass filter incident on the detector. Using this technique allows us to record electrical activity as if there were a 64 by 64 channel electrode array on the surface of the heart. In addition to the high density electrical recording, the signal from optical mapping of Di-4 ANEPPS gives direct information concerning the dynamic electrical behavior of the sarcolemma thus allowing measurements of parameters such as APD and diastolic interval (DI) which can only be obtained through inference with traditional extracellular recording electrodes by measuring parameters such as activation recovery intervals. In addition, I was able to obtained high-density spatial information that allowed determination of inexcitable tissue and visualize the highly heterogeneous pattern of electrical depression and failure in response to uniform global ischemia.

The down sides of optical mapping are that motion from contraction can contaminate the signal, only signals from superficial layers are collected, large concentrations of dye can result in phototoxicity, the signal-to-noise ration is high compared to electrical recordings, and only relative changes in $V_m$ can be measured. To minimize some of these pitfalls, the following precautions were taken. To reduce motion, hearts were either lightly pressed against the wall of the superfusion bath (canine hearts) or treated with an excitation-contraction uncoupler (rabbit hearts). Signal-to-noise was optimized by adjusting both the concentration of the dye and the intensity of illumination while attempting to minimize phototoxicity. To obtain information from the myocardial depth (greater than the first few hundred microns) I combined optical mapping with unipolar plunge needle electrodes (see Section 2.3.4). Figure 2.2C illustrates the data processing workflow. First, masks were created manually to exclude background and separate the LV and RV. Each pixel from the recorded movie yielded a series of APs. Signals were filtered in space and time, inverted, and normalized by background fluorescence.

The filtered APs are then passed through two separate algorithms. Figure 2.2C (center column, upper panel) illustrates the wavefront detection algorithm. This algorithm detects the rate of AP upstroke, the maximum $d\Delta F/dt$ (proportional to $dV/dt$ in the cardiac AP). This technique allows reliable detection of APs in the presence of motion artifact due to myocardial contraction since contraction occurs with a time delay following AP propagation. An area was considered silent/inexcitable if the max $dV/dt$ did not exceed two times the max $dV/dt$ of background noise. Figure 2.2C illustrates the impulse detection algorithm that allows detection of AP presence as well as some AP characteristics such as APD and DI. While the impulse detection algorithm provides more information concerning the APs, it is more easily contaminated by motion artifact. From these two algorithms, maps such as those illustrated in Figure 2.2C can be obtained. These maps can provide valuable spatial information concerning electrical activity at various time points during VF-SCA. Fluctuations that did not exceed both the local and global minimum were not counted as APs. Further details on the analysis of fluorescence data can be obtained in the relevant chapters.

### 2.3.4 Extracellular Potential Mapping

Extracellular potential was monitored by volume-conducted ECG and unipolar electrograms (EG) recorded using plunge needle electrodes made of fiberglass (10 leads 1.2 to 1.6 mm interlead distance for canine hearts) to span the transmural wall [90]. Figure 2.3A shows a plunge needle electrode with sample EG recording across the transmural wall at 5 minutes of VF-SCA in a canine heart. Figure 2.3E shows an example of how plunge needles could be arranged in the myocardium to extract information both transmurally and laterally.

Using plunge needles allows the measurement of three-dimensional electrical activity in the heart. Figure 2.3C and D show example surface plots of measurements obtained from EG mapping. It can be seen that using plunge needle recordings the heterogeneous evolution of electrical deterioration can be observed both transmurally (Figure 2.3C) and laterally (Figure 2.3D). Volume-conducted ECG recordings were used to determine time of asystole while EGs were analyzed for heterogeneities in transmural VF rate and the occurrence of local inexcitability.

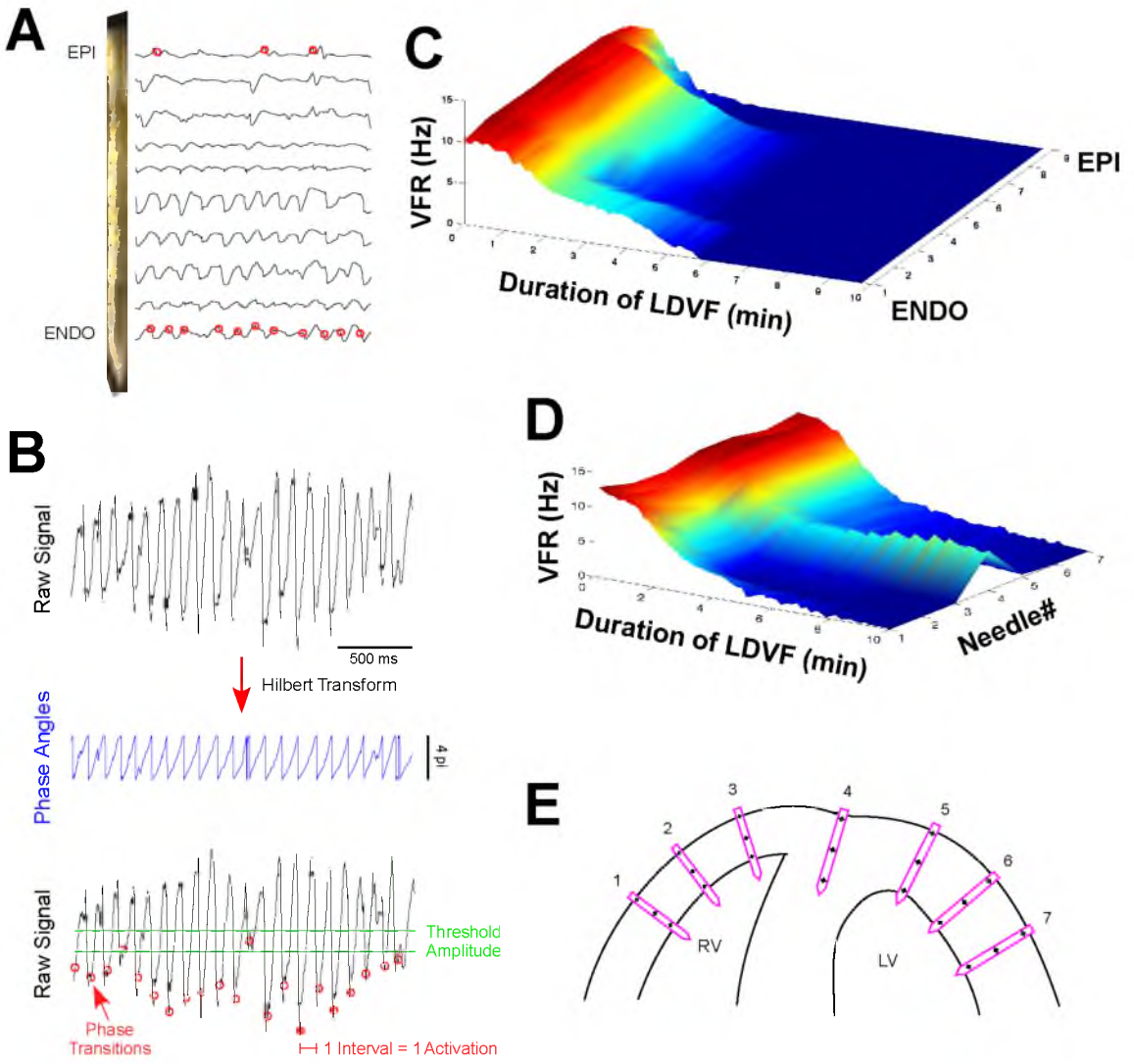


**Figure 2.3**: Plunge needle electrodes and recordings. **A.** An example plunge needle and unipolar EG recordings across the myocardial thickness at 5 minutes of VF-SCA. **B.** EG signal processing is performed by applying the Hilbert transform on the raw signal to obtain phase angles. Each transition of phase angle from $2\pi$ to $-2\pi$ is marked on the raw signal. Next, amplitude is measured in the raw signal between each consecutive phase transition. If the amplitude does not meet threshold the phase transition is rejected. The remaining phase transitions indicate transition between cycles in local AP firing or electrical activity. **C.** Example of transmural surface plot of VFR as a function of myocardial depth and duration of VF-SCA. **D.** Example of lateral surface plot of VFR across the EPI. **E.** Example arrangement of plunge needles for three-dimensional mapping of electrical failure.

ECG and EG recordings were amplified using a high impedance amplifier and fed to a multiplexing unit for data acquisition. Figure 2.3B shows the process of EG analysis. The Hilbert transform is applied to the raw signal, converting the signal to phase angles. Each transition from $2\pi$ to $-2\pi$ represents the start of a new cycle and is noted on the raw signal. Next, a minimum threshold amplitude is applied to the raw signal between phase transitions, thus ruling out small fluctuations and noise from being detected as activations. Each interval between remaining phase transitions represents an electrical activation in the local area. The lack of activation detection is interpreted as local electrical failure.

Like optical mapping, there are pros and cons of extracellular potential mapping. The benefit of ECG recordings is the ability to ascertain global rhythm and the occurrence of asystole, the down side is that there is no information about localized electrical activity from the single lead system used in the subsequent studies. EGs on the other hand provide more localized information and plunge needles can record information from deeper regions of the myocardium. The largest problem with plunge needles is the physical damage inflicted on the myocardial tissue, which produces immediate effects on the recorded electrical activity in the form of injury currents. To minimize injury current plunge needles were placed early in the experimental protocol and the injuries were allowed to recover for approximately half an hour. It is also difficult to know the exact volume from which measurements are obtained. Neither ECG nor EG recordings provide direct information about the APs and traditional methods for the inference of AP characteristics during normal rhythm (i.e., activation recovery intervals for APD) cannot be used during VF. Nevertheless, extracellular potentials provide useful insight into the nature of electrical failure as will be seen in the subsequent chapters.

### 2.3.5 Extracellular Potassium Mapping

$K^+$ sensitive electrodes were constructed from a valinomycin based membrane [91] and housed in a hypodermic needle to protect the delicate membrane. Electrodes were calibrated pre- and post experimental protocol using the Nernst equation:

$$K_2 = \exp\left(\ln(K_1) + (V_2 - V_1)\frac{F}{RT}C\right) \quad (7)$$

where $K_1$ is the baseline $[K^+]$, $K_2$ is the measured $[K^+]$, F is Faraday's constant, R is the universal gas constant, T is the temperature in Kelvin, and C (a value which describes variability in the system) is determined experimentally pre- and postexperimental protocol using 3 and 10 mM KCl solution. Electrodes that fail to shift 30 ± 4 mV both pre- and postexperiment were rejected as broken and the data discarded. $K_1$ was set to either the $[K^+]$ for Tyrode's solution or the measured $[K^+]$ in the recirculating purfusate. Baseline $[K^+]$ was determined by a Nova8 ion analyzer (Nova Biomedical Waltham, MA U.S.A.). Using these calibrated $K^+$ needles, I obtained transmural measurements of $[K^+]_o$ at the ENDO, mid-myocardium (MID), and the EPI during VF-SCA. A description of the detailed approach to transmural measurements can be found in the methods section of Chapter 5.

## 2.4 Timeline of Study: Problems Encountered and Solutions Found

By necessity the spatial and temporal pattern of electrical depression and failure needed to be determined prior to setting out what caused the pattern. As such, the open-chest canine heart was chosen as a starting point in the summer of 2008. The open-chest model represented a whole organism system, relevant to human subjects, for studying the consequences of VF-SCA while still allowing access to the heart with high-density data acquisition equipment. Initially, work was done to develop an optical mapping system capable of acquiring usable data from the open-chest animal. The hurdles for open-chest optical mapping were significant including the delivery of sufficient amounts of fluorophore to the heart, fluorophore toxicity, and the motion artifact due to contraction of the heart. I concluded that for mechanistic insight, especially utilizing pharmacological interventions or modulating extracellular ion concentrations, isolated hearts allowed much finer control of the environment. Thus, I performed simulated VF-SCA studies in isolated canine hearts that reproduced the characteristic patterns I observed in open-chest canine hearts, although the event timing was left-shifted (published in summer 2010,

Chapter 3). From these efforts it was decided to use the isolated heart model to probe the mechanisms of electrical failure.

Concurrent to these efforts was the attempt to measure $[K^+]_o$ in both the open chest and isolated canine hearts during VF-SCA using the valinomycin based $K^+$ sensitive electrodes described above Although I started with the understanding that success rates for acquiring usable data would be low, I collected no usable data from the first 100 or so electrodes that were fabricated. I concluded that the epicardial layers on the surface of the canine heart were too thick to allow placement of the $K^+$ electrodes without destroying them. Thus I developed the $K^+$ needle electrode (described in detail in Chapter 5), which boosted my success rate for usable data acquisition from virtually 0% to approximately 80%. Sufficient data for transmural comparison of $[K^+]_o$ accumulation during VFSCA was finally obtained in Spring 2012.

As I continued to collect $[K^+]_o$ measurements, I started my work on testing the role of $K_{ATP}$ in electrical failure using pharmacological interventions in VF-SCA using an ischemic model in the spring of 2009. The primary difficulty with this project was optimizing the concentration of the $K_{ATP}$ channel blocker. The problem was that the role of $K_{ATP}$ could only be observed with high concentrations that created a concern about nonspecific effects. This lead to a more than doubling of the number of experiments to show that the nonspecific effects could not account for the results of the $K_{ATP}$ blocker. The results of this effort were published in summer of 2012 (Chapter 4).

With the $[K^+]_o$ data from the ischemic model in hand, in the spring of 2012 I set out to determine the role of hyperkalemia in electrical failure during VF-SCA. This was when the idea to use normal oxygenated perfusion instead of ischemia was developed. The idea was to exclude ischemia as a factor and see if the consequences of ischemia such as hyperkalemia or $K_{ATP}$ opening can reproduce the electrical pattern observed with ischemia. I then took the idea one step further and decided to combine the two conditions to see if I could reproduce what the leading theory at the time claimed was the mechanism of electrical failure. The results were negative. The long believed factors for electrical failure, namely hyperkalemia and $K_{ATP}$ opening—individually or combined—did not reproduce the pattern of electrical failure during VF-SCA. There are additional factors at play. This result was published in summer 2013 (Chapter 5).

The question since then has been, "What are the additional factors?" Although I had some hypotheses the large number of possible mechanisms made it impractical to pursue these studies in dogs. To allow higher data throughput I chose to transition to a rabbit model a plan to investigate promising mechanisms in the canine model in the future. The difficulty in transitioning was that rabbit hearts do not experience sustained fibrillation under normal conditions. My attempts to create a sustained VF model in rabbits instead led me to develop a model of simulated VF (i.e., rapid pacing and β-AS). Using th1is model I was able to prove the hypothesized roles of excitation rate and β-AS in electrical failure. Using this rabbit model of VF-SCA I have also tested the potential role of $K_{Na}$ and reproduced my findings for $K_{ATP}$ (Chapter 6) and am in the process of investigating other hypothesized mechanisms of electrical failure (Chapter 7.3.1 Future Work).

## 2.5 Organization of the Remaining Chapters

The following sections of this dissertation describe the results and conclusions of the effort described above. Chapter 3 is a reprint of my first publication (as cofirst author) in the American Journal of Physiology: Heart and Circulatory Physiology (AJP) in which I first established detailed three-dimensional phenomenology/pattern of electrical depression and failure in both in situ and ex vivo canine heart models of VF-SCA. Chapter 4 is a reprint of my second publication in AJP addressing the role of $I_{KATP}$ in electrical depression and failure in the isolated canine heart. Chapter 5 contains my most recent publication, also in AJP, addressing the combined effects of hyperkalemia and $K_{ATP}$ activation in the isolated canine heart leading to the conclusion that additional mechanisms besides these two factors plays a key role in electrical depression and failure during VF-SCA. Chapter 6 is a manuscript currently in preparation elucidating the synergistic effects of β-AS and high excitation rate in promoting electrical failure in the isolated rabbit heart with insights into the mechanism. Chapter 7 contains conclusions drawn from this body of work, proposed mechanisms yet unproved and currently under investigation, future directions, and potential clinical implications for my findings.

An important note is that each paper contained in Chapters 3 through 6 have been presented at American Heart Association's annual Resuscitation Science Symposium where the work contained in Chapter 5 received a Young Investigator Award. In addition to the work featured in Chapters 3 through 6 (in which I played a primary role), Chapter 7 contains a discussion of work complimentary to this thesis in which I played an ancillary role.

# CHAPTER 3

## COMPLEX STRUCTURE OF ELECTROPHYSIOLOGICAL GRADIENTS EMERGING DURING LONG-DURATION VENTRICULAR FIBRILLATION IN THE CANINE HEART

The research in this chapter was published in the *American Journal of Physiology: Heart and Circulatory Physiology*. Paul W. Venable, Tyson G. Taylor, Junko Shibayama, Mark Warren, and Alexey V. Zaitsev.: 'Complex structure of electrophysiological gradients emerging during long-duration ventricular fibrillation in the canine heart.' Am J Physio Heart Circ Physiol, 2010, 299, pp. H1405-H1418. Reprinted with permission of the American Physiological Society.

*Am J Physiol Heart Circ Physiol* 299: H1405–H1418, 2010.
First published August 27, 2010; doi:10.1152/ajpheart.00419.2010.

# Complex structure of electrophysiological gradients emerging during long-duration ventricular fibrillation in the canine heart

**Paul W. Venable,* Tyson G. Taylor,* Junko Shibayama, Mark Warren, and Alexey V. Zaitsev**
*Nora Eccles Harrison Cardiovascular Research and Training Institute, University of Utah, Salt Lake City, Utah*

Submitted 30 April 2010; accepted in final form 25 August 2010

**Venable PW, Taylor TG, Shibayama J, Warren M, Zaitsev AV.** Complex structure of electrophysiological gradients emerging during long-duration ventricular fibrillation in the canine heart. *Am J Physiol Heart Circ Physiol* 299: H1405–H1418, 2010. First published August 27, 2010; doi:10.1152/ajpheart.00419.2010.—Long-duration ventricular fibrillation (LDVF) in the globally ischemic heart is a common setting of cardiac arrest. Electrical heterogeneities during LDVF may affect outcomes of defibrillation and resuscitation. Previous studies in large mammalian hearts have investigated the role of Purkinje fibers and electrophysiological gradients between the endocardium (Endo) and epicardium (Epi). Much less is known about gradients between the right ventricle (RV) and left ventricle (LV) and within each chamber during LDVF. We studied the transmural distribution of the VF activation rate (VFR) in the RV and LV and at the junction of RV, LV, and septum (Sep) during LDVF using plunge needle electrodes in opened-chest dogs. We also used optical mapping to analyze the Epi distribution of VFR, action potential duration (APD), and diastolic interval (DI) during LDVF in the RV and LV of isolated hearts. Transmural VFR gradients developed in both the RV and LV, with a faster VFR in Endo. Concurrently, large VFR gradients developed in Epi, with the fastest VFR in the RV-Sep junction, intermediate in the RV, and slowest in the LV. Optical mapping revealed a progressively increasing VFR dispersion within both the LV and RV, with a mosaic presence of fully inexcitable areas after 4–8 min of LDVF. The transmural, interchamber, and intrachamber VFR heterogeneities were of similar magnitude. In both chambers, the inverse of VFR was highly correlated with DI, but not APD, at all time points of LDVF. We conclude that the complex VFR gradients during LDVF in the canine heart cannot be explained solely by the distribution of Purkinje fibers and are related to regional differences in the electrical depression secondary to LDVF.

ischemia; optical mapping; inexcitability

VENTRICULAR FIBRILLATION (VF) is a major cause of sudden cardiac death. The spatiotemporal organization of VF evolves as global ischemia progresses and alters electrophysiological properties of the myocardium. Concurrent with the metabolic and electrophysiological changes, the chance of successful defibrillation and resuscitation diminishes with every minute of VF, approaching zero at ~10 min after the onset of VF (31). Unfortunately, the delayed response time of emergency medical services often approaches the time when successful resuscitation is unlikely. This perhaps explains the fact that the overall survival of victims of out-of-hospital cardiac arrest is a dismal 5% (14). The mechanisms determining successful defibrillation and survival under these conditions remain poorly understood but may be related to the nature of the sources maintaining VF (reentrant or focal) and electrical depression caused by ischemia, culminating in a complete loss of electrical response (asystole). The evolution of the organization of VF lasting 10–20 min in the globally ischemic heart [termed long-duration VF (LDVF)] has been the focus of several recent studies (2, 5, 8, 15, 19, 20, 27, 34, 42). These studies revealed large gradients in the VF activation rate (VFR) between the left ventricular (LV) endocardium (Endo) and LV epicardium (Epi) in the dog and the rabbit but not in the pig. In the rabbit heart, a transmural VFR gradient is present only in the LV but not in the right ventricle (RV) (42). Based on principal differences in the organization of Purkinje fibers in these species (exclusively Endo in the dog and rabbit vs. transmural in the porcine heart), as well as analysis of the directionality of the transmural wave propagation in the dog and pig, the differences in the organization of LDVF between the dog and pig were interpreted in terms of the leading role of focal activity (e.g., abnormal automaticity) arising from Purkinje fibers in maintaining advanced stages of LDVF (2, 8, 34). The idea of focal sources driving VF is a significant shift of the current paradigm of VF based on the notion of reentry in the form of spiral waves and may have important implications for defibrillation and resuscitation during LDVF. Recently, an elegant study (19) using a transmural multilevel optrode in the LV showed that the gradient in VFR is mostly determined by the gradient in the diastolic interval (DI), whereas the action potential (AP) duration (APD) remains conserved across the LV wall as the LDVF evolves. This can be interpreted as evidence that a gradient of excitability and/or postrepolarization refractoriness occurs across the LV wall, which enables Endo to support more rapid activations during LDVF. The presence of such a gradient may be due to the transmural distribution of ionic channel properties unrelated to but coincidental with the distribution of Purkinje fibers. Thus, the question arises as to whether the sites of the fastest activation at advanced stages of LDVF are universally associated with Endo, where Purkinje fibers are localized in the canine heart.

In that regard, it is important to note that in addition to the transmural VFR gradient, optical mapping studies (4, 42) in the rabbit heart have revealed a large Epi VFR gradient between the RV (faster activation) and LV during LDVF. However, little is known about right-to-left gradients during LDVF in large mammalian hearts, in particular in the canine heart, which is considered to be the closest to the human heart in terms of the dynamics of LDVF (2). The purpose of this study was to provide a comprehensive description of both transmural and lateral [RV to septum (Sep) to LV] electrophysiological gradients during LDVF in the canine heart during the first 10 min of LDVF using information from both transmural needle electrodes and high-resolution Epi optical mapping. From optical data, we analyzed the distribution of APD, DI, and sustained sources of activation in the RV and LV during

* P. W. Venable and T. G. Taylor contributed equally to this work.

Address for reprint requests and other correspondence: A. V. Zaitsev, Cardiovascular Research and Training Institute, Univ. of Utah, 95 S. 2000 E., Salt Lake City, UT 84112-5000 (e-mail: zaitsev@cvrti.utah.edu).

  

LDVF. Our results revealed an unprecedented complexity of electrophysiological gradients emerging during LDVF, with large heterogeneities both between chambers as well as locally within each chamber. Importantly, the magnitudes of interchamber and intrachamber VFR gradients were comparable to the magnitude of the transmural gradient, with Epi sites at the RV-Sep junction being activated as fast as LV Endo. We also found that Epi right-to-left VFR gradients were determined by the gradients in DI amid relatively constant APD, which is similar to the pattern observed transmurally across the LV wall (19). We concluded that VFR gradients during LDVF in the canine heart cannot be fully explained by special properties of Purkinje fibers but may be universally determined by nonuniform electrical depression reflected in the prolongation of postrepolarization refractoriness and eventual loss of excitability. We propose possible factors contributing to the highly nonuniform response of the canine heart to the stress imposed by LDVF and global ischemia.

## METHODS

This investigation conformed with the National Institutes of Health *Guide for the Care and Use of Laboratory Animals* (NIH Pub. No. 85-23, Revised 1996). The animal protocols were approved by the Institutional Animal Care and Use Committee of the University of Utah. A total of 19 dogs were used in this study (5 dogs for the multielectrode mapping of LDVF in situ, 10 dogs for the optical mapping of LDVF in isolated hearts, and 4 dogs for the assessment of regional differences in refractoriness during global ischemia in isolated hearts).

*Experiments in situ.* Five dogs of either sex (30.8 ± 10.5 kg) were anesthetized with acepromazine (0.1 ml/10 kg) and pentobarbital sodium (32.5 mg/kg). Anesthesia was maintained through intravenous injections of pentobarbital sodium. Intubation was accomplished with a cuffed endotracheal tube, and mechanical ventilation was maintained at 10–15 cycles/min (tidal volume: 15–20 ml/kg). The heart was exposed via a midline sternotomy. The chest opening was covered with polyethylene film, and warm, humidified air was blown into the chest to maintain temperature at the surface of the heart between 35 and 37°C during LDVF. Lead I ECG was recorded continuously throughout the experiment. Blood gases, pH, electrolyte concentrations, and glucose were analyzed in arterial blood samples before the onset of VF. Plunge needle electrodes with 10 evenly spaced unipolar leads were manufactured in house following the design developed by Rogers et al. (30). Electrodes in the LV had an interlead distance of 1.6 mm, and those in the RV and Sep had an interlead distance of 1.2 mm. Three needle electrodes were inserted in the anterior RV, one in the Sep, and three in the anterior LV, as shown schematically in Fig. 1*A*. The distance between needles was 10–15 mm. Needles were placed along a transverse plane bisecting the heart approximately at half-distance between the apex and base. The Sep needle was placed just to the right of the left anterior descending coronary artery (LAD). VF was induced by a brief (~1 s) application of current from a 9-V battery to the RV outflow tract. Unipolar electrograms from all contacts of the needle electrodes were recorded continuously during the first 10 min of VF at a sampling rate of 1 kHz using a custom-made multichannel data-acquisition system, as previously described (35).

*Electrode data analysis.* Unipolar electrograms were analyzed using custom software developed in a Matlab framework. Activations were chosen as the maximum negative derivatives that exceeded a minimum of 3 V/s within a 20-ms search window, which is similar to previously described approaches (8, 9). VFR was calculated as the average number of activations per second over 10-s intervals taken at 10 s after VF induction and at *minutes 1-9* of LDVF. For simplicity, the first time point is referred to as *minute 0* of LDVF.

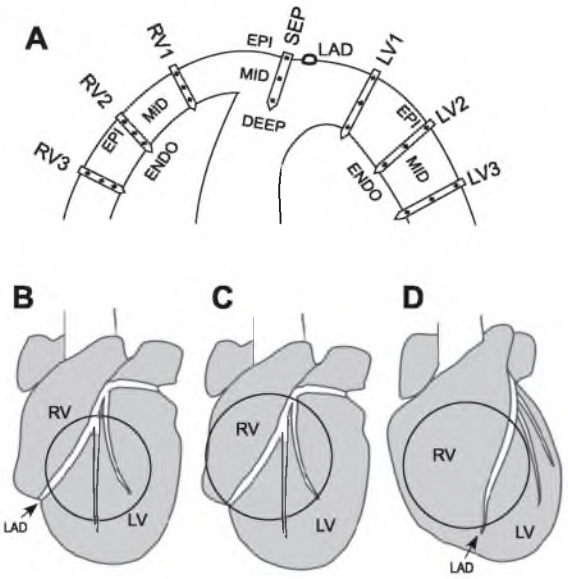


Fig. 1. Schematic representation of the mapping modalities used in this study. *A*: approximate positions of the plunge needle electrodes. RV1, RV2, and RV3 indicate electrodes in the right ventricle (RV). LV1, LV2, and LV3 indicate electrodes in the left ventricle (LV). The electrode in the anterior projection of the interventricular septum (Sep) is also shown. All electrodes were in the transverse plane located at approximately middistance between the base and apex. The epicardial (Epi) and midmyocardial (Mid) leads in the plunge needle electrodes are indicated, as is the endocardial (Endo) lead in the RV and LV electrodes. Deep indicates the lead in the Sep electrode that is the most distant electrode from Epi and is located in the depth of Sep. See text for more detail. *B–D*: three positions of the imaged area (circles) used in the optical mapping experiments. *B*: the imaged area mostly covers the LV with a narrow region of the RV. *C*: the imaged area covers approximately equal portions of the RV and LV. *D*: the imaged area mostly covers the RV with a narrow region of the LV. LAD, left anterior descending coronary artery.

Whereas the length of the RV and LV needles was constant and designed to span the largest thickness observed in the respective chambers of the canine heart, the actual thickness of the ventricular wall is highly nonuniform, especially in the RV. Thus, in some cases, plunge needle electrodes were longer than the wall thickness at the site of insertion. The contacts outside the ventricular wall were excluded from analysis based on the following criteria: *1*) low VFR at 0 min of LDVF (slower by 5 Hz or more compared with the average VFR measured in all locations), *2*) decrease of VFR to below 2 Hz within the first minute of LDVF, and *3*) observation of a progressively decreasing electrogram amplitude toward more distal leads while maintaining the same morphology as more proximal leads in the same needle. In the latter case, the most proximal lead from the group of leads with identical morphology was designated as the Endo location in the needle. This approach could potentially falsely reject some of the true Endo leads in the RV and LV and thus underestimate the magnitude of the Endo-to-Epi difference in VFR, which, however, would not affect the main conclusions of this study (this issue is further discussed in *Limitations*). The position of the Epi lead could be easily ensured by visual inspection. After determination of the most distal lead in contact with the myocardial wall (Endo), the midmyocardial (Mid) lead was chosen as the one closest to being equidistant between Epi and Endo. Note that, unlike in RV or LV needles, the most distal recording site in the Sep needle was always in the depth of

the Sep (see Supplemental Material, Supplemental Fig. 1).[1] Accordingly, in the Sep needle, we identified the Epi, Mid, and Deep sites for the purposes of analysis and comparison with RV and LV locations. At later stages of LDVF, some electrograms appeared to lack any local activation. However, due to a far-field signal always being present in unipolar electrograms, it was sometimes difficult to ascertain a clear-cut case of complete loss of excitability. Therefore, local inexcitabilty was defined in unipolar electrograms when VFR fell below 0.5 Hz, whereas at least some other leads in the same experiment exhibited fibrillatory activity with VFR $>$ 4 Hz.

*Experiments in isolated hearts.* Hearts were obtained from dogs of either sex ($n$ = 14, 27.5 ± 2.7 kg) after premedication, anesthesia, and surgery performed as described above. After isolation via a midline sternotomy, the heart was perfused in a Langendorff apparatus with a mixture of blood and Tyrode solution as described in detail in our previous publications (16, 43). Briefly, the blood-Tyrode mixture was oxygenated (5% $CO_2$-95% $O_2$), heated (37°C), and filtered using standard pediatric heart perfusion units from various vendors. The whole mixture was collected for recirculation with collector tubes inserted into the RV and LV via cuts in the appendages of the respective atria. The heart was then placed in a temperature-controlled bath with heated water-jacketed transparent glass walls. The bath was filled with warmed Tyrode solution, which was continuously pumped, without recirculation, at a rate 80–150 ml/min. The $O_2$ content in the superfusate was removed by continuous gassing with a 95% $N_2$-5% $CO_2$ mixture. Temperatures in the LV cavity, superfusate, and water jacket were maintained at 37 ± 0.5°C during both normal coronary perfusion and ischemia. The gradient of temperature across the LV wall did not exceeded 1°C. Ten hearts were used for the optical mapping of LDVF. In four additional hearts, we performed programmed stimulation during global ischemia to access regional differences in refractoriness (see Supplemental Figs. 6–8).

*Optical recordings.* Optical mapping of activation during VF was performed using an electron-multiplied charge-coupled device camera (iXon DU-860D, Andor Technology, Belfast, UK) with a 6- or 12-mm objective lens (Computar, Commack, NY) at a resolution of 64 × 64 pixels and frame interval of 2 ms. Excitation light came from a 532-nm green solid-state laser (Coherent, Santa Clara, CA), and the fluorescent signal was filtered with a 640 ± 50-nm filter (Omega Optical, Brattleboro, VT). The voltage-sensitive dye di-4-ANEPPS (Molecular Probes, Carlsbad, CA) was delivered to the heart as a bolus via an injection into the aortic cannula. The field of view covered portions of Epi of the anterior RV, Sep, and LV. Even though the sites immediately adjacent to the LAD most certainly overlay the Epi projection of the Sep, the exact boundaries between the Sep and RV and LV free walls could not be reliably determined for the purposes of optical mapping. Therefore, in optical maps, we followed previously used approaches (4, 32, 42) and defined the area to the right of the LAD as the RV and the area to the left of the LAD as the LV (Fig. 1*B*). The size of the field of view varied between 40 × 40 and 65 × 65 mm. Due to the relatively large size of the dog heart and curvature of the ventricular wall, it was not possible to have large portions of both ventricles simultaneously in the field of view. Therefore, optical mapping experiments were divided into three subgroups. In the first group ($n$ = 4), the field of view predominantly covered the LV with a rim of the RV ~15 mm wide. In the second group ($n$ = 3), the areas to the right and left of the LAD were approximately equal. In the third group ($n$ = 3), the field of view predominantly covered the RV with a rim of the LV ~15 mm wide. The approximation of the respective fields of view is schematically shown in Fig. 1*B*. To minimize motion artifacts, the heart was gently pressed against the glass chamber wall as previously described (16, 43). No electromechanical uncouplers were used.

The heart was perfused with blood before the onset of LDVF; however, immediately before the induction of ischemia, the perfusion was switched to Tyrode solution with the dual purpose of ensuring constant composition of the extracellular milieu at the onset of LDVF and enhancing the voltage-sensitive signal for the purpose of better resolving low-amplitude signals at advanced stages of LDVF. VF was induced using a 9-V direct current battery 10 s to 5 min before the onset of global ischemia initiated by interruption of aortic perfusion. No perceptible differences in the measured parameters were found between experiments depending on the duration of VF before the onset of ischemia; therefore, in all experiments, the time of LDVF was counted from the moment when perfusion was stopped. LDVF was maintained for 10 min; 4–6-s-long movies were acquired every 30 s. After the last LDVF movie, the perfusion pump was restarted, and additional movies were acquired every minute during 5 min of reperfusion.

*Analysis of optical signals.* Spatial distributions of VFR, APD, and DI at different time points during LDVF were estimated in optical mapping data using custom routines developed in PV-Wave software (Visual Numerics, Boulder, CO). The dominant frequency of the Fourier spectrum was not used to estimate VFR because it did not reliably represent the perceived number of activations per unit of time at advanced stages of LDVF, when the AP is characterized by very short APD and long DI. Instead, we used an algorithm to detect individual APs in single-pixel recordings, similar to that described in our previous publication (16). In brief, the depolarization and repolarization phases of each optical AP were detected. The time points at which the depolarization and repolarization phases crossed a line drawn at the 40% level of the absolute maximum in the respective signal ($\Delta F_{max}$) were determined. From these time points, APD, DI, and VF cycle length (VFCL) could be calculated for each cycle. The algorithm rejected noise based on thresholds set for APD ($<$10 ms), VFCL ($<$30 ms), absolute AP amplitude ($<$15 levels of brightness), and percent AP amplitude with respect to the time sequence maximum ($<$5% of $\Delta F_{max}$). VFR maps were created by dividing the number of APs by duration of the analyzed movie. Areas with no APs detected throughout the entire movie were considered to be inexcitable and having a VFR = 0. Such areas were counted for the purposes of determining the average VFR but were excluded from the calculation of average APD and DI. Singularity points were identified in Hilbert-transformed movies of voltage-sensitive fluorescence as points where all AP phases converged, as previously described (13, 39). Rotors were defined as singularity points that lasted for more than one cycle of rotation. The maximal lifespan and maximal number of rotations of rotors were computed for the RV and LV at 0 and 6 min of LDVF.

*Statistical analysis.* Within the data collected from the plunge needle electrodes, the time course of VFR was statistically compared in a 3 × 3 grid of principal locations (RV Epi, RV Mid, RV Endo, Sep Epi, Sep Mid, Sep Deep, LV Epi, LV Mid, and LV Endo; see Fig. 1A). In each experiment, the RV and LV were represented by average values from all three electrodes in the respective chambers. Two-way ANOVA was performed with a post hoc Bonferroni test to make all 36 pairwise comparisons of the VFR time course between the 9 locations (see Supplemental Table 1). Note that the statistical significance indicated the differences between the means at all time points of LDVF in different locations. No conclusions regarding differences at individual time points were possible due to the prohibitively large number of required pairwise comparisons.

In the data collected from optical recordings, average values of VFR, APD, and DI were calculated for areas to the right (RV) and left (LV) of the LAD. Despite differences in the distribution of the field of view between the RV and LV in different experiments, the average values for the two areas were similar; therefore, data from all optical mapping experiments were combined into respective regions. Two-way ANOVA was performed with a post hoc Bonferroni test to compare the time course of VFR, APD, and DI during LDVF between the RV and LV. Similar to the statistical treatment of the electrode

[1] Supplemental Material for this article is available online at the *American Journal of Physiology-Heart and Circulatory Physiology* website.

data, the statistical significance indicated the differences between the mean values of measured parameters at all time points of LDVF. A linear regression analysis was performed to correlate the mean APD versus the mean VFCL and the mean DI versus the mean VFCL throughout all time points analyzed during LDVF. Data are expressed as means ± SE. Differences at $P < 0.05$ were considered statistically significant.

## RESULTS

*Multielectrode mapping in situ.* Representative examples of unipolar electrograms obtained from plunge needle electrodes inserted into the RV, Sep, and LV are shown in Fig. 2. At 0 min of LDVF, VFR was relatively uniform among all locations and all layers. At 10 min of LDVF, a prominent Endo-to-Epi gradient in VFR was typically observed in both LV and RV free walls (Endo faster), whereas in the Sep, the fastest VFR was observed in Epi or Mid locations with slower VFR in the Sep Deep. After 3 min of LDVF, the sites of the fastest VFR in the RV occurred in Endo in four of five (80%) experiments; in one experiment, VFR was uniform across the RV wall. In the LV, the fastest sites were in Endo in three of five (60%) of experiments; in the other two experiments, Endo and Mid had similar VFRs, with both being faster than Epi VFR. In the Sep, the fastest sites were in Epi and/or Mid in 100% of the experiments, with Sep Deep locations being consistently slower than Sep Mid locations. In many cases, we observed what appeared to be a complete lack of activation in some electrograms. Such events occurred starting from ~4 min of LDVF and were often local, so that adjacent needles or different contacts in the same needle still reflected some activation. Using our criterion for inexcitability (see METHODS), local inexcitability was most frequently observed in LV Epi and RV Epi (100% and 60% of experiments, respectively). Much less frequent were cases of inexcitability in LV Endo, RV Endo, RV Mid, LV Mid, and Sep Deep locations (20% of experiments in each case). Finally, inexcitability was never observed in Sep Epi and Sep Mid.

Figure 3 shows the average time course of VFR during the first 9 min of LDVF in the nine ventricular locations shown in Fig. 1*A* (RV Epi, RV Mid, RV Endo, Sep Epi, Sep Mid, Sep Deep, LV Epi, LV Mid, and LV Endo). Data for individual experiments are shown in Supplemental Fig. 2. In both Fig 3 and Supplemental Fig. 2, the wall types are distinguished by different colors (LV, red; Sep, green; and RV, blue) and the distance from the Epi surface is indicated by different symbols (Epi, circle; Mid, square; Endo, triangle; and Sep Deep, ×). Note that in Fig. 3 the VFR curves are presented redundantly in *A–C* and *D–F*. Figure 3, *A–C*, groups the curves by wall type and thus facilitates a visual analysis of transmural gradients. Figure 3, *D–F*, on the other hand, groups the same curves by depth and thus highlights the lateral gradients (between the LV, Sep, and RV) at each depth.

Figure 3*A* shows the time course of VFR during LDVF at three transmural levels in the LV. Consistent with previous results, the difference between Endo, Mid, and Epi progressively increased over time of LDVF, with LV Endo being consistently the fastest location. Note, however, that the largest gradient occurred in the outer half of the LV wall, between Mid and Epi. Accordingly, the time course of VFR was significantly different ($P < 0.05$) between Endo and Epi and between Mid and Epi but not between Endo and Mid.

Figure 3*B* shows the time course of VFR at three transmural levels in the Sep. It is important to note that the Sep Deep location was at approximately the same distance from Epi as RV Endo but at least 4–5 mm away from any Endo surface (see Fig. 1*A*). Within the Sep, Epi and Mid VFR curves stayed very close together throughout the first 9 min of LDVF. After 3 min of LDVF, VFR in Sep Epi and Sep Mid stabilized at ~7 Hz, whereas VFR in Sep Deep continued to fall, leading to a progressive separation of the Sep Deep curve from both Sep Epi and Sep Mid. This separation, however, did not reach statistical significance due to the relatively large variation between individual experiments (see Supplemental Fig. 2).

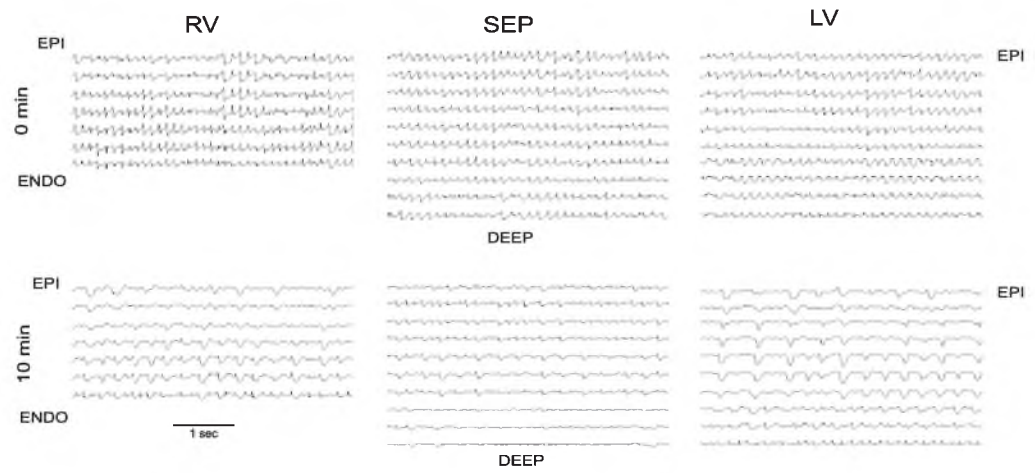


Fig. 2. Unipolar electrograms recorded from different leads of plunge needle electrodes during long-duration ventricular fibrillation (LDVF) in a representative experiment. *Top*: 0 min of LDVF; *bottom*: 10 min of LDVF. Shown are recordings from the RV3 (*left*), Sep (*middle*), and LV3 (*right*) electrodes. See Fig. 1*A* for electrode locations and other definitions.

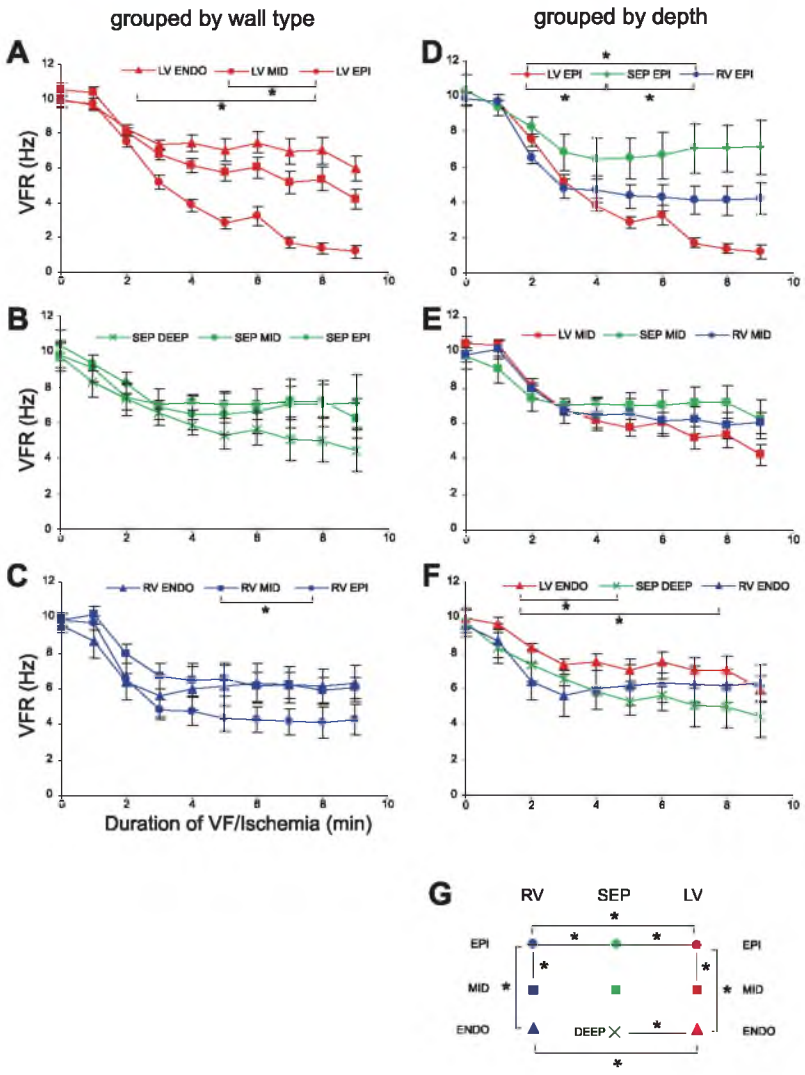


Fig. 3. Time course of VF activation rate (VFR) in a matrix of 3 × 3 of nine principal locations (LV Endo, LV Mid, LV Epi, Sep Deep, Sep Mid, Sep Epi, RV Endo, RV Mid, and RV Epi) during 0–9 min of LDVF. Colors indicate different wall types (LV, red; Sep, green; RV, blue). Symbols indicate different distances from Epi (Endo, triangles; Mid, squares; Epi, circles; Sep Deep, ×). *A–C*: the nine VFR curves grouped by wall type (LV, Sep, and RV, respectively). *D–F*: the same nine VFR curves grouped by distance from Epi (Epi, Mid, and Endo/Deep, respectively). *Statistically significant difference between the VFR curves by two-way ANOVA. *G*: summary of statistically significant differences in VFR time courses between different locations.

Figure 3*C* shows the time course of VFR at three transmural levels in the RV. RV Mid was faster than RV Epi throughout the entire course of LDVF, with the difference being statistically significant ($P < 0.05$). However, there were no significant differences between RV Endo and RV Mid. Thus, the transmural VFR gradient in RV was present mostly between Mid and Epi layers. Note that VFR in all RV layers reached a plateau after 3–4 min of LDVF, similar to Sep Epi and Sep Mid, but dissimilar to all LV layers and Sep Deep.

Figure 3, *D–F*, shows the same data as Fig. 3, *A–C*, but grouped by the distance from Epi. Figure 3*D* shows the VFR time course in the Epi layer of the LV, Sep, and RV. In all Epi locations, there was an initial decrease in VFR up to 3 min of LDVF, which was slightly faster in LV Epi and RV Epi than in Sep Epi. After that, however, VFR in RV Epi and Sep Epi stabilized (albeit at different levels), whereas VFR in LV Epi continued to fall. As a result, VFR was significantly different between all pairs of Epi locations ($P < 0.05$), with Sep Epi being the fastest, RV Epi intermediate, and LV Epi slowest.

Figure 3*E* shows the VFR time course in the Mid layers of the LV, Sep, and RV. There was very little difference in the VFR time course between these locations during the first 3 min of LDVF. After that, the curves slightly diverged, with Sep Mid being the fastest, LV Mid slowest, and RV Mid in between. In a way, this pattern repeats the divergence observed in Epi locations (see Fig. 3*D*) but at a much lower scale. As a result, there were no statistical differences between VFR time courses in all Mid locations.

Finally, Fig. 3*F* shows the VFR time course in Endo layers of the LV and RV and the Deep layer in the Sep. The LV Endo location was consistently faster than both RV Endo and Sep Deep, although LV Endo and RV Endo converged by 9 min of LDVF.

The differences between LV Endo and RV Endo and between LV Endo and Sep Deep were statistically significant ($P < 0.05$). Figure 3*G* diagrammatically shows the VFR gradients in the directions tangential and perpendicular to the anterior ventricular wall. The results of all pairwise comparisons between the nine measured locations are shown in Supplemental Table 1.

The data presented above can be summarized as follows: *1*) VFR is uniform over all locations at the onset of LDVF; *2*) during LDVF, there are significant right-to-left gradients in Epi and Endo but not in Mid; *3*) the largest transmural gradients in both the LV and RV develop between Mid and Epi, whereas the gradient between Endo and Mid is modest in the LV and practically nonexistent in the RV; and *4*) overall, LV Epi exhibits the largest and Sep Epi the smallest decline in VFR during LDVF, so that the largest overall difference in VFR during LDVF was observed between Sep Epi and LV Epi. Figure 4 further highlights the special role of the Sep in the pattern of activation during LDVF, showing that in all experiments the highest Epi VFR was observed either in Sep Epi or the adjacent RV Epi location (electrode RV1). Finally, it is worth noting that throughout the entire length of LDVF studied, the VFR time course was very similar in LV Endo, Sep Mid, and Sep Epi (see Supplemental Fig. 3). Since Sep Epi and Sep Mid do not have Purkinje fibers and are not adjacent to LV Endo in canine hearts, these data indicate that Purkinje fiber distribution and function may not be the main determinants of the VFR time course during LDVF.

*Optical mapping in isolated hearts.* The purpose of optical mapping experiments was to analyze the right-to-left and intrachamber gradients in VFR, APD, and DI during LDVF with high spatial resolution. Typical examples of VFR distribution maps and individual optical recordings during LDVF are shown in Fig. 5. In the experiment shown in Fig. 5*A*, the field of view predominantly covered the LV and a small portion of RV. At the onset of LDVF, the VFR distribution was relatively uniform, and there were no large-scale differences between the LV and RV. At 8 min of LDVF, the VFR distribution was markedly heterogeneous, with the fastest domain (~4.5 Hz, green) situated in the RV and LV adjacent to the LAD. The largest part of the LV was activated at a VFR of ~3 Hz (blue). Importantly, there was an area in the LV with an extremely low activation rate (<1 Hz, dark purple). The single-pixel recordings (Fig. 5*A*, *sites a*--*c*) were selected in such a way as to represent the three major frequency domains in the LV observed at 8 min of LDVF. At the onset of LDVF, the activation rate was similar between the three locations. However, at 8 min of LDVF, *site a* was the fastest, *site c* was intermediate, and in *site b* there was a single large-amplitude AP followed by a few small deflections, which are most likely due to electrotonus from the adjacent *site c*. Based on selected threshold criteria (see METHODS), our algorithm picked only the first (large) AP during the 4-s recording in *site b* compared with many more in *sites a* and *c* (asterisks in Fig. 6*A*). Note that *site c*, which exhibited a rhythmic series of suprathreshold APs,

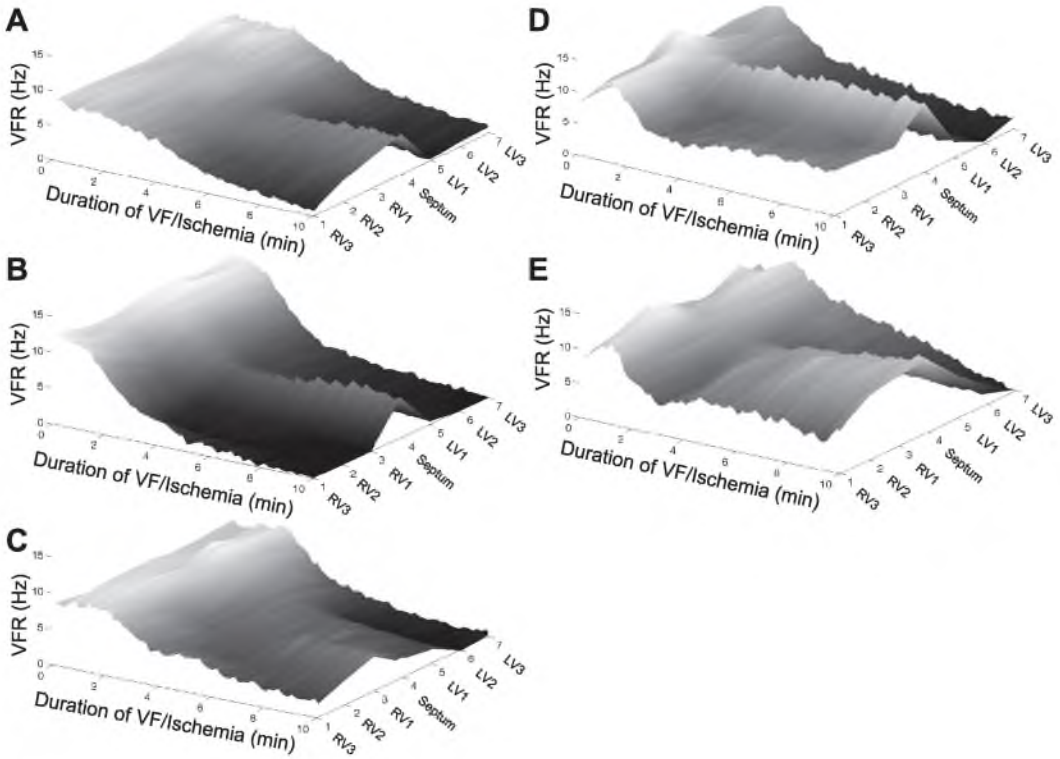


Fig. 4. Epicardial distribution of VFR during LDVF in five experiments in situ (*A*–*E*). Lighter shades of grey indicate higher VFR. Note that in all experiments there is a local maximum in Epi VFR distribution either in the Sep or adjacent RV position (RV1) after 3–4 min of LDVF.

was only ~2 mm away from *site b*, which was barely excitable. *Site b* became completely silent by 10 min of LDVF, whereas the RV-Sep portion and rightmost part of the LV were still excitable (not shown).

In the experiment shown in Fig. 5*B*, the field of view predominantly covered the RV and a small portion of LV. Similar to the preceding example, at the onset of LDVF, the VFR distribution was relatively uniform, and there were no large-scale differences between the LV and RV. At 10 min of LDVF, however, the VFR distribution was extremely heterogeneous. The highest VFR was observed in an apical part of RV (~6 Hz, green). There were also two active areas in the more basal portions of the RV (~3 Hz, blue), whereas the rest of the RV and the visible region of the LV had a VFR below 1 Hz (dark purple) or were completely inexcitable (black). Individual recordings from *sites a–c* showed similar fast activations at the onset of LDVF and striking differences at 10 min of LDVF. Specifically, *site a* exhibited fast and highly periodic activity, *site b* was completely silent, and *site c* was also highly periodic but was activated at half the rate of *site a*. Waves originating in the 6-Hz domain (green) did not propagate into the 3-Hz domain (blue) within the field of view. In fact, these two domains were separated by a thin inexcitable area (indicated by a white arrow in Fig. 6*B*) such that the waves from both domains converged and stopped at this area (not shown). Yet, *sites a* and *c* were phase locked in a 2:1 pattern, as shown in Fig. 5*C*. Indeed, activation in *site c* followed every other activation in *site a* with a fixed time delay. Thus, unless this is a perfect coincidence, which is highly unlikely, *site c* is electrically connected to *site a*, perhaps via an intramural excitable pathway.

A highly heterogeneous VFR distribution with patches of inexcitable areas in the RV and LV, as shown in Fig. 5, was typical for advanced stages of LDVF (after 4–5 min of no perfusion). The transitions between high and low VFR could be very sharp, with local VFR gradients reaching 4–5 Hz/mm (not shown). A common feature of VFR maps was the presence of the highest VFR in the RV localized near the LAD. Examples of heterogeneous VFR maps from each optical mapping experiment are shown in Supplemental Fig. 4. Consistent with the presence of areas with VFR = 0 in VFR maps, activation maps showed areas of no activation at advanced stages of LDVF (see examples in Supplemental Fig. 5*D*).

Figure 6 shows a quantitative analysis of the differences between the RV and LV that emerged during LDVF. Figure 6*A* shows that the average VFR was consistently higher in the RV than in the LV throughout 10 min of LDVF, with the exception of 0 min of LDVF. Figure 6*B* shows that average DI was longer in the LV than in the RV. Figure 6*C* shows that average APD was slightly shorter in the LV than in the RV between 2 and 8 min of LDVF. Note that whereas DI increased quickly during LDVF in both the LV and RV, APD changed little with time of LDVF in both chambers. Finally, Fig. 6*D* shows percentages of excitable areas in the LV and RV maps as a function of LDVF duration. Note that after 3 min of LDVF, the

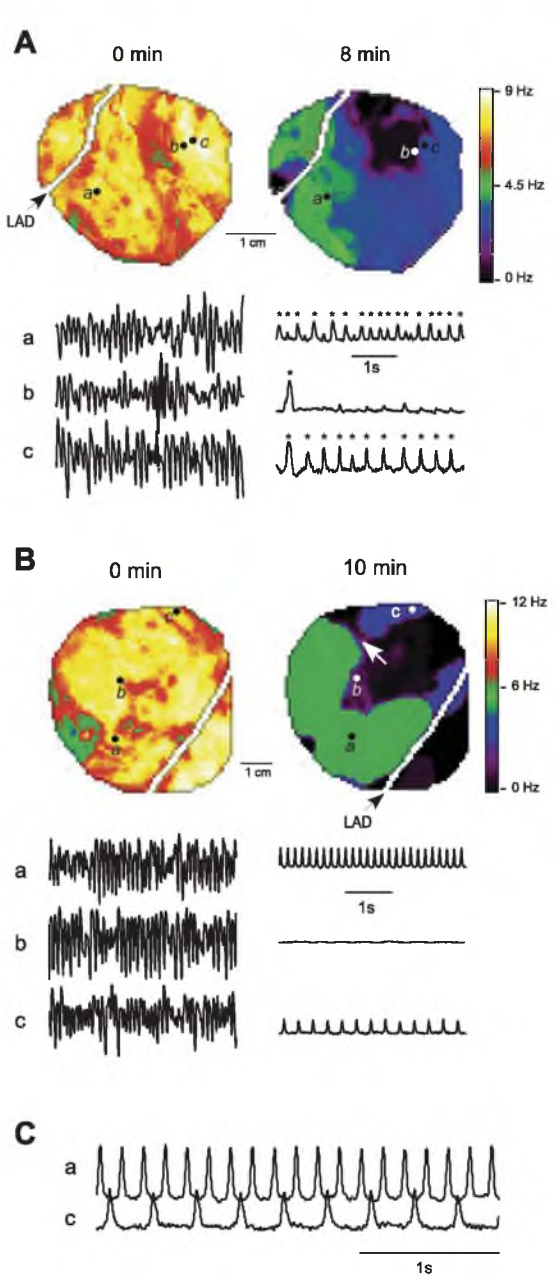


Fig. 5. Examples of VFR distribution measured in Epi optical maps in isolated hearts at the early and late stages of LDVF. *A*: experiment with predominantly LV optical mapping. *Top*, VFR maps at 0 min (*right*) and 8 min (*left*) of LDVF. *Bottom*, single-pixel recordings from *sites a–c* (indicated on the respective VFR maps with circles). *B*: experiment with predominantly RV optical mapping. *Top*, VFR maps at 0 min (*right*) and 10 min (*left*) of LDVF. The arrow in the 10-min map indicates a thin inexcitable area (black, VFR = 0) separating two active areas (green, VFR ~ 6 Hz; blue, VFR ~ 3 Hz). *Bottom*, the same layout as in *A*. *C*: single-pixel recordings of *sites a* and *c* from *B* shown with an expanded time scale. Note the fixed 2:1 phase relationship between activations in these two locations, suggesting that *sites a* and *c* have a common source of excitation even though they do not communicate within the imaged area. Note the extremely high level of VFR heterogeneity in both the RV and LV at the advanced stages of LDVF.

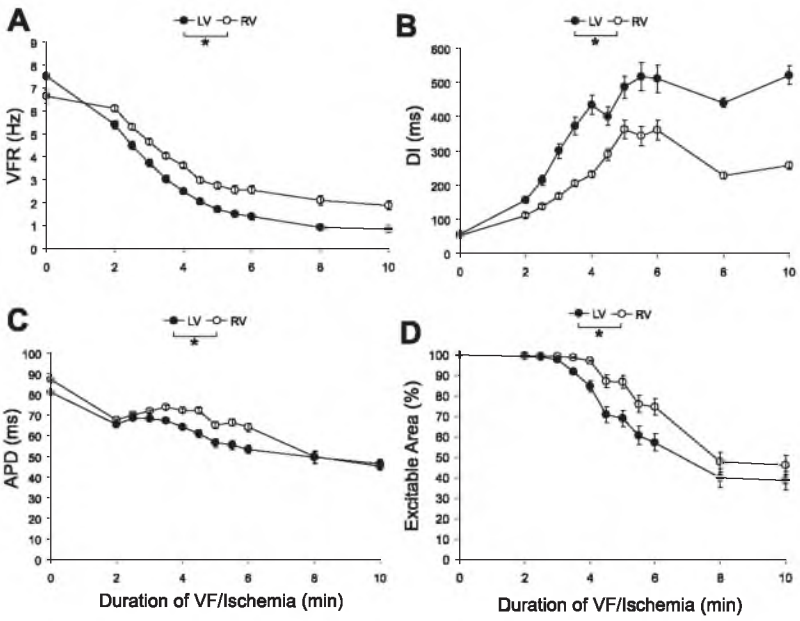


Fig. 6. Right-to-left differences in the time courses of VFR (*A*), diastolic interval (DI; *B*), action potential duration (APD; *C*), and percentage of excitable area (*D*) in Epi optical maps during LDVF. *Statistically significant difference between respective curves by two-way ANOVA.

percentage of the excitable area in the LV progressively decreased, followed by a similar decrease in the RV after an ~1-min delay. The differences between the time courses of all measured parameters in the RV versus LV were statistically significant using two-way ANOVA ($P < 0.05$).

Figure 7 shows that average VFCL (inverse of VFR) was strongly correlated with the duration of average DI in both chambers at all time points during LDVF. In contrast, VFCL was only weakly inversely correlated with the average APD. Thus, VFCL was not determined by APD dispersion but rather by dispersion in DI, which reflects the degree of postrepolarization refractoriness. It should also be noted that no functional relationship could be found between APD and the preceding DI at any stage of LDVF (not shown), which is consistent with previous reports (16, 19).

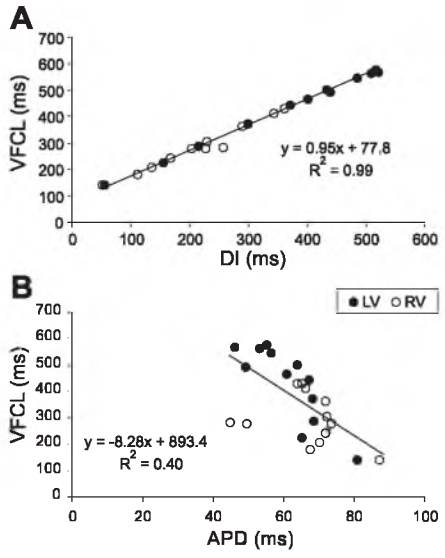


Fig. 7. *A* and *B*: scatterplots of VF cycle length (VFCL) measured in the RV and LV at all time points of LDVF versus DI (*A*) and APD (*B*). There was a strong direct correlation between VFCL and DI (*A*) and a weak inverse correlation between VFCL and APD (*B*).

*Stability of reentry and breakthrough patterns in optical maps.* Epi optical maps revealed multiple wavelets/short-living rotors in both chambers until relatively late stages of LDVF (~5–6 min). During this period of time, Epi activation maps were extremely complex and fragmented with only rare occasions of complete reentrant patterns (see Supplemental Fig. 5). At 0 min of LDVF, the maximum duration and number of rotations of reentrant circuits were larger in the RV than in the LV (see Table 1). At 6 min of LDVF, the maximum number of rotations in the RV was not different from that at 0 min LDVF, whereas the maximum lifespan was longer, consistent with prolonged VFCL at this later stage of LDVF. No reentry was observed in the LV at 6 min of LDVF. In 7 of 10 experiments,

Table 1. *Maximal lifespan of repetitive reentrant patterns in epicardial optical maps*

| | Maximum Lifespan, ms | Maximum Number of Rotations |
|---|---|---|
| Right ventricle | | |
| 0 min of LDVF | 504 ± 188 | 4.3 ± 1.2 |
| 6 min of LDVF | 906 ± 278* | 4.7 ± 1.5 |
| Left ventricle | | |
| 0 min of LDVF | 166.6 ± 3.0* | 1.7 ± 0.6* |
| 6 min of LDVF | No reentry | No reentry |

Values are means ± SE. LDVF, long-duration ventricular fibrillation. *$P <$ 0.05 vs. the right ventricle at 0 min of LDVF.

repetitive breakthrough patterns were observed in the RV close to the LAD at least in one of the movies recorded after 4 min of LDVF (see Fig. 8*D*). The breakthrough patterns appeared in approximately the same location in at least 50% of activations recorded in the same movie, and transitions from a breakthrough to a reentrant pattern and vice versa in the same location were observed. Repetitive breakthrough patterns were not present in the RV at 0 min of LDVF and were not present in the LV throughout the entire duration of LDVF.

An example of transitions between focal and reentrant pattern in the same location at a late stage of LDVF are shown in Fig. 8, *A–C*. Figure 8*A*,*1* shows a snapshot of a phase movie taken at 8 min of LDVF, which revealed a total of seven coexisting singularity points in the mapped area. The white arrowhead indicates the rotor, which was sustained for about seven rotations and was the dominant source in the area. The rotor was replaced by a breakthrough pattern in the same location (black arrows in Fig. 8*A*,*2*) which lasted for another 9–10 cycles. The breakthrough pattern then reverted back to reentry (white arrow in Fig. 8*A*,*3*). Figure 8*B* shows an activation map computed for the movie taken at 10 min of LDVF. On this map, the colors from red to magenta show a progression of wavefronts emanated by a stable and highly periodic focal source in the RV (black arrows in Fig. 9*B*). The focal source was situated approximately in the same site as the focal/reentrant source observed 2 min earlier and shown in Fig. 8*A*. The waves emitted by the RV source failed to cross the LAD and activate the LV. However, a portion of the LV was activated, at a much slower rate, by a repetitive planar wave (white arrow in Fig. 9*B*), which was apparently unrelated to the fast source in the RV.

Figure 8*C* shows a unique case of stable Epi reentry observed in the same experiment at 16 min of LDVF (and hence beyond the standard duration of LDVF analyzed in this study). The reentrant circuit was located in the basal RV not far from the LAD (counterclockwise arrow in Fig. 8*C*) and was sus-

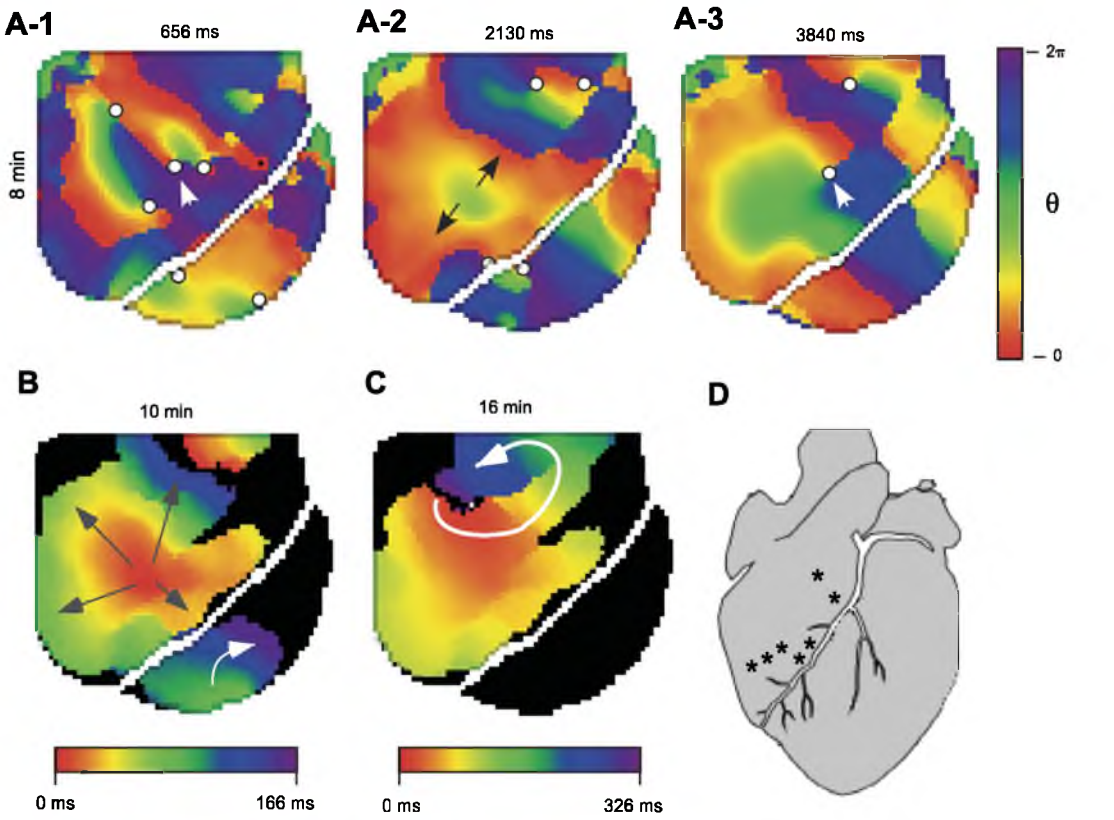


Fig. 8. Examples of transitions between the focal and reentrant pattern in the RV at the late stages of LDVF. *A*: individual frames of a phase movie at 8 min of LDVF. In *1*, several singularity points coexist in the mapped area; the point indicated by the white arrow is the leading source of activation in the mapped area for at least seven cycles. In *2*, the reentrant source is replaced by a repetitive focal source in approximately the same location (black arrows). In *3*, the focal source has reverted back to a repetitive reentrant source (white arrow) in approximately the same location. *B*: activation map at 10 min of LDVF showing a stable focal pattern (black arrows) in the same location as the focal and reentrant sources shown in *A*,*1–3*. This focal source activates the RV but not the LV. The LV is activated by a planar wave (white arrow), which is apparently unrelated to the source in the RV. Red, early activation; magenta, late activation. The red front in the basal RV (*B*, *top*) shows the excitation wave generated in the previous cycle that is exiting the field of view when a new focal wave emerges. *C*: unique example of stable Epi reentry in the RV (white arrow) at a very late stage of LDVF (16 min). *D*: approximate locations of repetitive breakthrough patterns observed in 7 of 10 hearts.

tained throughout the 6-s-long movie. Note that the reentrant waves did not penetrate into the LV, which was completely silent at this late stage of LDVF. Figure 8*D* shows the approximate locations of repetitive breakthrough patterns observed in 7 of 10 hearts.

## DISCUSSION

This study provides an extensive analysis of heterogeneous electrical alterations occurring in the canine heart in response to the combined challenges of high excitation rate and ischemia during LDVF. The main finding of this study is the evidence of interchamber and intrachamber heterogeneities of a magnitude comparable to the much more studied gradients between Endo and Epi. In particular, our study revealed the presence of fully inexcitable areas interweaved with still excitable areas in both ventricles during the later stages of LDVF. Additionally, our optical mapping data complement and extend previous work by Kong et al. (19) showing that the right-to-left VFR gradient, similarly to the Endo-to-Epi VFR gradient, is largely determined by the nonuniform distribution of postrepolarization refractoriness amid a relatively invariant APD.

*Gradients of the activation rate and sources of fastest activation during VF in globally ischemic hearts.* The progressive disparity of VFR between Endo and Epi of both the LV and RV (higher VFR in Endo) during VF in a nonperfused canine heart has been previously shown by several groups (5, 27, 41). It was also documented that RV Epi was faster than LV Epi after 3 min of LDVF and that LV Endo was faster than RV Endo during the first 10 min of LDVF (5). In the rabbit heart, there was an Endo-to-Epi gradient in the LV, but not in the RV, and a right-to-left VFR gradient was present in Epi (42). In contrast to dog and rabbit hearts, in the pig heart, LV Epi was slightly faster than LV Endo and LV Epi was slightly faster than RV Epi at least during the first 3 min of LDVF (see Fig. 3 in Ref. 27). From these results, one can conclude that the overall pattern of VFR distribution during LDVF is complex and species dependent. Yet, the most striking feature is the consistent presence of a large Endo-to-Epi gradient in the LV of both dog and rabbit hearts and the absence thereof (or a slight inverse gradient) in the LV of the pig heart. Based on the principally different arrangement of the Purkinje network (confined to Endo in the dog and rabbit and transmural in the pig), it was postulated that the transmural distribution of VFR during LDVF reflects the dominant role of Purkinje fibers in the maintenance of VF in the ischemic heart. Hence, in dog and rabbit ventricles, the rapid sources of VF are concentrated in Endo, whereas in the pig heart they are distributed throughout the wall thickness. More direct evidence for this hypothesis stemmed from experiments in which Endo ablation with Lugol solution eliminated the transmural VFR gradient (5, 8) or accelerated spontaneous VF termination in isolated LV preparation (8) and from the observation of an increasing incidence of focal patterns in intramural layers of the porcine heart during LDVF (20).

Our quantification of spatial VFR gradients in the canine LV and RV is consistent with a previous report (27) showing the simultaneous presence of both Endo-to-Epi and RV-to-LV gradients of VFR during LDVF. In addition, we found that patterns of activation of the RV and LV during LDVF differ in several respects. First, in the RV, there are no significant differences between Endo and Mid, and, thus, the VFR gradient is mostly present in the outer half of the RV wall. In the LV, however, there is a significant gradient between Endo and Mid as well as between Mid and Epi. Second, RV Epi maintains excitability for a longer time than LV Epi. Third, repetitive reentrant activity is present in the RV but not in the LV at late stages of LDVF. We also found that activation of the Sep (at least at its anterior junction with the RV and LV) deviates from the Purkinje paradigm for LDVF maintenance. In fact, the sites of fastest activation in the Sep were found within 5–6 mm from Epi, which is at least 4 to 5 mm away from the nearest Endo surface containing the Purkinje layer (see Supplemental Fig. 1). Sep Epi locations were consistently faster than surrounding RV Epi and LV Epi locations (see Figs. 3 and 4). Moreover, throughout 10 min of LDVF, the activation rate in Sep Epi and Sep Mid was similar to that in LV Endo (see Supplemental Fig. 3*B*). Thus, based on the fastest VFR criterion, it is possible that Sep Epi and Sep Mid layers may harbor sources maintaining LDVF. This possibility is confirmed by observations of sustained focal and reentrant sources in the vicinity of the RV-Sep junction in Epi optical maps (see Fig. 8). A similar preferential clustering of sustained Epi sources near the Sep has been previously observed during LDVF in the rabbit heart (42). Those authors attributed Sep Epi breakthroughs to a possibility that sub-Endo structures such as papillary muscle insertions located at or near the Sep can anchor and stabilize intramural reentrant sources, which would appear as stable Epi breakthroughs.

This explanation may hold true for the case of the canine heart, where a large papillary muscle is located on the right side of the Sep. However, relatively stable reentrant circuits are also present on Epi of the RV-Sep junction. We think it is possible that the special fiber arrangement with abrupt changes in fiber orientation in the RV-Sep junction may favor the stabilization of reentrant sources in this area, especially when combined with the very slow conduction velocity, short APD, and partial cell-to-cell uncoupling present during ischemia. The ability of the RV-Sep junction to support high-frequency sources during LDVF may also be related to increased mechanical stretch in this area (which is often thinner than the lateral RV wall and Sep) resulting from the sustained RV pressure increase occurring during LDVF (22, 26). Due to the activation of mechanosensitive channels and/or modulation of other ionic channels and transporters, stretch promotes conduction block and reentry and may contribute to the generation of ectopic triggers during ischemia (17, 25). It has also been shown that stretch increases VFR and/or the density of singularity points during normoxemic VF (6, 26) and thus potentially can modulate the organization of VF in ischemic hearts. In conclusion, the unique pattern of activation of the RV-Sep junction during LDVF may be due to a combination of structural and mechanical properties of this region that set it apart from the adjacent RV and LV free walls. However, these assumptions await experimental confirmation.

*Mosaic inexcitability during LDVF.* A novel finding of this study is the highly heterogeneous pattern of electrical depression in Epi of both the RV and LV during later stages of LDVF (see Fig. 6). Indeed, even though on average VFR was higher in the RV than in the LV, in both chambers there were fully unexcitable regions interweaved with regions maintaining electrical activity. Such areas of local inexcitability were not

observed during LDVF in porcine hearts (16). Clearly, these local Epi gradients cannot be explained in terms of Purkinje fiber distribution and function. The mechanisms responsible for these local gradients remain unknown. One possible mechanism is related to the heterogeneous activation of ATP-sensitive $K^+$ channel current ($I_{K,ACh}$) secondary to mitochondrial depolarization during ischemia caused by opening of the mitochondrial inner membrane anion channel (IMAC) (1). During global ischemia in the guinea pig heart, an agonist of IMAC, FGIN-127, exacerbated the electrical depression caused by ischemia and induced regional inexcitability at ~10 min of ischemia. It should be noted, however, that the study by Akar et al. (1) did not directly demonstrated the link between regional inexcitability and mitochondrial depolarization. A study (24) using confocal microscopy to image the mitochondrial potential in rat hearts revealed a mosaic presence of cells with depolarized mitochondrial potential among cells with mitochondria still fully polarized. However, the cells exhibiting mitochondrial depolarization appeared only relatively late in ischemia (~20–30 min) and were observed much more frequently upon reperfusion. In addition, they did not form macroscopically continuous regions, which could explain the inexcitable areas observed in our experiments. Thus, the link between mitochondrial depolarization and electrical depression in early ischemia remains unconfirmed. We cannot exclude, however, that the electrical depression dependent on IMAC channel activation is more pronounced under conditions used in our study (LDVF in canine hearts) than in previous studies using small mammalian hearts without VF. It is also possible that the regional inexcitability in Epi of the canine ventricles is promoted by partial cellular uncoupling, which may help to establish a sharp separation between inexcitable and excitable areas. Canine ventricular Epi may be more susceptible to uncoupling during ischemia due to lower expression of connexin43 in Epi compared with deeper layers of the ventricular wall (29). The inexcitable areas observed in this study may hamper the ability of defibrillation shocks applied during advanced stages of LDVF to synchronize the ventricles and may also facilitate the formation of reentrant circuits, which would reinitiate VF after shock application.

*Right-to-left gradients in APD and DI during LDVF.* To the best of our knowledge, this is the first reported analysis of right-to-left differences in DI and APD during LDVF in the canine heart. In general, VFCL reflects the local effective refractory period (ERP) under the assumption that the tissue is activated as soon as it is capable of conducting an electrical wave. This assumption is reasonable if conduction is not restricted by anatomic barriers and is sustained predominantly by functional reentrant circuits. With the normal availability of fast $Na^+$ current ($I_{Na}$), the tissue is able to generate an AP almost immediately upon repolarization from previous excitation, ERP approximates APD well, and, therefore, DIs are short during VF. However, as ischemia develops and causes a decrease in excitability, ERP extends beyond APD (postrepolarization refractoriness). Consequently, DIs during ischemic VF are prolonged (19, 28, 43). Thus, one can assume that in the ischemic heart, the length of DI during VF is a reasonably good indicator of local postrepolarization refractoriness.

Our results clearly show that the right-to-left gradients in VFCL are determined by gradients in DI (and, hence, presumably, by postrepolarization refractoriness) amid a relatively invariant APD over both chambers and all time points of LDVF (see Fig. 8). In fact, there was a slightly longer APD in the RV versus in the LV, which is consistent with observations of a gradient of the same direction observed during pacing in the ischemic rabbit heart (23). In any case, despite the slightly longer APD in the RV than in the LV, VFCL was shorter in the RV than in the LV. Overall, the relationship between VFCL, DI, and APD was very similar to that recently reported by Kong et al. (19). These authors showed that the transmural gradient of VFCL across the LV wall was due to the differences in DI amid a relatively constant APD. Thus, an Endo-to-Epi APD gradient observed in normoxemic canine and human hearts at physiological pacing rates (3, 12) is not present during LDVF and does not influence the VFR gradient in the canine heart. While it is not practically possible to measure ERP in a rigorous manner during the fast and irregular rhythms characteristic of LDVF, our rough estimates of ERP differences between Epi and Endo locations in the LV and RV paced at a relatively fast frequency of 4 Hz during global ischemia are consistent with the presence of ERP gradients both between Endo and Epi and between the RV and LV (see Supplemental Figs. 6–8). Taken together, the arguments above support the notion that both transmural and right-to-left VFR gradients during ischemia in the canine heart are universally determined by the distribution of postrepolarization refractoriness.

*LDVF mechanism: sources versus substrate.* As mentioned above, the focus of recent relevant studies was on the role of Purkinje fibers as sources of activation maintaining LDVF. The strongest evidence supporting the leading role of Purkinje fibers in the dog heart is the elimination of the transmural gradient after the ablation of Endo with Lugol solution and also earlier spontaneous termination of LDVF in isolated slab preparations (5, 8). As we argued above, the outer layers of the RV-Sep junction may be another source of fast activations apparently unrelated to the fast sources in Endo. Thus, the observation of earlier termination in ablated isolated slabs of the LV free wall (8) may not be applicable to whole hearts with an intact Sep and RV.

It should be noted, however, that the identification of the sources is only one aspect of LDVF. The picture of LDVF will remain incomplete without an understanding of the "substrate," i.e., the response of the ventricles to fast sources of electrical activity. Regardless of whether or not Purkinje fibers are the predominant source of electrical waves, the question remains as to why the electrical depression develops faster in some regions of the ventricle than in others. The large left-to-right and intrachamber VFR gradients shown in this study are most likely unrelated to Purkinje fiber distribution. We argued above that VFR may be regarded as an important index of local electrical depression (and ensuing postrepolarization refractoriness) that appears to be highly nonuniform in the canine heart. During ischemia and VF, a number of ionic currents as well as other factors can contribute to heterogeneous electrical depression. It has been shown that $I_{K,ATP}$ activation can be different between Endo and Epi myocytes (10). We could not find any evidence of differential activation of $I_{K,ATP}$ in the RV versus in the LV during ischemia in the relevant literature. However, the fact that the LV simultaneously has a shorter APD and longer DIs than the RV during LDVF (see Fig. 7) would be consistent with larger $I_{K,ATP}$ in the LV than in the

RV. Indeed, increased time-independent outward $K^+$ current in the partially depolarized myocardium is expected to accelerate repolarization, on one hand, and to prolong postrepolarization refractoriness, on the other hand. Other $K^+$ currents whose activation is enhanced under conditions of ischemia and/or a high rate of excitation may also be involved, such as $Na^+$-activated $K^+$ current (18). Another possible mechanism of heterogeneous electrical depression during LDVF is the dispersion in the inactivation properties of $I_{Na}$. Cordeiro at al. (7) have recently shown that Epi cells have a more negative half-inactivation voltage than Endo cells. This property confers a greater sensitivity of ventricular Epi to electrical depression caused by an elevation of extracellular $K^+$ and thus may contribute to the transmural VFR gradient observed during VF in the globally ischemic heart. Although right-to-left differences in the voltage dependence of $I_{Na}$ inactivation were not reported, in the rabbit heart the right-to-left VFR gradient during LDVF was reproducible by elevating $K^+$ in the normally oxygenated fibrillating heart (4), indicating chamber-specific differences in the sensitivity to hyperkalemia. We have already mentioned a possible role of mechanical stretch in the maintenance of fast and sustained sources in the RV-Sep area. It is also possible that the distribution of stretch contributes to the transmural gradient of VFR and excitability, since both experimental and computational studies (11, 17, 38) have indicated larger strain in Endo. In particular, right-to-left and/or transmural gradients in mechanical stretch may modulate the spatial distribution of $I_{K,ATP}$ activation, since a reduction in ATP content under ischemic conditions sensitizes ATP-sensitive $K^+$ channels to stretch (21, 36, 37).

Although the mechanisms discussed above seem to be the most relevant because they are enhanced under conditions presented by LDVF, a number of heterogeneously distributed ionic channels, such as those associated with transient outward $K^+$ current, the rapid component of delayed rectifier $K^+$ current, and inward rectifier $K^+$ current (33), may be involved in nonuniform electrical depression during LDVF.

*VF evolution: comparison with previous studies.* In his seminal work, Wiggers (40) described four different stages of VF in the open-chested dog: *1*) undulatory or tachysystolic (1–2 s); *2*) convulsive incoordination (15–40 s); *3*) tremulous incoordination (2–3 min); and *4*) progressive atonic incoordination, which usually starts 2–5 min after the onset of VF. This classification was based on the visual analysis of high-speed movies of cardiac contraction. In a more recent study in the same animal model, Huang et al. (15) distinguished five stages (*stages i–v*) during the first 10 min of VF, based on a quantitative analysis of spatiotemporal dynamics of wavefronts extracted from multielectrode Epi maps. They found a nonmonotonic evolution of activation patterns during LDVF, with a transient phase of increased organization and the incidence of reentry between 1 and 3 min after VF onset and a rapid decrease in these parameters in later phases of VF. These authors also observed a steady decrease in the number of wavefronts as LDVF progressed concomitant with a steady increase in the number of breakhtroughs and the incidence of conduction block.

To the extent that it is possible to compare results obtained with different recording and analysis techniques, our present study is consistent with previous observations in several aspects. Similar to Huang et al. (15), we observed a transitory increase in the occurrence of reentry between ~2 and 4 min of LDVF (see Supplemental Fig. 5, *B* and *C*). This approximately corresponds to Wigger's tremulous incoordination phase, during which he noted the presence of "contraction waves. . .circling around in very limited areas" (40). During the next stage (atonic incoordination), Wiggers (40) noted that some areas completely lost contractility, whereas in other areas, especially those close to large vessels and to the right side of the LAD, contractions still persisted. These early observations are fully confirmed by our optical mapping results showing a mosaic distribution of excited and nonexcited areas during this stage of LDVF, with excitability more preserved in areas close to the LAD and in the RV (see Supplemental Fig. 4). Similarly, Huang et al. (15) reported a progressive decrease in the number of wavefronts in LV Epi, which approached zero by 10 min of LDVF. Thus, different studies in dogs agree in their observation of a rapid loss of excitability in LV Epi. It is worth noting, however, that in porcine and rabbit hearts, LV Epi maintains excitability throughout the first 10 min of LDVF (16, 42). This difference may be due to interspecies differences in the ionic channel distribution/function and/or differences in the severity of metabolic stress caused by combined effects of ischemia and LDVF.

*Conclusion and significance.* Recent studies of LDVF have been focused on the role of Purkinje fibers in LDVF maintenance. Our data indicate that both sources of activity and substrate during LDVF in the canine heart are not exclusively determined by the relationship between Purkinje fibers and the working myocardium. The pattern of activation becomes ever more divergent during the course of LDVF, revealing simultaneous differences between Endo and Epi, RV, LV, and Sep, and within each chamber or wall type. Regardless of whether or not Purkinje fibers maintain self-sustained electrical activity at advanced stages of LDVF, for the purposes of successful defibrillation and resuscitation, it is at least as important whether or not a critical mass of the myocardium can respond in a synchronous manner to an electric shock and any stimulus after defibrillation shock. The presence of large inexcitable areas in the LV and RV may affect the outcome of defibrillation shock and raises the possibility of forming reentrant circuits around inexcitable regions after shock and reinitiation of VF. Thus, future studies concerning LDVF should be more focused on understanding the reasons why the electrical depression develops faster in some regions of the ventricle than in others and how electrical depression heterogeneities interact with the defibrillation shock.

*Limitations.* In our experiments, LDVF began when perfusion was stopped. In a patient, the termination of perfusion may be more gradual. However, most likely, this difference would affect, at most, the first 1–3 min of LDVF. The main limitation of any mapping technique is incomplete coverage of the three-dimensional pattern of ventricular activation. However, the magnitude of the observed heterogeneities could only increase if we mapped larger regions. The thickness of the ventricular wall is highly nonuniform, whereas the length of the plunge needle electrodes used in both the RV and LV was fixed to accommodate the largest wall thickness in the respective chambers. Thus, in some locations, the most Endo leads were outside the ventricular wall. Despite our best efforts to identify and exclude such leads (see METHODS), an error in this process could have led to an underestimation of the transmural

VFR gradient in the RV and LV. However, the fact that transmural gradients were still detected in both chambers and were consistent with a previous report (5) indicates that this potential problem was of limited influence. Whereas residual motion artifacts could have been present at the early stage of LDVF despite mechanical restraint, the largest interchamber and intrachamber gradients were observed after contractility was completely abolished by the ischemic process. Therefore, the presence of motion artifacts could not have overestimated the magnitude of the gradients. Other common limitations of optical mapping were discussed in our previous publication (16).


## ACKNOWLEDGMENTS

The superb technical assistance of Jayne Davis, Alicja Booth, and Nancy Allen is greatly appreciated.

## GRANTS

This work was supported by National Heart, Lung, and Blood Institute Grant 5-R01-HL-088444 and by Nora Eccles Treadwell Foundation research grant (to A. V. Zaitsev).


## DISCLOSURES

No conflicts of interest, financial or otherwise, are declared by the author(s).

## REFERENCES


1. **Akar FG, Aon MA, Tomaselli GF, O'Rourke B.** The mitochondrial origin of postischemic arrhythmias. *J Clin Invest* 115: 3527–3535, 2005.
2. **Allison JS, Qin H, Dosdall DJ, Huang J, Newton JC, Allred JD, Smith WM, Ideker RE.** The transmural activation sequence in porcine and canine left ventricle is markedly different during long-duration ventricular fibrillation. *J Cardiovasc Electrophysiol* 18: 1306–1312, 2007.
3. **Antzelevitch C, Sicouri S, Litovsky SH, Lukas A, Krishnan SC, Di Diego JM, Gintant GA, Liu DW.** Heterogeneity within the ventricular wall. Electrophysiology and pharmacology of epicardial, endocardial, and M cells. *Circ Res* 69: 1427–1449, 1991.
4. **Caldwell J, Burton FL, Smith GL, Cobbe SM.** Heterogeneity of ventricular fibrillation dominant frequency during global ischemia in isolated rabbit hearts. *J Cardiovasc Electrophysiol* 18: 854–861, 2007.
5. **Cha YM, Uchida T, Wolf PL, Peters BB, Fishbein MC, Karagueuzian HS, Chen PS.** Effects of chemical subendocardial ablation on activation rate gradient during ventricular fibrillation. *Am J Physiol Heart Circ Physiol* 269: H1998–H2009, 1995.
6. **Chorro FJ, Trapero I, Guerrero J, Such LM, Canoves J, Mainar L, Ferrero A, Blasco E, Sanchis J, Millet J, Tormos A, Bodi V, Alberola A.** Modification of ventricular fibrillation activation patterns induced by local stretching. *J Cardiovasc Electrophysiol* 16: 1087–1096, 2005.
7. **Cordeiro JM, Mazza M, Goodrow R, Ulahannan N, Antzelevitch C, Di Diego JM.** Functionally distinct sodium channels in ventricular epicardial and endocardial cells contribute to a greater sensitivity of the epicardium to electrical depression. *Am J Physiol Heart Circ Physiol* 295: H154–H162, 2008.
8. **Dosdall DJ, Tabereaux PB, Kim JJ, Walcott GP, Rogers JM, Killingsworth CR, Huang J, Robertson PG, Smith WM, Ideker RE.** Chemical ablation of the Purkinje system causes early termination and activation rate slowing of long-duration ventricular fibrillation in dogs. *Am J Physiol Heart Circ Physiol* 295: H883–H889, 2008.
9. **Evans FG, Rogers JM, Smith WM, Ideker RE.** Automatic detection of conduction block based on time-frequency analysis of unipolar electrograms. *IEEE Trans Biomed Eng* 46: 1090–1097, 1999.
10. **Furukawa T, Kimura S, Furukawa N, Bassett AL, Myerburg RJ.** Role of cardiac ATP-regulated potassium channels in differential responses of endocardial and epicardial cells to ischemia. *Circ Res* 68: 1693–1702, 1991.
11. **Gallagher KP, Osakada G, Matsuzaki M, Miller M, Kemper WS, Ross J Jr.** Nonuniformity of inner and outer systolic wall thickening in conscious dogs. *Am J Physiol Heart Circ Physiol* 249: H241–H248, 1985.
12. **Glukhov AV, Fedorov VV, Lou Q, Ravikumar VK, Kalish PW, Schuessler RB, Moazami N, Efimov IR.** Transmural dispersion of repolarization in failing and nonfailing human ventricle. *Circ Res* 106: 981–991, 2010.
13. **Gray RA, Pertsov AM, Jalife J.** Spatial and temporal organization during cardiac fibrillation. *Nature* 392: 75–78, 1998.
14. **Hong MF, Dorian P.** Update on advanced life support and resuscitation techniques. *Arrhythmias Curr Opin Cardiol* 20: 1–6, 2005.
15. **Huang J, Rogers JM, Killingsworth CR, Singh KP, Smith WM, Ideker RE.** Evolution of activation patterns during long-duration ventricular fibrillation in dogs. *Am J Physiol Heart Circ Physiol* 286: H1193–H1200, 2004.
16. **Huizar JF, Warren MD, Shvedko AG, Kalifa J, Moreno J, Mironov SF, Jalife J, Zaitsev AV.** Three distinct phases of VF during global ischemia in the isolated blood-perfused pig heart. *Am J Physiol Heart Circ Physiol* 293: H1617–H1628, 2007.
17. **Jie X, Gurev V, Trayanova N.** Mechanisms of mechanically induced spontaneous arrhythmias in acute regional ischemia. *Circ Res* 106: 185–192, 2010.
18. **Kameyama M, Kakei M, Sato R, Shibasaki T, Matsuda H, Irisawa H.** Intracellular $Na^+$ activates a $K^+$ channel in mammalian cardiac cells. *Nature* 309: 354–356, 1984.
19. **Kong W, Ideker RE, Fast VG.** Transmural optical measurements of $V_m$ dynamics during long-duration ventricular fibrillation in canine hearts. *Heart Rhythm* 6: 796–802, 2009.
20. **Li L, Jin Q, Huang J, Cheng KA, Ideker RE.** Intramural foci during long duration fibrillation in the pig ventricle. *Circ Res* 102:1256–1264, 2008.
21. **Li W, Kohl P, Trayanova N.** Myocardial ischemia lowers precordial thump efficacy: an inquiry into mechanisms using three-dimensional simulations. *Heart Rhythm* 3: 179–186, 2006.
22. **Mashiro I, Cohn JN, Heckel R, Nelson RR, Franciosa JA.** Left and right ventricular dimensions during ventricular fibrillation in the dog. *Am J Physiol Heart Circ Physiol* 235: H231–H236, 1978.
23. **Pandit SV, Shibayama J, Mironov S, Anumonwo J, Vikstrom K, Jalife J.** Electrophysiological changes in left versus right ventricle during global ischemia and reperfusion: role of sarcolemmal K-ATP channels (Abstract). *Heart Rhythm* 5: S112, 2008.
24. **Matsumoto-Ida M, Akao M, Takeda T, Kato M, Kita T.** Real-time 2-photon imaging of mitochondrial function in perfused rat hearts subjected to ischemia/reperfusion. *Circulation* 114: 1497–1503, 2006.
25. **McNary TG, Sohn K, Taccardi B, Sachse FB.** Experimental and computational studies of strain-conduction velocity relationships in cardiac tissue. *Prog Biophys Mol Biol* 97: 383–400, 2006.
26. **Moreno J, Zaitsev AV, Warren M, Berenfeld O, Kalifa J, Lucca E, Mironov SF, Guha PK, Jalife J.** Effect of remodelling, stretch and ischaemia on ventricular fibrillation frequency and dynamics in a heart failure model. *Cardiovasc Res* 65: 158–166, 2005.
27. **Newton JC, Smith WM, Ideker RE.** Estimated global transmural distribution of activation rate and conduction block during porcine and canine ventricular fibrillation. *Circ Res* 94: 836–842, 2004.
28. **Robertson PG, Huang J, Chen KA, Chen X, Dosdall DJ, Tabereaux PB, Smith WM, Ideker RE.** Increased cycle length during long-duration ventricular fibrillation is caused by decreased upstroke velocity as well as prolonged refractoriness. *Heart Rhythm* 6: 378–384, 2009.
29. **Poelzing S, Akar FG, Baron E, Rosenbaum DS.** Heterogeneous connexin43 expression produces electrophysiological heterogeneities across ventricular wall. *Am J Physiol Heart Circ Physiol* 286: H2001–H2009, 2004.
30. **Rogers JM, Melnick SB, Huang J.** Fiberglass needle electrodes for transmural cardiac mapping. *IEEE Transact Biomed Eng* 49: 1639–1641, 2002.
31. **Roth R, Stewart R, Rogers K.** Out-of-hospital cardiac arrest: factors associated with survival. *Ann Emerg Med* 13: 237–243, 1984.
32. **Samie FH, Berenfeld O, Anumonvo J, Mironov SF, Udassi S, Beaumont J, Taffet S, Pertsov AM, Jalife J.** Rectification of the background potassium current. A determinant of rotor dynamics in ventricular fibrillation. *Circ Res* 89: 1216–1223, 2001.
33. **Schram G, Pourrier M, Melnyk P, Nattel S.** Differential distribution of cardiac ion channel expression as a basis for regional specialization in electrical function. *Circ Res* 90: 939–950, 2002.
34. **Tabereaux PB, Walcott GP, Rogers JM, Kim J, Dosdall DJ, Robertson PG, Killingsworth CR, Smith WM, Ideker RE.** Activation patterns of purkinje fibers during long-duration ventricular fibrillation in an isolated canine heart model. *Circulation* 116: 1113–1119, 2007.

35. **Taccardi B, Punske BB, Macchi E, MacLeod RS, Ershler PR.** Epicardial and intramural excitation during ventricular pacing: effect of myocardial structure. *Am J Physiol Heart Circ Physiol* 294: H1753–H1766, 2008.
36. **Van Wagoner DR.** Mechanosensitive gating of atrial ATP-sensitive potassium channels. *Circ Res* 72: 973–983, 1993.
37. **Van Wagoner DR, Lamorgese M.** Ischemia potentiates the mechanosensitive modulation of atrial ATP-sensitive potassium channels. *Ann NY Acad Sci* 723: 392–395, 1994.
38. **Vetter F, McCulloch A.** Mechanoelectric feedback in a model of the passively inflated left ventricle. *Ann Biomed Eng* 29: 414–426, 2001.
39. **Warren M, Guha PK, Berenfeld O, Zaitsev A, Anumonwo JMB, Dhamoon AS, Bagwe S, Taffet SM, Jalife J.** Blockade of the inward rectifying potassium current terminates ventricular fibrillation in the guinea pig heart. *J Cardiovasc Electrophysiol* 14: 621–631, 2003.
40. **Wiggers CJ, Bell JR, Paine M.** Studies of ventricular fibrillation caused by electric shock. II. Cinematographic and electrocardiographic observations of the natural process in the dog's heart: its inhibition by potassium and the revival of coordinated beats by calcium. *Am Heart J* 5: 351–365, 1930.
41. **Worley SJ, Swain JL, Colavita PG, Smith WM, Ideker RE.** Development of an endocardial-epicardial gradient of activation rate during electrically induced, sustained ventricular fibrillation in dogs. *Am J Cardiol* 55: 813–820, 1985.
42. **Wu TJ, Lin SF, Hsieh YC, Ting CT, Chen PS.** Ventricular fibrillation during no-flow global ischemia in isolated rabbit hearts. *J Cardiovasc Electrophysiol* 17: 1112–1120, 2006.
43. **Zaitsev AV, Guha PK, Sarmast F, Kolli A, Berenfeld O, Pertsov AM, de Groot JR, Coronel R, Jalife J.** Wavebreak formation during ventricular fibrillation in the isolated, regionally ischemic pig heart. *Circ Res* 92: 546–553, 2003.

3.8 Online Supplemental Material

**Supplemental Table 1**

| | RV EPI | RV MID | RV ENDO | SEP EPI | SEP MID | SEP DEEP | LV EPI | LV MID | LV ENDO |
|---|---|---|---|---|---|---|---|---|---|
| RV EPI | | X | X | X | X | | X | X | X |
| RV MID | X | | | | | | X | | |
| RV ENDO | X | | | | | | X | | X |
| SEP EPI | X | | | | | | X | | |
| SEP MID | X | | | | | | X | | |
| SEP DEEP | | | | | | | X | | X |
| LV EPI | X | X | X | X | X | X | | X | X |
| LV MID | X | | | | | | X | | |
| LV ENDO | X | | X | | | X | X | | |

**Online Data Supplement**

**Supplemental Figure 1**

Approximate position of SEP plunge needle electrode superimposed onto an MRI image of a canine heart. All symbols are the same as in Figure 1 of the main text.

**Supplemental Figure 2**

The time course of VFR in RV, SEP and LV in all 5 experiments in which plunge needle electrodes were used.

**Supplemental Table 1.**

Results of pairwise comparisons between the time course of VFR in all pairs of 9 principal locations studied using plunge needle electrodes. Crosses indicate statistical significance ($p<0.05$) using two-way ANOVA and Bonferroni post-hoc test. Note that the comparisons were performed between all time points of respective VFR curves and indicate overall dissimilarity in the time course of VFR between any pair of locations. Note also that LV EPI is the only site that is statistically different from all other locations. Thus, LV EPI is unique in its sensitivity to the stress imposed by the combination of VF and global ischemia.

**Supplemental Figure 3**

Superimposed VFR curves from SEP MID, SEP EPI and LV ENDO (the data is he same as in Figure 3 of the main text). One can see that throughout the entire course of LDVF

these curves closely track each other, even though SEP MID and SEP EPI are not adjacent to LV ENDO. These data suggest that the presence of Purkinje fibers is not the only determinant of VFR during LDVF.

**Supplemental Figure 4**

Examples of highly non-uniform VFR distribution at advanced stages of LDVF. Panels A-K represent different hearts. Time above the maps indicate the time of no-flow ischemia. The white line crossing the field of view represent LAD. Note the presence of completely inexcitable areas (black, VFR=0) adjacent to areas still maintaining fibrillatory activity. Note also that most of the time the sites with the highest VFR were situated either in RV or in regions of LV adjacent to LAD.

**Supplemental Figure 5**

Examples of LV activation maps taken at different time points of LDVF in the same heart. ***A to D,*** sets of consecutive activation maps from movies taken at approximately 0, 2, 4.5 and 10 min of LDVF, respectively. Different colors in activation maps denote activation times with respect to the start time. The start time in the first activation map in each set is chosen arbitrarily, but in subsequent maps the start time is the same as the latest activation time in the previous map. The range of activation times is shown in color bars to the right of respective maps. White arrows indicate examples of complete or incomplete reentrant patterns. At 0 min of LDVF (***A***), complete reentrant patterns are present, but typically do not repeat themselves. Thus, a complete reentrant pattern seen in Panel A2 is not present either before (A1) or after (A3). Between 2 and 5 min of LDVF

(***B*** and ***C***), more stable reentrant patterns could be observed. Thus, both Panels B1-B3 (2 min of LDVF) and Panels C1-C3 (4.5 min of LDVF) show repetitive reentrant pattern in three consecutive activation maps (in Panel C1 it is likely that a portion of the reentrant circuit is outside the mapped area). At 10 min of LDVF (***D***), only incomplete reentrant pattern were observed in LV coincident with emergence of large areas of epicardium not invaded by excitation waves propagating in adjacent areas (white cross in Panels D1-D4). This was typical of LV activation after 5-6 min of LDVF. Note that, in contrast to LV, in RV repetitive reentrant circuits could be observed even at very late stages of LDVF (see Fig. 8 in the main text).

**Regional differences in response to rapid pacing during global ischemia (Supplemental Figures 6-8)**

In 4 experiments we performed rapid pacing during global ischemia simultaneously in 4 locations: LV EPI, LV ENDO, RV EPI and RV ENDO (see Supplemental Figure 6). Six needles containing 10 evenly spaced unipolar electrodes were inserted in myocardium of both the LV and RV anterior free walls (Supplemental Figure 6A). Using the 2 most EPI and ENDO electrodes (see Supplemental Figure 6B), we repeatedly applied a series of ten S1 stimuli at CL=250 ms followed by a single extrastimulus (S2) at CL=180 ms throughout 10 minutes of global ischemia. The amplitudes of both S1 and S2 stimuli were set at 3 times end-diastolic excitation threshold measured in normally perfused heart.

This setup allowed us to compare the effective refractory period (ERP) in a given pacing location and at a given time of ischemia with 180 ms and 250 ms, based on the sequence of activation in adjacent electrodes. If an activation sequence followed an S1 or S2 stimulus with a short delay and propagated away from a pacing site, we postulated that the ERP at that pacing site was shorter than 250 or 180 ms, respectively. If an activation sequence followed an S1 or S2 stimulus with a long delay and propagated towards the pacing site, we postulated that the ERP at that pacing site was longer than 250 ms or 180 ms, respectively. Obviously, a complete lack of response to either S1 or S2 in the neighborhood of a particular pacing site indicated that ERP at that site exceeded either 250 ms or 180 ms, respectively.

Typically, at the very beginning of ischemia (within the first minute) EPI locations had shorter ERP than ENDO locations. An example in shown in Supplemental Figure 7 A. One can see that at 9 seconds of ischemia S1 stimulus generates local responses in both EPI and ENDO locations with activation waves spreading from both sites and converging in MID. In contrast, S2 stimulus generates local response only in EPI which propagates to ENDO and activates the latter after a delay. However, in a short order (at 124 seconds of ischemia) the sequence of activation in response to S2 stimulus is reversed (see Supplemental Figure 7B) indicating that at this time point ENDO ERP is shorter than EPI ERP. At the same time, S1 stimulus still generates local responses in both EPI and ENDO locations with activation waves spreading from both sites and converging in MID. At 130 seconds of ischemia (see Supplemental Figure 7C), there is no longer local response to

S1 stimulus in EPI, so that local response to both S1 and S2 stimuli occurs only in ENDO whereas EPI is activated by planar waves originated in ENDO.

In all experiments, EPI locations failed to respond to S2 stimulus earlier than ENDO locations in both LV and RV. We did not find a consistent difference between RV and LV. Pooled together, LV and RV EPI locations failed to respond to S2 stimulus at 184±59.4 s, whereas LV and RV ENDO locations responded to S2 up to 363±149.3 s of global ischemia. The difference was statistically significant ($p=0.022$). Thus, between ~3-6 min of ischemia, the effective refractory period (ERP) on EPI was > 180 ms, whereas the ERP on ENDO was <180 ms, indicating a transmural gradient in ERP.

By 10 min of ischemia, in 3 out of 4 hearts all ENDO locations followed S1 pacing (CL=250 ms) in 1:1 ratio. In 1 experiment, the entire ventricles responded to S1 stimuli in 1:2 ratio. In all 4 experiments at least some of EPI locations failed to follow S1 stimuli in 1:1 ratio with rate transformations in ratios 1:2, 1:3 or higher (See Supplemental Figure 8). There was a clear trend towards higher number of EPI sites following S1 stimulation in RV than in LV (4.0±2.7 vs. 0.50±0.58, $p=0.060$). Excluding the experiment in which all locations failed to follow every S1 stimulus (and thus the shortest testing interval was 500 ms), the difference between RV and LV in the number of EPI sites following pacing at CL=250 ms in 1:1 manner became significant (5.3±0.58 vs. 0.7±0.58, $p=0.005$). In all EPI sites excitability recovered and ERP fell below 180 ms within 1 minute of reperfusion (not shown).

Taken together, these findings indicate that during global ischemia in the canine heart ENDO sites are capable of following faster pacing rates than EPI sites, which is equivalent to an ERP gradient between ENDO and EPI. Moreover, there is a clear trend towards a higher degree of electrical depression in LV EPI than in RV EPI. Combining these observations with previously published data indicating the lack of APD gradient across the ventricular wall during VF/ischemia (1) and our data showing slightly longer APD in RV than in LV (see Figure 6C), one can make the conclusion that the ERP difference between ENDO and EPI is determined by the differences in post-repolarization refractoriness rather than differences in APD. More detailed and accurate measurements of post-repolarization refractoriness during global ischemia will require specially designed hardware and will be a subject of future studies.

**Supplemental Figure 6**

Electrode configuration used for assessment of regional differences in ERP during global ischemia. A, approximate positions of 6 plunge needle electrodes in RV and LV (open circles denote plunge needle electrodes used for EPI and ENDO stimulation). B, localization of leads in designated plunge needle electrodes used for pacing.

**Supplemental Figure 7**

Typical examples of the activation sequences along a plunge needle electrode induced by an S1 and S2 stimuli applied to the most epicardial and the most endocardial pairs of contacts along the needle at different time points of global ischemia. ***A-C***, unipolar

electrograms recorded from leads 3-8. Dashed red lines denote the direction of propagation. ***D***, a diagram of the plunge needle electrode showing the leads used for stimulation and recording.

**Supplemental Figure 8**

A typical example of transmural activation patterns in response to S1-S2 stimulation in LV and RV at 0 and 10 min of global ischemia. Note that at 10 min of ischemia LV subepicardial sites (# 8, 9 and 10) show a progressive failure to follow S1 stimuli culminating in complete lack of response in site #10. See text for more detail.

**Bibliography**

1**. Kong W, Ideker RE, Fast VG.** Transmural optical measurements of Vm dynamics during long-duration ventricular fibrillation in canine hearts. *Heart Rhythm* 6: 796-802, 2009

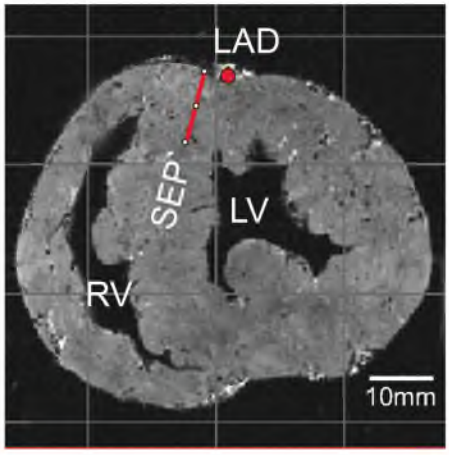


Supplemental Figure 1

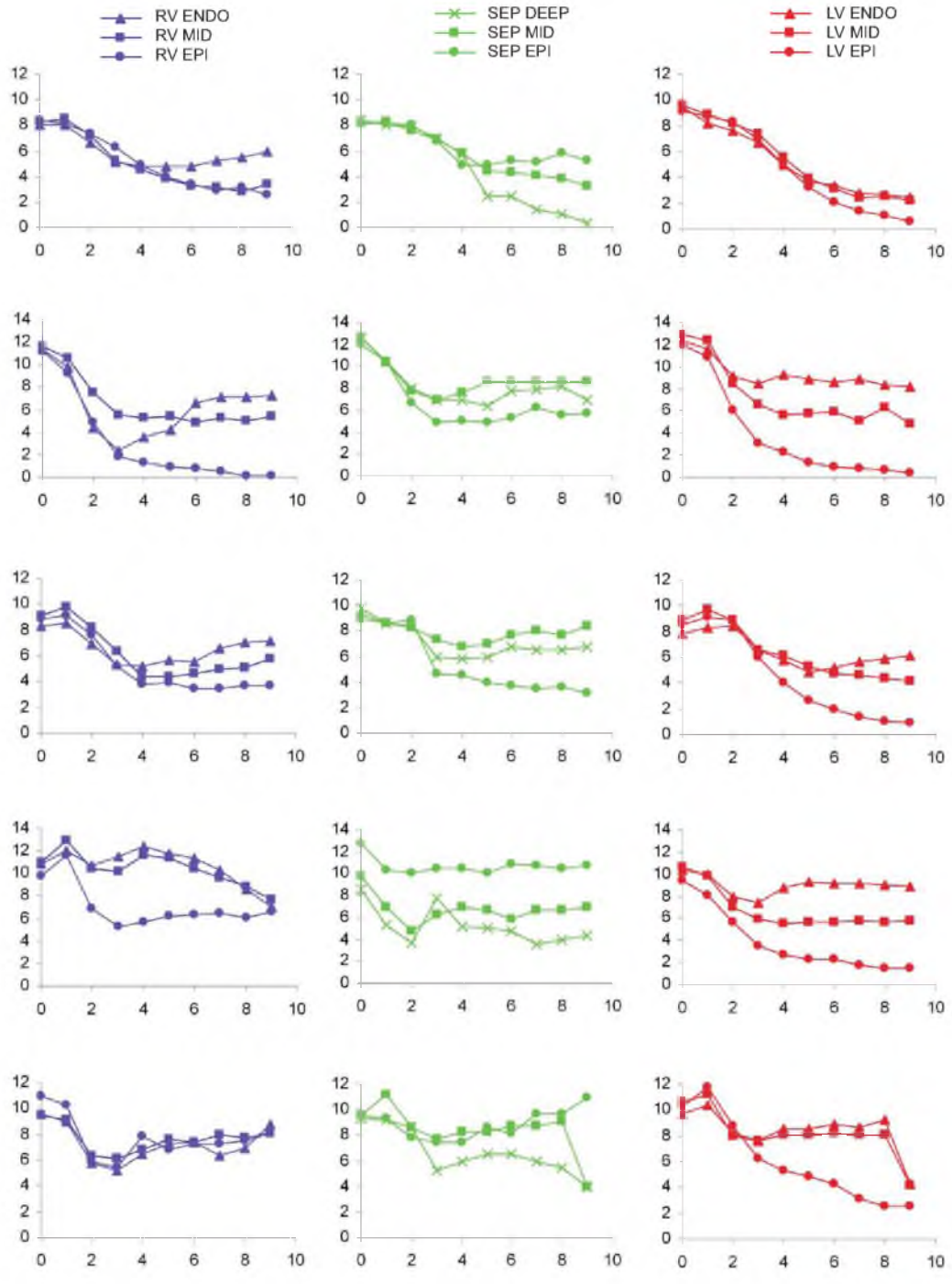


Supplemental Figure 2

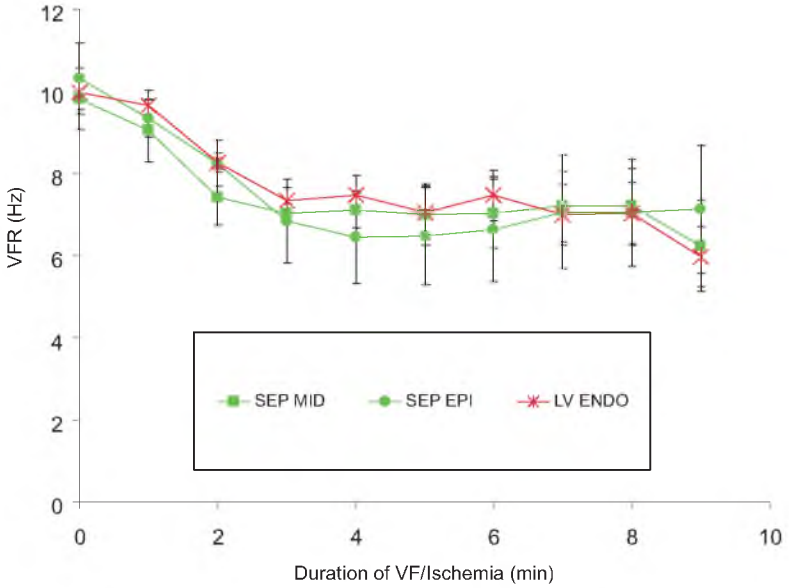


Supplemental Figure 3

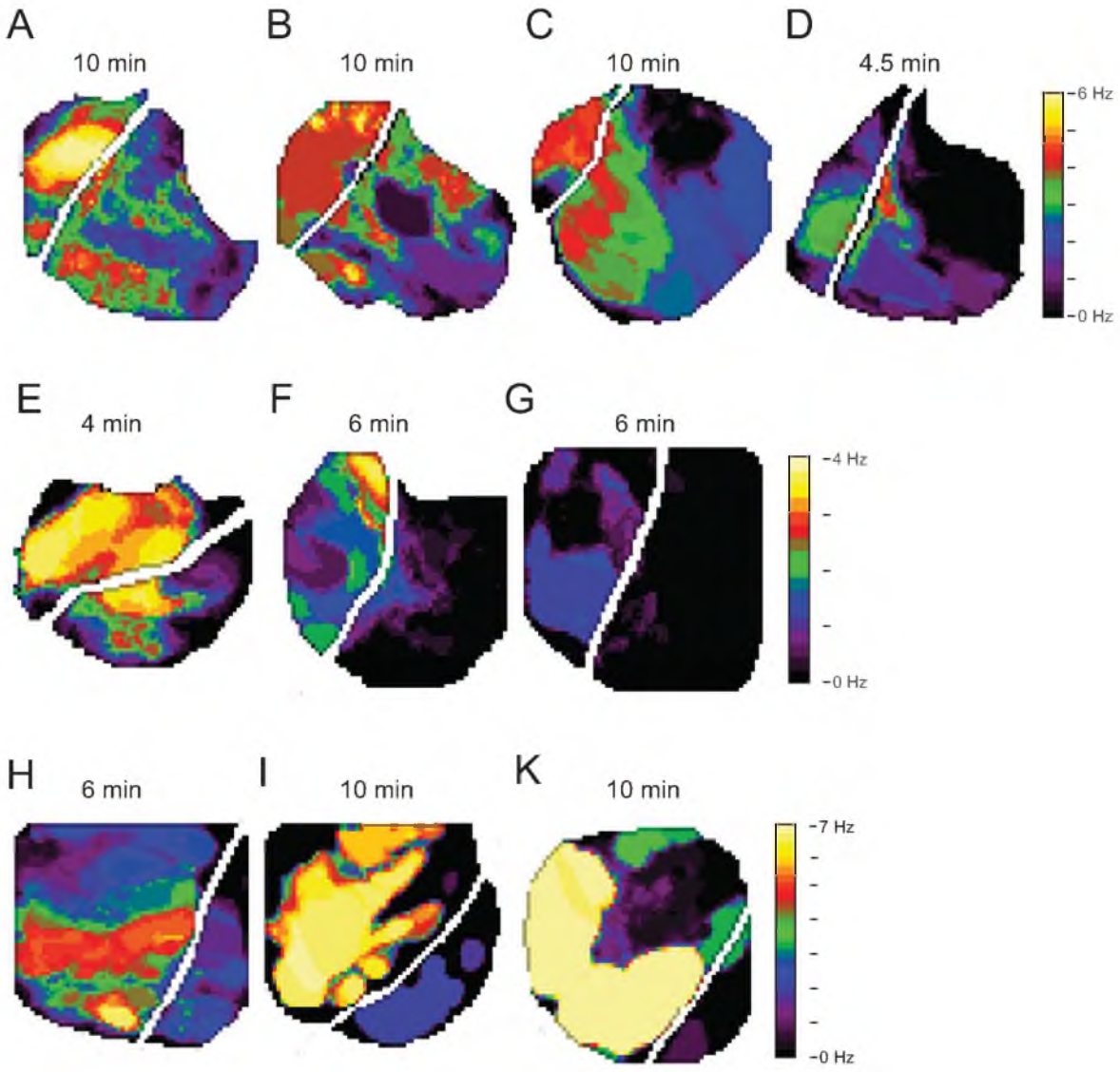


Supplemental Figure 4

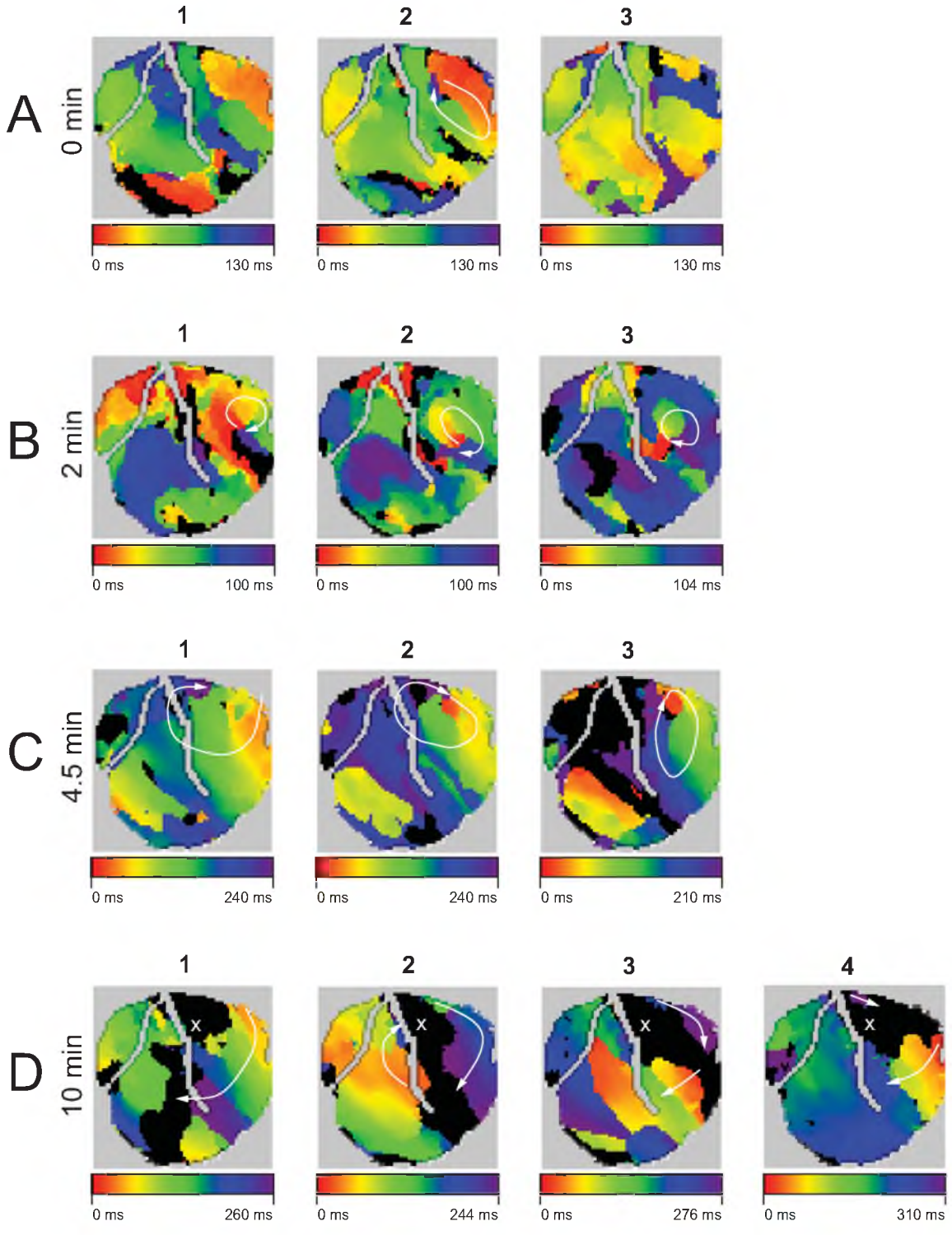


Supplemental Figure 5

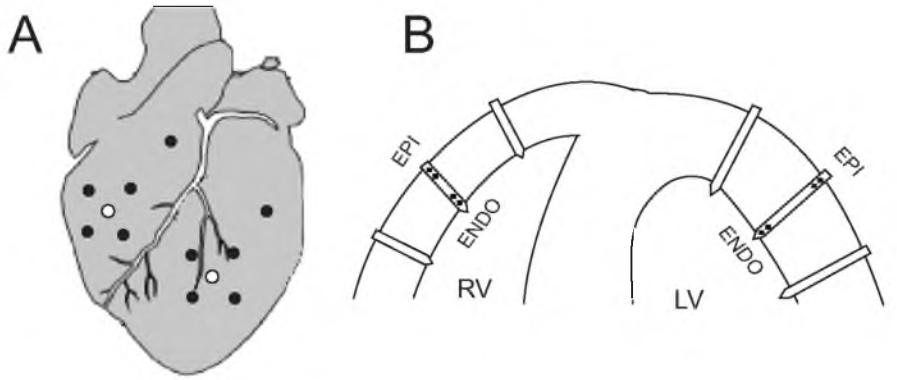


Supplemental Figure 6

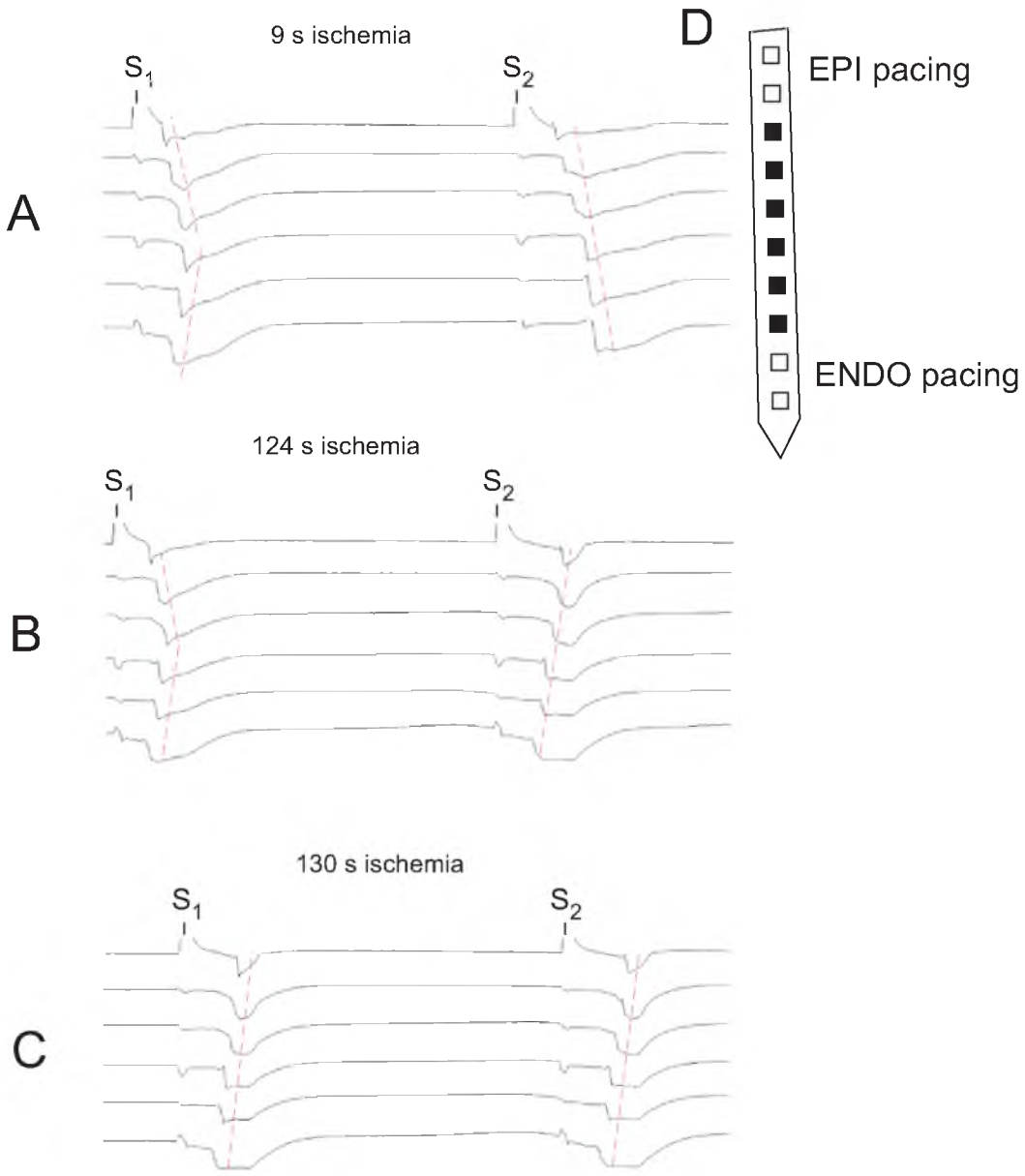


Supplemental Figure 7

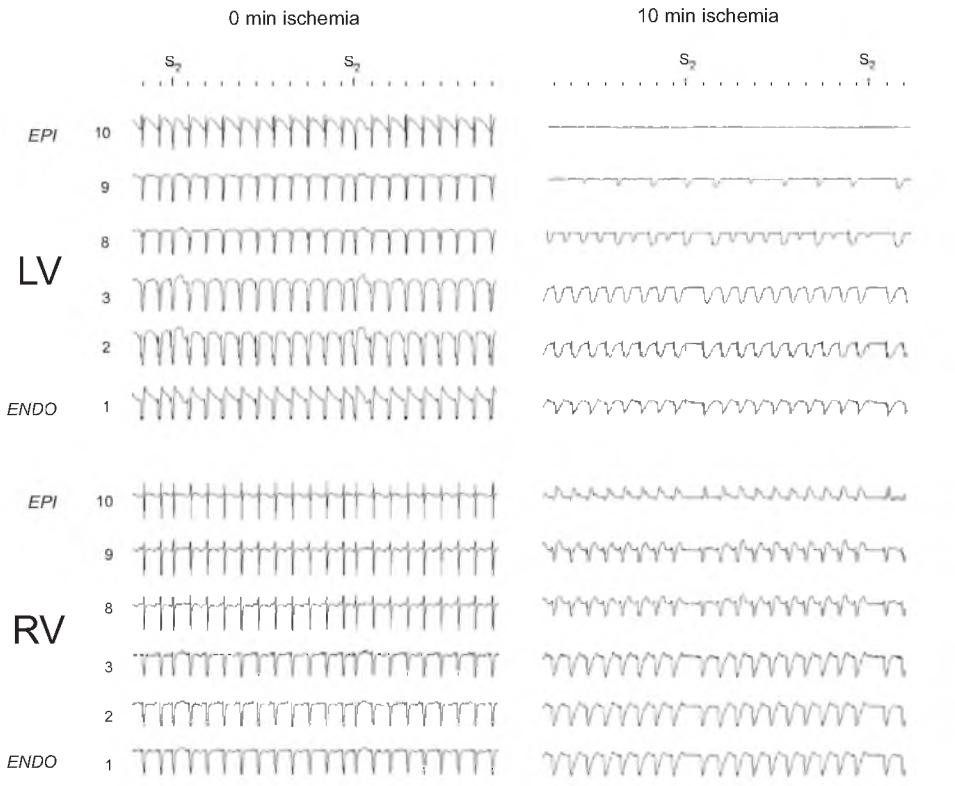


Supplemental Figure 8

# CHAPTER 4

## ROLE OF KATP CHANNEL IN ELECTRICAL DEPRESSION AND ASYSTOLE DURING LONG-DURATION VENTRICULAR FIBRILLATION IN EX VIVO CANINE HEART

The research in this chapter was published in the *American Journal of Physiology: Heart and Circulatory Physiology*. Tyson G. Taylor, Paul W. Venable, Junko Shibayama, Mark Warren, and Alexey V. Zaitsev.: 'Role of $K_{ATP}$ channel in electrical depression and asystole during long-duration ventricular fibrillation in ex vivo canine heart.' Am J Physio Heart Circ Physiol, 2012, 302, pp. H2396-H2409. Reprinted with permission of the American Physiological Society.

*Am J Physiol Heart Circ Physiol* 302: H2396–H2409, 2012.
First published March 31, 2012; doi:10.1152/ajpheart.00752.2011.

# Role of $K_{ATP}$ channel in electrical depression and asystole during long-duration ventricular fibrillation in ex vivo canine heart

**Tyson G. Taylor,* Paul W. Venable,* Junko Shibayama, Mark Warren, and Alexey V. Zaitsev**
*Nora Eccles Harrison Cardiovascular Research and Training Institute, University of Utah, Salt Lake City, Utah*

Submitted 29 July 2011; accepted in final form 22 March 2012

**Taylor TG, Venable PW, Shibayama J, Warren M, Zaitsev AV.** Role of $K_{ATP}$ channel in electrical depression and asystole during long-duration ventricular fibrillation in ex vivo canine heart. *Am J Physiol Heart Circ Physiol* 302: H2396–H2409, 2012. First published March 31, 2012; doi:10.1152/ajpheart.00752.2011.—Long-duration ventricular fibrillation (LDVF) in the globally ischemic heart is characterized by transmurally heterogeneous decline in ventricular fibrillation rate (VFR), emergence of inexcitable regions, and eventual global asystole. Rapid loss of both local and global excitability is detrimental to successful defibrillation and resuscitation during cardiac arrest. We sought to assess the role of the ATP-sensitive potassium current ($I_{KATP}$) in the timing and spatial pattern of electrical depression during LDVF in a structurally normal canine heart. We analyzed endo-, mid-, and epicardial unipolar electrograms and epicardial optical recordings in the left ventricle of isolated canine hearts during 10 min of LDVF in the absence (control) and presence of an $I_{KATP}$ blocker glybenclamide (60 μM). In all myocardial layers, average VFR was the same or higher in glybenclamide-treated than in control hearts. The difference increased with time of LDVF and was overall significant in all layers ($P < 0.05$). However, glybenclamide did not significantly affect the transmural VFR gradient. In epicardial optical recordings, glybenclamide shortened diastolic intervals, prolonged action potential duration, and decreased the percentage of inexcitable area (all differences $P < 0.001$). During 10 min of LDVF, asystole occurred in 55.6% of control and none of glybenclamide-treated hearts ($P < 0.05$). In three hearts paced after the onset of asystole, there was no response to LV epicardial or atrial pacing. In structurally normal canine hearts, $I_{KATP}$ opening during LDVF is a major factor in the onset of local and global inexcitability, whereas it has a limited role in overall deceleration of VFR and the transmural VFR gradient.

adenosine 5′-triphosphate-sensitive potassium channel; glybenclamide; myocardial ischemia; optical mapping

VENTRICULAR FIBRILLATION (VF) is a major cause of sudden cardiac death and a common context of cardiopulmonary resuscitation. In the setting of out-of-hospital cardiac arrest, VF intervention is often delayed for at least several minutes until first responders arrive at the scene, detect cardiac rhythm, and initiate life-saving procedures. Such relatively long-duration VF (LDVF) is characterized by a nonuniform depression of electrical activity, manifested as a transmural gradient in VF rate (VFR) in canine (2, 6, 14, 30, 43, 56, 62, 67) and human (37) hearts. An extreme form of heterogeneous electrical depression was observed in epicardial optical maps, where sharply demarcated inexcitable areas emerged within the fibrillating myocardium (62). Heterogeneous loss of excitability may promote initiation of VF upon reperfusion of a globally ischemic heart (1).

Untreated, LDVF eventually degenerates into asystole, a complete cessation of electrical activity in the heart. In the context of out-of-hospital cardiac arrest, asystole is a "non-shockable" rhythm associated with a very poor prognosis of survival to hospital discharge (22, 25, 44). In recent years, the reported incidence of asystole as the first recorded rhythm during sudden cardiac arrest (SCA) has increased compared with the incidence of VF (8, 48). This may indicate a trend towards faster degeneration of VF into asystole in the clinical setting. Considering that the window of opportunity for successful resuscitation is limited to ~10 min after the onset of SCA (52), the rapidity at which electrical depression develops during the course of LDVF may have a significant impact on survival in this setting.

The factors determining the timing of local and global electrical standstill in the course of LDVF remain largely unknown. One of the most prominent mechanisms linking metabolic stress and electrical activity during ischemia is the ATP-sensitive potassium current ($I_{KATP}$; Ref. 17). $I_{KATP}$ is principally regulated by the blocking effect of ATP and activating effect of MgADP but is also modulated by a plethora of signaling pathways (17). The complexity of $I_{KATP}$ regulation at least partially explains the difficulty to pinpoint the actual events and conditions that trigger opening of the channel during ischemia. A possible role of $I_{KATP}$ in the maintenance of LDVF was recently highlighted by Farid et al. (15). These authors found that blockade of $I_{KATP}$ in hearts explanted from patients with end-stage heart failure resulted in an increased incidence of spontaneous VF termination, an overall decrease in VFR, and a diminished transmural difference in VFR compared with control conditions. The authors attributed these effects of glybenclamide to the prevention of the action potential duration (APD) shortening presumably caused by $I_{KATP}$ activation in this model of LDVF (15). Furthermore, these authors suggested that $I_{KATP}$ blockade could be a rational strategy to improve outcomes of SCA caused by VF. The importance of their results notwithstanding, the study by Farid at al. has left several important questions unanswered. First, their study was performed in hearts explanted from patients with end-stage heart failure, which is an extreme and terminal condition even within the population afflicted with this disease. Moreover, in these patients VF is not a predominant rhythm causing SCA (35); thus LDVF in these hearts may not be representative of the cases of SCA due to VF, which are often a consequence of acute triggering events occurring in hearts without advanced structural abnormalities (7). Second, they studied the effect of $I_{KATP}$ blockade only during the first 3 min of LDVF, a time window that is much shorter than the typical interval between collapse and initiation of life-saving proce-

* T. G. Taylor and P. W. Venable contributed equally to this study.

Address for reprint requests and other correspondence: A. V. Zaitsev, Cardiovascular research and Training Institute,Univ. of Utah, 95 South 2000 East, Salt Lake City, UT 84112-5000 (e-mail: zaitsev@cvrti.utah.edu).

dures (54). The outcomes could be different at later stages of LDVF, which may be more relevant to out-of-hospital SCA. Third, the rhythm following VF termination was not reported. Clearly, if VF termination was followed by global inexcitability, such an outcome of $I_{KATP}$ blockade could hardly be considered beneficial. Lastly, APD prolongation by glybenclamide may not necessarily prolong the VF cycle length (VFCL). During LDVF, the excitation cycle lengths poorly correlates with APD and is largely determined by the length of diastolic intervals (DIs), which get progressively longer in the course of LDVF (30, 49, 62).

While ideally these questions would be addressed using hearts from human donors representing the general population, in practice this goal is hard to attain. Apart from the rarity of this research opportunity, it is almost impossible to control the history of ischemic or hypoxic exposure of human hearts rejected for the purposes of transplantation and made available for research. However, such exposure(s) may cause preconditioning effects that may not affect results obtained under normoxemic conditions but that may alter the outcomes of the tested LDVF (58). With the above considerations in mind we were motivated to perform a study aimed to ascertain the role of $I_{KATP}$ in the dynamics and outcomes of LDVF occurring in a structurally normal canine heart, which is close to human heart in terms of size, ionic channel make-up and Purkinje fiber distribution. In our study, we assessed the effects of $I_{KATP}$ blockade by glybenclamide on the transmural VFR gradient, APD derived from epicardial optical recordings, and the timing of the onset of local and global inexcitability in the course of LDVF. Contrary to the observations in explanted failed human hearts (15), we found that $K_{ATP}$ channel blockade did not significantly alter the transmural VFR gradient but delayed VF termination and maintained on average a slightly higher VF rate compared with control despite a slight increase in optical APD. Additional experiments were performed to exclude the role of side effects of glybenclamide with respect to other potassium currents such as the rapid component of the delayed rectifier current ($I_{Kr}$) and the transient outward current ($I_{to}$). We conclude that in structurally normal hearts $K_{ATP}$ channels are a major factor in the transition from a state of depressed excitability to complete electrical standstill, but they have a limited role in the transmural VFR gradient during LDVF. These results underscore the important differences in the effects of $I_{KATP}$ blockade in normal vs. severely failing hearts. Possible reasons for these differences are discussed.

## MATERIALS AND METHODS

This investigation conformed to the *Guide for the Care and Use of Laboratory Animals* published by the National Institutes of Health (NIH publication No. 85-23, revised 1996). The animal protocols were approved by the University of Utah Institutional Animal Care and Use Committee (Protocol No. 10-09005).

*Study groups.* A total of 28 dogs, 14 random source dogs (27.0 ± 1.3 kg, 9 males, 5 females) and 14 purpose-bred dogs (21.6 ± 0.8 kg, 7 males, 7 females) were used in this study. The source of dogs changed in the course of the study due to recently enacted institutional mandates. Nine hearts served as the control group. Six hearts were treated with an $I_{KATP}$ blocker glybenclamide (GLYB; 60 μM). To exclude the possibility that the observed effects of glybenclamide were confounded by partial blockade of $I_{Kr}$ (51), an additional six hearts were treated with a selective blocker of $I_{Kr}$ dofetilide (DOF; 1 μM). To exclude the possibility that the observed effects of glybenclamide were confounded by partial blockade of the transient outward potassium current $I_{to}$ (53) (26), a group of six hearts was treated with a combination of a $K_{ATP}$ channel opener chromakalim (10 μM) and $I_{to}$ blocker 4-aminopyridine (1 mM; CRO + 4AP). Assuming that glybenclamide at a concentration of 60 μM induces a significant degree of $I_{to}$ blockade, our comparison between CRO + 4AP and GLYB groups allowed us to contrast the effects of $I_{KATP}$ activation and blockade under relatively uniform conditions of $I_{to}$ inhibition. One additional heart was treated with cromakalim only and was used for assessment of the effect of this drug on VFR under conditions of normal perfusion and oxygenation.

*Experimental protocol.* The dogs were premedicated with acepromazine (0.1 ml/10 kg), Telazol (0.1 ml/kg), or propofol (7.45 mg/kg) and maintained with sodium pentobarbital (32.5 mg/kg). Intubation was accomplished with a cuffed endotracheal tube, and mechanical ventilation was maintained at 10–15 cycles/min (tidal volume: 15–20 cc/kg). Following isolation via midline sternotomy, the hearts were perfused in a Langendorff apparatus with a mixture of blood and Tyrode solution as described in detail in our previous publications (27, 68). Briefly, the blood-Tyrode mixture was oxygenated ($CO_2$ 5%-$O_2$ 95%), heated (37°C), and filtered using standard pediatric heart perfusion units from various vendors. Perfusate was collected for recirculation with collector tubes inserted into the right and the left ventricles via cuts in the appendages of the respective atria. The heart was then placed in a temperature-controlled bath with heated water-jacketed transparent glass walls. The bath was filled with warmed Tyrode solution, which was continuously pumped, without recirculation, at a rate of 80–150 ml/min. The oxygen content in the superfusate was removed by continuous gassing with a 95% $N_2$/5% $CO_2$ mixture. The temperatures in the right ventricular cavity, superfusate, and water jacket were maintained at 37 ± 0.5°C during both normal coronary perfusion and ischemia. The gradient of temperature across the left ventricular wall did not exceed 1°C. In all hearts, immediately preceding the induction of ischemia, the perfusion was switched to Tyrode solution with the dual purpose of ensuring constant composition of the extracellular milieu at the onset of LDVF and enhancing the voltage-sensitive signal for the purpose of improving resolution of low-amplitude signals at advanced stages of LDVF. VF was induced using a 9V DC battery 10 s to 5 min before the onset of global ischemia initiated by interruption of aortic perfusion. No perceptible differences in the measured parameters were found between experiments with respect to the duration of VF before the onset of ischemia; therefore, in all experiments the time of LDVF was counted from the moment when perfusion was stopped.

In the GLYB group, glybenclamide (60 μM) was added to the recirculating blood-Tyrode mixture 20–30 min before the onset of LDVF and its successful delivery to the heart was verified by observing an increase in the aortic pressure caused by the vasoconstricting effect of glybenclamide (12). In this study, the aortic pressure increased by 35 ± 5% after administration of glybenclamide. In the DOF group, dofetilide (1 μM) was added to the circulating solution 10 min prior to the onset of LDVF in six hearts. In the CRO + 4AP group, cromakalim (10 μM) and 4-aminopyridine (1 mM) were added to the recirculating mixture in alternating order 20 and 10 min before the onset of LDVF; in three hearts cromakalim was added first while in three more hearts 4-aminopyridine was added first. Thus, in a total of six hearts constituting the CRO + 4AP group, both cromakalim and 4-aminopyridine were present in the perfusate for ≥10 min before the onset of LDVF. In DOF and CRO + 4AP groups, brief (1-min) episodes of VF were induced before and 10 min after administration of each drug and VFR was measured during the last 4 s of 1-min VF episodes. In this way, the individual effects of all drugs on VFR in normally perfused hearts could be assessed. After that, VF was promptly terminated by a defibrillation shock with the remaining experimental protocol being the same as in control and GLYB groups.

In all experiments only data from the first 10 min of LDVF were compared. If asystole occurred with abrupt and continued silence (>60 s) during LDVF the right atrium, LV epicardium and LV

endocardium were paced at 3 and 10 times end-diastolic preischemic threshold to determine excitability.

*High-resolution epicardial optical mapping.* Details of optical mapping are given in our previous publication (62). Briefly, we used a high-resolution electron-multiplied CCD camera (iXon DU-860D; Andor Technology, Belfast, UK) to image fluorescence of the voltage-sensitive dye Di-4-ANEPPS (Molecular Probes, Carlsbad, CA). The field of view covered the epicardial surface of the anterior LV including a portion of the left anterior descending coronary artery (Fig. 1). The size of the field of view varied between 40 × 40 mm and 65 × 65 mm. To minimize motion artifacts, the heart was gently pressed against the glass chamber wall as previously described (27, 68). No electromechanical uncouplers were used. Five second-long movies were acquired every 30 s from 0 to 10 min of LDVF. To minimize phototoxicity, exposure to the excitation light was limited to 7 s per movie by means of an electronic shutter synchronized with the video camera.

*Analysis of optical signals.* Spatial distributions of VFR, APD, and DI at different time points during LDVF were estimated in optical mapping data using custom routines developed in PV-Wave software (Visual Numerics, Boulder, CO). Dominant frequency of the Fourier spectrum was not used to estimate VFR because it did not reliably represent the perceived number of activations per unit of time at advanced stages of LDVF when the action potential is characterized by very short APD and long DI. Instead, we used an algorithm to detect individual action potentials in single pixel recordings similar to that described in our previous publications (27, 62). In brief, the depolarization and repolarization phases of each optical action potential (OAP) were detected. The time points at which the depolarization and repolarization phases crossed a line drawn at 40% level of the absolute maximum in the respective signal ($\Delta F_{max}$) were determined. From these time points, APD, DI, and VFCL were calculated for each cycle. The algorithm rejected noise based on thresholds set for APD (<10 ms), VF cycle length (<30 ms), absolute O AP amplitude (<15 levels of brightness), and percent O AP amplitude with respect to the time sequence maximum (<5% of $\Delta F_{max}$). VFR maps were created by dividing the number of OAPs by the duration of the analyzed movie. Areas with no OAPs detected throughout the entire movie were considered to be inexcitable and having a VFR = 0. The lack of activation in continuous areas having VFR = 0 was confirmed by visual inspection of movies. Such areas were counted for the purposes of determining the average VFR and percentage of inexcitable area but were excluded from the calculation of average APD and DI.

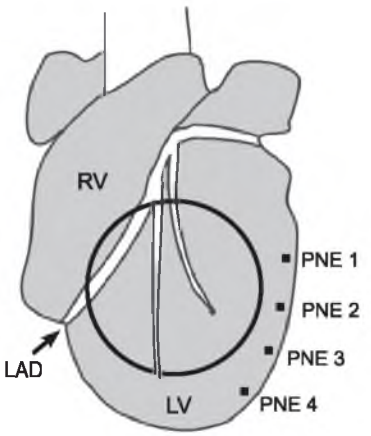


Fig. 1. Schematic representation of mapping modalities used in this study. Circle denotes the area imaged with the optical mapping system, including predominantly anterior left ventricular (LV) and a narrow region of right ventrice (RV; the latter was excluded from analysis). Black squares denote approximate positions of plunge needle electrodes (PNE 1-PNE 4). Electrodes were placed in the lateral LV close to the margin of the imaged area. LAD, left anterior descending coronary artery.

*Electrical recordings.* Volume-conducted ECG were recorded from two electrodes attached to the walls of the superfusion chamber with ground electrode attached to the bottom. Plunge needle electrodes with 10 evenly spaced unipolar leads (inter-lead, distance, 1.6 mm) were manufactured in-house following the design developed by Rogers et al. (50). The needles were placed in the lateral LV free wall adjacent to the optically mapped area as shown schematically in Fig. 1. The distance between needles was 10–15 mm. Unipolar electrograms from all contacts of the needle electrodes and volume-conductor ECG were recorded continuously during the first 10 min of LDVF at a sampling rate of 1 kHz using a custom-made multichannel data acquisition system as described previously (57). VF termination was defined as the first time point at which the ECG no longer showed VF/VT for 20 consecutive seconds. Asystole was defined as spontaneous VF termination and complete electrical silence (ECG signal indistinguishable from noise with amplitude <10% of ECG amplitude measured at 0 min of LDVF) lasting for ≥20 s.

*Electrode data analysis.* Unipolar electrograms were analyzed using custom software developed in the Matlab (MathWorks, Natick, MA) framework. The electrograms were first filtered using a 60-Hz notch filter. We applied the Hilbert Transform to unipolar electrograms as previously described (36, 41). Hilbert transform converts fluctuating voltage signal into its corresponding phase so that consecutive cycles of activation are represented by changes in phase from 0 to $2\pi$. Thus the number of phase transitions from $2\pi$ to 0 per unit of time gives an estimate of frequency. To decrease the influence of noise, the activation cycles with length <33 ms and amplitude of the waveform between two consecutive phase transitions <10% of the electrogram amplitude measured at 0 min of LDVF were excluded from the total cycle counts. After that, VFR was calculated as the average number of activations per second over 4-s intervals taken at 4 s after LDVF induction and at min 1 to 10 of LDVF. For simplicity, the first time point will be referred to as 0 min LDVF.

Whereas the length of the plunge needle electrodes was constant and designed to span the largest thickness observed in LV of the canine heart, the actual thickness of the ventricular wall is highly nonuniform. Thus in some cases plunge needle electrodes were longer than the wall thickness at the site of insertion. The contacts protruding from the ventricular wall were excluded from analysis based on the following criteria (62): *1*) leads with signal-to-noise ratio <200%; *2*) low VFR at 0 min of LDVF (slower by 5 Hz or more compared with the average VFR measured in all locations); *3*) decrease of VFR to below 2 Hz within the first min of LDVF; and *4*) observation of a progressively decreasing electrogram amplitude towards more distal leads while maintaining the same morphology as more proximal leads in the same needle. In the latter case, the most proximal lead from the group of leads with identical morphology was designated as the endocardial (ENDO) location in the needle. The position of the epicardial (EPI) lead could be easily ensured by visual inspection. In some experiments, the LV cavity was opened after the experiment and the positions of the ENDO leads in plunge needles were verified by visual inspection of the endocardium. After determination of the most distal lead in contact with the myocardial wall (ENDO), the mid-myocardial lead (MID) was chosen as the one closest to being equidistant between EPI and ENDO.

*Statistical analysis.* In the data collected from the plunge needle electrodes, the time course of VFR was statistically compared in a 2 × 3 matrix with dimensions of experimental group (control and GLYB) and location (EPI, MID, and ENDO) using a two-way ANOVA with post hoc multiple comparisons and Bonferroni correction. In each experiment, the data from EPI, MID, and ENDO locations were represented by average values from all four plunge needle electrodes inserted in the LV lateral wall (see Fig. 1). Note that


Fig. 2. Examples of volume-conducted ECGs obtained from a control heart with early asystole (*control A*), control heart with no asystole within 10 min of long-duration ventricular fibrillation (LDVF; *control B*) and a heart treated with glybenclamide (GLYB).

the statistical significance indicated the differences between the means at all time points of LDVF in different locations. No conclusions regarding differences at individual time points were made due to a prohibitively large number of required pairwise comparisons. In the data collected from optical recordings, average values of VFR, APD, DI, and percentage of inexcitable area were calculated for each time point during LDVF. A two-way ANOVA was performed with post hoc multiple comparisons and Bonferroni correction to compare the time courses of these parameters between control and GLYB groups. Similar to statistical treatment of the electrode data, the statistical significance indicated the differences between the mean values of measured parameters at all time points of LDVF. Timing of asystole was compared between control and GLYB hearts using a log-rank test applied to Kaplan-Meier survival curves. Comparisons of VFR between multiple groups at baseline and 10 min of LDVF were made using *t*-tests with Bonferroni correction for multiple pairwise comparisons. Data are given in mean ± SE. A difference at $P < 0.05$ was considered statistically significant.

## RESULTS

*Effect of glybenclamide on the timing of global asystole.* Figure 2 shows examples of volume-conducted ECG in two control hearts (*control A* and *control B*) and one GLYB heart. In the *control A* heart, the ECG shows abrupt termination of VF followed by the lack of any electrical activity. In *control B* and GLYB hearts, LDVF persists for the entire 10-min interval. In all cases, the event of asystole detected in volume-conductor ECG coincided with the lack of activity in all optical and electrical recordings.

Figure 3 shows the cumulative probability of asystole in the absence and the presence of glybenclamide (60 μM). It can be seen that in the absence of the drug the likelihood of asystole cumulatively increased between 4 and 10 min of LDVF reaching 55.6% (5 out of 9 hearts) by the end of the tested interval. In four out of five asystolic hearts, VF terminated abruptly. In one heart, VF was followed by ~30 s of ventricular tachycardia at a cycle length of ~360 ms followed by asystole. In contrast, in the presence of 60 μM glybenclamide asystole did not occur in six out of six hearts within the first 10 min of LDVF. The difference in the timing of asystole between control and glybenclamide-treated hearts was statistically significant ($P < 0.05$) by log-rank test.

In three control hearts that experienced complete asystole we applied pacing in LV EPI, LV ENDO and right atrium following VF termination. The stimulus strength was set at 3 times and 10 times preischemic end-diastolic excitation threshold. In two of three hearts, none of the locations elicited a response, while in one heart only LV ENDO responded, and only to the largest stimulus (10 times preischemic threshold). Thus asystole in these hearts was associated with profound depression of excitability.

*Effect of glybenclamide on the transmural VFR distribution.* Examples of transmural unipolar electrograms can be found in Fig. 4. Statistical analysis of transmural VFR distribution in the presence and the absence of glybenclamide is presented in Fig. 5. Figure 5, *A* and *B*, shows VFR values vs. time of no perfusion in different layers of LV wall (ENDO, MID, and EPI) in control and GLYB hearts, respectively. It is clear that an ENDO-to-EPI gradient in VFR was consistently present both in the absence and in the presence of glybenclamide. In both groups, most of the transmural VFR difference was concentrated between EPI and MID. Accordingly, both ENDO and MID were statistically different from EPI, but there was no statistical difference between ENDO and MID in both groups.

Figure 5*C* shows the time course of the transmural VFR gradient (estimated as the difference between ENDO and EPI) in the two groups derived from the same data as shown in Fig. 5, *A* and *B*. In the control group, the transmural VFR gradient reached peak at 7 min of LDVF and decreased again by 10 min of LDVF, when VFR in all layers converged to very low values (see Fig. 5*A*). Interestingly, the dynamics of VFR gradient in GLYB group was somewhat reciprocal to that in the control group, such that the maximal gradient was reached at 3 min, decreased between 3 and 8 min, and then increased again at 10 min of LDVF. In any case, the overall dynamics of the VFR gradient was not statistically different between GLYB and control groups.

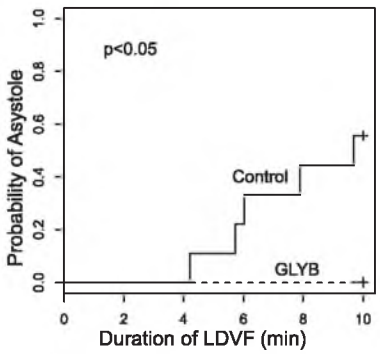


Fig. 3. Cumulative probability of asystole during 10 min of LDVF in the absence (solid line) and the presence (dashed line) of glybenclamide (60 μM). In control ~50% of hearts experienced asystole, whereas in the presence of glybenclamide asystole did not occur (significantly different at $P < 0.05$).

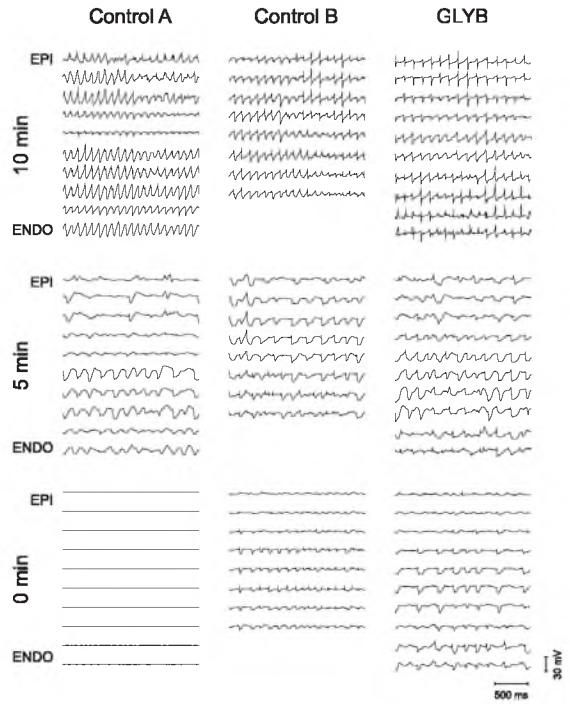


Fig. 4. Representative examples of unipolar electrograms from a plunge needle electrode spanning the thickness of the lateral LV wall during LDVF. *Control A* (*left column*) shows data from a control heart in which LDVF deteriorated to asystole. *Control B* (*center column*) show data from a control heart which maintained VF for at least 10 min of ischemia. GLYB (*right column*) shows data from a heart representing the glybenclamide group. At 0 min of ischemia (*top row*), VFR is similar between the different LV layers and between the *control A*, *control B*, and GLYB hearts. At 5 min of ischemia (*middle row*) an ENDO-to-EPI gradient (VFR faster in ENDO) develops in all hearts regardless of the absence or presence of glybenclamide. At 10 min of ischemia (*bottom row*), no activity can be seen in *control A* heart, whereas *control B* heart and GLYB heart still maintain electrical activity in ENDO and mid-myocardial leads (MID) but not EPI. Note that in the *control B* example only 8 electrograms are shown because the two most distal leads of the plunge needle were in the LV cavity and were not in contact with the myocardium. See text for more detail.

Figure 6 shows the same data as in Fig. 5, but this time the VFR curves are grouped by myocardial layer (EPI, MID, and ENDO). It can be seen that VFR in GLYB group was never lower, but became progressively higher than in control group throughout 10 min of LDVF. The divergence between control and GLYB groups was apparent first in ENDO (at ~1 min of LDVF) then in MID (at 2~3 min of LDVF) and then in EPI (at ~4 min of LDVF). The difference in VFR between control and GLYB groups was statistically significant in all layers.

*Effect of glybenclamide on the epicardial VFR, APD, DI, and percentage of inexcitable area.* While the electrode data described above enabled us to estimate the effect of glybenclamide on VFR in transmural layers of myocardium, optical mapping, albeit limited to the epicardial surface, enabled us to assess the effect of glybenclamide on APD, DI, and the extent of unexcited regions during LDVF (62). Examples of single pixel recordings are presented in Fig. 7. Figure 8 shows spatial distribution of VFR in a representative control (Fig. 8, *top*) and GLYB heart (Fig. 8, *bottom*). A palette of colors (from red to black) denotes different VFRs (from 11 to 0 Hz). Progressive decrease in VFR can be seen in both hearts; however, in the control heart the VFR decline occurs much faster. Focal loss of excitability emerges in the center of the mapped area as early as 4 min of LDVF and spreads to the entire mapped area by 5.5 min of LDVF. Later (at 8 min of LDVF), a small pocket of activity (VFR: ~1.5 Hz) reemerges in the right ventricular-septal area adjacent to the LAD, but it fails to activate LV. In contrast, in the representative GLYB heart (Fig. 8, *bottom*) activity is maintained in the entire mapped area throughout the first 10 min of LDVF. Note that a heterogeneous depression of activity is still present, but it does not reach the critical point of complete inexcitability.

Figure 9 shows the results of statistical analysis of OAPs obtained from the LV epicardium. Figure 9, *A–D*, shows the average values of VFR, APD, DI and percent of inexcitable

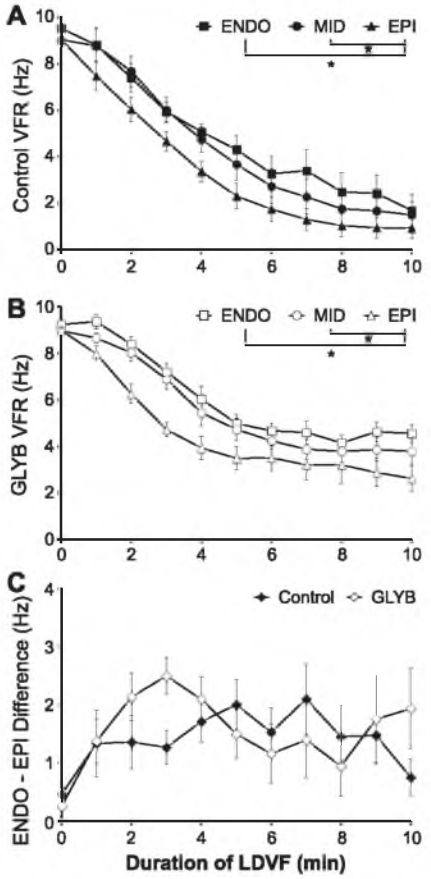


Fig. 5. Transmural distribution of VFR in LV during LDVF. *A* and *B*: VFR time course in ENDO (■, □), MID (●, ○), and EPI (▲, △) in control and glybenclamide groups, respectively. *C*: ENDO-EPI VFR difference in control and glybenclamide groups (derived from the same data as shown in *A* and *B*). ◆, controls; ◊ glybenclamide. *$P < 0.05$, significant difference between the curves by two-way ANOVA. Note that glybenclamide does not have a significant effect on the transmural VFR gradient.

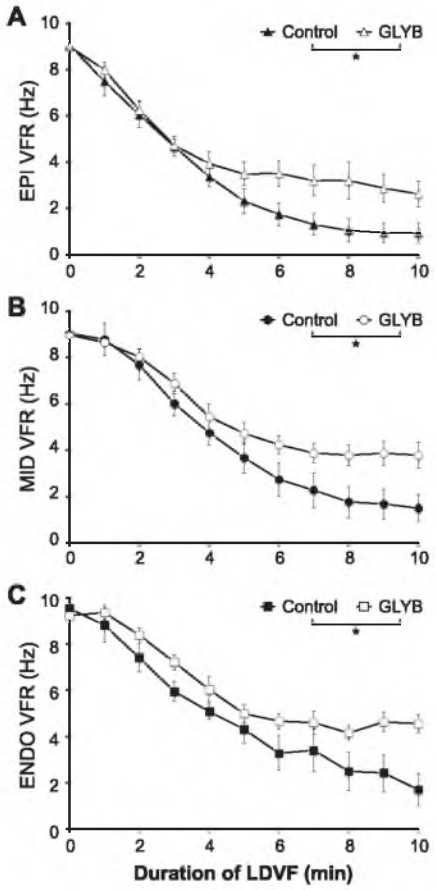


Fig. 6. Effect of glybenclamide on VFR time course in different layers of LV wall. Data are the same as in Fig. 5, but VFR curves are grouped by layer. *A–C*: represent EPI, MID, and ENDO, respectively. It is seen that glybenclamide maintained higher VFR in all layers, the difference increasing with the time of LDVF. This effect was statistically significant in all layers ($P < 0.05$).

area as a function of LDVF duration, respectively. It can be seen that glybenclamide postponed VFR decline in the epicardium; at each time point starting from 2 min of LDVF VFR was higher in GLYB than in control groups (Fig. 9*A*). The difference in VFR between control and GLYB groups increased with time reaching 1.5–2.0 Hz after 6 min of LDVF. Concomitant with VFR increase, glybenclamide significantly decreased average DI (Fig. 9*B*) while increasing APD (Fig. 9*C*). The most dramatic effect of glybenclamide treatment, however, was the prevention of local epicardial inexcitability (Fig. 9*D*). On average 57% of the mapped area in LV epicardium was inexcitable in control hearts vs. only 14% in GLYB hearts, by 10 min of LDVF. All differences shown in Fig. 9 were statistically significant ($P < 0.001$).

*Possible confounding effects of glybenclmide.* Figures 10 and 11 compare the VFR data obtained in control and GLYB groups with the data obtained from additional groups (CRO + 4AP and DOF, see MATERIALS AND METHODS), which served the purpose of addressing possible confounding effects of glybenclamide. In Fig. 10, VFR averaged across all myocardial layers was compared in the four groups during nonischemic VF (Fig. 10*A*) and at 10 min of ischemic VF (i.e., LDVF; Fig. 10*B*). In addition, Fig. 10*A* shows VFR measured in the presence of CRO and 4-AP alone, which was possible in CRO + 4AP group due to alternate order of the administration of the two drugs before the onset of LDVF (see MATERIALS AND METHODS). Figure 11 shows the VFR time course during LDVF in the four groups (control, GLYB, CRO + 4AP, and DOF). The data from control and GLYB groups are the same as in Figs. 5 and 6. VFR time course was compared among the four groups during late stage LDVF (from 5 to 10 min).

The first confounding factor to address is a substantial block of $I_{to}$ by glybenclamide at the concentration used in this study (26). It was shown that blockade of $I_{to}$ by 4-aminopyridine has a differential effect on the canine epicardium and endocardium during myocardial ischemia (33, 34), thus raising a possibility that $I_{to}$ could contribute to the transmural VFR gradient during LDVF. However, 4-aminopyridine is not selective and was also shown to be a potent blocker of $K_{ATP}$ (24). Thus the effects of both 4-aminopyridine and glybenclamide can be confounded by blockade, to various degrees, of both $K_{ATP}$ and $I_{to}$. In this situation we tested the effect of 4-aminopyridine on VFR in the presence of $K_{ATP}$ channel opener cromakalim. As shown in Fig. 10*A*, cromakalim very significantly increased VFR in nonischemic hearts (9.22 ± 0.27 vs. 19.00 ± 0.57 $P <$ 0.05). However, 4-aminopyridine did not have any significant effect on VFR in either untreated (9.22 ± 0.27 vs. 8.78 ± 0.40) or cromakalim-treated (19.00 ± 0.57 vs. 17.57 ± 0.76) hearts under conditions of normal perfusion (see Fig. 10*A*). Despite the fact that during nonischemic VF the hearts from CRO + 4AP group had a much higher VFR than GLYB group, at 10 min of ischemic VF (LDVF) the relationship was reversed, that is, VFR in CRO + 4AP group was significantly lower than in GLYB group (0.40 ± 0.21 vs. 3.66 ± 0.33, $P < 0.05$; see Fig. 10*B*). As can be seen in Fig. 11, the reversal of the difference in VFR between the two groups occurred around ~4 min of LDVF. Collectively, these observations can be interpreted as follows: *1*) $K_{ATP}$ activation increases VFR in nonischemic hearts but decreases VFR at advanced stages of ischemia; *2*) $K_{ATP}$ blockade by glybenclamide prevents VFR decrease when $K_{ATP}$ channel is activated at advanced stages of ischemia; and *3*) $I_{to}$ blockade does not affect VFR regardless of opened or closed state of $K_{ATP}$ channel. These arguments are further substantiated in the DISCUSSION.

Another potential confounding factor is a partial blockade by glybenclamide of the rapid component of the delayed rectifier potassium current, $I_{Kr}$ (51). To address this issue, we treated six additional hearts with dofetilide (1 μM) before the onset of LDVF. As can be seen in Fig. 10A, dofetilide significantly decreased VFR in nonischemic hearts (9.22 ± 0.27 vs. 6.51 ± 0.24, $P < 0.05$). Also, at 10 min of LDVF VFR averaged across all layers was significantly lower in DOF group than in GLYB group (0.35 ± 0.29 vs. 3.66 ± 0.33, $P < 0.05$, see Fig. 10*B*). In fact, dofetilide caused a decrease in VFR in all layers throughout the entire episode of LDVF, the effect almost opposite to that of glybenclamide (see Fig. 11). Thus dofetilide did not reproduce the effects of glybenclamide in the setting of LDVF.

Finally, it should be noted that 6/6 GLYB hearts remained in VF, whereas only 4/9 Control, 2/6 CRO + 4AP, and 0/6 DOF hearts remained in VF at 10 min of ischemia. This further

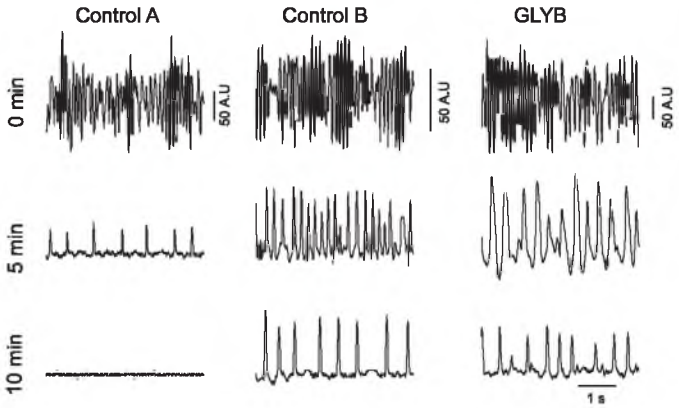


Fig. 7. Representative examples of single pixel recordings of optical action potential (OAPs) at different time points of LDVF. *Control A* (*left column*) shows data from a control heart in which LDVF deteriorated to asystole. *Control B* (*center column*) show data from a control heart which maintained VF for at least 10 min of ischemia. GLYB (*right column*) shows data from a heart representing glybenclamide group. At 0 min of ischemia (*top row*), high frequency activations with virtually absent diastolic intervals can be seen in all presented recordings. At 5 of ischemia (*middle row*), the OAP from *control A* heart exhibits a large degree of electrical depression manifested as very slow VFR and short APD amid very long diastolic interval (DI). At the same time, in both *control B* and GLYB hearts the respective OAPs exhibit more robust fibrillatory activity, albeit with slower VFR and longer DIs than at 0 min of LDVF. At 10 min of ischemia (*bottom row*), no activity is detectable in *control A* heart. In *control B* and GLYB hearts the fibrillatory activity is still present but VFR is slower and DIs are longer than at 5 min of LDVF. The large difference in the speed of electrical depression between the two selected control hearts is representative of large variation observed in the entire control group, which is also reflected in the large values of standard error in the measurements of DI and percentage of inexcitable area (see Fig. 9, *C* and *D*).

supports the unique role of glybenclamide in maintaining VF in structurally normal globally ischemic canine hearts.

## DISCUSSION

In this study we investigated the role of $K_{ATP}$ channels in the evolution of LDVF in structurally normal canine heart. The main finding is that $K_{ATP}$ channel blockade by glybenclamide significantly delayed the transition from depressed excitability to complete electrical standstill during LDVF. However, $K_{ATP}$ channel blockade had only modest effect on the speed of VFR decline and the transmural VFR gradient.

*Efficacy and specificity of glybenclamide as an $I_{KATP}$ blocker during LDVF.* It should be noted that efficacy of glybenclamide and other sulfonylureas may be limited in the presence of elevated intracellular ADP concentration ($[ADP]_i$) during ischemia, so that concentrations from 30 to 100 μM may be required to achieve significant blockade of $K_{ATP}$ channels (63). The extent of $[ADP]_i$ elevation during acute ischemia is not well known and may differ between different species and/or experimental models. Our experiments using glybenclamide in concentrations ~30 μM showed only marginal differences between treated and nontreated hearts (not shown) whereas other investigators were able to see effects of glybenclamide during ischemia with respect to various electrophysiological parameters at concentrations as low as 1–10 μM (3, 13, 46). However, most of the studies using low concentrations of glybenclamide were performed in isolated cells or thin superfused preparations. In our experiments, glybenclamide was delivered via coronary circulation which could reduce the effective concentration of the drug visible to cardiac myocytes due to drug binding with the membranes of blood cells and/or endothelium (9). Furthermore, the apparently lower efficacy of glybenclamide in our study could be due to more pronounced rise in $[ADP]_i$, presumably as a result of greater energy imbalance during LDVF as opposed to ischemia alone. In any case, the concentration of glybenclamide used in our study was sufficient to reveal a significant role of $K_{ATP}$ channels in the development of inexcitability and asystole during LDVF. However, we cannot exclude that the role of $I_{KATP}$ with respect to the speed of VFR decline and transmural VFR distribution during LDVF is larger than what can be inferred from the results of this study.

Whereas a relatively high concentration of glybenclamide (60 μM) was necessary to achieve a sufficient blockade of $K_{ATP}$, this concentration could also potentially block other channels. Previous studies (31) have shown that glybenclamide can also reduce both the sodium-potassium pump (Na-K pump) current and L-type calcium current ($I_{CaL}$) by ~18% at 60 μM. Despite the partial blockade of the Na-K pump Venkatesh et al. (63) have shown that during ischemia, high concentrations of glybenclamide (up to 100 μM) reduces extracellular $K^+$ accumulation, suggesting Na-K pump blockade plays a limited role, if any. It is unlikely that partial $I_{CaL}$ blockade by glybenclamide affected the main results of this study (delay of inexcitability and asystole), since decrease in $I_{CaL}$ should promote inexcitability because during ischemia $I_{CaL}$ plays a larger role in supporting propagation in partially depolarized myocardium (55). One could argue that an inhibition of $I_{CaL}$ by glybenclamide can preserve electrical activity by reducing contractility and thus energy expenditure during LDVF. However, glybenclamide at a concentration similar to that used in this study (100 μM) actually moderately increases contractility in nonischemic hearts and does not affect the decline in contractility during ischemia (e.g., see Fig. 6 in Ref. 63). The increase in contractility by glybenclamide was also demonstrated in isolated ventricular myocytes (28). This effect occurred despite decrease in the peak $I_{CaL}$ and was associated with increase in intracellular calcium by a mechanism not fully understood

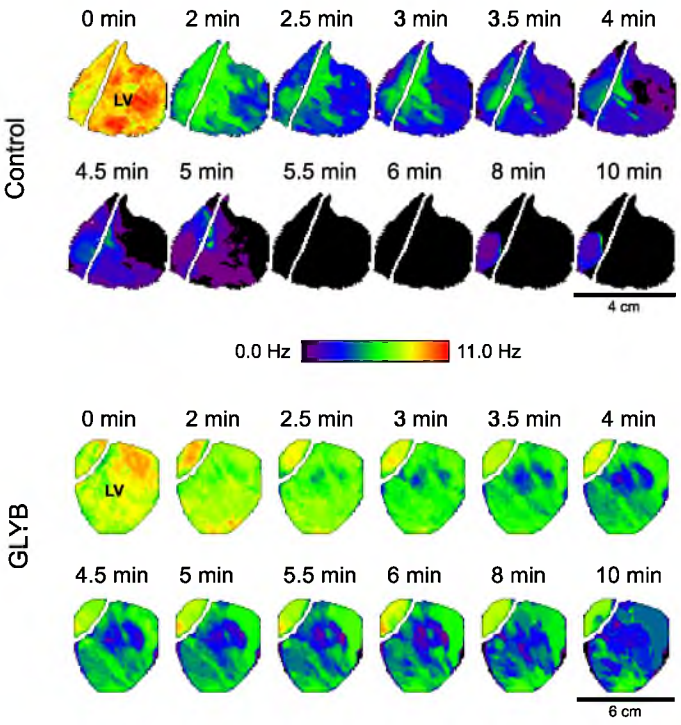


Fig. 8. Representative examples of VFR distribution maps derived from optical mapping of anterior LV during LDVF in a control (*top*) and a glybenclamide-treated (*bottom*) heart. Labels above the maps indicate the respective time points during LDVF. Colors (from black to red) indicate VFR in Hz (from 0 to 11 Hz). Note that the overall VFR decline occurs faster in the control than in the glybenclamide heart. Note also that in the control heart inexcitable areas (black) start to emerge as early as at 4 min of LDVF and culminate in complete absence of activation by 5.5 min of ischemia. At 8 min, highly localized and slow activity reemerges at the RV-septal junction but fails to activate LV. In GLYB heart, VFR decline occurs slower than in control and, despite VFR slowing, the entire mapped area maintains excitability throughout 10 min of global ischemia.

(28). Thus neither electrophysiological nor contractile factors associated with modest $I_{CaL}$ inhibition caused by glybenclamide can explain the outcomes of this study.

Another concern is a reported 40% reduction in $I_{Kr}$ in the presence of 60 μM glybenclamide (51). To address the potential effect of glybenclamide on $I_{Kr}$ during ischemia, we elected to determine what role $I_{Kr}$ blockade would play in electrical depression during LDVF. Dofetilide was chosen due to its properties as a highly specific and effective $I_{Kr}$ blocker: dofetilide blocks almost 100% of $I_{Kr}$ at 1 μM and has virtually no effect on the slow component of the delayed rectifying potassium current (5). Dofetilide shows dose-dependent block of

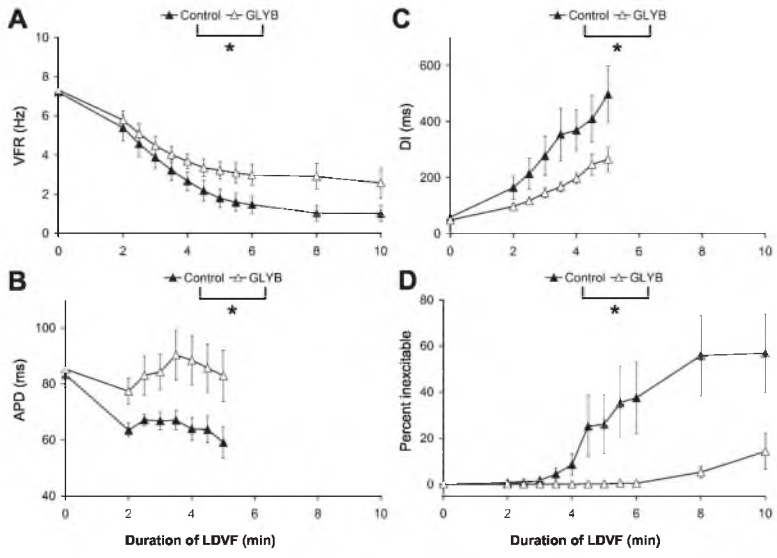


Fig. 9. Comparison of the time courses of VFR (*A*), DI (*B*), APD (*C*), and the percentage of inexcitable area (*D*) in epicardial optical maps during LDVF in control and GLYB hearts. $*P < 0.05$, statistically significant difference between the respective curves by two-way ANOVA.

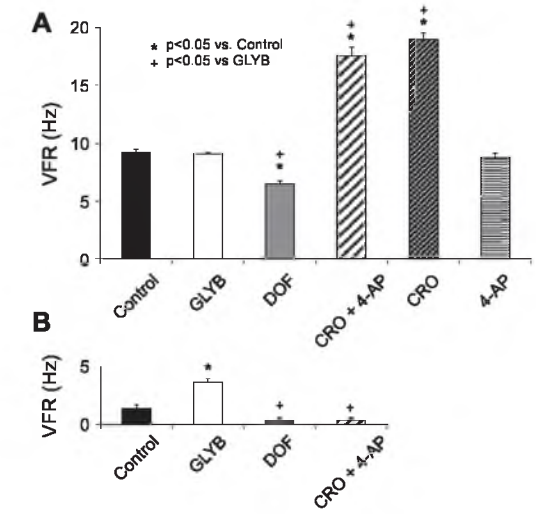


Fig. 10. Comparison of VFR averaged across all myocardial layers in different groups during nonischemic VF (*A*) and at 10 min of LDVF (*B*). GLYB, 60 μM; DOF, dofetilide (1 μM); CRO, cromakalim (10 μM); 4-AP, 4-aminopyridine (1 mM); CRO + 4AP, combination of cromakalim and 4-aminopyridine. See text for more detail.

$I_{KATP}$ but at much higher concentrations than what was used in our study ($EC_{50}$ of 51 ± 1 μM in inside-out patches, and lesser efficacy when dofetilide is applied outside the cell; Ref. 65). Comparing the effects of glybenclamide and dofetilide in our study suggests that potential blockade of $I_{Kr}$ by 60 μM glybenclamide does not affect the main phenomenon, since dofetilide lowered VFR whereas glybenclamide increased VFR (see Fig. 11). Also, dofetilide aborted LDVF in all experiments, whereas glybenclamide maintained LDVF in all experiments, within the tested 10-min interval. It is of interest that dofetilide appeared to preferentially decrease VFR in ENDO (see Fig. 11). Assuming a leading role of endocardial Purkinje fibers in maintaining LDVF in dog heart (56), the prominent antifibrillatory effect of dofetilide observed in this study could be explained in terms of efficient suppression of arrhythmic sources associated with ischemic Purkinje fibers. This intriguing possibility is beyond the scope of the current study but merits further investigation.

Another concern caused by the use of 60 uM of glybenclamide is the substantial (~60%) blockade of $I_{to}$ (26). It was suggested that $I_{to}$ plays an important role in setting up conditions for heterogeneous APD distribution and reentry during simulated ischemia by promoting loss of the action potential "dome" on the epicardium, which could be prevented by the $I_{to}$ blocker 4-aminopyridine (33, 34). Thus blockade of $I_{to}$ by glybenclamide could, in theory, contribute to the effects of glybenclamide on LDVF observed in this study. It should be noted however, that the effects of 4-aminopyridine on APD during ischemia were sensitive to stimulation rates and were largely absent at rates >2 Hz (the lower bound of activation rates observed during LDVF in our study). This can be explained by relatively slow reactivation kinetics of $I_{to}$ in canine ventricular myocytes (32) and/or reverse use dependence of block by 4-aminopyridine (4). In addition, the suggested role of $I_{to}$ was demonstrated only during "simulated" ischemia (33, 34) and was exclusively based on the effects of 4-aminopyridine, a relatively nonselective potassium channel blocker. At millimolar concentrations needed for efficient $I_{to}$ blockade 4-aminopyridine can cause significant inhibition of $I_{KATP}$ ($IC_{50}$ of 2.1 ± 0.3 mM; Ref. 24).

In our study, we tested the combined effects of 4-aminopyridine and a $K_{ATP}$ opener cromakalim. In nonischemic hearts, 4-aminopyridine did not have any significant effect on VFR both in the absence and in the presence of cromakalim (see Fig. 10*A*). This suggests that blockade by 4-aminopyridine of either $I_{to}$ or $K_{ATP}$ does not have any significant role in determining the excitation rate during VF. In contrast, activation of $K_{ATP}$ had a dramatic effect on VFR in nonischemic hearts, increasing VFR almost twofold over nontreated hearts. In the course of LDVF the difference in VFR between CRO + 4AP and GLYB groups progressively diminished until the VFR curves in the two groups crossed over, so that VFR in CRO + 4AP group became lower than in GLYB group (see Fig. 11). It is striking that whenever the effect of glybenclamide was detectable

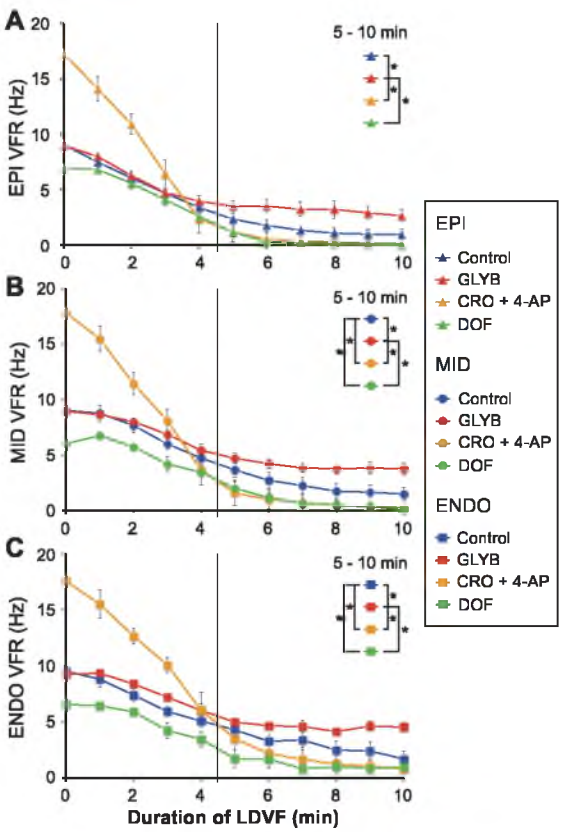


Fig. 11. VFR time course during LDVF in control, GLYB, CRO + 4AP, and DOF groups. Data from control and GLYB groups are the same as in Figs. 5 and 6. VFR time course was compared among the 4 groups during late stage LDVF (from 5 to 10 min) using a two-way ANOVA. *A–C*: represent EPI, MID, and ENDO, respectively. *Statistical differences between individual groups.

(namely, 2–4 min after the onset of LDVF) it was opposite to the effect exerted by the combination of cromakalim and 4-aminopyririne. Assuming that inhibition of $I_{to}$ was at least the same (or larger) in CRO + 4AP than in GLYB group, the polar difference between these two groups can hardly be explained in terms of $I_{to}$ blockade. Rather, this difference would be consistent with the idea that after 4 min of LDVF activation of $K_{ATP}$ by cromakalim further promotes electrical depression manifested as VFR decline, whereas blockade of $K_{ATP}$ by glybenclamide prevents that effect.

Summarizing arguments above, we conclude that the main effects of glybenclamide observed in this study, namely, maintenance of higher VFR and excitable state during LDVF are best explained in terms of $K_{ATP}$ blockade since among all known possible targets of glybenclamide only $K_{ATP}$ channel opening is relevant to loss of excitability during ischemia, as discussed in more detail below.

*$I_{KATP}$ and electrical depression during LDVF.* During myocardial ischemia, a number of factors promote depression of excitability and conduction failure including hyperkalemia, acidosis, and activation of $I_{KATP}$ (55). Opening of $K_{ATP}$ channels during LDVF may facilitate loss of excitability in two ways: first, by its contribution to the level of extracellular $K^+$ concentration ($[K^+]_o$) increase (66), and second, by creating conditions of source-sink mismatch when $I_{Na}$ is already reduced due to elevated $[K^+]_o$ (55). In isolated ventricular cardiomyocytes, complete loss of excitability can occur when $K_{ATP}$ is sufficiently activated in response to mitochondrial depolarization, even without any increase in $[K^+]_o$ (1). We are not aware of any published data regarding the dynamics of $[K^+]_o$ during LDVF. Although, in the center of the ischemic zone of regionally ischemic isolated canine hearts paced at cycle length of 350–450 ms, $[K^+]_o$ reached ~8 mM after 8 min of coronary occlusion (11). At that level of $K^+$ elevation, ~20% of unipolar electrograms in the ischemic zone exhibited "block" morphology (i.e., lack of negative intrinsic deflection), which can be interpreted as indicative of conduction block at the recording site. In our study, a similar percentage of inexcitable sites was achieved ~4 min earlier in the course of LDVF (see Fig. 9*D*). This comparison suggests that either the level of $[K^+]_o$ or the level of $I_{KATP}$ activation, or both, could be considerably higher during LDVF than ischemia alone, perhaps due to ionic and/or metabolic consequences of very high excitation rate.

*$K_{ATP}$ channel activation and heterogeneities in VFR and excitability during LDVF.* It has been shown that epicardial myocytes are more susceptible to the electrophysiological effects of ischemia than are endocardial cells, in particular with regard to ischemia-induced APD shortening. Several studies (19, 39, 40) have implicated the higher level of $K_{ATP}$ channel expression and/or activation on the epicardium in this phenomenon. In contrast to those earlier studies, Farid et al. (15) reported a higher expression of $K_{ATP}$ subunits in the endocardium of failing human hearts, which was consistent in their study with preferential effect of glybenclamide (slowing of the excitation rate during LDVF ) in the endocardium. The authors attributed this effect to preferential prolongation of APD by glybenclamide in endocardial cells but provided very limited evidence to support that statement.

In our study, pretreatment with glybenclamide slightly prolonged APD in the epicardium during the combination of VF and ischemia, which is consistent with the known effect of $I_{KATP}$ blockade with respect to APD during ischemia alone. However, this was of little consequence for the dynamics of VFR. If prolongation of APD were the only effect of glybenclamide, then we would expect a prolongation of VFCL (hence, a decrease in VFR). On the contrary, epicardial VFCL shortened and VFR increased in the presence of glybenclamide, despite prolongation of APD although concomitant with shortening of DI. Therefore, at least in the epicardium, the effect of glybenclamide on VFR was determined by its effect on DI. Using intramural optrodes, Kong et al. (30) recently showed that the activation rate during LDVF in all layers of the ventricular wall was predominantly determined by DI amid a relatively constant APD. Unfortunately, we did not have means to measure the effect of glybenclamide on APD and DI during LDVF in intramural layers. However, extrapolating the results obtained with optical mapping on the epicardium, it is likely that the VFR increase observed in mid- and endocardial electrograms in the presence of glybenclamide is also associated with shortening of DI.

In light of previous studies suggesting differential properties of $K_{ATP}$ channels in the endocardium vs. epicardium (39, 40). it is surprising that $K_{ATP}$ channel blockade did not affect the transmural VFR gradient in our study (see Fig. 5). If the VFR gradient were predominantly due to transmural differences in $K_{ATP}$ activation, then blockade of this channel should have abolished the gradient. In fact, such abolishment was observed during LDVF in explanted failed human hearts (15), in stark contrast to our results (possible reasons for this discrepancy will be discussed below). The lack of effect of glybenclamide in our study indicates that other factor(s) are sufficient to create conditions for the VFR gradient during LDVF in the structurally normal canine heart. Note that once a VFR gradient is established due to these other factors, the (presumably) higher availability of $K_{ATP}$ channels in the epicardium can be offset by a lower value of total depolarization time in the epicardium due to fewer action potentials with shorter APDs. As a result, even though more channels are opened, the total current over a period of time will be small because most of the time the membrane potential will be close to the potassium equilibrium potential. Factors contributing to the transmural VFR gradient during LDVF may include transmural differences in properties of $I_{Na}$ inactivation (10); transmural distribution of mechanical stress (20, 64) with attendant changes in the function of stretch-activated channels and other channels, including $K_{ATP}$ (60, 61); lower expression of connexin 43 in the epicardium compared with deeper layers of the ventricular wall (47); and heterogeneous expression/function of several other channels and tranporters [for more detailed discussion, see our previous publication (62)].

Even though $K_{ATP}$ channel blockade markedly reduced the percentage of inexcitable area, it did not remove local (at the scale of millimeters) heterogeneities observed with optical mapping in the epicardium. Such local heterogeneities in the degree of electrical depression during LDVF may be related to spatially heterogeneous elevation of $[K^+]_o$, which can be observed even during global ischemia (29). The reasons for small-scale heterogeneities in the electrophysiological effects of (apparently uniform) global ischemia remain unknown.

*Role of $K_{ATP}$ channel in asystole and outcomes of resuscitation.* During global ischemia associated with cardiac arrest of any etiology, asystole should inevitably occur, if not intervened, as a natural step towards death. However, the timing and the circumstances of asystole do matter. In the setting of out-of-hospital sudden cardiac arrest (OHSCA), asystole is not treatable with defibrillation shock and is associated with an extremely low rate of survival (23). In recent years, the incidence of asystole as the initial presenting rhythm remained the same or increased, amid a robust decrease in the incidence of VF (8, 48). At this point, one can only speculate what has caused the change in the proportion between VF and asystole in the OHSCA population. In most cases, the rhythm precipitating cardiac arrest in the out-of-hospital setting is not known. Recordings obtained from postmortem interrogation of Holter monitors, implantable cardioverter defibrillators, or implantable loop recorders in selected groups of patients with prior history of heart disease showed that from 40 to 80% of these patients had VF as the terminal rhythm at the time of unexpected death (21, 35, 38). The incidence of VF as the rhythm preceding death was generally lower in patients with advanced stages of heart failure (35) and higher in patients with prior myocardial infarction (21). It should be noted that the high-risk sudden cardiac death patients being monitored either in hospital or ambulatory are likely to be different from the residents in the general community that have sudden cardiac death, often as the very first manifestation of heart disease (7). Thus it is very difficult to estimate at this point what proportion of asystole in OHSCA is due to early transition from VF to asystole as opposed to asystole as a culmination of severe bradycardia and pulseless electrical activity (45). However, in both scenarios the mechanism of rapid deterioration to asystole may involve enhanced activation of $I_{KATP}$, which may affect not only ventricles but also atria and/or the specialized conducting system of the heart. At least in the three asystolic hearts where we attached pacing and recording electrodes to the right atrium, atria did not show any spontaneous activity and did not respond to stimulation after VF termination. This observation warrants closer attention to the role of supraventricular tissues in the events occurring during cardiac arrest. Indeed, suppression of the sinus node activity due to activation of $I_{KATP}$ (18) alone may be sufficient to prevent restoration of spontaneous circulation under these conditions. These assumptions have to be tested in future studies.

Our study shows that activation of $I_{KATP}$ is a major determinant of asystole as the outcome of LDVF. That is, blockade of $K_{ATP}$ channel supports maintenance of VF within the clinically relevant time window. This is consistent with a previous study by Tang et al. (58) using an open-chest rat model of resuscitation, where activation of $K_{ATP}$ channel either by use of a $K_{ATP}$ channel agonist or by ischemic preconditioning promoted spontaneous VF termination. In our study, however, VF termination was followed by asystole (adverse outcome) whereas in that study it was followed by restoration of sinus rhythm (benign outcome). The discrepancy may be due to differences between species and/or experimental conditions. However, it brings up an important point that in the setting of LDVF the net effect of $K_{ATP}$ channel activation/blockade depends on the balance between the effects with respect to VF dynamics and the effects with respect to generation and delivery of the sinus node impulses to the ventricles.

*Comparison to explanted cardiomyopathic human heart.* A recently published study by Farid et al. (15) investigated the role of $I_{KATP}$ in the dynamics and the outcome of LDVF induced in Langendorff-perfused hearts explanted from human patients with end-stage heart failure. The difference between our study and that by Farid et al. is quite striking; essentially, the results are opposite in many respects. The most important difference is that in our study glybenclamide prevented VF termination, whereas in their study this drug promoted VF termination in the globally ischemic heart. In our study, there was no major effect of glybenclamide with respect to the difference in excitation rate during LDVF between ENDO and EPI; in their study, this difference was effectively eliminated by glybenclamide. Lastly, in our study, there was no detectable effect of glybenclamide at the onset of LDVF; in their study that effect was profound (see their Fig. 4*A*).

The latter difference, in fact, may be key to the discrepant results. Excluding trivial explanations in terms of unintentional metabolic stresses associated with various stages of preparation preceding the actual experiment, the prominent effect of glybenclamide in an essentially nonischemic heart may be related to the fact that the hearts at advanced stages of dilated cardiomyopathy are metabolically compromised to such extent that $I_{KATP}$ is activated even without overt ischemia. This assumption would be consistent with reports indicating severe energy deprivation in failing hearts (42), and a possibility that $K_{ATP}$ channel regulation is altered in response to congestive heart failure (16).

Another factor in the difference between LDVF dynamics in normal vs. failing hearts (ignoring for the moment interspecies differences) may be related to downregulation of repolarizing potassium currents such as $I_{to}$ and $I_{Kr}$ in failing hearts (59). This may lead to a significant prolongation of APD, which in turn may slow down the excitation rate during VF. In agreement with this conjecture, blockade of $I_{Kr}$ with dofetilide in our model significantly decreased VF rate in both nonischemic and ischemic hearts (see Figs. 10 and 11). Moreover, dofetilide affected VF maintenance so that in two out of six hearts treated with dofetilide VF stopped spontaneously within 1 or 2 min after its induction (not shown), an event never observed in untreated canine hearts.

If the two assumptions mentioned above (downregulation of voltage-dependent potassium currents and an apparent upregulation of $I_{KATP}$ in failing human hearts) are correct, the difference between our study and that by Farid et al. could be explained in terms of different timing of $K_{ATP}$ activation in the two models and varying role of $I_{KATP}$ in LDVF dynamics depending on the stage of ischemia. Our data show that when $K_{ATP}$ is deliberately activated, its effect changes in the course of LDVF, which might depend on the magnitude of other detrimental factors of ischemia such as extracellular potassium accumulation. Namely, $K_{ATP}$ activation increases VFR in the early stage (3–4 min) and decreases VFR at the late stage (5–10 min) of LDVF (see Fig. 11). Based on the effects of $K_{ATP}$ blockade by glybenclamide, it appears that the principal difference between the normal canine heart and failing human hearts is the level of $K_{ATP}$ activation at the early stage of LDVF: high in failing human hearts vs. low in normal canine hearts. Note that the study by Farid et al. (15) was limited to only the first 3 min of LDVF, the time frame when $K_{ATP}$ activation is expected to increase VFR and, conversely, $K_{ATP}$

blockade is expected to reduce VFR if $K_{ATP}$ channel is activated. Note also that in failing human hearts the very existence of sustained VF may require $K_{ATP}$ activation to overcome the antifibrillatory effect of dramatic APD prolongation caused by downregulation of repolarizing potassium currents. In this regard, it is interesting to note that prevalence of VF as the rhythm causing cardiac arrest is low in patients with advanced stages of heart failure compared with other cardiac conditions (21, 35, 38).

*Clinical implications.* Together with previous publications, our study underscores the very complex role of $K_{ATP}$ channel in cardiac arrest. While in the structurally normal canine heart, $K_{ATP}$ channel blockade supports maintenance of VF in globally ischemic heart (this study), in failing human heart the effect is exactly opposite: VF termination (15). The latter outcome is good only if it is followed by restoration of spontaneous rhythm, but is lethal if it is followed by asystole. $K_{ATP}$ channel activation can promote loss of excitability (this study) and postreperfusion arrhythmias (1), yet upon resuscitation and reperfusion enhanced $K_{ATP}$ channel activation can also afford better recovery of hemodynamics and, ultimately, survival (58). Future therapeutic strategies aimed at improving the outcomes of cardiac arrest must therefore address the challenge of separating the adverse effects of $K_{ATP}$ channel activation from the protective ones.

*Limitations.* Limitations related to the reduced blocking efficacy of glybenclamide in the presence of elevated $[ADP]_i$ (63) and potential blockade of $I_{Kr}$, $I_{to}$, and other nonspecific effects have been thoroughly addressed above. Other common limitations of the ex vivo model of LDVF, plunge needle electrodes, and optical mapping are discussed in our previous publications (27, 62).

## ACKNOWLEDGMENTS

We are indebted to Jayne H. Davis, Alicja Booth, and Nancy C. Allen for excellent technical support.

## GRANTS

This work was supported by National Heart, Lung, and Blood Institute Grants 5R01-HL-088444 and 1RO1-HL-103877 (to A..V. Zaitsev) and 1F32-HL-097576 (to J. Shibayama) and a Nora Eccles Treadwell Foundation Research Grant (to A. V. Zaitsev).

## DISCLOSURES

No conflicts of interest, financial or otherwise, are declared by the author(s).

## AUTHOR CONTRIBUTIONS

Author contributions: T.G.T. and A.V.Z. conception and design of research; T.G.T., P.W.V., J.S., M.W., and A.V.Z. performed experiments; T.G.T., P.W.V., and A.V.Z. analyzed data; T.G.T., P.W.V., J.S., M.W., and A.V.Z. interpreted results of experiments; T.G.T. and P.W.V. prepared figures; T.G.T. and A.V.Z. drafted manuscript; T.G.T. and A.V.Z. edited and revised manuscript; T.G.T. and A.V.Z. approved final version of manuscript.

## REFERENCES

1. **Akar FG, Aon MA, Tomaselli GF, O'Rourke B.** The mitochondrial origin of postischemic arrhythmias. *J Clin Invest* 115: 3527–3535, 2005.
2. **Allison JS, Qin H, Dosdall DJ, Huang J, Newton JC, Allred JD, Smith WM, Ideker RE.** The transmural activation sequence in porcine and canine left ventricle is markedly different during long-duration ventricular fibrillation. *J Cardiovasc Electrophysiol* 18: 1306–1312, 2007.
3. **Baker JE, Contney SJ, Gross GJ, Bosnjak ZJ.** KATP channel activation in a rabbit model of chronic myocardial hypoxia. *J Mol Cell Cardiol* 29: 845–848, 1997.
4. **Campbell DL, Qu Y, Rasmusson RL, Strauss HC.** The calcium-independent transient outward potassium current in isolated ferret right ventricular myocytes. II. Closed state reverse use-dependent block by 4-aminopyridine. *J Gen Physiol* 101: 603–626, 1993.
5. **Carmeliet E.** Voltage- and time-dependent block of the delayed K+ current in cardiac myocytes by dofetilide. *J Pharmacol Exp Ther* 262: 809–817, 1992.
6. **Cha YM, Uchida T, Wolf PL, Peters BB, Fishbein MC, Karagueuzian HS, Chen PS.** Effects of chemical subendocardial ablation on activation rate gradient during ventricular fibrillation. *Am J Physiol Heart Circ Physiol* 269: H1998–H2009, 1995.
7. **Chugh SS, Reinier K, Teodorescu C, Evanado A, Kehr E, Al Samara M, Mariani R, Gunson K, Jui J.** Epidemiology of sudden cardiac death: clinical and research implications. *Prog Cardiovasc Dis* 51: 213–228, 2008.
8. **Cobb LA, Fahrenbruch CE, Olsufka M, Copass MK.** Changing incidence of out-of-hospital ventricular fibrillation, 1980–2000. *JAMA* 288: 3008–3013, 2002.
9. **Conway MA, Nelson MT, Brayden JE.** 2-Deoxyglucose-induced vasodilation and hyperpolarization in rat coronary artery are reversed by glibenclamide. *Am J Physiol Heart Circ Physiol* 266: H1322–H1326. 1994.
10. **Cordeiro JM, Mazza M, Goodrow R, Ulahannan N, Antzelevitch C, Di Diego JM.** Functionally distinct sodium channels in ventricular epicardial and endocardial cells contribute to a greater sensitivity of the epicardium to electrical depression. *Am J Physiol Heart Circ Physiol* 295: H154–H162, 2008.
11. **Coronel R, Fiolet JW, Wilms-Schopman JG, Opthof T, Schaapherder AF, Janse MJ.** Distribution of extracellular potassium and electrophysiologic changes during two-stage coronary ligation in the isolated, perfused canine heart. *Circulation* 80: 165–177, 1989.
12. **Daut J, Maier-Rudolph W, von Beckerath N, Mehrke G, Gunther K, Goedel-Meinen L.** Hypoxic dilation of coronary arteries is mediated by ATP-sensitive potassium channels. *Science* 247: 1341–1344, 1990.
13. **Di Diego JM, Antzelevitch C.** Pinacidil-induced electrical heterogeneity and extrasystolic activity in canine ventricular tissues. Does activation of ATP-regulated potassium current promote phase 2 reentry? *Circulation* 88: 1177–1189, 1993.
14. **Dosdall DJ, Tabereaux PB, Kim JJ, Walcott GP, Rogers JM, Killingsworth CR, Huang J, Robertson PG, Smith WM, Ideker RE.** Chemical ablation of the Purkinje system causes early termination and activation rate slowing of long-duration ventricular fibrillation in dogs. *Am J Physiol Heart Circ Physiol* 295: H883–H889, 2008.
15. **Farid TA, Nair K, Masse S, Azam MA, Maguy A, Lai PF, Umapathy K, Dorian P, Chauhan V, Varro A, Al-Hesayen A, Waxman M, Nattel S, Nanthakumar K.** Role of KATP channels in the maintenance of ventricular fibrillation in cardiomyopathic human hearts. *Circ Res* 109: 1309–1318, 2011.
16. **Fedorov VV, Glukhov AV, Ambrosi CM, Kostecki G, Chang R, Janks D, Schuessler RB, Moazami N, Nichols CG, Efimov IR.** Effects of KATP channel openers diazoxide and pinacidil in coronary-perfused atria and ventricles from failing and non-failing human hearts. *J Mol Cell Cardiol* 51: 215–225, 2011.
17. **Flagg TP, Nichols CG.** Sarcolemmal K(ATP) channels: what do we really know? *J Mol Cell Cardiol* 39: 61–70, 2005.
18. **Fukuzaki K, Sato T, Miki T, Seino S, Nakaya H.** Role of sarcolemmal ATP-sensitive $K^+$ channels in the regulation of sinoatrial node automaticity: an evaluation using Kir6.2-deficient mice. *J Physiol* 586: 2767–2778, 2008.
19. **Furukawa T, Kimura S, Furukawa N, Bassett AL, Myerburg RJ.** Role of cardiac ATP-regulated potassium channels in differential responses of endocardial and epicardial cells to ischemia. *Circ Res* 68: 1693–1702, 1991.
20. **Gallagher KP, Osakada G, Matsuzaki M, Miller M, Kemper WS, Ross J Jr.** Nonuniformity of inner and outer systolic wall thickening in conscious dogs. *Am J Physiol Heart Circ Physiol* 249: H241–H248, 1985.
21. **Gang UJ, Jons C, Jorgensen RM, Abildstrom SZ, Haarbo J, Messier MD, Huikuri HV, Thomsen PE.** Heart rhythm at the time of death documented by an implantable loop recorder. *Europace* 12: 254–260, 2010.
22. **Hallstrom A, Herlitz J, Kajino K, Olasveengen TM.** Treatment of asystole and PEA. *Resuscitation* 80: 975–976, 2009.
23. **Hallstrom A, Rea TD, Mosesso VN Jr, Cobb LA, Anton AR, Van Ottingham L, Sayre MR, Christenson J.** The relationship between

shocks and survival in out-of-hospital cardiac arrest patients initially found in PEA or asystole. *Resuscitation* 74: 418–426, 2007.

24. **Haworth RA, Goknur AB, Berkoff HA.** Inhibition of ATP-sensitive potassium channels of adult rat heart cells by antiarrhythmic drugs. *Circ Res* 65: 1157–1160, 1989.
25. **Herlitz J, Svensson L, Engdahl J, Silfverstolpe J.** Characteristics and outcome in out-of-hospital cardiac arrest when patients are found in a non-shockable rhythm. *Resuscitation* 76: 31–36, 2008.
26. **Hernandez-Benito MJ, Maciankiene R, Sipido KR, Flameng W, Mubagwa K.** Suppression of transient outward potassium currents in mouse ventricular myocytes by imidazole antimycotics and by glybenclamide. *J Pharmacol Exp Ther* 298: 598–606, 2001.
27. **Huizar JF, Warren MD, Shvedko AG, Kalifa J, Moreno J, Mironov S, Jalife J, Zaitsev AV.** Three distinct phases of VF during global ischemia in the isolated blood-perfused pig heart. *Am J Physiol Heart Circ Physiol* 293: H1617–H1628, 2007.
28. **Khatib SY, Boyett MR.** Effects of glyburide (glibenclamide) on myocardial function in Langendorff perfused rabbit heart and on myocardial contractility and slow calcium current in guinea-pig single myocytes. *Mol Cell Biochem* 242: 81–87, 2003.
29. **Kim JJCS, Gabris B, Waggoner A, Salama G.** Optical measurements of extracellular potassium accumulation (EKA) during ischemia with new potassium sensitive dyes. *Heart Rhythm* 7: S261, 2010.
30. **Kong W, Ideker RE, Fast VG.** Transmural optical measurements of Vm dynamics during long-duration ventricular fibrillation in canine hearts. *Heart Rhythm* 6: 796–802, 2009.
31. **Lee SY, Lee CO.** Inhibition of $Na^+$-$K^+$ pump and L-type $Ca^{2+}$ channel by glibenclamide in Guinea pig ventricular myocytes. *J Pharmacol Exp Ther* 312: 61–68, 2005.
32. **Liu DW, Gintant GA, Antzelevitch C.** Ionic bases for electrophysiological distinctions among epicardial, midmyocardial, and endocardial myocytes from the free wall of the canine left ventricle. *Circ Res* 72: 671–687, 1993.
33. **Lukas A, Antzelevitch C.** Differences in the electrophysiological response of canine ventricular epicardium and endocardium to ischemia. Role of the transient outward current. *Circulation* 88: 2903–2915, 1993.
34. **Lukas A, Antzelevitch C.** Phase 2 reentry as a mechanism of initiation of circus movement reentry in canine epicardium exposed to simulated ischemia. *Cardiovasc Res* 32: 593–603, 1996.
35. **Luu M, Stevenson WG, Stevenson LW, Baron K, Walden J.** Diverse mechanisms of unexpected cardiac arrest in advanced heart failure. *Circulation* 80: 1675–1680, 1989.
36. **Massé S, Downar E, Chauhan V, Sevaptsidis E, Nanthakumar K.** Ventricular fibrillation in myopathic human hearts: mechanistic insights from in vivo global endocardial and epicardial mapping. *Am J Physiol Heart Circ Physiol* 292: H2589–H2597, 2007.
37. **Masse S, Farid T, Dorian P, Umapathy K, Nair K, Asta J, Ross H, Rao V, Sevaptsidis E, Nanthakumar K.** Effect of global ischemia and reperfusion during ventricular fibrillation in myopathic human hearts. *Am J Physiol Heart Circ Physiol* 297: H1984–H1991, 2009.
38. **Mitchell LB, Pineda EA, Titus JL, Bartosch PM, Benditt DG.** Sudden death in patients with implantable cardioverter defibrillators: the importance of post-shock electromechanical dissociation. *J Am Coll Cardiol* 39: 1323–1328, 2002.
39. **Miyoshi S, Miyazaki T, Asanagi M, Moritani K, Ogawa S.** Differential role of epicardial and endocardial K(ATP) channels in potassium accumulation during regional ischemia induced by embolization of a coronary artery with latex. *J Cardiovasc Electrophysiol* 9: 292–298, 1998.
40. **Miyoshi S, Miyazaki T, Moritani K, Ogawa S.** Different responses of epicardium and endocardium to KATP channel modulators during regional ischemia. *Am J Physiol Heart Circ Physiol* 271: H140–H147. 1996.
41. **Nash MP, Mourad A, Clayton RH, Sutton PM, Bradley CP, Hayward M, Paterson DJ, Taggart P.** Evidence for multiple mechanisms in human ventricular fibrillation. *Circulation* 114: 536–542, 2006.
42. **Neubauer S.** The Failing Heart - An Engine Out of Fuel. *N Engl J Med* 356: 1140–1151, 2007.
43. **Newton JC, Smith WM, Ideker RE.** Estimated global transmural distribution of activation rate and conduction block during porcine and canine ventricular fibrillation. *Circ Res* 94: 836–842, 2004.
44. **Olasveengen TM, Samdal M, Steen PA, Wik L, Sunde K.** Progressing from initial non-shockable rhythms to a shockable rhythm is associated with improved outcome after out-of-hospital cardiac arrest. *Resuscitation* 80: 24–29, 2009.
45. **Parish DC, Dinesh Chandra KM, Dane FC.** Success changes the problem: why ventricular fibrillation is declining, why pulseless electrical activity is emerging, and what to do about it. *Resuscitation* 58: 31–35, 2003.
46. **Picard S, Rouet R, Ducouret P, Puddu PE, Flais F, Criniti A, Monti F, Gerard JL.** KATP channels and "border zone": arrhythmias: role of the repolarization dispersion between normal and ischaemic ventricular regions. *Br J Pharmacol* 127: 1687–1695, 1999.
47. **Poelzing S, Akar FG, Baron E, Rosenbaum DS.** Heterogeneous connexin43 expression produces electrophysiological heterogeneities across ventricular wall. *Am J Physiol Heart Circ Physiol* 286: H2001–H2009, 2004.
48. **Polentini MS, Pirrallo RG, McGill W.** The changing incidence of ventricular fibrillation in Milwaukee, Wisconsin (1992–2002). *Prehosp Emerg Care* 10: 52–60, 2006.
49. **Robertson PG, Huang J, Chen KA, Chen X, Dosdall DJ, Tabereaux PB, Smith WM, Ideker RE.** Increased cycle length during long-duration ventricular fibrillation is caused by decreased upstroke velocity as well as prolonged refractoriness. *Heart Rhythm* 6: 378–384, 2009.
50. **Rogers JM, Melnick SB, Huang J.** Fiberglass needle electrodes for transmural cardiac mapping. *IEEE Trans Biomed Eng* 49: 1639–1641, 2002.
51. **Rosati B, Rocchetti M, Zaza A, Wanke E.** Sulfonylureas blockade of neural and cardiac HERG channels. *FEBS Lett* 440: 125–130, 1998.
52. **Roth R, Stewart RD, Rogers K, Cannon GM.** Out-of-hospital cardiac arrest: factors associated with survival. *Ann Emerg Med* 13: 237–243, 1984.
53. **Schaffer P, Pelzmann B, Bernhart E, Lang P, Mächler H, Rigler B, Koidl B.** The sulphonylurea glibenclamide inhibits voltage dependent potassium currents in human atrial and ventricular myocytes. *Br J Pharmacol* 128: 1175–1180, 1999.
54. **Schneider T, Martens PR, Paschen H, Kuisma M, Wolcke B, Gliner BE, Russell JK, Weaver WD, Bossaert L, Chamberlain D.** Multicenter, randomized, controlled trial of 150-j biphasic shocks compared with 200- to 360-j monophasic shocks in the resuscitation of out-of-hospital cardiac arrest victims. *Circulation* 102: 1780–1787, 2000.
55. **Shaw RM, Rudy Y.** Electrophysiologic effects of acute myocardial ischemia. A mechanistic investigation of action potential conduction and conduction failure. *Circ Res* 80: 124–138, 1997.
56. **Tabereaux PB, Walcott GP, Rogers JM, Kim J, Dosdall DJ, Robertson PG, Killingsworth CR, Smith WM, Ideker RE.** Activation patterns of Purkinje fibers during long-duration ventricular fibrillation in an isolated canine heart model. *Circulation* 116: 1113–1119, 2007.
57. **Taccardi B, Punske BB, Macchi E, Macleod RS, Ershler PR.** Epicardial and intramural excitation during ventricular pacing: effect of myocardial structure. *Am J Physiol Heart Circ Physiol* 294: H1753–H1766, 2008.
58. **Tang W, Weil MH, Sun S, Pernat A, Mason E.** KATP channel activation reduces the severity of postresuscitation myocardial dysfunction. *Am J Physiol Heart Circ Physiol* 279: H1609–H1615, 2000.
59. **Tsuji Y, Opthof T, Kamiya K, Yasui K, Liu W, Lu Z, Kodama I.** Pacing-induced heart failure causes a reduction of delayed rectifier potassium currents along with decreases in calcium and transient outward currents in rabbit ventricle. *Cardiovasc Res* 48: 300–309, 2000.
60. **Van Wagoner DR.** Mechanosensitive gating of atrial ATP-sensitive potassium channels. *Circ Res* 72: 973–983, 1993.
61. **Van Wagoner DR, Lamorgese M.** Ischemia potentiates the mechanosensitive modulation of atrial ATP-sensitive potassium channels. *Ann NY Acad Sci* 723: 392–395, 1994.
62. **Venable PW, Taylor TG, Shibayama J, Warren M, Zaitsev AV.** Complex structure of electrophysiological gradients emerging during long-duration ventricular fibrillation in the canine heart. *Am J Physiol Heart Circ Physiol* 299: H1405–H1418, 2010.
63. **Venkatesh N, Lamp ST, Weiss JN.** Sulfonylureas, ATP-sensitive K+ channels, and cellular K+ loss during hypoxia, ischemia, and metabolic inhibition in mammalian ventricle. *Circ Res* 69: 623–637, 1991.
64. **Vetter FJ, McCulloch AD.** Mechanoelectric feedback in a model of the passively inflated left ventricle. *Ann Biomed Eng* 29: 414–426, 2001.
65. **West PD, Bursill JA, Wyse KR, Martin DK, Campbell TJ.** Effect of Dofetilide and d-Sotalol on the ATP-Sensitive Potassium Channel of Rabbit Ventricular Myocytes. *J Cardiovasc Pharmacol Ther* 1: 307–312, 1996.

66. **Wilde AA, Escande D, Schumacher CA, Thuringer D, Mestre M, Fiolet JW, Janse MJ.** Potassium accumulation in the globally ischemic mammalian heart. A role for the ATP-sensitive potassium channel. *Circ Res* 67: 835–843, 1990.
67. **Worley SJ, Swain JL, Colavita PG, Smith WM, Ideker RE.** Development of an endocardial-epicardial gradient of activation rate during electrically induced, sustained ventricular fibrillation in dogs. *Am J Cardiol* 55: 813–820, 1985.
68. **Zaitsev AV, Guha PK, Sarmast F, Kolli A, Berenfeld O, Pertsov AM, de Groot JR, Coronel R, Jalife J.** Wavebreak formation during ventricular fibrillation in the isolated, regionally ischemic pig heart. *Circ Res* 92: 546–553, 2003.

# CHAPTER 5

## DOES THE COMBINATION OF HYPERKALEMIA AND KATP ACTIVATION DETERMINE EXCITATION RATE GRADIENT AND ELECTRICAL FAILURE IN THE GLOBALLY ISCHEMIC FIBRILLATING HEART?

The research in this chapter was published in the *American Journal of Physiology: Heart and Circulatory Physiology*. Tyson G. Taylor, Paul W. Venable, Alicja Booth, Junko Shibayama, Alexey V. Zaitsev.: 'Does the combination of hyperkalemia and $K_{ATP}$ activation determine excitation rate gradient and electrical failure in the globally ischemic fibrillating heart?' Am J Physiol Heart Circ Physiol, 2013, 305, pp. H903-H912. Reprinted with permission of the American Physiological Society.

*Am J Physiol Heart Circ Physiol* 305: H903–H912, 2013.
First published July 19, 2013; doi:10.1152/ajpheart.00184.2013.

# Does the combination of hyperkalemia and $K_{ATP}$ activation determine excitation rate gradient and electrical failure in the globally ischemic fibrillating heart?

**Tyson G. Taylor, Paul W. Venable, Alicja Booth, Vivek Garg, Junko Shibayama, and Alexey V. Zaitsev**
*Nora Eccles Harrison Cardiovascular Research and Training Institute, University of Utah, Salt Lake City, Utah*

Submitted 8 March 2013; accepted in final form 16 July 2013

**Taylor TG, Venable PW, Booth A, Garg V, Shibayama J, Zaitsev AV.** Does the combination of hyperkalemia and $K_{ATP}$ activation determine excitation rate gradient and electrical failure in the globally ischemic fibrillating heart? *Am J Physiol Heart Circ Physiol* 305: H903–H912, 2013. First published July 19, 2013; doi:10.1152/ajpheart.00184.2013.—Ventricular fibrillation (VF) in the globally ischemic heart is characterized by a progressive electrical depression manifested as a decline in the VF excitation rate (VFR) and loss of excitability, which occur first in the subepicardium (Epi) and spread to the subendocardium (Endo). Early electrical failure is detrimental to successful defibrillation and resuscitation during cardiac arrest. Hyperkalemia and/or the activation of ATP-sensitive $K^+$ ($K_{ATP}$) channels have been implicated in electrical failure, but the role of these factors in ischemic VF is poorly understood. We determined the VFR-extracellular $K^+$ concentration ($[K^+]_o$) relationship in the Endo and Epi of the left ventricle during VF in globally ischemic hearts (Isch group) and normoxic hearts subjected to hyperkalemia (HighK group) or a combination of hyperkalemia and the $K_{ATP}$ channel opener cromakalim (HighK-Crom group). In the Isch group, Endo and Epi values of $[K^+]_o$ and VFR were compared in the early (0–6 min), middle (7–13 min), and late (14–20 min) phases of ischemic VF. A significant transmural gradient in VFR (Endo > Epi) was observed in all three phases, whereas a significant transmural gradient in $[K^+]_o$ (Epi > Endo) occurred only in the late phase of ischemic VF. In the Isch group, the VFR decrease and inexcitability started to occur at much lower $[K^+]_o$ than in the HighK group, especially in the Epi. Combining $K_{ATP}$ activation with hyperkalemia only shifted the VFR-$[K^+]_o$ curve upward (an effect opposite to real ischemia) without changing the $[K^+]_o$ threshold for asystole. We conclude that hyperkalemia and/or $K_{ATP}$ activation cannot adequately explain the heterogeneous electrical depression and electrical failure during ischemic VF.

extracellular potassium accumulation; myocardial ischemia; ventricular fibrillation; ATP-sensitive potassium channel; asystole

HETEROGENEOUS ELECTRICAL DEPRESSION and the eventual loss of excitability occurring in the course of cardiac arrest are major adverse outcomes determining the incidence of reperfusion arrhythmias (1) and asystole, with the latter usually being the point of ultimate failure in resuscitation practice (10). In the ex vivo blood-perfused canine heart, simulated cardiac arrest produced by a combination of ventricular fibrillation (VF) and global ischemia causes a prominent transmural gradient in the VF rate (VFR) followed by the emergence of inexcitable areas in the epicardium (Epi), which spread across the ventricular wall and culminate in global asystole within a clinically relevant timeframe (32, 34). The transmural VFR gradient is also present in explanted human hearts subjected to global ischemia and VF (9). Given the similarity between the canine heart and human heart, understanding the mechanisms of heterogeneous electrical depression in the canine model may help to improve the outcomes of resuscitation from cardiac arrest in patients, based on mechanistic knowledge.

Electrical depression during ischemia without VF has been studied for many years, and the classical teaching posits that the main factor determining excitability during ischemia is the elevation of the extracellular $K^+$ concentration ($[K^+]_o$; hyperkalemia), which leads to depolarization of the resting potential and a subsequent reduction in the availability of $Na^+$ channels for activation (30). Moreover, because $Na^+$ channel inactivation occurs at more negative potentials in the Epi than in the endocardium (Endo), even a transmurally uniform increase in $[K^+]_o$ can bring about a selective depression of Epi action potentials and transmural frequency-dependent conduction block (6). Thus, assuming that the primary sources of high-frequency activation during ischemic VF are harbored by Endo Purkinje fibers (8), global uniform hyperkalemia may be sufficient to explain the VFR gradient during ischemic VF. However, this possibility has not been tested in experiments. The second factor implicated in the loss of excitability during ischemia is activation of ATP-sensitive $K^+$ ($K_{ATP}$) channels, which, in theory, can oppose sarcolemmal depolarization caused by the opening of $Na^+$ channels to the degree at which spread of excitation becomes impossible, leading to so-called "sink block" (1). Moreover, the two factors (hyperkalemia and $K_{ATP}$ activation) in theory can be synergistic, such that in the presence of $K_{ATP}$ activation, conduction block would occur at lower $[K^+]_o$ than hyperkalemia alone (30). To the best of our knowledge, however, such synergism has not been tested in experimental studies.

Cardiac arrest secondary to VF presents a more complex context than ischemia alone because the high excitation rate of VF aggravates metabolic challenge by increasing energy demand (16) and can potentially contribute to ionic imbalances that develop in the course of ischemia. For example, it was shown that the high excitation rate present during atrial fibrillation causes a moderate but detectable elevation of $[K^+]_o$ even in the presence of coronary circulation (19). It is thus possible that VF in globally ischemic hearts would aggravate hyperkalemia, but the time course of $[K^+]_o$ elevation in ischemic VF has not yet been reported.

The relationship between ionic alterations caused by ischemia and the excitation rate of VF is complex and remains controversial. The VF cycle length, the inverse of VFR, is correlated with the duration of the refractory period, which, in turn, is determined by the sum of the action potential duration and the duration of the period after repolarization during which

Address for reprint requests and other correspondence: A. V. Zaitsev, Nora Eccles Harrison Cardiovascular Research and Training Institute, Univ. of Utah, 95 S. 2000 E., Salt Lake City UT 84112-5000 (e-mail: zaitsev@cvrti.utah.edu).

  

$Na^+$ channels recover from inactivation. The latter period, termed postrepolarization refractoriness, is extremely short under normal conditions but becomes a prominent component of the refractory period and a major determinant of VFR during ischemia (15, 34). Hyperkalemia causes a decrease in VFR (4. 17, 26), most likely due to an increase in postrepolarization refractoriness (26). In the rabbit heart, a moderate increase in $[K^+]_o$ (to 8 mM) appeared to be sufficient to reproduce the decrease in VFR caused by low-flow ischemia (4); however, the actual $[K^+]_o$ during ischemia was not measured, and the case of no-flow ischemia was not tested in that study.

If, indeed, hyperkalemia were sufficient for determining VFR during ischemic VF, this would leave no role for the direct effect of increased $K_{ATP}$ current. However, blockade of $K_{ATP}$ channels has been shown to modulate VFR during ischemic VF in the canine heart (32) and failing human heart (9). Of interest, the effects of the $K_{ATP}$ blocker glybenclamide on ischemic VFR were somewhat opposite in the two above-mentioned studies. In explanted failing human hearts, glybenclamide eliminated the transmural VFR gradient and facilitated the termination of ischemic VF (9). In contrast, in the ex vivo canine heart, glybenclamide had little effect on the transmural VFR gradient but postponed the termination of ischemic VF (32). The disparate outcomes of $K_{ATP}$ blockade in these studies could be related to differences in the (unknown) ischemic level of $[K^+]_o$, if the assumption of synergism between $K_{ATP}$ activation and hyperkalemia with regard to the reduction of excitability (30) is correct. It also cannot be excluded that the outcomes were confounded by the off-target effects of glybenclamide, although many of the possible nonspecific effects were ruled out in the canine model (32). Thus, the role of $K_{ATP}$ activation in VFR dynamics and loss of excitability during ischemic VF remains controversial.

This study was designed to test the hypothesis that hyperkalemia and/or $K_{ATP}$ activation can explain the transmural VFR gradient and loss of excitability observed during VF and no-flow ischemia in the ex vivo blood-perfused canine heart. The results of our study showed that even though a transmural $[K^+]_o$ gradient is present during ischemic VF, hyperkalemia alone cannot reproduce the VFR suppression observed during ischemic VF, especially in the Epi. Moreover, pharmacological $K_{ATP}$ activation alone or in combination with hyperkalemia produced an effect opposite to that of real ischemia: a VFR increase instead of a VFR decrease. These results suggest the presence of yet unknown but powerful ionic mechanisms of electrical depression during ischemic VF not mediated by hyperkalemia or $K_{ATP}$ activation. Possible additional/alternative mechanisms are discussed.

## METHODS

This investigation conformed with the National Institutes of Health *Guide for the Care and Use of Laboratory Animals* (NIH Pub. No. 85-23, Revised 1996) and was approved by the Institutional Animal Care and Use Committee of the University of Utah (Protocol No. 10–09005).

*Experimental protocol.* A total of 36 dogs (12 mongrel dogs and 24 purpose-bred dogs, weight: 24.6 ± 0.7 kg, 20 male and 16 female) were euthanized for this study. Animals were premedicated with acepromazine (0.4 mg/kg), propofol (8 mg/kg), or Telazol (9 mg/kg), and a deep plane of anesthesia was maintained with pentobarbital in all dogs (initial dose: 50 mg/kg, additional doses as needed to maintain deep anesthesia for the duration of surgery, <1 h). Hearts were exposed via a midline sternotomy and rapidly excised for perfusion on a Langendorff apparatus with a mixture of heparinized blood and Tyrode solution as previously described (12, 37). After isolation, hearts were placed in either a vapor chamber or immersed in Tyrode superfusion to maintain an Epi temperature of 37 ± 1°C. Twenty-six hearts were subjected to 20 min of ischemic VF by inducing VF with a 9-V battery 10 s before the onset of global ischemia initiated by the interruption of aortic perfusion (Isch group). In these hearts, $[K^+]_o$ increased naturally during ischemia and was measured using $K^+$-sensitive electrodes (see below). In the remaining 10 hearts, VF was induced the same way, and normal oxygenated perfusion was maintained in the fibrillating heart while $[K^+]_o$ was varied between 4 and 15 mM by altering $[K^+]$ in the perfusate. In five of these hearts, hyperkalemia was the only factor tested (HighK group). In the remaining five hearts, 20–34 μM cromakalim (a $K_{ATP}$ channel opener) was administered before $[K^+]_o$ was increased (HighK-Crom group). In the HighK and HighK-Crom groups, $[K^+]$ was increased stepwise by adding 1–3 ml of 600 mM KCl solution at a time to the recirculating blood-Tyrode mixture while the resulting $[K^+]$ in the perfusate was measured every 2–3 min using a NOVA 8 ion analyzer (Nova Biomedical, Waltham, MA). A VFR measurement was accepted for analysis if it was bracketed by two venous $[K^+]_o$ measurements within 0.5 mM of each other, and the average of the two $[K^+]_o$ values was used for analysis.

*$K^+$-sensitive electrodes and $[K^+]_o$ measurements.* $K^+$-sensitive electrodes were prepared following as close as possible the process described by Johnson et al. (13). However, the electrodes manufactured in this fashion turned out to be extremely fragile, with many not surviving the experimental protocol. To improve our success rate, the prepared electrodes were then housed in a 20-gauge hypodermic needle with an aperture exposing the sensing part of the $K^+$-sensitive electrode to the interstitial fluid (Fig. 1, *A* and *B*). The depth of the $K^+$-sensitive electrode could be adjusted by sliding the thin polymer tubing (arrow in Fig. 1*A*) along the shaft of the needle. The assembled $K^+$-sensitive electrode and housing are referred to as "$K^+$ needle" below.

$K^+$ needles were calibrated both before and after the experiment using 3 and 10 mM KCl solution; any electrode that showed a voltage shift outside the range of 30 ± 4 mV before or after the experiment was excluded as damaged, and the data collected was discarded. Figure 1*C* shows an example calibration of Endo and Epi $K^+$ needles. Note that both electrodes showed stable measurements over 30-min periods in both 3 and 10 mM KCl solution with an ~30-mV shift between solutions. The *inset* in Fig. 1*C* shows the rapid (in the order of seconds) response of the $K^+$ needles to the transition from 3 to 10 mM solution. Millivolt values were converted to millimolar values using the Nernst equation [for details of the calibration, see Johnson et al. (13)]. Since the calibration constant could be slightly different pre- and postexperiment, we used the average of the pre- and post-experimental calibration values for conversion purposes. In addition, the response of $K^+$ needles placed in hearts was tested by adding a bolus of 600 mM KCl solution to the recirculating blood-Tyrode mixture. Figure 1*D* shows an example of recordings from Endo and Epi $K^+$ needles (squares and triangles, respectively) verified by measurements using a blood ion analyzer (large Xs). The initial value of $[K^+]_o$ in the perfusate was 2.2 mM. The indicated target concentration was calculated based on the estimated dilution factor. The two vertical dashed lines indicate the timing of bolus injection and washout. Washout was performed by replacing ~700 ml of the $K^+$-enriched perfusate with an equivalent amount of a surplus blood-Tyrode mixture. Since all of the blood with elevated $[K^+]$ could not be removed (due to the limited volume of the blood-Tyrode mixture), the final $[K^+]$ remained elevated (5.4 mM) compared with before the $K^+$ bolus (2.2 mM). Note, however, that during steady-state conditions both before and after the $K^+$ bolus there was a close match between $[K^+]$ values obtained by $K^+$ needles and the blood ion analyzer.

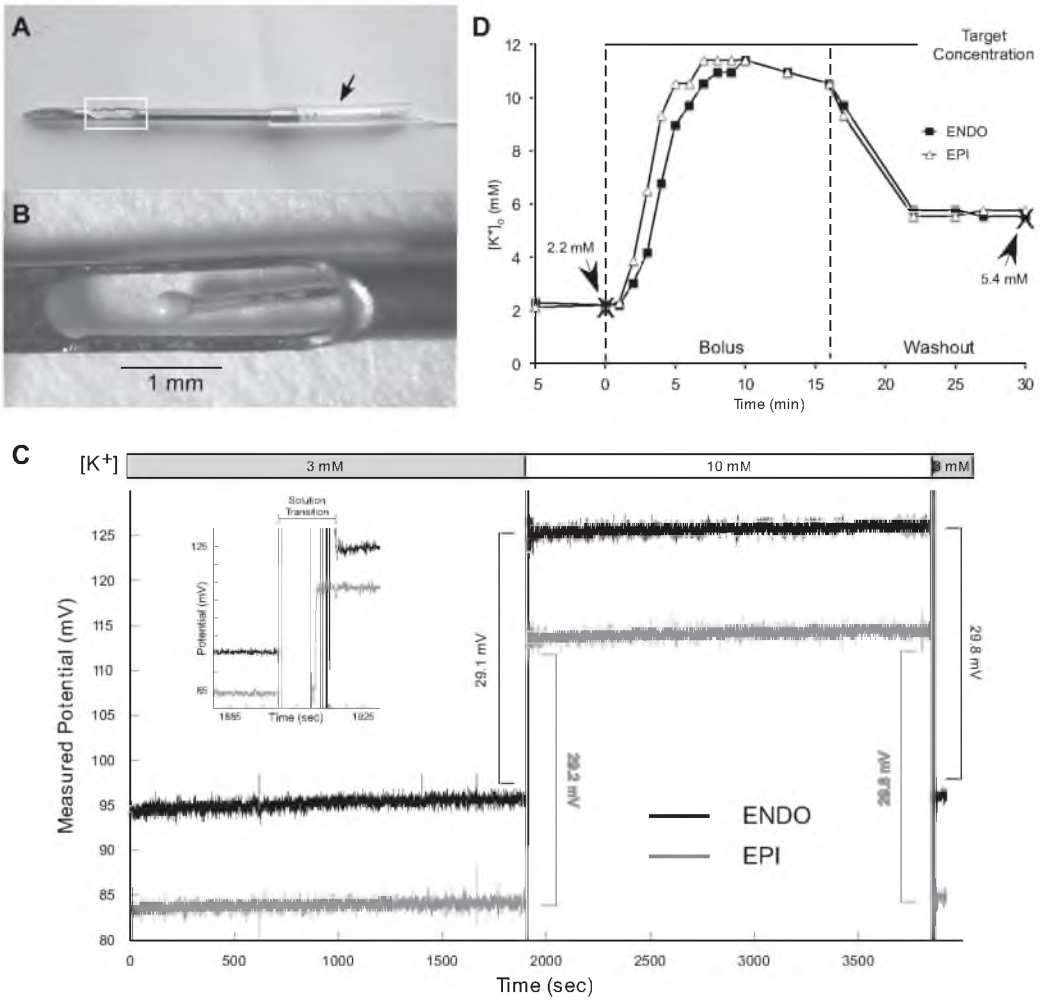


Fig. 1. Custom-made $K^+$-sensitive electrodes. *A*: $K^+$-sensitive electrodes were enclosed in a 20-gauge hypodermic needle that contained a window (white box) that exposed the $K^+$ sensor to the myocardial tissue. The polymer tubing (arrow) could be moved along the shaft of the needle to adjust the position of the $K^+$ sensor at the desired distance from the epicardial (Epi) surface. *B*: close up of the sensing part of the $K^+$ needle indicated by the white box in *A*. This design provided both adjustable depth and protection for the delicate sensor. *C*: example of calibration of endocardial (Endo) and Epi $K^+$ needles. Note that both electrodes showed stable measurements over 30-min periods in both 3 and 10 mM KCl solution with an ~30-mV shift between solutions. The *inset* shows the rapid (in the order of seconds) response of the $K^+$ needles to the transition from 3 to 10 mM solution. *D*: response of Endo (squares) and Epi (triangles) $K^+$ needles placed in a heart to a bolus of 600 mM KCl solution added to the recirculating blood-Tyrode mixture. The indicated target concentration was calculated based on the estimated dilution factor. The two vertical dashed lines indicate the timing of bolus injection and (partial) washout. Note that during steady-state conditions both before and after the KCl bolus, there was a close match between extracellular $K^+$ concentration ($[K^+]_o$) values obtained by $K^+$ needles and those obtained using the blood ion analyzer (large Xs).

$K^+$ needles were placed in the anterior left ventricular (LV) free wall. Epi $K^+$ needles were manufactured to have the sensor reliably submerged into the tissue, and the actual depth of the Epi $[K^+]_o$ measurement was ~3 mm from the epicardial surface. The depth of the Endo $[K^+]_o$ measurement could not be determined at the moment of the needle insertion due to the trabeculated structure of the LV Endo (in our estimates, the thickness of the LV wall varied between 5 mm at the thinnest part and 20 mm at locations where the papillary muscles were attached to the LV free wall). Thus, it was not possible to have a fixed depth of the sensing aperture in Endo $K^+$ needles. To address the irregular thickness of the LV free wall and to make sure that the sensing portion of the $K^+$ needle was located close to the Endo surface, we used two complementary approaches. First, we performed "pacing threshold mapping" using one of the multicontact plunge needle electrodes used for recording unipolar electrogams across the LV wall (see below). In essence, we applied pacing stimuli to consecutive pairs of adjacent leads (starting from the most Endo leads: 1 and 2, 2 and 3, etc.) and measured the end-diastolic threshold for excitation. Based on the observation that Endo pacing thresholds were typically the lowest across the LV wall and very high in the LV cavity (not shown), the pacing cathode location yielding the lowest excitation threshold between 5 and 16 mm from the Epi surface was

considered to be the best estimate for the Endo location. With this estimate, the depth of the sensing window on the Endo $K^+$ needle was adjusted by sliding the Epi cuff (see arrow in Fig. 1*A*) along the shaft of the needle, and the needle was inserted within 2 mm of the multicontact electrode used for the pacing mapping. Second, to obtain the actual position of sensors in Endo $K^+$ needles, we exposed the LV Endo after finishing our experimental protocol and visually determined the distance of the sensing portion of the $K^+$ needles from the Endo. The accepted Endo $[K^+]_o$ measurements were collected at a distance of 1–6 mm from the Endo surface. One to three Epi $K^+$ needles and one to three Endo $K^+$ needles were used in each experiment, with the goal of having at least one measurement from both the Endo and Epi after discarding any electrodes not meeting our requirements for calibration and the intramural position of the sensor. In those experiments in which two or (rarely) three acceptable $K^+$ recordings were obtained either from the Epi or Endo, the data from these individual measurements were averaged to represent the respective layer in that particular experiment.

*Electrical recordings and analysis.* Plunge needle electrodes with 10 evenly spaced unipolar leads (interlead distance: 1.6 mm) were manufactured in house following the design developed by Rogers et al. (27). Ten needles were placed across the anterior surface of the heart, and three needles in close proximity to the $K^+$ needles were chosen for analysis. The distance between needles was 10–15 mm. Unipolar electrograms from all contacts of the needle electrodes were recorded continuously during the first 20 min of ischemic VF at a sampling rate of 1 kHz using a custom-made multichannel data-acquisition system (31). Unipolar electrograms were analyzed using custom software developed in the Matlab (Mathworks, Natick, MA) framework. Electrograms were first filtered using a 60-Hz notch filter including several shorter harmonics. We applied the Hilbert transform to unipolar electrograms as previously described (18, 23, 32). Briefly, the Hilbert transform converts a fluctuating voltage signal into its corresponding phase so that consecutive cycles of activation are represented by changes in phase from $-2\pi$ to $2\pi$. Thus the number of phase transitions from $2\pi$ to $-2\pi$ gives an estimate of frequency. To decrease the influence of noise, activation cycles with a length of <33 ms and amplitude of the waveform between two consecutive phase transitions of <10% of the electrogram amplitude measured at 0 min of ischemic VF were excluded from the total cycle counts. After that, VFR was calculated as the average number of activations per second over 4-s intervals taken at 4 s after ischemic VF induction and at *minutes 1–20* of ischemic VF. For simplicity, the first time point is referred to as 0 min of ischemic VF. Local tissue was considered inexcitable if VFR was 0 Hz (no detectable activations). The percentage of Endo or Epi leads that were inexcitable was determined at each time point of ischemia.

Whereas the length of the plunge needle electrodes was constant and designed to span the largest thickness observed in the LV of the canine heart, as previously mentioned the actual thickness of the ventricular wall is highly nonuniform. Thus, in some cases, plunge needle electrodes were longer than the wall thickness at the site of insertion. In the beginning of this study, we used our elaborate set of criteria to exclude the contacts protruding from the ventricular wall based on the analysis of the electrograms that we previously described (34). However, in the vast majority of experiments, we determined the relationship between plunge needle length and LV wall thickness by visual inspection and wall thickness measurements after opening the LV cavity at the end of the experiments, simultaneous with determining the depth of sensor location in Endo $K^+$ needles.

*Plots of VFR and percentage of inexcitable sites versus $[K^+]_o$.* VFR and the percentage of inexcitable sites in the Endo and Epi were plotted against measured $[K^+]_o$ for all three experimental groups (Isch, HighK, and HighK-Crom groups). Data were grouped into increments of 1 mM $[K^+]_o$ for comparison. In some experiments from the HighK and HighK-Crom groups, $[K^+]_o$ measurements were sparse and were apart by >1 mM. In these cases, VFR and the percentage of inexcitable sites for intermediate $[K^+]_o$ values were linearly interpolated. In addition, in some early experiments from the HighK and HighK-Crom groups when full asystole was observed at $[K^+]_o$ between 10 and 15 mM, higher levels of $[K^+]_o$ were not tested. In those cases, we assumed that VFR would remain at 0 Hz and that the percentage of inexcitable sites would remain at 100%, for all $[K^+]_o$ above the highest $[K^+]_o$ for which asystole was actually observed.

*Statistical analysis.* All curves were compared using two-way ANOVA. The time course of VFR and $[K^+]_o$ during ischemic VF was compared separately for three phases: early (0–6 min), middle (7–13 min), and late (14–20 min) ischemia. Data are given as means ± SE. Differences of $P < 0.05$ were considered statistically significant.

## RESULTS

*Time course of $[K^+]_o$, VFR, and the occurrence of inexcitability during ischemic VF.* Figure 2*A* shows the time course of $[K^+]_o$ elevation in the Endo and Epi during ischemic VF. Extracellular $K^+$ accumulation started immediately upon the onset of ischemic VF and monotonically increased over the entire 20-min ischemic interval. The total increase ($\Delta[K^+]_o$) was greater in the Epi than in the Endo (8.3 vs. 6.6 mM). However, the Epi-to-Endo difference was statistically significant only during the late phase of ischemic VF (14–20 min). This relationship persisted when the Endo $[K^+]_o$ measurements used for analysis were limited only to those collected within 0–3 mm from the Endo surface (not shown). The transmural difference in VFR (Fig. 2*B*) was much more pronounced than the difference in $[K^+]_o$ and was statistically significant throughout all three phases of ischemic VF, consistent with previous studies (8, 34, 36). When measurements with VFR = 0 were excluded from analysis, the transmural VFR difference was overall similar and remained statistically significant throughout all three phases of ischemic VF (not shown). Figure 2*C* shows the percentage of electrodes with undetectable electrical activity (thus deemed inexcitable according to the formal criterion; see METHODS) as a function of ischemia duration. As shown in Fig. 2*C*, the prevalence of inexcitable sites steadily increased during ischemic VF in both the Endo and Epi, but at a much higher rate in the Epi than in the Endo. The transmural difference in this parameter was statistically significant during all three phases of ischemic VF. Note that the largest Endo-to-Epi difference in VFR and excitability was observed during the middle phase of ischemic VF (7–13 min), after which time point these parameters converged, indicating nearly complete electrical suppression by 20 min of ischemia.

*Relationship between $[K^+]_o$ and VFR under various experimental conditions.* To assess the role of hyperkalemia in the progressive VFR decline and eventual inexcitability during ischemic VF, we compared the relationship between VFR and $[K^+]_o$ during ischemic VF (Isch group), normoxic VF in the presence of hyperkalemia (HighK group), and normoxic VF in the presence of hyperkalemia in combination with the $K_{ATP}$ channel opener cromakalim (HighK-Crom group). In normoxic experiments, $[K^+]_o$ was varied between 4 and 15 mM. Note that in ischemic hearts, the elevated K+ concentration was achieved naturally, whereas in all other experiments it was adjusted by adding boluses of KCl to the perfusate (see METHODS).

Figure 3 shows examples of transmural unipolar electrograms recorded at approximately normal $[K^+]_o$ (3.7–4.3 mM;

*left*) and at high $[K^+]_o$ (9.1–9.4 mM; *right*) in the three experimental groups (from *top* to *bottom*: Isch, HighK, and HighK-Crom groups). Figure 3, *top left*, shows electrograms obtained at 0 min of ischemic VF when the level of $[K^+]_o$ was 3.7 mM. Figure 3, *top right*, shows electrograms obtained at 7 min of ischemic VF when the level of $[K^+]_o$ was 9.1 mM in the Epi and 9.3 mM in the Endo. As was the typical situation at 0 min and between 5 and 9 min of ischemic VF (see Fig. 2*A*), in this example, there was no significant difference between $[K^+]_o$ in the Epi and Endo. As shown in Fig. 3, at 0 min of ischemia and $[K^+]_o$ = 3.7 mM, there was no perceptible difference in VFR between the Epi and Endo. In contrast, at 7 min of ischemia and $[K^+]_o \sim 9$ mM, there was a drastic difference in VFR between the Epi and Endo, despite the relative uniformity of $[K^+]_o$. In fact, the outer half of the LV wall did not have detectable activations at all (VFR = 0).

Figure 3, *middle*, shows a representative example of transmural unipolar electrograms from a HighK heart subjected to $[K^+]_o$ = 3.7 mM (*left*) and $[K^+]_o$ = 9.3 mM (*right*). As shown in Fig. 3, *middle*, at both levels of $[K^+]_o$, VFR was uniform across the ventricular wall and the actual VFR was virtually unaffected by the increase in $[K^+]_o$ from 3.7 to 9.3 mM. Figure 3, *bottom*, shows a representative example of transmural unipolar electrograms from a HighK-Crom heart subjected to $[K^+]_o$ = 4.3 mM (*left*) and $[K^+]_o$ = 9.4 mM (*right*). As shown in Fig. 3, *bottom*, activation of $K_{ATP}$ channels by cromakalim induced a huge and transmurally uniform increase in VFR compared with the absence of the drug. Note that VFR remained exceedingly high even when $[K^+]_o$ was raised to 9.4 mM, with no appreciable transmural VFR gradient. Moreover, note the striking contrast between VFR during real ischemia (Fig. 3, *top right*) and VFR during hyperkalemia in combination with $K_{ATP}$ activation (Fig. 3, *bottom right*), despite the same level of $[K^+]_o$.

Figure 4*A* shows the statistical summary of the VFR-$[K^+]_o$ relationship in all three experimental groups. The different colors represent the different experimental groups; open triangles and solid squares represent Epi VFR and Endo VFR, respectively. The diagram shown in the *inset* in Fig. 4*A* shows relevant pairwise comparisons. The vertical brackets indicate statistically significant difference between the same layer in different experimental groups; the horizontal brackets indicate statistically significant difference between the Endo and Epi in the same experimental group. As shown in Fig. 4, in the HighK group (red), an appreciable decrease in VFR in both the Endo and Epi occurred only at $[K^+]_o$ exceeding 8 mM and VFR approached zero at $[K^+]_o$ between 12 and 14 mM. Even though

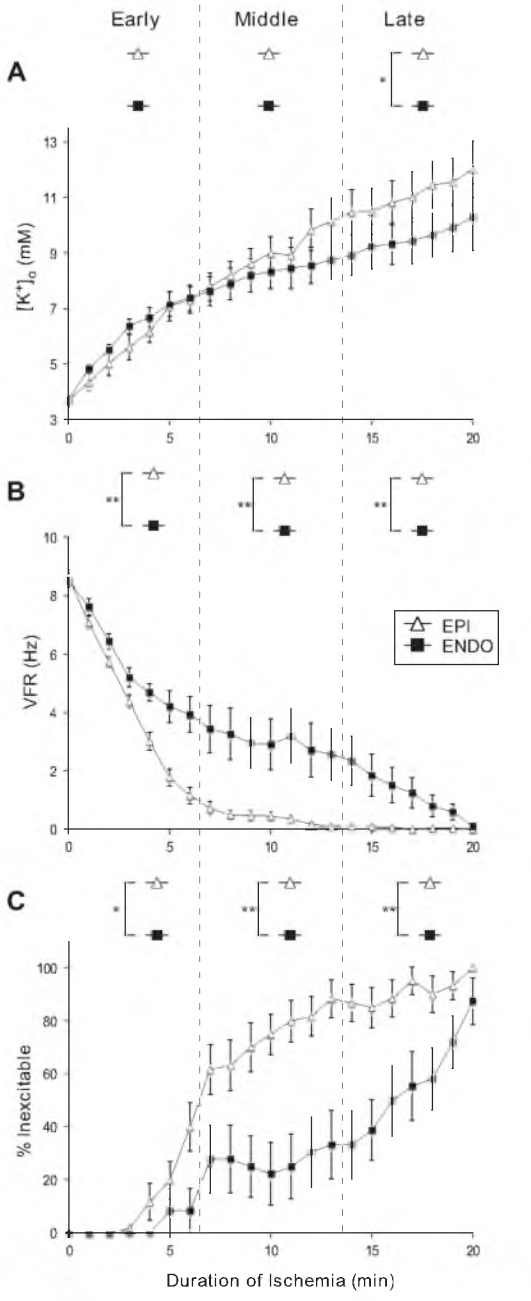


Fig. 2. Time course of $[K^+]_o$ (*A*), ventricular fibrillation (VF) rate (VFR; *B*), and the percentage of inexcitable sites (%Inexcitable; *C*) during 20 min of ischemic VF. The open triangles and filled squares represent the Epi and Endo, respectively. The vertical dashed lines denote the early, middle, and late phases of ischemic VF. *A*: $[K^+]_o$ progressively increased in both the Epi and Endo throughout 20 min of ischemic VF. Note that the difference between Endo and Epi $[K^+]_o$ was statistically significant ($P < 0.05$) only during the late phase of ischemic VF. *B*: time course of VFR decline. VFR decreased faster in the Epi than in the Endo, creating a prominent and statistically significant Endo-to-Epi difference during all phases of ischemic VF. The magnitude of the VFR gradient eventually decreased, as both Epi and Endo VFR values converged to zero by 20 min of ischemic VF. *C*: progressive increase in the percentage of inexcitable sites. The Epi showed a more rapid onset and greater extent of local inexcitability compared with the Endo, but both Endo and Epi locations approached 100% inexcitability by the end of 20-min episodes of ischemic VF. The Endo-to-Epi difference in the percentage of inexcitable sites was statistically significant during all phases of ischemic VF. Note the discrepancy between the dynamics of the $[K^+]_o$ gradient and the gradients of VFR and excitability: the largest transmural difference in the electrical parameters was observed when there was no transmural difference in $[K^+]_o$, and vice versa. *$P < 0.05$; **$P < 0.0001$.

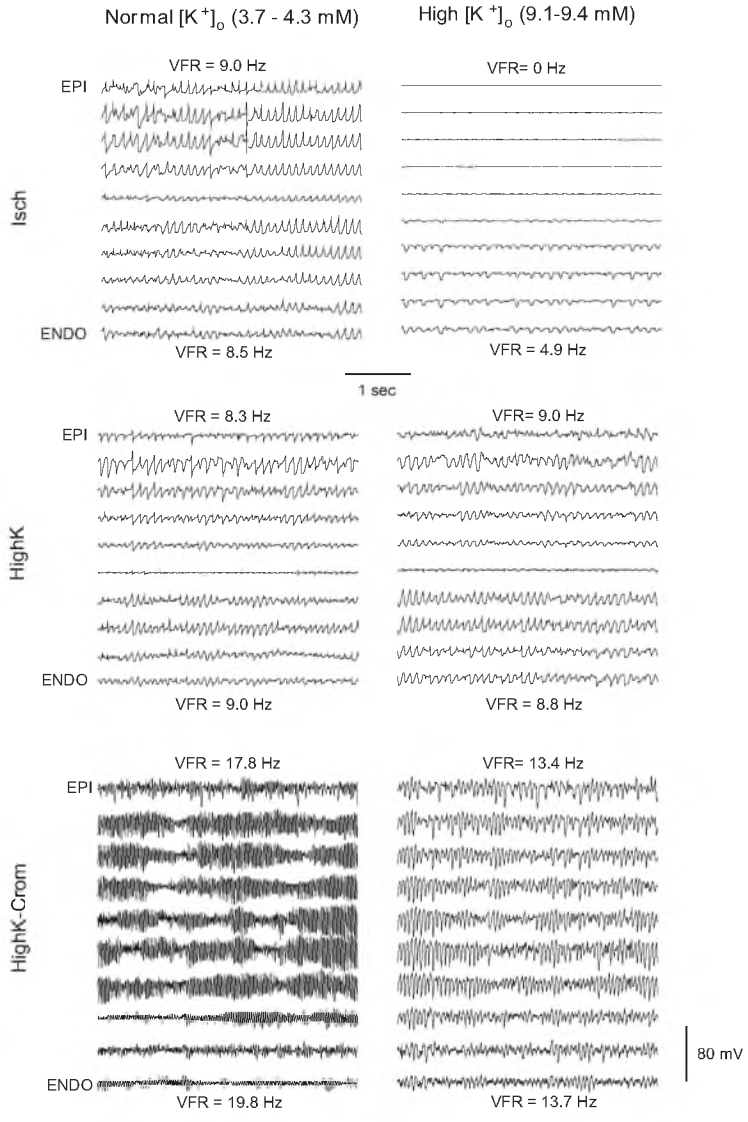


Fig. 3. Representative transmural unipolar electrograms from globally ischemic hearts (Isch group), normoxic hearts subjected to hyperkalemia (HighK group), and normoxic hearts subjected to a combination of hyperkalemia and the ATP-sensitive $K^+$ ($K_{ATP}$) channel opener cromakalim (HighK-Crom group) (*top* to *bottom*) at approximately normal $[K^+]_o$ (*left*) and elevated $[K^+]_o$ (*right*). Epi and Endo VFR values are shown next to the respective electrogram recordings. Note that at $[K^+]_o$ close to normal (3.7–4.3 mM), there were no appreciable transmural VFR gradients in any group, but $K_{ATP}$ activation in the HighK-Crom group caused a dramatic increase in VFR (*bottom left*). At high $[K^+]_o$ (9.1–9.4 mM), a prominent VFR gradient (with Epi VFR = 0) was observed only in the Isch group (*top right*) but not in the HighK or HighK-Crom groups. This suggests that the ischemic VFR gradient and regional inexcitability are not caused by hyperkalemia or $K_{ATP}$ activation.

Endo VFR appeared to be slightly higher than Epi VFR at each tested $[K^+]_o$, the difference was not statistically significant. In the Isch group (black in Fig. 4), the relationship between $[K^+]_o$ and VFR was profoundly different from that in the HighK group. First, at each $[K^+]_o$, VFR in the Isch group was lower than the respective VFR in the HighK group. Second, in the Isch group, there was also a large and significant difference in the sensitivity of VFR to $[K^+]_o$ between the Epi and Endo. Note that the average Epi VFR was much lower than the Endo VFR in the range of $[K^+]_o$ between 6 and 9 mM. Also, uniquely among all groups, the average Epi VFR in the Isch group was very slow (<1 Hz) starting from a concentration of $[K^+]_o$ equal to 8 mM. This made a stark contrast with the HighK group, in which at 8 mM $[K^+]_o$, Epi VFR was barely different from that observed at normal $[K^+]_o$.

The combination of hyperkalemia and $K_{ATP}$ activation by cromakalim (HighK-Crom group; blue in Fig. 4) poorly reproduced the VFR-$[K^+]_o$ relationship observed during ischemia. $K_{ATP}$ activation caused a massive increase in VFR, which was maintained at all $[K^+]_o$ between 4 and 11 mM, in contrast to VFR slowing observed in the Isch group. Even though in the HighK-Crom group there was a trend of slower VFR in the Epi than in the Endo, especially at $[K^+]_o$ between 7 and 8 mM, the transmural VFR difference was not statistically significant.

Figure 4*B* shows the statistical summary of the relationship between $[K^+]_o$ and the percentage of inexcitable LV locations

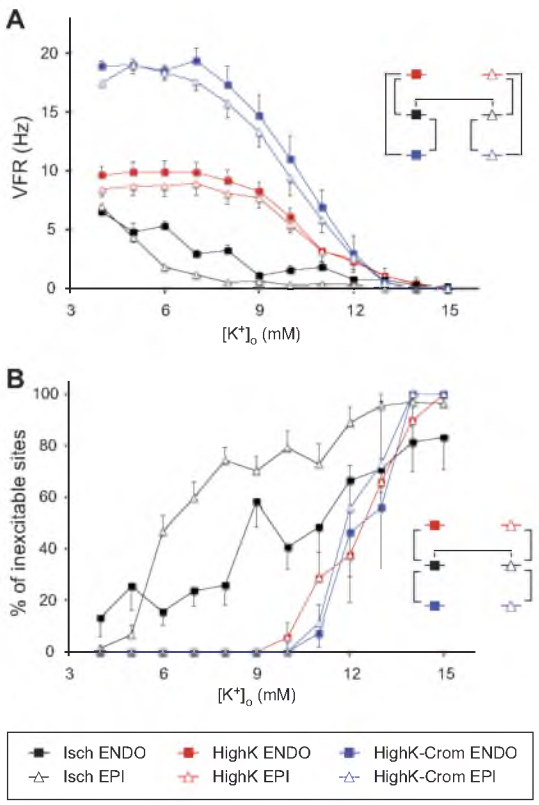


Fig. 4. Statistical analysis of VFR (*A*) and the percentage of inexcitable sites (*B*) as functions of $[K^+]_o$ in the Isch, HighK, and HighK-Crom groups (black, red, and blue, respectively). In each group, the Epi and Endo are represented by open triangles and filled squares, respectively. The *insets* in both *A* and *B* indicate relevant pairwise comparisons that yielded statistically significant difference ($P < 0.05$). The vertical brackets indicate differences between experimental groups in a given myocardial layer; the horizontal brackets indicate differences between the Endo and Epi in the same experimental group. *A*: VFR as the function of $[K^+]_o$. VFR in the Isch group was lower, whereas VFR in the HighK-Crom was higher, than VFR in the HighK group at all $[K^+]_o$ between 4 and 11 mM. Transmural differences in VFR were statistically significant only in the Isch group. Note that hyperkalemia combined with $K_{ATP}$ activation did not reproduce the $[K^+]_o$-VFR relationship observed during ischemia. *B*: percentage of inexcitable sites as a function of $[K^+]_o$. Note the difference between the Isch group and the two normoxic groups (HighK and HighK-Crom groups). In the Isch group, inexcitable sites appeared at relatively low $[K^+]_o$, and there was a large difference in the percentage of inexcitable sites between the Epi and Endo at intermediate levels of $[K^+]_o$. In contrast, both the HighK and HighK-Crom groups started to exhibit a loss of excitability only at $[K^+]_o$ above 10 mM, and there was no transmural difference in the percentage of inexcitable sites. Note that the upper limit of excitability in all experimental groups and myocardial layers was at $[K^+]_o$ ~14–15 mM, a level consistent with the inactivation of fast $Na^+$ channels, which are necessary to maintain propagation of cardiac impulse (30).

(VFR = 0) in all tested groups. Note that this information is somewhat related to the relationship between $[K^+]_o$ and VFR shown in Fig. 4*A*, especially given the fact that sites with VFR = 0 were included in the average VFR values shown in Fig. 4*A*. Yet, the results shown in Fig. 4*B* underscore the uniqueness of the ischemic data, especially in the Epi, in that during ischemic VF loss of excitability occurred at very modest levels of $[K^+]_o$. Note that in the Epi, almost 50% of recorded locations were inexcitable at $[K^+]_o$ as low as 6 mM. In contrast, both HighK and HighK-Crom groups showed a significant loss of excitability only at $[K^+]_o$ above 12 mM, thus approaching the canonical level of $K^+$-induced inexcitability (30). It is of interest that $K_{ATP}$ activation did not enhance the loss of excitability in the presence of hyperkalemia, despite the theoretical possibility of a synergistic relationship between these two factors with respect to electrical depression (30).

## DISCUSSION

VF is a frequent cause of sudden cardiac arrest and, in combination with ensuing global myocardial ischemia, determines the context of cardiopulmonary resuscitation and other life-saving procedures. VF evolving in globally ischemic hearts (sometimes termed long-duration VF) is a highly dynamic process featuring progressive transmural dispersion of VFR (8, 34, 36), which, at least in part, reflects the transmurally heterogeneous increase in postrepolarization refractoriness (15, 34). This increase is unbounded and culminates in a complete loss of excitability first in the LV Epi and subsequently in the rest of the ventricles (32, 34). Total loss of excitability (asystole) is in many cases the early point of no return after out-of-hospital cardiac arrest. Regional inexcitability can contribute to postreperfusion lethal arrhythmias (1), which is a major complication of cardiac arrest in the aftermath of successful defibrillation (33).

Despite the obvious significance of progressive electrical depression in the course of ischemic VF, little is known about the major determinants of this phenomenon. Shaw and Rudy (30) used a numeric model to analyze the relative roles of hyperkalemia, acidosis, and $K_{ATP}$ activation in conduction failure during ischemia. In this study, elevation of $[K^+]_o$ to ~14 mM was fully sufficient to cause conduction block. Acidosis did not have a significant additional effect, but a large degree of $K_{ATP}$ activation (20% channel availability assuming an intracellular ATP concentration of 0.5 mM) lowered the threshold $[K^+]_o$ necessary to cause conduction block from 14 to 10 mM. From this, it would be reasonable to assume that elevated $[K^+]_o$ and a massive activation of $K_{ATP}$ channels are major determinants of electrical failure during ischemic VF.

*Hyperkalemia.* To the best of our knowledge, our study is the first to measure the progressive accumulation of $[K^+]_o$ during ischemic VF. We found a larger $K^+$ efflux in the Epi than in the Endo, but the difference was significant only in the late phase of ischemic VF (14–20 min). We can compare these results only to previous studies performed in nonfibrillating hearts. In an in situ canine model of regional ischemia (20, 21), there was no transmural difference in $[K^+]_o$, and the total $K^+$ accumulation in the Epi and Endo during 20 min of left anterior descending coronary artery (LAD) occlusion was similar to that observed in the Endo after 20 min of ischemic VF in our study (~9–10 mM). In another study (7) using isolated blood-perfused canine hearts, $[K^+]_o$ was measured in the regionally ischemic myocardium at a depth of 5 mm from the Epi surface during pacing at a normal heart rate. In that study, at the end of an 8-min LAD occlusion period, the level of $[K^+]_o$ in the ischemic zone reached ~8 mM, which was very close to both Endo and Epi values of $[K^+]_o$ observed at the same duration of ischemia in our study (see Fig. 2*B*). Those authors also mea-

sured the incidence of inexcitability as the percentage of unipolar electrograms exhibiting "monophasic" morphology and found that after 8 min of ischemia, only ~25% of recording sites were inexcitable (see Fig. 5*A* in Ref. 7). In our case, the degree of inexcitability was drastically different between the Endo and Epi. Whereas in the Endo the percentage of inexcitable sites at 8 min of ischemia (28%) was similar to that observed by Coronel et al. (7) in the midmyocardium, in the Epi at the same time point of ischemia, it was much larger (63%). In stark contrast to ischemic conditions, raising $[K^+]_o$ to the level of 8 mM during normal perfusion in our study never caused inexcitability in any layer of the LV wall, and even the effect with respect to VFR was minimal (see Fig. 4*A*). These results disagree with those obtained during ischemic VF in the isolated rabbit heart, where an elevation of $[K^+]_o$ to 8 mM in normoxemic hearts reproduced the decrease in VFR observed during ischemia (4). Apart from the differences in species, another important difference between the rabbit study and our study is the degree of ischemia, which was complete (no flow) in our experiments and was only partial (remaining flow at 15% of normal) in the study by Caldwell et al. (4).

Because $Na^+$ channel inactivation occurs at more negative potentials in the Epi than in the Endo, even a transmurally uniform increase in $[K^+]_o$ can cause differential electrical depression in the Epi and Endo, leading, in particular, to the inability of the Epi to follow a rapid rate of excitation waves coming from the Endo (6). If this effect were significant in our study, we would expect that uniform hyperkalemia due to an elevation of $[K^+]_o$ in the perfusate would induce the transmural difference in VFR and/or the percentage of inexcitable sites. In fact, neither of these occurred in our study. Hyperkalemia in normoxemic hearts caused a transmurally uniform VFR decline at $[K^+]_o$ above 8 mM, culminating in a transmurally uniform loss of excitability when $[K^+]_o$ exceeded 12–14 mM. Thus, it is unlikely that the differential properties of $Na^+$ channel inactivation (6) contribute significantly to the transmural differences in VFR and excitability observed during ischemic VF.

*$K_{ATP}$ channels.* The timing, conditions, and electrophysiological consequences of $K_{ATP}$ activation during real ischemia in intact hearts remain as controversial now as three decades ago, when the channel was first discovered (25). While the principal role of $K_{ATP}$ channels in ischemic action potential duration shortening appears to be undisputable, its potential contribution to decreased membrane excitability and conduction failure during ischemia is far less clear. In their theoretical analysis of factors influencing conduction failure during early ischemia, Shaw and Rudy (30) concluded that the contribution of $K_{ATP}$ activation to conduction failure is limited unless the degree of activation of this channel is very large, which would require intracellular ATP concentration to reach very low (submillimolar) levels, much below what is typically observed within the first 10–15 min of ischemia. However, since it is not possible to directly measure activation of $K_{ATP}$ channels in intact tissues during ischemia, and because the regulation of this channel is dependent on a number of metabolites besides ATP, the possibility of any degree of $K_{ATP}$ activation during early ischemia remains open. Akar et al. (1) asserted the role of $K_{ATP}$ channel opening as the primary mechanism of ischemic inexcitability by an experimental demonstration of "metabolic sink block" resulting from $K_{ATP}$ activation secondary to mitochondrial depolarization (1). Noteworthy, in isolated ventricular cardiomyocytes, complete loss of excitability can occur without any increase in $[K^+]_o$, provided that the $K_{ATP}$ channel is sufficiently activated in response to mitochondrial depolarization (1, 22).

Since hyperkalemia alone failed to reproduce the $[K^+]_o$-VFR relationship observed during ischemic VF, we tested the possibility that in the presence of a strong activation of $K_{ATP}$ channels, the $[K^+]_o$-VFR relationship observed during normoxic VF would approach more closely the relationship observed during ischemic VF. However, this was not the case. The $K_{ATP}$ opener cromakalim caused a dramatic increase in VFR in the range of $[K^+]_o$ between 5 and 10 mM, which was opposite to the effect of ischemia. Also, cromakalim did not decrease the critical $[K^+]_o$ at which excitability is lost (it remained in the range of 12–14 mM). The concentration of cromakalim used in this study is expected to activate ~50% of the channels (24), which exceeds even what Shaw and Rudy (30) considered to be a result of extreme anoxia (20% of channels available). Yet even such an extreme level of $K_{ATP}$ activation failed to cause VFR suppression or loss of excitability up to $[K^+]_o$ of 12 mM, the concentration at which ~40% of the Endo locations and ~80% of the Epi locations exhibited loss of activity during ischemic VF (see Fig. 4*B*). These observations speak against the principal role of $K_{ATP}$ activation in electrical depression during ischemic VF, somewhat contradicting the concept of metabolic sink block (1) and our own previous finding that the blockade of $K_{ATP}$ channels by glybenclamide slightly postponed VFR decline and the emergence of local and global inexcitability during ischemic VF (32). To reconcile these apparent discrepancies, we suggest that $K_{ATP}$ activation does contribute to electrical depression during ischemic VF, but perhaps only in the presence of other ischemic factors yet to be established.

*Possible additional factors.* The $Na^+$-activated $K^+$ ($K_{Na}$) channel could theoretically contribute to electrical depression in the course of ischemic VF. This channel has conductance even larger than that of $K_{ATP}$ channels (35), and, thus, the consequences of its activation during ischemia could be similar to those of $K_{ATP}$ activation [i.e., sink block (1)]. The effects of $K_{ATP}$ and $K_{Na}$ activation could be synergistic with respect to electrical depression. Even though the available experimental evidence speaks against functional expression of $K_{Na}$ channels in the sarcolemma of canine ventricular myocytes (28), one cannot exclude that the lack of functioning $K_{Na}$ channels in single canine myocytes is a consequence of the cell isolation procedure.

As Shaw and Rudy (29) pointed out, the ability of $K_{ATP}$ channels to oppose the excitatory $Na^+$ current depends very much on the driving force for $K^+$ at the foot of the action potential, in other words, on the deviation of the resting potential ($V_{rest}$) from the $K^+$ equilibrium potential ($E_K$). Assuming, as they did, that during ischemia $V_{rest}$ is close to $E_K$ (and therefore the magnitude of the $K_{ATP}$ current to oppose the $Na^+$ current is small), the effect of $K_{ATP}$ activation on excitability should be limited. The difference between $V_{rest}$ and $E_K$ depends on the magnitude of inward leak currents present during diastole. Assuming that the ischemic $K^+$ leak is due to an increased conductance through $K^+$-selective channels (currently the most accepted theory), Carmeliet (5) postulated the necessity of a substantial inward leak to explain the presence of

significant rate-independent $K^+$ efflux, observed even after the cessation of electrical activity (14). Note that in our experiments, Epi $[K^+]_o$ continued to rise throughout 20 min of ischemia, even though the average Epi VFR was already close to zero at 10 min of ischemia (see Fig. 2). Whereas the Endo had a much higher VFR, the level of $K^+$ accumulation was lower in the Endo than in the Epi, clearly indicating that the frequency of excitations did not influence the intensity of $K^+$ efflux.

The extent to which $V_{rest}$ during ischemia can deviate from $E_K$ remains controversial. Kleber (14) showed that these two parameters, separated by 7–8 mV under normal conditions, converge to within 1 mV after 6–7 min of ischemia. However, an intriguing study by Blake et al. (3) suggests that in the ischemic canine heart, the relationship between $V_{rest}$ and $E_K$ is frequency dependent, such that in the presence of an increased excitation rate (180 vs. 90 beats/min), depolarization of $V_{rest}$ significantly exceeds that predicted by the ischemic level of $E_K$. Clearly, these conditions are relevant to the case of ischemic VF, where the excitation rate is initially in excess of 300–400 beats/min. Those authors showed that a $Ca^{2+}$ infusion had a similar effect and that the two factors combined enhanced deviation of $V_{rest}$ from $E_K$ during ischemia. This suggests a possibility that the effect of rapid activations on $V_{rest}$ during ischemia is mediated via an attendant increase in the intracellular $Ca^{2+}$ concentration. The depolarizing effects of metabolic inhibition on $V_{rest}$ were observed in spontaneously beating chick embryo myocytes (11) and adult rat ventricular myocytes subjected to cyanide (2) but not in adult mammalian ventricular myocytes subjected to a mitochondrial uncoupler (1, 22). The mechanisms of depolarizing effects of metabolic stress that are not related to hyperkalemia remain largely unknown and warrant further studies.

*Conclusions.* This is the first study to measure $[K^+]_o$ accumulation during ischemic VF. Comparison with published data obtained in the same species suggests that the presence of VF during ischemia has little impact on the rate of $K^+$ efflux compared with ischemia alone. Moreover, the higher level of $[K^+]_o$ in the sub-Epi than in the sub-Endo, despite the opposite distribution of the VFR, further supports the relative independence of ischemic $K^+$ efflux from excitation rate.

This study tested, and rejected, the hypothesis that the VFR decline and loss of excitability during ischemic VF in the canine heart can be explained in terms of "canonical" factors of electrical depression, hyperkalemia and $K_{ATP}$ activation, by showing a great disparity in the relationship between $[K^+]_o$ and VFR in the absence of ischemia (with or without a $K_{ATP}$ agonist), on the one hand, and the presence of ischemia, on the other hand. The alternative mechanisms of electrical depression during ischemic VF remain wide open for speculation but may include enhancement of inward leak currents, which could promote sarcolemmal depolarization beyond the level induced by extracellular $K^+$ accumulation.

## ACKNOWLEDGMENTS

The authors thank Jayne H. Davis and Nancy C. Allen for the excellent technical support and Curtis Booth for proofreading the manuscript and providing suggestions in English language and style.

## GRANTS

This work was supported by the National Heart, Lung, and Blood Institute Grants 5-R01-HL-088444 and 1-RO1-HL-103877 (to A. V. Zaitsev) and 1-F32-HL-097576 (to J. Shibayama) and by a Nora Eccles Treadwell Foundation Research Grant (to A. V. Zaitsev).

## DISCLOSURES

No conflicts of interest, financial or otherwise, are declared by the author(s).

## AUTHOR CONTRIBUTIONS

Author contributions: T.G.T., A.B., and A.V.Z. conception and design of research; T.G.T., P.W.V., A.B., V.G., J.S., and A.V.Z. performed experiments; T.G.T., P.W.V., A.B., J.S., and A.V.Z. analyzed data; T.G.T. and A.V.Z. interpreted results of experiments; T.G.T. and A.V.Z. prepared figures; T.G.T. and A.V.Z. drafted manuscript; T.G.T., P.W.V., A.B., V.G., J.S., and A.V.Z. edited and revised manuscript; T.G.T., P.W.V., A.B., V.G., J.S., and A.V.Z. approved final version of manuscript.

## REFERENCES

1. **Akar FG, Aon MA, Tomaselli GF, O'Rourke B.** The mitochondrial origin of postischemic arrhythmias. *J Clin Invest* 115: 3527–3535, 2005.
2. **Baczkó I, Giles WR, Light PE.** Resting membrane potential regulates $Na^+$-$Ca^{2+}$ exchange-mediated $Ca^{2+}$ overload during hypoxia-reoxygenation in rat ventricular myocytes. *J Physiol* 550: 889–898, 2003.
3. **Blake K, Clusin WT, Franz MR, Smith NA.** Mechanism of depolarization in the ischaemic dog heart: discrepancy between T-Q potentials and potassium accumulation. *J Physiol* 397: 307–330, 1988.
4. **Caldwell JANE, Burton FL, Smith GL, Cobbe SM.** Heterogeneity of ventricular fibrillation dominant frequency during global ischemia in isolated rabbit hearts. *J Cardiovasc Electrophysiol* 18: 854–861, 2007.
5. **Carmeliet E.** Cardiac ionic currents and acute ischemia: From channels to arrhythmias. *Physiol Rev* 79: 917–1017, 1999.
6. **Cordeiro JM, Mazza M, Goodrow R, Ulahannan N, Antzelevitch C, Di Diego JM.** Functionally distinct sodium channels in ventricular epicardial and endocardial cells contribute to a greater sensitivity of the epicardium to electrical depression. *Am J Physiol Heart Circ Physiol* 295: H154–H162, 2008.
7. **Coronel R, Fiolet JW, Wilms-Schopman JG, Opthof T, Schaapherder AF, Janse MJ.** Distribution of extracellular potassium and electrophysiologic changes during two-stage coronary ligation in the isolated, perfused canine heart. *Circulation* 80: 165–177, 1989.
8. **Dosdall DJ, Tabereaux PB, Kim JJ, Walcott GP, Rogers JM, Killingsworth CR, Huang J, Robertson PG, Smith WM, Ideker RE.** Chemical ablation of the Purkinje system causes early termination and activation rate slowing of long-duration ventricular fibrillation in dogs. *Am J Physiol Heart Circ Physiol* 295: H883–H889, 2008.
9. **Farid TA, Nair K, Masse S, Azam MA, Maguy A, Lai PF, Umapathy K, Dorian P, Chauhan V, Varro A, Al-Hesayen A, Waxman M, Nattel S, Nanthakumar K.** Role of $K_{ATP}$ channels in the maintenance of ventricular fibrillation in cardiomyopathic human hearts. *Circ Res* 109: 1309–1318, 2011.
10. **Hallstrom A, Herlitz J, Kajino K, Olasveengen TM.** Treatment of asystole and PEA. *Resuscitation* 80: 975–976, 2009.
11. **Hasin Y, Barry WH.** Myocardial metabolic inhibition and membrane potential, contraction, and potassium uptake. *Am J Physiol Heart Circ Physiol* 247: H322–H329, 1984.
12. **Huizar JF, Warren MD, Shvedko AG, Kalifa J, Moreno J, Mironov S, Jalife J, Zaitsev AV.** Three distinct phases of VF during global ischemia in the isolated blood-perfused pig heart. *Am J Physiol Heart Circ Physiol* 293: H1617–H1628, 2007.
13. **Johnson TA, Engle CL, Kusy RP, Knisley SB, Graebner CA, Gettes LS.** Fabrication, evaluation, and use of extracellular $K^+$ and $H^+$ ion-selective electrodes. *Am J Physiol Heart Circ Physiol* 258: H1224–H1231, 1990.
14. **Kléber AG.** Resting membrane potential, extracellular potassium activity, and intracellular sodium activity during acute global ischemia in isolated perfused guinea pig hearts. *Circ Res* 52: 442–450, 1983.
15. **Kong W, Ideker RE, Fast VG.** Transmural optical measurements of $V_m$ dynamics during long-duration ventricular fibrillation in canine hearts. *Heart Rhythm* 6: 796–802, 2009.
16. **Kusuoka H, Chacko VP, Marban E.** Myocardial energetics during ventricular fibrillation investigated by magnetization transfer nuclear magnetic resonance spectroscopy [Erratum. *Circ Res* 72(1): 237, 1993]. *Circ Res* 71: 1111–1122, 1992.

17. **Mandapati R, Asano Y, Baxter WT, Gray RA, Davidenko JM, Jalife J.** Quantification of effects of global ischemia on dynamics of ventricular fibrillation in isolated rabbit heart. *Circulation* 98: 1688–1696, 1998.
18. **Masse S, Downar E, Chauhan V, Sevaptsidis E, Nanthakumar K.** Ventricular fibrillation in myopathic human hearts: mechanistic insights from in vivo global endocardial and epicardial mapping. *Am J Physiol Heart Circ Physiol* 292: H2589–H2597, 2007.
19. **Miyata A, Dowell JD, Zipes DP, Rubart M.** Rate-dependent $[K^+]_o$ accumulation in canine right atria in vivo: electrophysiological consequences. *Am J Physiol Heart Circ Physiol* 283: H506–H517, 2002.
20. **Miyoshi S, Miyazaki T, Moritani K, Ogawa S.** Different responses of epicardium and endocardium to $K_{ATP}$ channel modulators during regional ischemia. *Am J Physiol Heart Circ Physiol* 271: H140–H147, 1996.
21. **Miyoshi S, Miyazakt T, Asanagi M, Moritani K, Ogawa S.** Differential role of epicardial and endocardial $K_{ATP}$ channels in potassium accumulation during regional ischemia induced by embolization of a coronary artery with latex. *J Cardiovasc Electrophysiol* 9: 292–298, 1998.
22. **Morley GE, Anumonwo JM, Delmar M.** Effects of 2,4-dinitrophenol or low $[ATP]_i$ on cell excitability and action potential propagation in guinea pig ventricular myocytes. *Circ Res* 71: 821–830, 1992.
23. **Nash MP, Mourad A, Clayton RH, Sutton PM, Bradley CP, Hayward M, Paterson DJ, Taggart P.** Evidence for multiple mechanisms in human ventricular fibrillation. *Circulation* 114: 536–542, 2006.
24. **Ng B, Kang Y, Xie H, Sun H, Gaisano HY.** Syntaxin-1A inhibition of P-1075, cromakalim, and diazoxide actions on mouse cardiac ATP-sensitive potassium channel. *Cardiovasc Res* 80: 365–374, 2008.
25. **Noma A.** ATP-regulated $K^+$ channels in cardiac muscle. *Nature* 305: 147–148, 1983.
26. **Pandit SV, Warren M, Mironov S, Tolkacheva EG, Kalifa J, Berenfeld O, Jalife J.** Mechanisms underlying the antifibrillatory action of hyperkalemia in guinea pig hearts. *Biophys J* 98: 2091–2101, 2010.
27. **Rogers JM, Melnick SB, Huang J.** Fiberglass needle electrodes for transmural cardiac mapping. *IEEE Trans Biomed Eng* 49: 1639–1641, 2002.
28. **Saxena NC, Fan JS, Tseng GN.** Effects of elevating $[Na]_i$ on membrane currents of canine ventricular myocytes: role of intracellular Ca ions. *Cardiovasc Res* 33: 548–560, 1997.
29. **Shaw RM, Rudy Y.** Electrophysiologic effects of acute myocardial ischemia: a theoretical study of altered cell excitability and action potential duration. *Cardiovasc Res* 35: 256–272, 1997.
30. **Shaw RM, Rudy Y.** Electrophysiologic effects of acute myocardial ischemia. A mechanistic investigation of action potential conduction and conduction failure. *Circ Res* 80: 124–138, 1997.
31. **Taccardi B, Punske BB, Macchi E, Macleod RS, Ershler PR.** Epicardial and intramural excitation during ventricular pacing: effect of myocardial structure. *Am J Physiol Heart Circ Physiol* 294: H1753–H1766, 2008.
32. **Taylor TG, Venable PW, Shibayama J, Warren M, Zaitsev AV.** Role of $K_{ATP}$ channel in electrical depression and asystole during long-duration ventricular fibrillation in ex vivo canine heart. *Am J Physiol Heart Circ Physiol* 302: H2396–H2409, 2012.
33. **van Alem AP, Post J, Koster RW.** VF recurrence: characteristics and patient outcome in out-of-hospital cardiac arrest. *Resuscitation* 59: 181–188, 2003.
34. **Venable PW, Taylor TG, Shibayama J, Warren M, Zaitsev AV.** Complex structure of electrophysiological gradients emerging during long-duration ventricular fibrillation in the canine heart. *Am J Physiol Heart Circ Physiol* 299: H1405–H1418, 2010.
35. **Wang Z, Kimitsuki T, Noma A.** Conductance properties of the $Na^+$-activated $K^+$ channel in guinea-pig ventricular cells. *J Physiol* 433: 241–257, 1991.
36. **Worley SJ, Swain JL, Colavita PG, Smith WM, Ideker RE.** Development of an endocardial-epicardial gradient of activation rate during electrically induced sustained ventricular fibrillation in dogs. *Am J Cardiol* 1985: 813–820, 1985.
37. **Zaitsev AV, Guha PK, Sarmast F, Kolli A, Berenfeld O, Pertsov AM, de Groot JR, Coronel R, Jalife J.** Wavebreak formation during ventricular fibrillation in the isolated, regionally ischemic pig heart. *Circ Res* 92: 546–553, 2003.

CHAPTER 6

# β-ADRENERGIC STIMULATION AND HIGH EXCITATION RATE MUTUALLY PROMOTE HETEROGENEOUS ELECTRICAL FAILURE AND VENTRICULAR FIBRILLATION IN THE GLOBALLY ISCHEMIC RABBIT HEART

## 6.1 Abstract

Ventricular fibrillation-induced sudden cardiac arrest (VF-SCA) is a leading killer in the U.S. Left untreated, VF-SCA is characterized by a progressive and heterogeneous decline in electrical activity culminating in asystole and death. The defining features of VF-SCA are high excitation rate and ischemia. In addition, due to current treatment guidelines combined with spontaneous release of catecholamines, β-adrenergic stimulation (β-AS) is greatly enhanced during VF-SCA. Taken together the combination of high excitation rate and β-AS could exacerbate metabolic challenge during ischemia leading to an increased propensity for recurrent arrhythmias and asystole, and is correlated with decreased survival probability. Here, I hypothesized that high excitation rate and β-AS would promote electrical failure and the effects would be synergistic. In addition, I hypothesized that the detrimental effects of β-AS and high excitation rate would be mediated by activation of ATP-sensitive $K^+$ channels ($K_{ATP}$) or $Na^+$-sensitive $K^+$ channels ($K_{Na}$).

Thirty-one rabbit hearts were isolated on a Langendroff apparatus and subjected to 30 minutes of global ischemia under six interventions whose parameters consisted of high (200 ms or tachy-pacing) or low (300 ms) pacing rate, presence or absence of the β-adrenergic agonist isoproterenol (Iso, 30 nM), and presence or absence of $K^+$ channel blockers (10 μM glybenclamide to block $I_{KATP}$ and 0.3 μM R56865 to block $I_{KNa}$). The groups were defined as 1) *300ms*, 2) *200ms*,

3) *300ms_Iso*, 4) *200ms_Iso*, 5) *200ms_Iso_Glyb*, and 6) *200ms_Iso_R56*. All hearts were treated with the electromechanical uncoupler BDM (20 mM) and stained with the voltage sensitive fluorophore Di-4 ANEPPS. Optical mapping was performed on the anterior surface of the hearts and the signals were processed to obtain measurements of the maximum upstroke velocity of the APs ($dV/dt_{max}$), percent of excitable area (%Excitable), and APD at 80% repolarization ($APD_{80}$).

I found that *200ms* and *300ms_Iso* accelerated the rate of $dV/dt_{max}$ decline, loss of excitability, and $APD_{80}$ shortening in both the left (LV) and right (RV) ventricles during ischemia where *300_Iso* had a greater effect than *200ms* in loss of excitability only. Furthermore, the combination of tachy-pacing and β-AS (*200ms_Iso*) exacerbated electrical decline in all three parameters compared to either intervention alone. Surprisingly, neither *200ms_Iso_Glyb* nor *200ms_Iso_R56* was able to rescue the detrimental effects of tachy-pacing and β-AS (*200ms_Iso*) when $dV/dt_{max}$ and % excitable area were compared. Expectedly, *200ms_Iso_Glyb* and *200ms_Iso_R56* both rescued $APD_{80}$ shortening compared to *200ms_Iso* with *200ms_Iso_Glyb* having a larger rescuing effect and *200ms_Iso_R56* having an effect only in the RV. In addition to the detrimental effects on electrical failure, I found that both tachy-pacing and β-AS promoted the initiation of VF during ischemia and a strong correlation between the onset of electrical failure and VF ($R^2$=0.76) was found.

I conclude that tachy-pacing and β-AS—individually and combined—promote electrical failure and induce the propensity for lethal arrhythmias. Furthermore, my results point to mechanism of arrhythmogenesis mediated primarily by the formation of reentrant substrate during ischemic heart disease rather than abnormal automaticity.

## 6.2 Introduction

Lethal ventricular tachyarrhythmias associated with acute myocardial ischemia remain one of the leading causes of death in developed countries [1-4]. Despite the long history of research and speculation, the exact mechanisms triggering such arrhythmias, and ventricular fibrillation (VF) in the first place, remain controversial. A major controversy is related to whether

VF in the ischemic heart is triggered/maintained by mechanisms related to abnormal impulse formation, such as early and delayed afterdepolarizations (EADs and DADs), or abnormal impulse propagation (unidirectional conduction block leading to self-sustained reentry). Once induced, VF leads to cardiac arrest and global myocardial ischemia, in which a complex bidirectional relationship takes place, such that ischemia modulates the dynamics of fibrillatory waves [51], whereas the high excitation rate associated with VF may aggravate the metabolic challenge [80] and ionic disturbances [92] caused by ischemia. To a large extent, this complex relationship determines the ability of countershocks and cardiopulmonary resuscitation (CPR) to restore sinus rhythm and spontaneous circulation in the aftermath of VF-induced sudden cardiac arrest (VF-SCA).

A prominent factor of myocardial ischemia and VF-SCA is a large increase in interstitial concentration of catecholamines [86, 93]. In particular, interstitial norepinephrine increased about a 7-fold during VF-SCA in an anesthetized pig, and progressed to over an 100-fold increase after defibrillation and reperfusion mimicking life-saving procedures in out-of-hospital cardiac arrest [86]. It is well established that beta-adrenergic stimulation (β-AS) increases the incidence of VF in the context of myocardial ischemia. These effects were usually explained in terms of "non-reentrant" mechanisms (EADs and DADs) downstream of increased cellular $Ca^{++}$ load, based on experiments in isolated cardiomyocytes partially reproducing ischemic conditions [94]. However, such implications have always been controversial, as in many studies a sufficiently "severe" simulated ischemia abolished DADs and EADs [94, 95]. While the possible effects on impulse propagation were postulated in terms of a "slow response" hypothesis (i.e., β-AS promotes extremely slow conduction driven exclusively by L-type $Ca^{++}$ current against the backdrop of significant hyperkalemia [96], the relevance of this mechanism to the conditions of real ischemia have never been demonstrated. On a more general note, little is known with regard to the effect of β-AS on conduction in the context of real ischemia.

It was noted that the anti-arrhythmic effect of beta-blockade is more pronounced at an increased rate of excitations [97]. Of interest, it was shown that slowing the heart rate below the normal physiological level by ivabradine reduced the incidence of postreperfusion VF and also

delayed the ischemia-induced slowing and block of conduction [98]. Both tachycardic rhythm and β-AS are likely to impose additional metabolic demand on the ischemic heart, and potentially aggravate ATP depletion. Activation of ATP-sensitive potassium channels ($K_{ATP}$) was implicated in pro-arrhythmic heterogeneous APD shortening during ischemia [99], as well as in ischemic loss of excitability and postischemic VF presumably mediated by conduction failure ("metabolic sink block") [82]. Theoretically, the sodium-sensitive potassium channel ($K_{Na}$), which is also sensitive to [ATP] [75] may contribute to "metabolic sink block," as this channel should be activated under conditions of ischemia and high excitation rate.

Based on the above, I hypothesized that an increased heart rate and β-AS may promote synergistically ischemic derangements of conduction and excitability, thus forming substrate for VF due to formation of reentrant pathways. I also hypothesized that these effects might be mediated via metabolically sensitive $K^+$ channels. I used an isolated heart model of global ischemia, in which the propagation of electrical waves can be scrutinized using high resolution optical mapping and the relative effects of a high excitation rate and β-adrenergic stimulation on conduction can be dissected with relative ease.

My study offers a radically new mechanism linking beta-adrenergic stimulation and VF in the ischemic heart. I show, for the first time, that beta-adrenergic stimulation promotes, synergistically with tachy-pacing, highly heterogeneous electrical depression and conduction failure in the globally ischemic heart, which correlates in time with the onset of VF driven by reentrant circuits. This suggests that the proarrhythmic effect of β-AS in ischemic hearts may be mediated via abnormal conduction rather than abnormal automaticity. Unexpectedly, I found little or no role of metabolically sensitive $K^+$ channels in electrical failure due to β-AS, negating a significant involvement of the metabolic sink block mechanism. I speculate that the observed synergism between high excitation rate and β-AS with respect to electrical depression may contribute to major adverse outcomes of VF-SCA, such as persistent/recurrent VF, pulseless electrical activity, and asystole. This provides further support to the idea that β-adrenergic blockade may be beneficial in the context of VF-SCA [86].

## 6.3 Methods

This investigation conformed with the National Institutes of Health *Guide for the Care and Use of Laboratory Animals* (8th Edition, 2011) and was approved by the Institutional Animal Care and Use Committee of the University of Utah (Protocols No. 12–09005 and 13-0005).

### 6.3.1 Langendorff-Purfused Rabbit Hearts

Adult New Zealand white rabbits of either sex (15 male and 16 female, weight 1.5 to 3.0 kg) were euthanized by sodium pentobarbital (130 mg/kg, i.v.) and heparin (1 ml, 10,000 USP) was given to prevent clotting. Hearts were rapidly excised, cannulated on a Langendorff apparatus and perfused with Tyrode's solution (130 mM NaCl, 24 mM $NaHCO_3$, 1.2 mM $NaH_2PO_4$, 1.0 mM $MgCl_2$, 5.6 mM glucose, 4.0 mM KCl, 1.8 mM $CaCl_2$ and 0.1 g/L albumin), gassed with an $O_2/CO_2$ mixture (adjusted to maintain pH at 7.4) at a fixed rate of 30 ml/min. The mitral valve was disrupted by inserting a drainage tube into the LV via a small cut in the left atrial appendage to prevent buildup of LV pressure due to venous efflux through Thebesian veins. Hearts were immersed in Tyrode's superfusion solution and temperature in the right ventricular (RV) cavity and the superfusion solution was maintained at 37.0±0.5 °C. The volume-conducted ECG was monitored continuously throughout the protocol.

After 15 minutes of stabilization, the electromechanical uncoupler 2,3-Butanedione 2-monoxime (BDM, 20 mM, Sigma-Aldrich, St. Louis, USA) was administered and continued for the rest of the duration of the experiment. About 10 minutes before the ischemic episode, hearts were stained with a bolus of the voltage-sensitive dye di-4-ANEPES (3 ml of 10.4 μM solution, Life Technologies, Carlsbad, CA, USA). Global ischemia was initiated by cessation of aortic perfusion and maintained for 30 minutes, followed by reperfusion. During global ischemia the temperature of the superfusate was maintained at 37.0±0.5 °C and the oxygen pressure in the superfusate was maintained at below ~40 mmHg by gassing the solution with a $N_2/CO_2$ gas mixture (adjusted to maintain pH at 7.4).

Pacing at either normal (CL = 300 ms) or fast (CL = 200 ms) rates (at 3 times end-diastolic excitation threshold) was performed using two pairs of Ag/AgCl plate electrodes

(diameter, 3 mm) positioned at the endocardial and the epicardial surface of the lateral right ventricular (RV) and left ventricular (LV) free wall. The relatively large size of the pacing electrodes, the application of the current across the ventricular wall, and the relatively large amplitude of the stimulus ensured efficient capture during ischemia, when excitability was progressively diminished. Pacing was started 2-3 minutes before ischemia.

### 6.3.2Experimental groups

A total of six experimental groups were used in this study. In the *300ms* group (n= 5), which served as the control, the hearts were paced at a CL=300 ms and no drugs (except BDM) were used. In the *200ms* group (n=5), the hearts were paced at a CL=200 ms. In the *300ms_Iso* and *200ms_Iso* groups (n= 5 and 6, respectively), the hearts were paced at CLs of either 300 or 200 ms in the presence of the β–adrenergic agonist isoproterenol (30 nM, Sigma-Aldrich, St. Louis, USA). In the *300ms_Iso_Glyb* group (n= 5), the hearts were paced at a CL of 200 ms in the presence of β–adrenergic agonist isoproterenol (30 nM) and $I_{KATP}$ blocker glybenclamide (10 μM, Sigma-Aldrich, St. Louis, MO, USA). Glybenclamide was administered 10 minutes before ischemia. In the *300ms_Iso_R56* group (n= 5), the hearts were paced at a CL of 200 ms in the presence of β–adrenergic agonist isoproterenol (30 nM) and $I_{KNa}$ blocker R56865 (0.3 μM, courtesy of Johnson & Johnson Pharmaceutical Research & Development, L.L.C., New Brunswick, NJ, USA). R56865 was administered 30 minutes before ischemia.

### 6.3.3 Optical mapping

Hearts were fully immersed in Tyrode's solution inside the imaging chamber to maintain the temperature at 37°C both during normoxic perfusion and no-flow ischemia. Optical mapping of changes in transmembrane voltage (optical action potential, OAP) was performed using an EMCCD camera (iXon DU-860D, Andor Technology, Belfast, UK) with a 6 mm objective lens, at a resolution of 64 X 64 pixels and frame interval of 2 ms. The voltage sensitive dye di-4-ANEPPS was excited by a 532 nm green solid-state laser (Coherent, Santa Clara, CA, USA). The imaging

area was 3 × 3 cm encompassing the entire anterior view of the right and left ventricles (see Figure 2.2C in Chapter 2). Emitted fluorescence was collected using either a 640±40 nm or 605±32 nm bandpass filter. Five-second long movies were acquired 2-3 minutes before ischemia, at each minute from 0 to 30 minutes of ischemia, and during 20 minutes of reperfusion (reperfusion movies were used only to check recovery of electrical activity). Data acquisition was performed using a custom software package (Alexey Zaitsev and Paul Venable) written in Java and using libraries from Micro-Manager open source microscopy software (Vale Lab, University of California in San-Francisco, USA) and NetBeans open source program development framework (netbeans.org, Oracle, Redwood City, CA, USA).

### 6.3.4 Data Processing and Analysis

The software program Scroll (Sergey Mironov, Center for Arrhythmia Research, University of Michigan, USA) was used for interactive analysis of movies and single pixel recordings, and also for manual selection of the mapped regions exclusive to RV and LV in each heart. All other analysis routines were written by Alexey Zaitsev using PV-WAVE software (Rogue Wave Software, Boulder, CO). I defined the area to the right of the LAD as RV and the area to the left of LAD as LV (Figure 2.2C Chapter 2). The optical recordings were background-subtracted, inverted and filtered in space and time as previously described [51]. The maximal time derivative of the OAP upstroke ($dV/dt_{max}$) was determined in each OAP of each single pixel recording in each movie. The average values of $dV/dt_{max}$ in each pixel were corrected for the background fluorescence. Specifically, $dV/dt_{max}$ in the brightest pixel (fluorescence level $F_{max}$) remained unhanged, whereas in all other pixels the value of $dV/dt_{max}$ was multiplied by the ratio of $F_{max}$ over F in the given pixel. This procedure compensated for the variation in $dV/dt_{max}$ due to nonuniform illumination and staining as well as curvature of the heart that cause deviation from the focal plane. The corrected values of $dV/dt_{max}$ were used to compute the average values for RV and LV and were plotted as a function of ischemia duration.

In order to detect the loss of excitability in individual locations in RV and LV, I applied a minimum $dV/dt_{max}$ criterion. The criterion was selected by trial and error and was just above

twice the level of the dF/dt of noise in the movies in which the full loss of excitability was undoubted, as was the case in all movies recorded in the *200ms_Iso* group at 30 minutes of ischemia. All movies analyzed for this study were carefully inspected to ensure that the computed inexcitable areas matched reasonably well the visually observable areas lacking propagating waves. The percent of pixels with $dV/dt_{max}$ values above the threshold (percent of excitable areas) was computed in the RV and the LV and plotted as the function of ischemia duration. Action potential duration was computed in OAPs at the level of 80% of repolarization ($APD_{80}$). Average values of $APD_{80}$ were computed for RV and LV and plotted as the function of ischemia duration. In experiments using isoproterenol a substantial motion artifact was present up to 3 minutes of ischemia despite the presence of BDM. This motion artifact had little effect on $dV/dt_{max}$ but significantly distorted the measurement of $APD_{80}$. In addition, in all but one experiments VF spontaneously occurred at some point in ischemia. $APD_{80}$ was compared between different experimental groups only in the time window in which such comparison was valid. The lower limit of this window was 3 minutes of ischemia, and the upper limit was the latest time point in ischemia at which at least 3 hearts in each experimental group still maintained regular paced rhythm. This time point was 8 minutes of ischemia.

### 6.3.5 Statistical analysis

The time course of $dV/dt_{max}$, percent of excitable area, and $APD_{80}$ were compared using a two-way ANOVA with Tukey posthoc test for multiple comparisons. The statement of significant difference in this case meant the significant separation between curves not time points. The time at which 50% of the mapped region in RV or LV lost excitability and the time of VF initiation were compared between groups using a one-way ANOVA followed by Tukey posthoc test for multiple comparisons. Data are given as means ± SE. Differences of $p < 0.05$ were considered statistically significant.

## 6.4 Results

### 6.4.1 Tachypacing and β-AS Mutually Promote the Progressive Decline in $dV/dt_{max}$ and the Emergence of Inexcitable Areas

Figure 6.1 summarizes the statistical analysis of $dV/dt_{max}$ and inexcitability data in four groups: *300ms*, *200ms*, *300ms_Iso* and *200ms_Iso*. All left-hand Panels describe RV, all right-hand panels describe LV. Panels A and B show the time course of $dV/dt_{max}$ during ischemia in RV and LV, respectively. One can see that in both chambers the slowest decline in $dV/dt_{max}$ occurs in the *300ms* group (control). In both chambers, the $dV/dt_{max}$ decline in *200ms* and *300ms_Iso* groups is accelerated, by a similar degree, as compared to that in the *300ms* group. This suggests that both tachycardia and β-AS, applied separately, promote electrical depression during ischemia. Lastly, the $dV/dt_{max}$ decline is further accelerated in the *200ms_Iso* group. The combination of tachycardia and β-AS led to a dramatic shift of the curve to the left as compared to the *300ms* group (control). Among all the pairs formed out of the four groups shown in Figure 6.1A-B, only the difference between *300ms_Iso* and *200ms* did not reach statistical significance.

Panels C and D of Figure 6.1 show the percent of excitable area as the function of ischemia duration in RV and LV, respectively. One can see that the overall relationship between the experimental groups is similar to that observed in the time course of $dV/dt_{max}$ shown in Figure 6.1A-B. Specifically, there was a progressively faster loss of excitable epicardial locations from *300ms* to *200ms* to *300ms_Iso* to *200ms_Iso* groups. I can conclude that β-AS promotes inexcitability more than tachy-pacing.

Panels E and F of Figure 6.1 show the average time of ischemia at which 50% of the mapped area in the RV and LV, respectively, lost excitability. The data are derived from the graphs shown in Figure 6.1, C and D, respectively, and seems to be a convenient way to compress the time-dependence of excitability loss during ischemia. Note that in all of the *300ms* experiments more than 50% of the RV remained excitable at 30 minutes of ischemia at which time the ischemic protocol was finished; this precluded an accurate estimate of the time at which the 50% loss in excitable sites in RV actually occurred. Because of this, the time of 50% loss in excitable sites in the RV was set at 30 minutes and was thus underestimated. Note also that the statistical

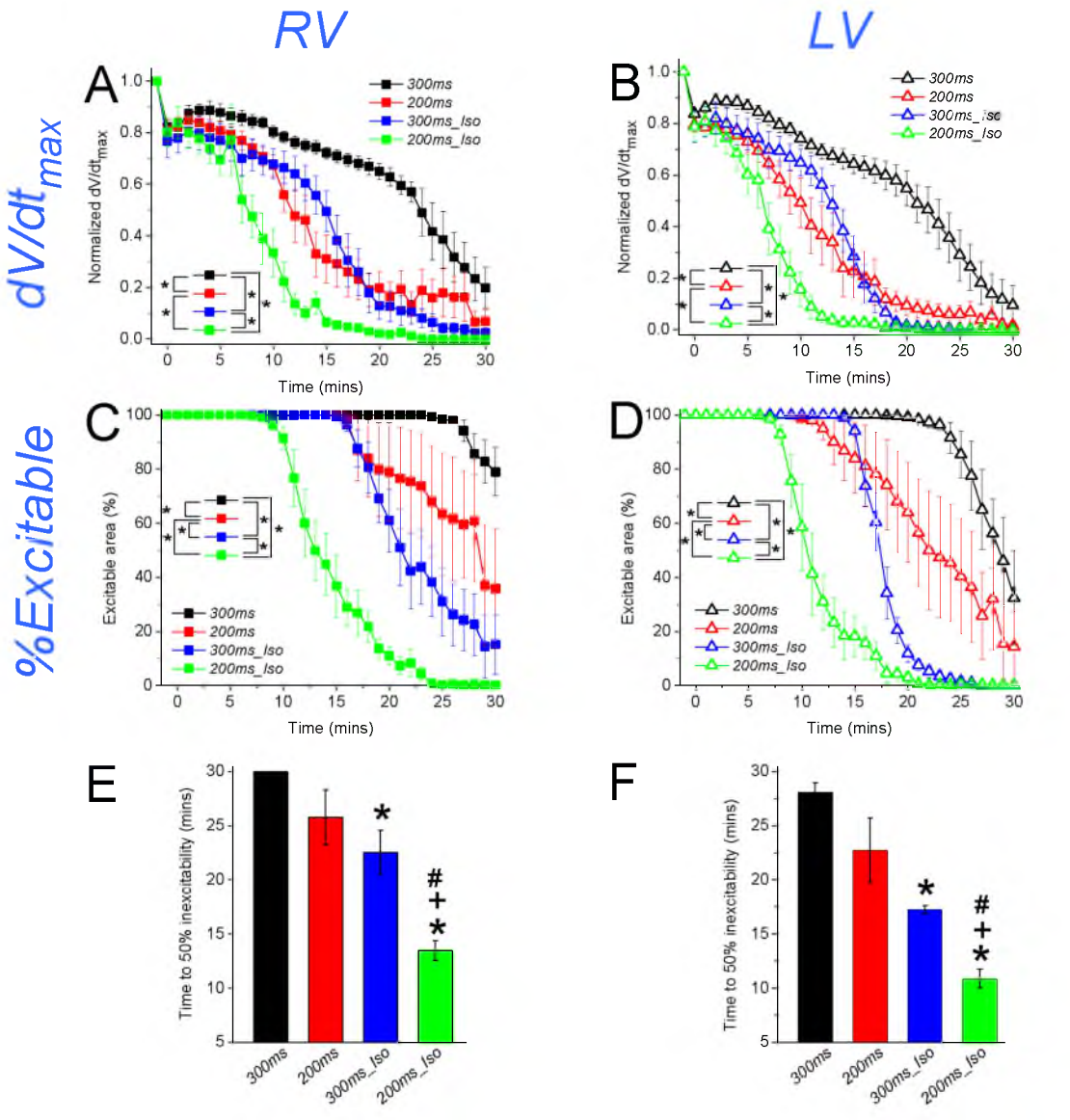


Figure 6.1: The effects of excitation rate and β-AS on the progressive decline in $dV/dt_{max}$ and percent excitability during ischemia. The right column shows data for RV and the left shows data for LV. **A-B.** normalized $dV/dt_{max}$ vs. time of ischemia in *300ms* (black), *200ms* (red), *300ms_Iso* (blue), and *200ms_Iso* (green) in the RV and LV, respectively. Both tachy-pacing and β-AS independently promote $dV/dt_{max}$ deterioration during ischemia while the combination further increases the rate of AP upstroke decline. **C-D.** Percent of excitable tissue on the epicardial surface vs. the duration of ischemia in the RV and LV, respectively. Similar to the effects on $dV/dt_{max}$, tachy-pacing and β-AS independently promote electrical failure. The effects of β-AS are greater than tachy-pacing where the effect on $dV/dt_{max}$ was not different between the two interventions. The combination of tachy-pacing and β-AS mutually promotes electrical failure. In panels A-D * indicates comparisons with $p<0.05$. **E-F.** Time to 50% inexcitability in the RV and LV, respectively. Note that the value for *300ms* in RV was truncated to 30 minutes in some experiments hence biasing the comparisons against difference from other interventions. Nevertheless, in both the RV and LV tachy pacing tended to accelerate the time to 50% inexcitability in ischemia though it did not reach significance. Both *300ms_Iso* and *200ms_Iso* significantly reduced time to 50% inexcitability compared to *300ms* (* $p<0.05$). The combination of tachy-pacing and β-AS also significantly reduced time to 50% inexcitability compared to both *200ms* and *300ms_Iso* (+ and #, respectively, $p<0.05$).

significance of the difference between *300ms* and *200ms* groups observable when the entire curves were compared (in Figures 6.1C and 6.1D) was no longer present when the time of 50% excitability loss is compared between these two groups (in Figures 6.1E and 6.1F). This is most likely due to reduced power of the test, because only one data point is used from each experiment, as opposed to over 30 time points used in the comparison of the entire curves. Nevertheless, the comparison of the time of 50% reduction in excitable area captures the main features of the phenomenon. Namely, it shows that in both chambers β-AS promotes the loss of excitability, which is further potentiated by tachycardia. Curiously, at least in the LV the effects of tachycardia and β-AS appear to be almost exactly additive (Figure 6.1F). Specifically, tachycardia (*200ms* vs. *300ms*) accelerates the loss of excitability by ~5 minutes, and β-AS (*300ms_Iso* vs. *300ms*) accelerates the loss of excitability by ~11 minutes. The acceleration induced by the combined intervention (*200ms_Iso* vs. *300ms*) is ~17 minutes, which is close to the sum of the effects induced by the individual interventions.

Figure 6.2 is redundant with Figure 6.1, but juxtaposes RV and LV curves in one graph, in order to highlight the interchamber differences in the development of electrical depression under various experimental conditions (*300ms*, *200ms*, *300ms_Iso* and *200ms_Iso)*. Summarizing Figure 6.2, both the decline in $dV/dt_{max}$ and the development of inexcitability occurs faster in LV than in RV in all of these groups. The difference in the time course of $dV/dt_{max}$ in each experimental group is small, but statistically significant. Regarding the time course of the loss of excitability, it is significantly different between the RV and LV in the *200ms*, *300ms_Iso* and *200ms_Iso* groups, but not in the *300ms* group. The latter observation is easily explained by the fact that most of the time both RV and LV are 100% excitable in this group (Figure 6.2B). If only the last 5 minutes of ischemia were compared, then the difference between RV and LV was significant ($p<0.05$).

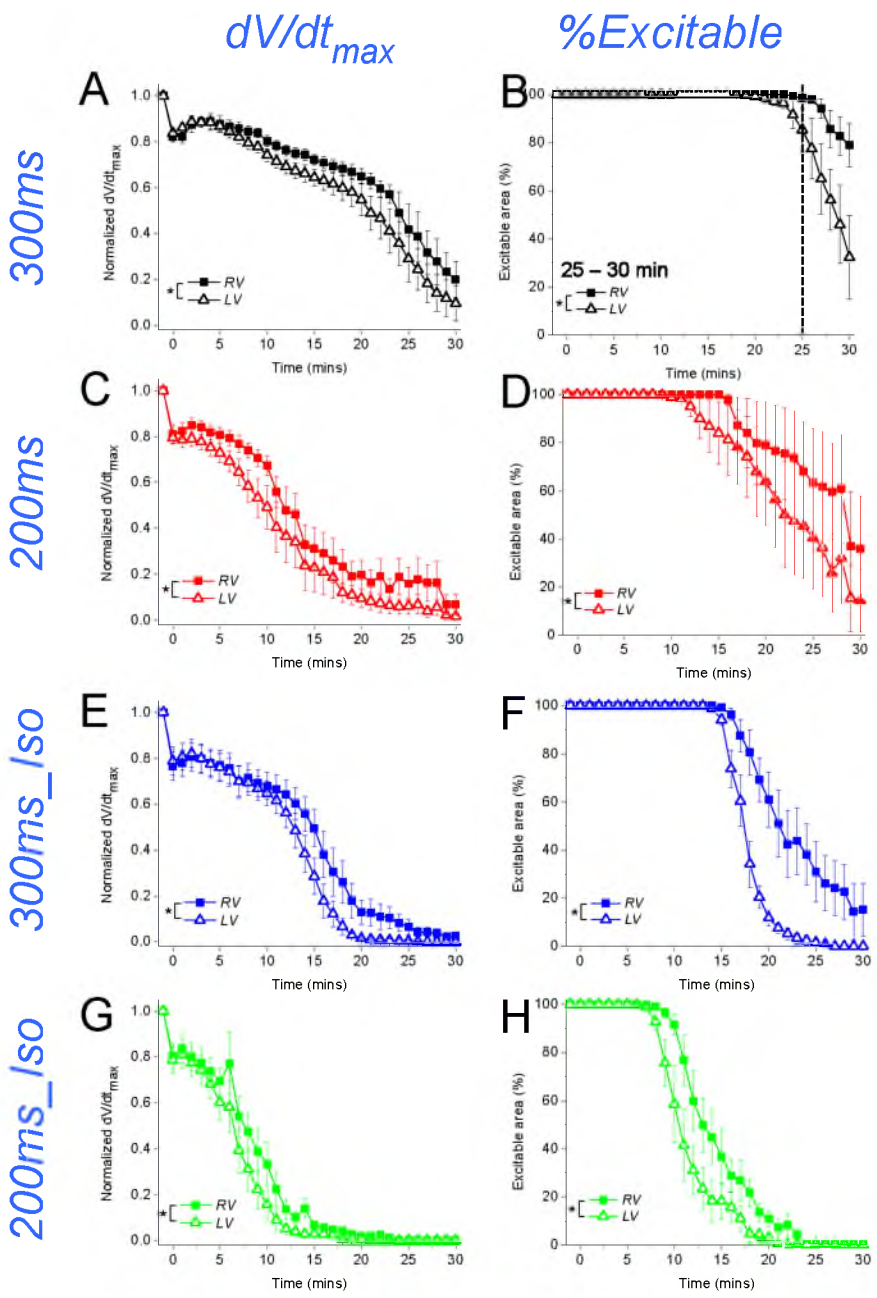


Figure 6.2: Effects of tachy-pacing and β-AS on the heterogeneous deterioration of electrical activity in the RV and LV. Shows the same data as in Figure 6.1 but grouped to compare RV and LV. **A, C, E, G** present $dV/dt_{max}$ data for all four groups and **B, D, F, H** present data for percent excitable area in all four groups. Note that an interchamber difference in time course is present in all groups in both $dV/dt_{max}$ and % excitability (* $p<0.05$). In the *300ms* group the difference between RV and LV was not significant when all time points were considered but was different during the last 5 minutes of ischemia. This can be explained by the fact that under conditions of the *300ms* group inexcitability did not develop in either chamber until late in ischemia. Note that neither tachy-pacing, β-AS nor the combination appeared to modulate the interchamber difference in electrical failure wherein the LV experienced a higher rate of electrical decline than the RV.

### 6.4.2 The Effects of Tachypacing and β-AS on APD Shortening and Electrical Failure During Ischemia

Despite the use of BDM, which almost completely removed motion artifact in isoproterenol-free hearts, the addition of isoproterenol substantially increased contraction and significantly distorted the repolarization phase of the optical action potentials in normoxemic hearts. In all groups the magnitude of motion artifact subsided during ischemia due to ischemic contraction failure. After careful inspection, I judged that after 3 minutes of ischemia (inclusive) the motion artifact was sufficiently suppressed by BDM in all groups. The upper limit of the ischemic time window during which the APD measurement was meaningful was determined by the onset of VF occurring in close to 100% of experiments, but at different time points in different groups (see below). The latest time in ischemia for APD measurement was determined as the time point at which at least 3 hearts in each experimental group were still free of VF, and this time point was 8 minutes of ischemia. Thus, the comparisons of APD between different groups were carried out for the time window between 3 and 8 minutes of ischemia. On the other hand, the comparisons between the RV and LV in individual groups were carried out taking into account all ischemic time points at which regular paced rhythm was maintained in that particular group (see Figure 6.3, C-F).

Figure 6.3 summarizes the statistical analysis of APD in four groups: *300ms*, *200ms*, *300ms_Iso* and *200ms_Iso*. Panels A and B show the time course of $APD_{80}$ during ischemia in the RV and LV, respectively. As mentioned above, in each group the measurements were performed for all ischemic time points at which at least 3 hearts remained in regular paced rhythm. So, indirectly, Figure 6.3 conveys the information that the onset of VF occurred at very different time points in different groups (earliest in the *200ms_Iso* group and latest in the *300ms* group, see more below). The two vertical dashed lines indicate the time window (3-8 minutes of ischemia) during which the comparison between groups was performed. One can see that both pacing rate and β-AS affected APD dynamics during ischemia. Assuming that at 3 minutes of ischemia (the earliest point of measurement) the APD values were not far from the preischemic values, it can be see that β-AS caused a large decrease in APD at the higher pacing rate.

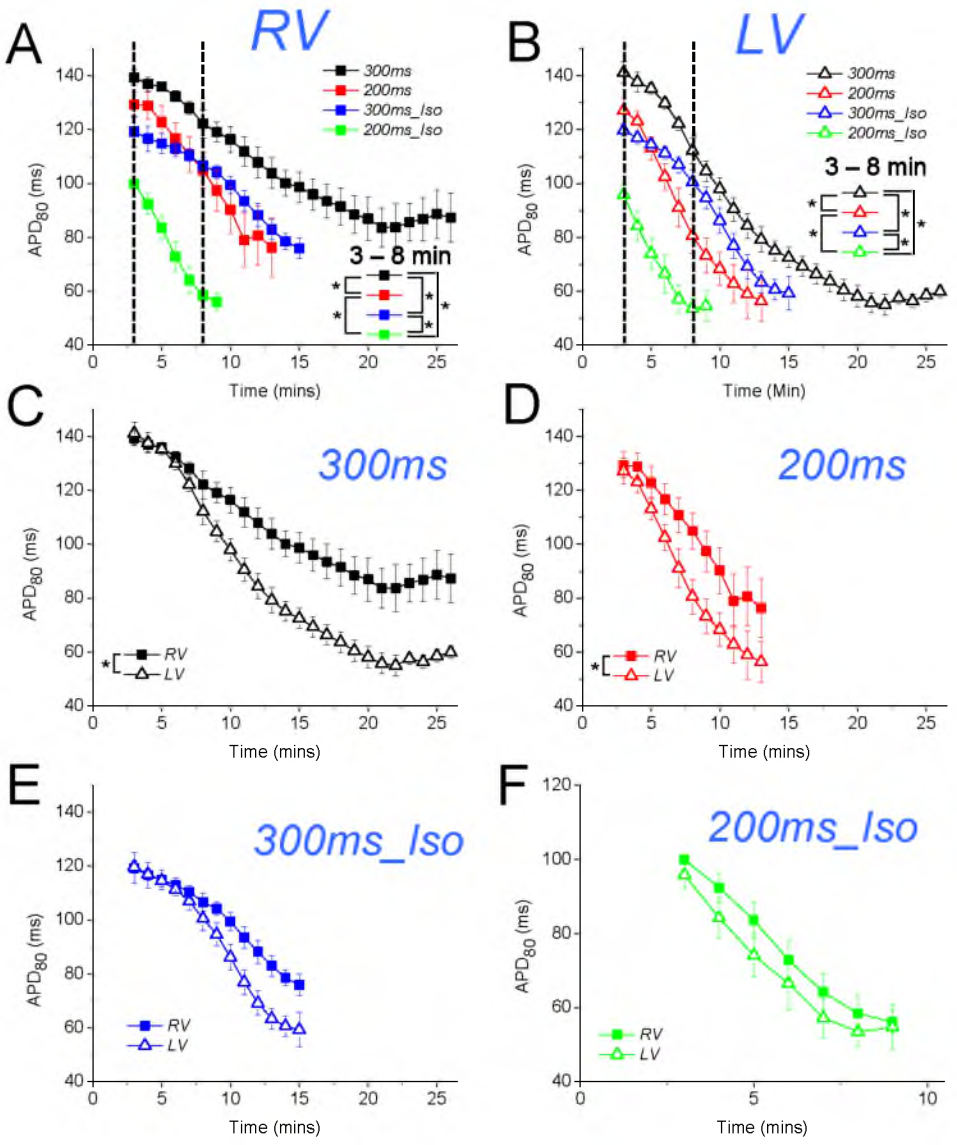


Figure 6.3: The effects of tachy-pacing and β-AS on $APD_{80}$ during ischemia. Note 0 to 3 minutes of $APD_{80}$ data are not shown due to motion artifact in the optical signal in isoproterenol treated groups; furthermore, curves continue only as long as three hearts in each group did not experience VF (see methods for details). Also note that intergroup comparisons were only made for the time points in which at least three hearts were available for comparison in each group, specifically 3 to 8 minutes. Comparisons between chambers were made for all time points with an n of at least 3 without the occurrence of VF in each group. **A-B.** $APD_{80}$ vs. duration of ischemia in the RV and LV, respectively. The relationship between treatment groups is similar in the RV and LV. Both tachy-pacing and β-AS significantly shorten $APD_{80}$ at all time points between 3 to 8 minutes and the combination of tachy-pacing and β-AS exacerbates $APD_{80}$ shortening further. It is indirectly apparent from this graph that tachy-pacing and β-AS independently and combined tend to accelerate the occurrence of VF during ischemia. **C-F.** The interchamber difference in $APD_{80}$ is significant only in the *300ms* and *200ms* groups. Suggesting that β-AS diminishes interchamber differences in $APD_{80}$ shortening. It can also be seen that in all groups VF appears to occur at an $APD_{80}$ around 35 to 70 ms; yet, in *300ms* $APD_{80}$ remains at this shortened duration for several minutes. This suggests that $APD_{80}$ shortening may be a contributor to VF induction during ischemia but is not the primary mechanism. Asterisks denote comparisons with $p<0.05$.

It also seems that the speed of APD shortening during ischemia is the fastest when tachycardia and β-AS are combined (green curves in Figure 6.3). It is of interest then that in the LV the shortest values of $APD_{80}$ measured in all groups before the onset of VF were similar (between 35 and 70 ms). However, note that in *300ms* group (black triangles in Figure 6.3B) $APD_{80}$ stayed around the minimal value for at lest 6 minutes without initiation of VF. Thus, the short APD in the LV may be a necessary, but probably not sufficient condition of VF initiation. In the RV, the $APD_{80}$ values measured before the onset of VF was very different among the different experimental groups (see Figure 6.3A). In both chambers, the $APD_{80}$ time course was significantly different in all pairwise comparisons between groups with the exception of the comparison between *200ms* and *300ms_Iso*, which did not yield statistical significance.

Panels C to F of Figure 6.3 show the same $APD_{80}$ curves as in Panels A and B, but rearranged to highlight the difference between the RV and LV in each group (*300ms*, *200ms*, *300ms_Iso* and *200ms_Iso*, respectively). One can see that a large RV-to-LV $APD_{80}$ gradient develops in the *300ms* group starting from 7 minutes of ischemia (Figure 6.3C). In the *200ms* group, an $APD_{80}$ gradient of the same direction develops earlier, starting from 4-5 minutes of ischemia, but is smaller in magnitude (Figure 6.3D). β-AS decreased the magnitude of the $APD_{80}$ gradient at both pacing frequencies (Figure 6.3, E-F), and almost fully eliminated it in the *200ms_Iso* group. The right-to-left $APD_{80}$ gradient was statistically significant in the *300ms* and *200ms* groups, but not in the *300ms_Iso* and *200ms_Iso groups*.

### 6.4.3 Role of $K_{ATP}$ and $K_{Na}$ in Electrical Depression Produced by the Combination of Tachy-Pacing and β-AS During Ischemia

The data presented above indicate that the combination of tachy-pacing and β-AS during ischemia had mutually potentiating effects in terms of aggravated electrical depression and APD shortening. Both of these effects could be mediated by activation of $K_{ATP}$ channels, perhaps due to enhanced metabolic demand and accelerated ATP depletion under the double challenge of anoxia and increased work of ionic pumps [98]. The possible role of $K_{ATP}$ channels in electrical failure during ischemia can be due to enhanced extracellular $K^+$ accumulation and/or due to the

enhanced sink for the excitatory current leading to source-sink mismatch and conduction failure (so called metabolic sink block [82]. $K_{Na}$ is another metabolically sensitive channel that might play a role under conditions of ischemia and tachycardia (see more in Discussion). Therefore, I performed experiments in which I applied a $K_{ATP}$ channel blocker glybenclamide (10 μM, *200ms_Iso_Glyb* group) or $K_{Na}$ blocker R56865 (0.3 μM, *200ms_Iso_R56* group). The results of these tests are shown in Figures 6.4, 6.5 and 6.6. Note that the data from the *200ms_Iso* group shown in Figures 6.4, 6.5 and 6.6 is the same as shown in Figures 6.1, 6.2, and 6.3. Since the $K^+$ channel blockers were used only against *200ms_Iso* group, I deemed is was easier to understand the data if the analysis of the interaction between tachy-pacing and β-AS was presented separately from the analysis of the $K_{ATP}$ and $K_{Na}$ role in electrophysiological alterations caused by the combination of tachy-pacing and β-AS.

Figure 6.4 shows the result of the statistical analysis of $dV/dt_{max}$ and inexcitability data in 3 groups: *200ms_Iso, 200ms_Iso_Glyb* and *200ms_Iso_R56*. The layout of this figure is the same as in Figure 6.1. All left-hand Panels describe RV, all right-hand Panels describe LV. Panels A and B of Figure 6.4 show the time course of $dV/dt_{max}$ during ischemia in RV and LV, respectively. One can see that in both chambers blockade of $K_{ATP}$ by glybenclamide had no effect on the dynamics of the $dV/dt_{max}$ during ischemia. Rather unexpectedly, R56865 accelerated $dV/dt_{max}$ decline during ischemia in both chambers; this effect, however, was statistically significant only in the RV.

Panels C and D of Figure 6.4 show the percent of excitable area as the function of ischemia duration in RV and LV, respectively. One can see that the overall relationship between the experimental groups is similar to that observed in the time course of $dV/dt_{max}$ shown in Figure 6.4, A-B. However, perhaps due to the threshold nature of excitability loss, the difference between groups is augmented. As a result, some effect of $K_{ATP}$ in terms of postponing the loss of excitability becomes apparent in the RV (see the separation between the green and the pink curves in Figure 6.4C), but the difference between *200ms_Iso* and *200ms_Iso_Glyb* still does not reach statistical significance. In the LV, the effect of $K_{ATP}$ with respect to development of inexcitability is fully absent. In both chambers there is a prominent (and statistically significant) effect of R56865 in

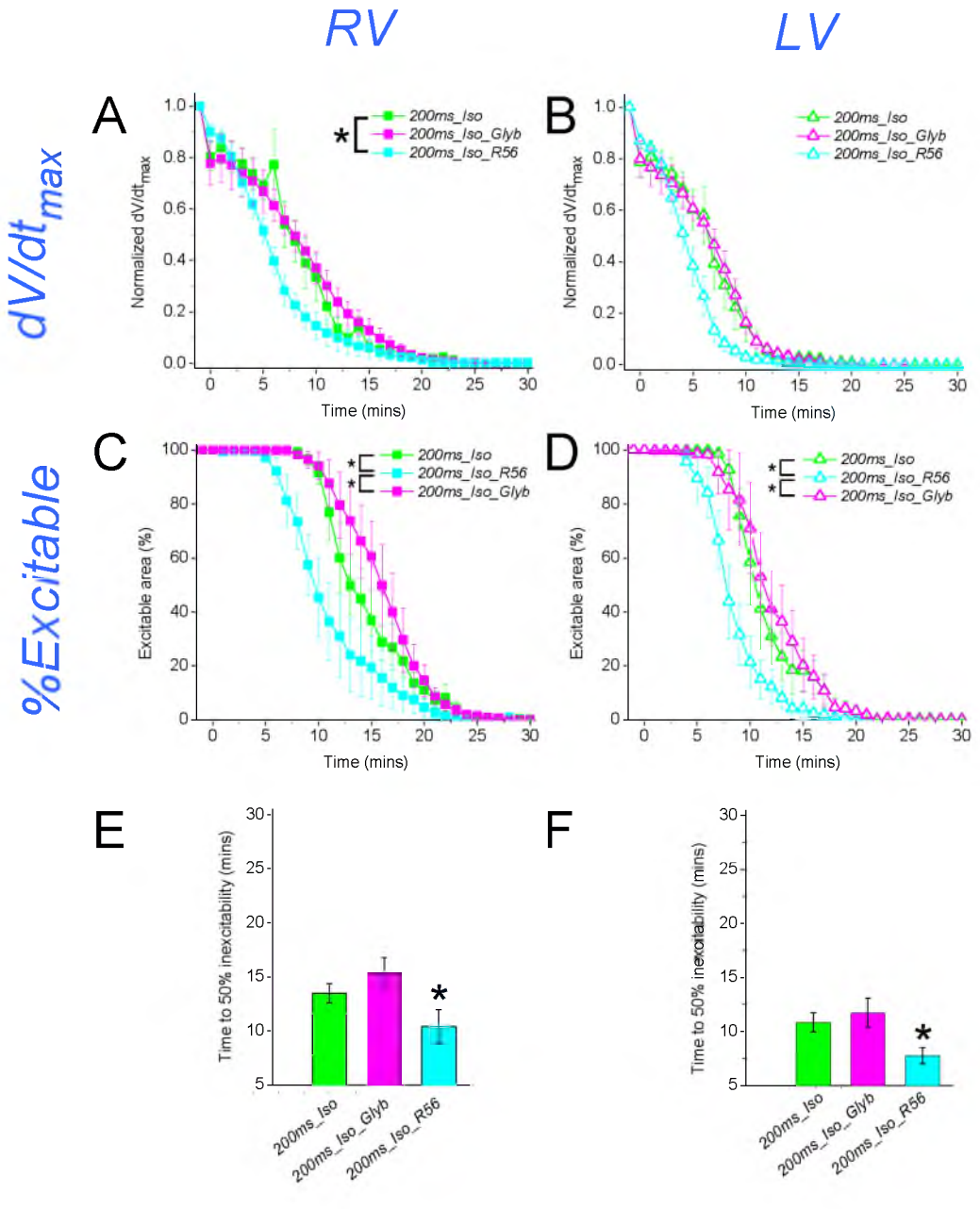


Figure 6.4: Do $K_{ATP}$ and $K_{Na}$ activation contribute to the detrimental effects of combined tachy-pacing and β-AS during ischemia? **A-B.** Effects of $K_{ATP}$ and $K_{Na}$ blockade on $dV/dt_{max}$ during ischemia in the RV and LV, respectively. *200ms_Iso_R56* accelerates deterioration of AP upstroke compared to *200ms_Iso* in the RV ($p<0.05$). **C-D.** Percent excitability is left shifted in *200ms_Iso_R56* compared to *200ms_Iso* and *200ms_Iso_Glyb* in both the RV and LV ($p<0.05$). **E-F.** Time to 50% inexcitability in each group for the RV and LV, respectively. Time to 50% inexcitability is shortened in *200ms_Iso_R56* compared to *200ms_Iso_Glyb* (* $p<0.05$). $K_{ATP}$ blockade appears to play little or no role in mediating the accelerated electrical failure due to tachy-pacing and β-AS during ischemia. Surprisingly, $K_{Na}$ blockade with R56865 further accelerated electrical failure compared to tachy-pacing and β-AS. The effects of R56865 may be explained by its effect on $I_{Na}$, which would exacerbate source-sink mismatch and promote electrical failure (see discussions for details).

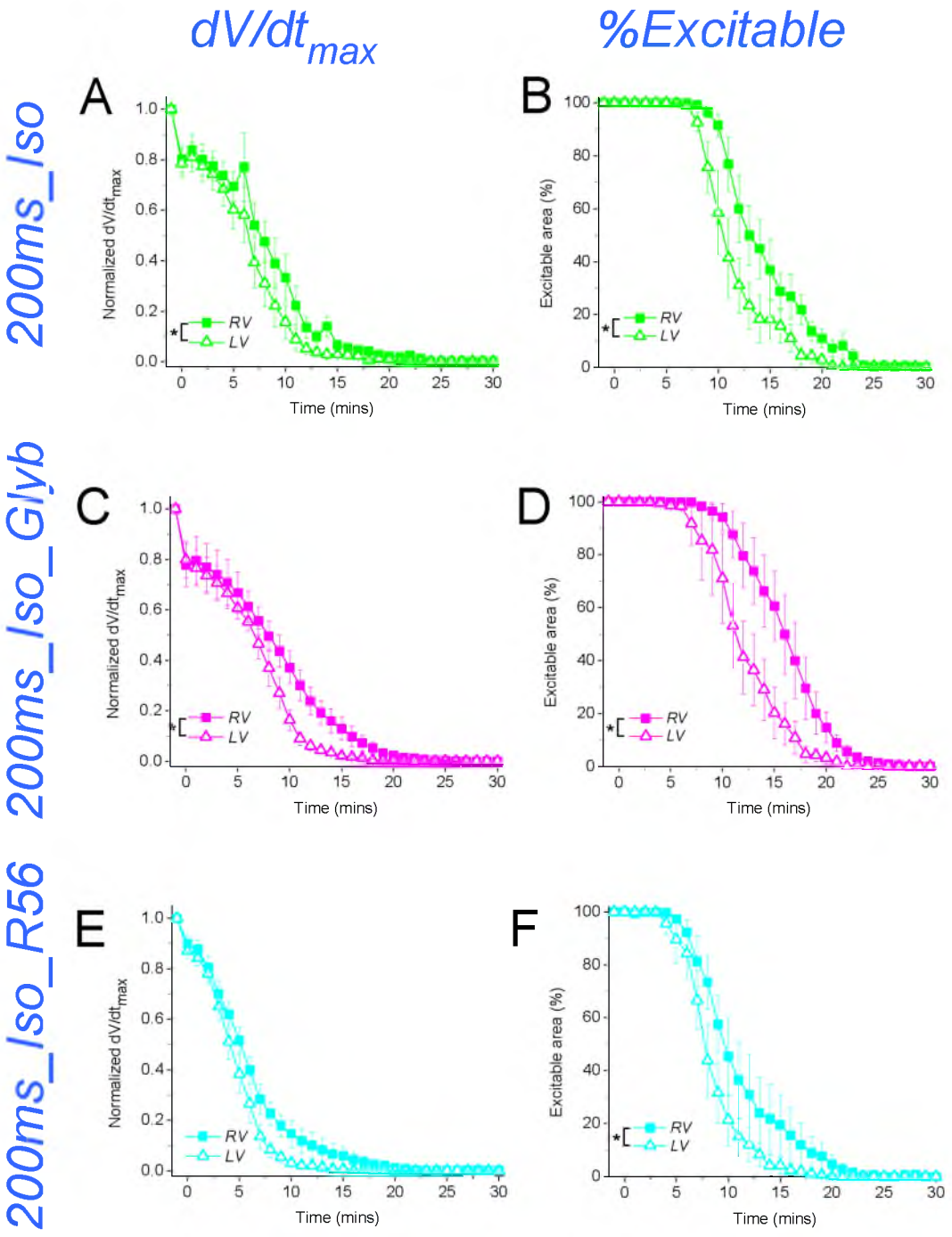


Figure 6.5. Role of $K_{ATP}$ and $K_{Na}$ in the interchamber difference in time course of electrical failure during ischemia. Shows the same data presented in Figure 6.4 but arranged to compare RV and LV. **A, C, E** show $dV/dt_{max}$ vs. duration of ischemia. **B, D, F** show % excitable area vs. duration of ischemia. Interchamber differences are significantly different in all groups for both % excitable area and $dV/dt_{max}$ except in *200ms_Iso_R56* where $dV/dt_{max}$ does not reach significant difference. Overall, $K_{ATP}$ and $K_{Na}$ appear not to be a significant factor in determining interchamber differences. The lack of significant difference in *200ms_Iso_R56* $dV/dt_{max}$ between the RV and LV is likely due to the significant depressant effect compared to *200_Iso,* which was limited to the RV thus diminishing the difference between RV and LV. This may be due to differential functional expression of $K_{Na}$ or $Na^+$ channels between the RV and LV.

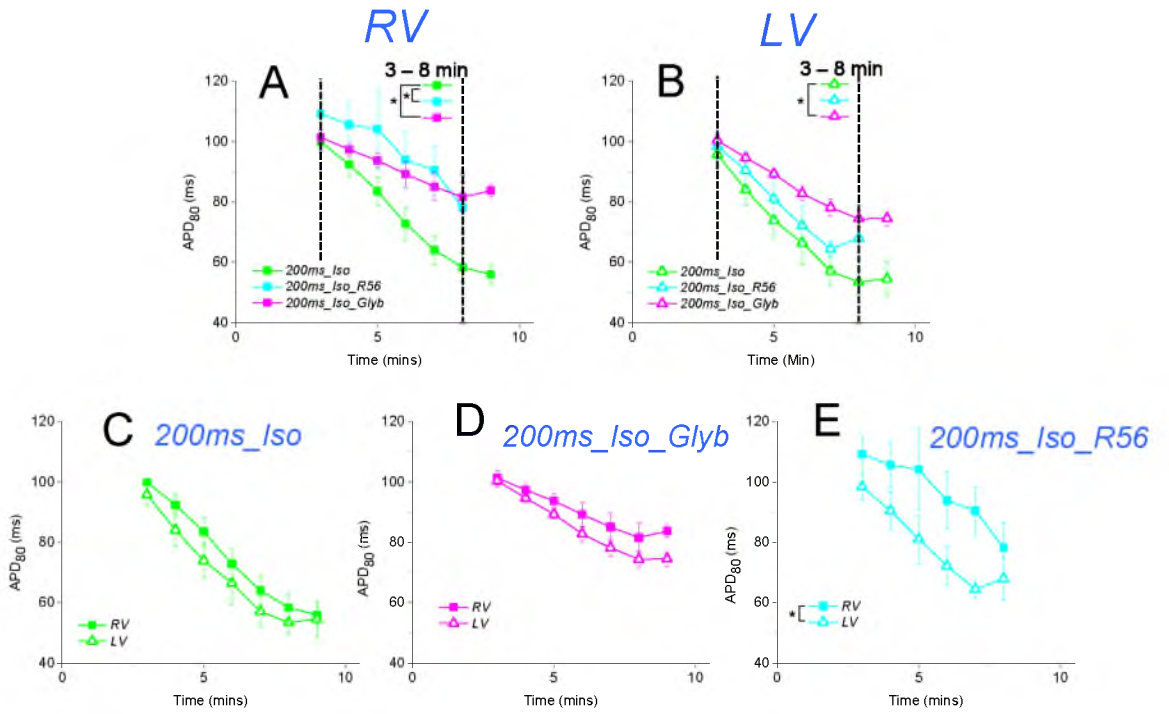


Figure 6.6: Do $K_{ATP}$ and $K_{Na}$ contribute to the shortening effects of tacy-pacing and β-AS on $APD_{80}$ during ischemia? Intergroup comparisons were limited from 3 minutes since motion artifact contaminated the first 2 minutes of $APD_{80}$ measurements in isoproterenol treated hearts and 8 minutes since VF occurred in a large number of hearts after this time point (see text for details). **A-B.** Comparison of $APD_{80}$ vs. duration of ischemia in *200ms_Iso*, *200ms_Iso_R56*, and *200ms_Iso_Glyb* groups (* $p<0.05$). Notice that both R56865 and glybenclamide rescue $APD_{80}$ shortening, and the rate of shortening, compared to *200ms_Iso*. Furthermore, in **C-E** $APD_{80}$ in the RV vs. the LV is only significantly different in the R56865 treated groups. These findings suggests that 1) both $K_{ATP}$ and $K_{Na}$ are being blocked by these interventions and 2) the effect of $K_{Na}$ blockade is larger in the RV than in the LV. The second observation points again to the presence of differential functional expression of $K_{Na}$ between the RV and LV. Also note that, indirectly, these plots suggest that prevention of $APD_{80}$ shortening by glybenclamide and R56865 does not delay the occurrence of VF (see Section 6.4.5 for details).

terms of the accelerated development of inexcitability, which appears to be larger in the RV. In fact, the fraction of excitable area as a function of time is significantly different in the *200ms_Iso_R56* group as compared to both the *200ms_Iso* and *200ms_Iso_Glyb* groups.

Panels E and F of Figure 6.4 show the average time of ischemia at which 50% of the mapped area in RV and LV, respectively, lost excitability. The data are derived from the graphs shown in Figure 6.4, C and D. As mentioned in relation to Figure 6.1 above, the power of the ANOVA test involving only the time points of 50% loss of excitability is less than the power of the test comparing all the time points. As a result, only the difference between the *200ms_Iso_R56* and *200ms_Iso_Glyb* groups is statistically significant. This is probably due to the fact that the

(weak) effect of glybenclamide is opposite to that of R56865, and the small addition to the contrast provided by glybenclamide is just sufficient to reach statistical significance.

Figure 6.5 is redundant with Figure 6.4, but juxtaposes RV and LV curves in one graph, in order to highlight the interchamber differences in the development of electrical depression in three experimental groups (*200ms_Iso*, *200ms_Iso_Glyb* and *200ms_Iso_R56)*. Summarizing Figure 6.5, in all three groups the electrical depression occurred earlier in the LV than in the RV. Glybenclamide apparently slightly increased the difference between the RV and the LV, whereas R56865 did not seem to have any effect.

It should be noted that R56865 has blocking effect with respect to the sodium channel [100-102], which may confound the interpretation of the findings of this study. This issue will be fully addressed in the Discussion taking also into account the APD data shown in Figure 6.6 below. In any event, the data shown in Figures 6.4 and 6.5 suggests that $K_{ATP}$ channels make little or no contribution to the aggravated electrical depression caused by the combination of tachycardia and β-AS.

### 6.4.4 Role of $K_{ATP}$ and $K_{Na}$ in APD Shortening Produced by the Combination of Tachy-Pacing and β-AS During Ischemia

Figure 6.6 summarizes the statistical analysis of APD in three groups: *200ms_Iso*, *200ms_Iso_Glyb*, and *200ms_Iso_R56*. Panels A and B show the time course of $APD_{80}$ during ischemia in RV and LV, respectively. The two vertical dashed lines indicate the time window (3-8 minutes of ischemia) during which the comparison between groups was performed. It can be seen that in the *200ms_Iso* group (green) $APD_{80}$ quickly declines during ischemia in both chambers, at a similar rate. Blockade of $K_{ATP}$ channels with glybenclamide (*200ms_Iso_Glyb* group, pink) dramatically slows down the $APD_{80}$ decline in both chambers between 3 and 9 minutes of ischemia. The effect of R56865 appears to be different in the RV vs. the LV. Namely, in the RV there was a large and statistically significant difference between the *200ms_Iso* and *200ms_Iso_R56* groups at all time points between 3 and 8 minutes of ischemia (measurements later in ischemia were precluded due to the onset of VF). In contrast, in the LV the difference

between *200ms_Iso* and *200ms_Iso_R56* groups was minimal between 3 and 7 minutes of ischemia, and only increased at the 8th minute of ischemia (see Figure 6.6B). It is unlikely that this "last minute" change in the R56865 effect is indicative of an increased $K_{Na}$ role at the 8th minute of ischemia. It is more likely that at this point slowing of the upstroke of the OAP due to electrical depression started to contribute to the APD leading to APD prolongation. In fact, this effect could have explained the plateauing or even the increase in $APD_{80}$, which occurred right before the onset of VF at least in one chamber in each group. In particular, this phenomenon was observed in the *300ms* group (RV and LV, see Figure 6.3C), *200ms* group (RV, see Figure 6.3D), *200ms_Iso* group (LV, see Figure 6.3B), *200ms_Iso_Glyb* (RV and LV, see Figure 6.6D), and *200ms_Iso_R56* (LV, see Figure 6.6B).

Panels C to F of Figure 6.6 show the same $APD_{80}$ curves as in Panels A and B, but rearranged to highlight the difference between the RV and LV in each group (*200ms_Iso*, *200ms_Iso_Glyb* and *200ms_Iso_R56*, respectively). One can see that in the *200ms_Iso* group the right-to-left gradient is very small and not statistically significant. Glybenclamide tends to increase the gradient, yet it remains not statistically significant. Finally, R56865 significantly increases the difference in $APD_{80}$ between the RV and the LV.

In summary, $K_{ATP}$ channels appear to contribute significantly to the progressive APD shortening under the combined conditions of ischemia, tachycardia and β-AS in both ventricular chambers, whereas $K_{Na}$ contributes significantly only in the RV, increasing the interchamber difference in $APD_{80}$.

### 6.4.5 The Relationship Between VF Initiation and Electrical Depression Under Different Experimental Conditions

In my experimental model VF occurred during ischemia in all groups with almost 100% probability. The exception was: one heart in the *200_Iso_R56* group. Overall, the conditions that accelerated electrical depression also promoted earlier initiation of VF. Figure 6.7 shows the time at which VF started in all experimental groups. One can see that both tachycardia (*200ms* group) and β-AS (*300ms_Iso* group) applied individually significantly shortened the time to VF as

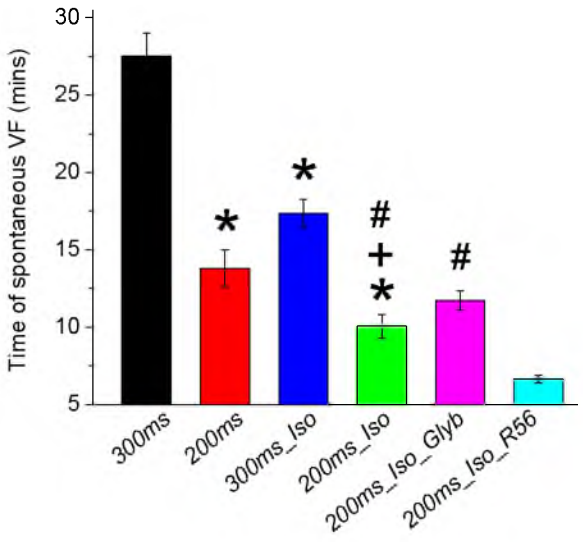


Figure 6.7: Time to spontaneous induction of VF in all six interventions. Note that comparisons with glybenclamide and R56865 were only made between groups with both tachy-pacing and β-AS (namely, *200ms_Iso*, 200ms*_Iso_R56*, and *200ms_Iso_Glyb*). Symbols indicate differences at $p<0.05$ from *300ms* (*), *300Iso* (+), and *200ms_Iso_R56* (#). Both tachy pacing and β-AS, individually and combined accelerated the time to spontaneous VF induction compared to *300ms*. R56865 significantly accelerated the time to VF compared to both *200ms_Iso* and *200ms_Iso_Glyb*. While glybenclamide treatment slightly delayed VF onset it did not reach significance. This may be due to the significant delay in $APD_{80}$ shortening as a result of treatment suggesting that while $APD_{80}$ may not be the primary predictor of VF onset, it may be a contributor.

compared to the control (*300ms* group). The combination of tachycardia and β-AS group) shortened the time to VF even more. Glybenclamide (*200ms_Iso_Glyb* group) was unable to antagonize the VF-promoting effect of the tachycardia/β-AS combination, and R56865 (*200ms_Iso_R56* group) further shortened the time to VF during ischemia.

I tested the relationship between electrical depression in the LV (which occurred earlier than in the RV under all conditions, see Figures 6.2 and 6.5) and VF initiation. In Figure 6.8, I plotted the time of VF initiation vs. the time at which 10% of the mapped region of LV became inexcitable. One can see the emergence of LV inexcitable regions is strongly correlated with the time of VF onset when all the groups are pooled together ($R^2=0.76$, $p<0.001$). It is of interest that the *200ms* group (red triangles) supplies the largest number of points deviating from the general trend.

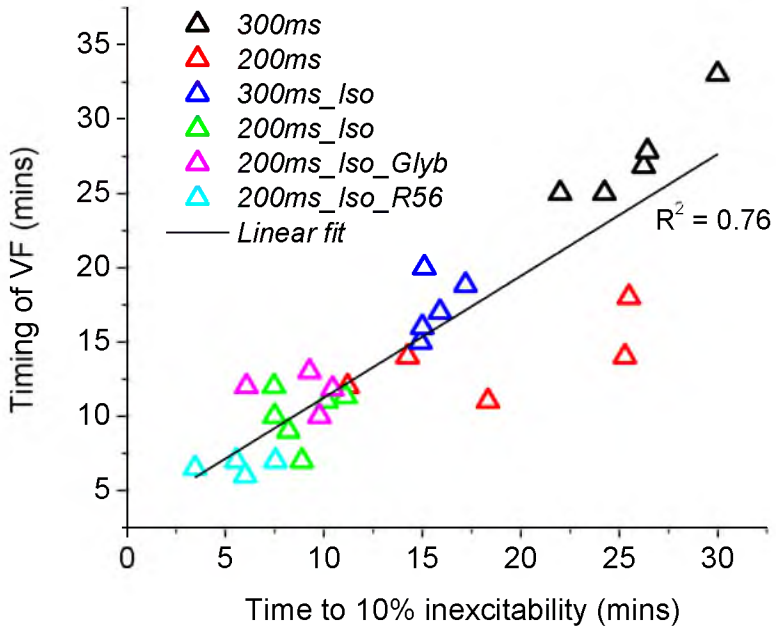


Figure 6.8: Local electrical failure as a predictor of spontaneous VF induction. Time to 10% inexcitability appears to be highly predictive of the time to spontaneous VF induction $R^2$=0.76. The most significant deviation comes from three hearts in the *200ms* group where VF occurs before inexcitability. This large separation within a single group is reminiscent of the dichotomy in the timing of asystole observed in canine hearts under VF, global ischemia, and the absence of isoproterenol [80]. The separation in time to VF in the 200ms group suggests the existence of a bifurcation point in the stress response to tachy-pacing under ischemia. Mechanisms mediating this bifurcation may be important in understanding the mechanism of VF induction.

## 6.5 Discussion

The major findings of this study can be summarized as follows. To my knowledge, this is the first study to show the depressant effect of β-AS on conduction and excitability in the ischemic myocardium. Moreover, this effect was potentiated by tachycardia and also correlated with the initiation of ischemic VF. Lastly, the mutual depressant effect of β-AS and tachycardia on conduction and excitability was not antagonized by the $K_{ATP}$ channel blocker glybenclamide (despite a large effect with respect to the APD) and was promoted by the (nonselective) $K_{Na}$ blocker R56865; which was unexpected considering both rate and β-AS would theoretically increase $Na^+$ influx and accumulation during ischemia. The unexpected outcome, however, may be explained by the off-target effects of R56865, most importantly by the blocking effect with respect to the fast sodium channel which is potentiated at depolarized potentials [102] expected

during ischemia. Despite these nonselective effects of R56865 I likely observed a substantial effect on $I_{KNa}$ as evidenced by decreased APD shortening compared to tachy-pacing and β-AS at least in the RV (see Figure 6.6A and B).

### 6.5.1 Relevant Effects of β-AS on Ion Channels in the Ischemic Myocardium

Myocardial ischemia is associated with large increases in the interstitial levels of epinephrine and norepinephrine. These increases are independent of plasma catecholamines. The excessively high local norepinephrine concentrations are combined with an enhanced responsiveness of the myocyte to catecholamines. According to Schomig et al., myocardial ischemia of 15 minute duration may result in a 100-fold increase in the interstitial catecholamine concentrations, a 2-fold increase in functionally coupled α-adrenoceptor, and a 30% increase in β-adrenoceptors [93]. In the study involving a porcine model of VF-SCA, interstitial norepinephrine increased 6-fold during VF, and progressed to an over 100-fold increase after defibrillation and reperfusion mimicking life-saving procedures in out-of-hospital SCA [86].

As reviewed by Carmeliet [103], β-AS results in stimulation of a number of ionic currents, whereas only a few are reduced. Kindly referring the interested reader to the full review [103], I postulate here that the most relevant affected currents are the fast $Na^+$ current, the slowly activating delayed-rectifier $K^+$ current ($I_{Ks}$), the L-type $Ca^{++}$ current ($I_{Ca,L}$) and $K_{ATP}$. It was shown that both $Na^+$ channel conductance and voltage-dependent availability curves are significantly shifted in the hyperpolarized direction by isoproterenol, the effect mediated by cAMP-dependent phosphorylation [104]. In depolarized cells during early ischemia the negative shift of the inactivation curve could add to the inhibition of the $Na^+$ current, with concomitant reduction in $dV/dt_{max}$ and slowing/block of conduction. However, in another study a (slight) inhibitory effect of isoproterenol with respect to $I_{Na}$ at depolarized potentials could be observed only at unphysiologically high concentration of 1 μM [105], 30 times higher that the concentration used in this study. Thus, it remains uncertain whether this mechanism made a significant contribution to the acceleration of electrical depression and inexcitability induced by β-AS in my study.

$I_{Ks}$ could potentially contribute to the accentuated electrical depression caused by the combination β-AS and tachycardia in my study because this current is enhanced by β-AS and also accumulates at higher excitation rates [106]. Thus, the significant presence of this current at the beginning of the action potential could increase the electrical sink and cause source-sink mismatch similar to the proposed role of $K_{ATP}$ [82]. However, this assumption remains highly speculative, as I found nothing in the literature pointing to such a possibility. However, $I_{Ks}$ is likely to contribute to the enhanced APD shortening caused by β-AS in my study (see Figure 6.3).

β-AS increases peak $I_{Ca,L}$ and slows inactivation, both effects leading to an increased $Ca^{++}$ loading of cardiomyocytes. In addition, β-AS upregulates $Ca^{++}$ uptake into the sarcoplasmic reticulum (SR), increases SR $Ca^{++}$ content, $Ca^{++}$-induced SR $C^{++}$ a release, and the amplitude of the intracellular $Ca^{++}$ transient [103]. The effects of β-AS with respect to $I_{Ca,L}$ gating clearly cannot explain either the decreased excitability and electrical failure, or the APD shortening observed in this study. However, increased peak $I_{Ca,L}$ and prolonged sustained current can contribute to arrhythmias mediated by EADs, whereas increased SR $Ca^{++}$ loading and SR $Ca^{++}$ release can contribute to arrhythmias mediated by DADs (the proarrhythmic mechanisms of β-AS in the ischemic heart are discussed further below).

β-AS can enhance activation of $I_{KATP}$, most likely indirectly, as a result of ATP depletion due to ATP consumption by a stimulated $Na^{+}$-$K^{+}$ pump, by enhanced cAMP synthesis (see Carmeliet in [103] and possibly by $Ca^{++}$ pumps. I observed a dramatic shortening of APD in the presence of β-AS stimulation during ischemia at both pacing rates, but especially at the higher rate (CL=200ms, see Figure 6.3). Based on my data, $K_{ATP}$ was responsible for about 50% of APD reduction occurring in *200ms_Iso* group between 3 and 8 minutes of ischemia (see Figure 2.2A).

### 6.5.2 β-AS and Electrical Depression During Myocardial Ischemia

My study revealed a depressant effect of β-AS on conduction and excitability in ischemic myocardium. Of interest, the depressant effect of β-AS was additive (if not synergistic) to that of the increase in pacing rate, but the effect of β-AS as compared to the effect of the decrease in cycle length from 300 to 200 ms appeared to be stronger. For example, in the LV the increase in pacing

rate decreased the time to 50% of inexcitability by approximately 5.5 minutes, whereas β-AS without increase in the pacing rate decreased the time to 50% of inexcitability by approximately 11 minutes. The two interventions combined decreased the time to 50% of inexcitability by ~17 minutes, which is almost exactly the sum of the effects of individual interventions (see Figure 6.1F). The pattern of electrical depression was highly nonuniform but with a similar pattern in all groups, such that LV experienced earlier depression than RV. I previously observed a similar pattern of nonuniform electrical depression in the epicardium of the RV and the LV of globally ischemic, fibrillating canine hearts [51]. The nonuniform electrical depression was first manifested as local slowing in VF rate (VFR), which eventually progressed to full loss of excitability in some regions while adjacent regions still maintained fibrillatory activity (see Figure 1.5) [51]. In the present study I analyzed the $dV/dt_{max}$ as the index of local excitability. $dV/dt_{max}$ reflects primarily the availability of $Na^+$ channels [103], but in the syncytium depends also on the source-sink relationship, so that a decreased sink (e.g., due to partial cellular uncoupling) may cause an increase in $dV/dt_{max}$ [107]. The canonical mechanism for reduction in $Na^+$ channel availability and $dV/dt_{max}$, as well as the complete loss of excitability during ischemia is the increase in the extracellular level of $[K^+]$ [79, 108]. However, in my previous study I showed that the level of $[K^+]_o$ actually attained in the globally ischemic fibrillating canine heart is too low to explain the observed degree of electrical depression and inexcitability [92]. Also, the depressant effect of isoproterenol observed in this study is difficult to explain in terms of accelerated $[K^+]_o$ elevation, since this beta-agonist was previously shown to reduce $[K^+]_o$ during global ischemia [109]. Also, the blockade of $K_{ATP}$, one of the major sources of ischemic $K^+$ leak by glybenclamide, had virtually no effect on the electrical depression, speaking against the primary role of $[K^+]_o$ in this phenomenon.

A mechanism which could explain the synergism in the effect of β-AS and tachy-pacing with regard to the depression of excitability is the potential presence of a transient inward leak current ($I_{ti}$) which is suggested in Carmiliet's comprehensive review [103] and demonstrated in isolated myocytes by Clusin et al. [110]. In essence, a small inward leak current would depolarize the resting membrane potential ($V_{rest}$) away from the $K^+$ reversal potential ($E_k$). Such a current

would simultaneously reduce source current through $I_{Na}$ inactivaiton and increase sink currents through increased $K^+$ driving force. The combination would lead to source-sink mismatch and hence electrical failure. Clusin points to the likely role of the $Na^+$-$Ca^{++}$ exchange as the molecular identity since $I_{ti}$ is abolished by low extracellular $Na^+$ or $Ca^{++}$.

### 6.5.3 β-AS and Ischemic Arrhythmias

It is well established that β-AS increases incidence of VF in the context of myocardial ischemia and infarction and that β-adrenergic receptor antagonists reduce the incidence of ischemic arrhythmias and sudden cardiac death [93, 97, 103, 111, 112]. The proarrhythmic effects of β-AS are usually explained in terms of "nonreentrant" mechanisms (EADs and DADs) downstream of increased $I_{Ca,L}$ and/or prolonged APD, or increased SR $Ca^{++}$ load and/or spontaneous SR $Ca^{++}$ release (for the sake of space, I will not discuss these diverse mechanisms in more detail here) [94, 112-116]. It should be noted, however, that when it comes to ischemic conditions, the evidence that EADs or DADs are responsible for arrhythmogenesis mediated by β-AS is limited and controversial. Essentially, the promotion of EADs and DADs by β-AS was observed only under conditions of hypoxia [94, 114], which poorly represents real ischemia since at least two critical factors ($K_{ATP}$ activation and hyperkalemia) are absent. More "severe" ischemic conditions, including hyperkalemia and a relatively complete metabolic inhibition (causing $K_{ATP}$ activation) abolish EADs and DADs [94, 95]. While the possible effects of β-AS on impulse propagation in ischemic myocardium were postulated in terms of a "slow response" hypothesis (i.e., β-adrenergic stimulation promotes extremely slow conduction driven exclusively by L-type $Ca^{++}$ current against the backdrop of significant hyperkalemia [96], the relevance of this mechanism to the conditions of real ischemia has never been demonstrated. One potential flaw of this hypothesis would be whether the diastolic $Ca^{++}$ accumulation known to occur during ischemia [103] would cause sufficient $Ca^{++}$ dependent inactivation of $I_{Ca,L}$ to prevent the slow response.

Thus, a careful analysis of the literature leaves us with a relative vacuum regarding the mechanisms that explain the proarrhythmic effects of β-AS in the context of acute but complete

myocardial ischemia. The observation of the temporal correlation between the initiation of ischemic VF and the emergence of inexcitable regions (see Figure 6.1) may help to fill this void by offering a mechanism for VF initiation (and possibly reinitiation after defibrillation shock) which is due to a highly heterogeneous electrical depression and conduction block, possibly downstream of increased intracellular $Ca^{++}$ load and activation of a depolarizing current formerly associated with the entity of $I_{ti}$ [110].

### 6.5.4 Relevance to the outcomes of VF-SCA

While the precise mechanism for the enhanced electrical failure due to β-AS is unclear, the findings of this study confirm the conclusion in the recently published retrospective analyses on clinical epinephrine use (an α- and β-adrenergic agonist) [42-44]. These studies have found that while epinephrine appears to improve return of spontaneous circulation (ROSC) during resuscitation long-term survival to hospital discharge is decreased compared to patients not treated with epinephrine. Presumably, epinephrine treatment enhances ROSC through increased inotropy promoting blood flow and hence reperfusion. Indeed, as I observed isoproterenol treatment enhanced contraction sufficiently to counteract the effects of BDM leading to significant motion artifact in the initial few minutes of my ischemic protocol (see Methods Section 6.3.4). Given that a major concern postresuscitation is recurrent disrhythmias and hemodynamics problems [117], I can speculate that epinephrine treatment may exacerbate these rhythm disorders leading to decreased long-term survival. Another consideration is whether or not accelerated electrical failure can lead to increased myocardial death following reperfusion. This is a topic currently under investigation [128]. The overall conclusion for clinical treatment of VF-SCA is that use of β-blockers or cessation of the use of epinephrine may be advisable but requires further investigation.

# CHAPTER 7

# CONCLUSIONS

Decreasing mortality from VF-SCA is a complex and multifaceted problem. The complexity is made more evident to the reader through the studies contained in the preceding chapters. The entire work described herein is dedicated to the single detail of electrical failure in VF-SCA and does not even touch upon contractile failure, metabolomics deterioration, cell death, or the process of resuscitation. Despite the limited scope, the body of work contained in this manuscript represents a substantial step forward in understanding the pattern and mechanisms of electrical failure in VF-SCA.

## 7.1 Complex VF Gradients and Electrical Failure

The pattern of electrical failure is complex (Chapter 3) and includes not only the previously described transmural gradient in electrical activity [45-50] but also manifests as heterogeneous depression between the LV, RV, and septum. Furthermore, on the surface of the heart, large gradients (up to 4 Hz/mm) develop including regions of electrical silence. Interestingly, the decrease in excitation rate and the occurrence of inexcitability appears to be a function of increased postrepolarization refractoriness rather than a consequence of APD shortening (which I showed was relatively modest during VF-SCA). As time spent in VF-SCA elapses the complexity of the pattern increases eventually leading to accumulation of inexcitable areas, culminating in global asystole. It is likely that this increasing heterogeneity and the development of regions with conduction block lead to reentry upon defibrillation resulting in

Refibrillation and lack of success in resuscitation explaining, in part, the progressive increase in mortality as a function of time following initiation of VF-SCA (see Chapter 1). In addition to the published work in Chapter 3, I observed a dichotomy in the timing of asystole [80, 118, 119] wherein approximately 50% of canine hearts experienced asystole prior to 10minutes of VF-SCA (early asysotle, EARLY ASYS) and the remaining hearts reached asystole at greater than 20 minutes (late asystole, LATE ASYS). It is of interest to ask 1) what are the mechanisms by which heterogeneities in electrical failure develop during VF-SCA, 2) what promotes EARLY ASYS and is it correlated to decreased survival (see Section 7.2.1.1), and 3) would reducing heterogeneities during VF-SCA result in greater success during resuscitation (see Section 7.2.1, Future Work).

## 7.2 Mechanisms of Electrical Failure

Having established the phenomenology of electrical failure in VF-SCA I sought to answer the first question. What are the mechanisms by which heterogeneities in electrical failure occur? Also, what causes electrical failure in general during VF-SCA? I first tested the roles of previously hypothesized mechanisms of electrical failure namely $K_{ATP}$ opening and hyperkalemia [79, 82].

### 7.2.1 $I_{KATP}$, Hyperkalemia, and Glycolysis

In Chapter 4 evidence was presented concerning the role of $K_{ATP}$ opening in heterogeneous electrical depression and failure. $K_{ATP}$ blockade delayed the heterogeneous electrical depression and failure on the EPI and eliminated the occurrence of asystole during the first 10 minutes of VF-SCA. An interesting note to this story is that $K_{ATP}$ blockade prevented the occurrence of EARLY ASYS in canine hearts, but the pattern of electrical depression and failure was similar in $K_{ATP}$ blocker treated hearts to that observed in LATE ASYS hearts [118]. This suggests that the occurrence of EARLY ASYS is modulated by $I_{KATP}$. Interestingly, two interventions promote the occurrence of EARLY ASYS. One is treatment with the $I_{KATP}$ activator cromakalim (Chapter 4), the other is the application of high serum glucose [80]. These observations point to the importance of glycolysis in modulating electrical failure. The work by Shibayama et al. showed that in EARLY ASYS hearts there was greater lactate accumulation early

in VF-SCA [80]. Combined with the finding by Weiss and Shine that glycolytic ATP is the key regulator of $I_{KATP}$ [81] it is plausible that increased serum glucose promotes early lactate inhibition of glycolysis leading to accelerated depletion of ATP resulting in $I_{KATP}$ activation and EARLY ASYS. Further evidence for the role of glycolytic ATP can be found in an abstract published by Venable et al. where the timing of asystole and mitochondrial potential depolarization were measured. Venable et al. found that the application of $Na^+$-Iodoacetate, a glycolysis inhibitor, greatly accelerated the occurrence of asystole and mitochondrial depolarization in leporine hearts [120]; thus, pointing to the likely role of glycolytic ATP in maintaining not only electrical activity but also mitochondrial potential. Despite the importance of $I_{KATP}$ observed in Chapter 4, pharmacological $K_{ATP}$ activation greater than what is expected during VF-SCA based on bulk tissue $[ATP]_i$ via cromakalim did not cause electrical failure (see Chapter 5). Indeed, the work contained in Chapter 5 not only shows lack of electrical failure from pharmacological $K_{ATP}$ activation but also shows that hyperkalemia alone is not sufficient to reproduce the pattern of electrical depression observed during VF-SCA. In addition, the combination of supramaximal $K_{ATP}$ activation and hyperkalemia is also insufficient to produce the degree and pattern of electrical depression seen during VF-SCA. Furthermore, measurements of $[K^+]_o$ accumulation during VFSCA show that $[K^+]_o$ accumulates more rapidly in EARLY ASYS hearts [119] again pointing to activation of $K^+$ currents such as $K_{ATP}$. Taken together these findings point to an additional mechanism, or mechanisms, modulating electrical failure and the important role of glycolysis in maintaining electrical excitability during VFSCA. The relationship between $K_{ATP}$/hyperkalemia and glycolysis warrants further investigation.

### 7.2.2 Excitation Rate and β-Adrenergic Stimulation

During the search to determine the additional mechanisms at play in electrical failure during VF-SCA I observed that in leporine hearts high excitation rate and β-AS promoted electrical failure, separately. In addition, I found that the effects of high rate and β-AS were synergistic whereby the combination promoted greater electrical failure that either intervention alone (Chapter 6). These findings have profound implications for current clinical practice in

resuscitation from VF-SCA. Namely, the administration of epinephrine to promote ROSC may be detrimental since β-AS increases the excitation frequency of VF [87]. Interestingly, the detrimental effects of high rate and β-AS were not abolished by $K_{ATP}$ channel blockade. In fact, an effect of $I_{KATP}$ blockade was not observed in electrical failure. Furthermore, blockade of $I_{KNa}$ using the compound R56865 caused acceleration of electrical failure, although this detrimental effect may be due to the effects of R56865 on $I_{Na}$ [100-102]. The lack of rescue from $I_{KATP}$ and $I_{KNa}$ blockade point again to additional mechanisms at play in electrical failure during VF-SCA, likely not through modulation of $K^+$ flux.

## 7.3 Future Work

### 7.3.1 Mechanisms of Electrical Failure: Inward Leak Current

This dissertation shows that the traditional theories for electrical failure during ischemia (hyperkalemia and $I_{KATP}$) are insufficient to explain the complex patterns of VF and electrical failure observed during VFSCA. The study by Blake et al. provides an interesting insight into a potential mechanism for electrical failure [89]. Blake et al. showed excitation rate plays a role in electrical deterioration during regional ischemia by measuring the deviation of $V_{rest}$ from the estimated $E_K$. It was also shown that the application of high $[Ca^{++}]_o$ and high rate was synergistic in promoting $V_{rest}$ deviation from $E_k$. By returning to the GHK equation (Equation 2) it is clear that for $V_{rest}$ to deviate from $E_K$ either $g_{Na}$, $g_{Ca}$, $g_{Cl}$, or other ion conductance for an inward current must be greater than zero. The consequences of such a current can be profound and 2-fold. First, as illustrated in Figure 7.1 (lower row) a small inward leak current can depolarize $V_{rest}$ slightly, leading to a substantial decrease in $Na^+$ channel availability due to the sharp downward slope of the sigmoid in this voltage range: in effect, reducing source current. Second, if $V_{rest}$ is greater than $E_K$ due to $Na^+$ and/or $Ca^{++}$ conductance being greater than zero there is an increase in *emf* for $K^+$ efflux: in effect, increasing sink current. A small inward leak current can exacerbate source-sink mismatch by both decreasing source and increasing sink and promote electrical failure. The question is whether there is evidence in literature for an inward leak current.

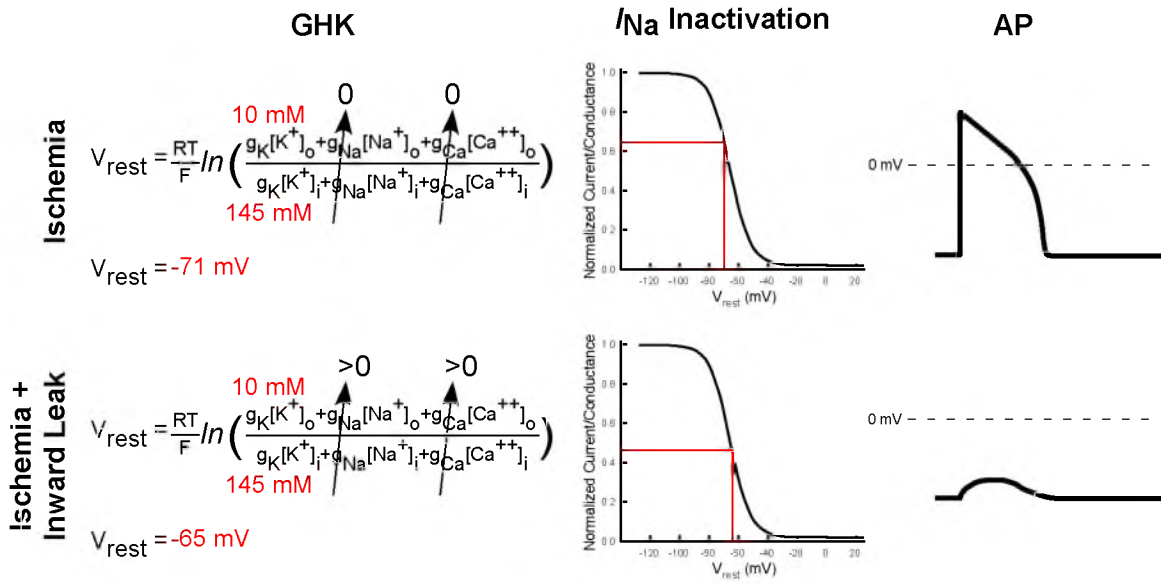


**Figure 7.1**: The consequences of inward leak current on electrical excitability. The upper row is a reproduction from Figure 1.4 showing the effects of hyperkalemia on the AP through effects on $Na^+$ channel availability. The lower row illustrates the consequences of a small $Na^+$ or $Ca^{++}$ leak current. A small inward leak current can depolarized $V_{rest}$ slightly but, due to the location on the sigmoidal curve, result in a relatively large reduction in $I_{Na}$ availability. Furthermore, $V_{rest}$ depolarization away from $E_k$ leads to greater *emf* for $K^+$, in essence, increasing sink. A small inward leak current can lead to increased source-sink mismatch and electrical failure.

While Blake et al. [89] show a deviation between estimated $E_K$ and $V_{rest}$ during high pacing rate and $Ca^{++}$ administration, Kleber et al. [121] shows no deviation between $V_{rest}$ and $E_k$ during ischemia. Yet both Blake and Kleber present an estimated $E_k$ (due to the difficulty in measuring intracellular $K^+$ concentration). Perhaps the most convincing evidence in favor of a deviation between $E_K$ and $V_{rest}$ during ischemia is the work by Weiss and Shine [122] where in a quiescent wedge preparation $[K^+]_o$ accumulation was observed during ischemia: $[K^+]_o$ accumulation cannot occur without $K^+$ efflux and $K^+$ efflux cannot occur without an *emf* for $K^+$, which requires that $E_k$ and $V_{rest}$ are not equal. In addition to the work in whole heart and tissue preparations described above, Clusin et al. [110] showed in chick embryonic myocytes a sustained inward current in response to pharmacological metabolic challenge. Furthermore, Clusin et al. found that this sustained inward current was modulated by altering extracellular $Ca^{++}$ or $Na^+$ concentrations. This finding points to the possible roles of the $Na^+$-$Ca^{++}$ exchange (NCX), or potentially a combination of ischemic effects on $I_{CaL}$, or $I_{Na}$. For example, ischemia has been shown to enhance a noninactivating component of $I_{Na}$ (late-$I_{Na}$) [123]. My preliminary results

indicate that the late-$I_{Na}$ is not likely the identity of the inward leak current but the possible role of NCX remains to be tested. Interestingly, studies have found detrimental effects of $Ca^{++}$ administration during resuscitation in patients in VF-SCA—hence $Ca^{++}$ is not recommended by the ACLS guidelines for patients found in VF except under special circumstances [124].

Another intriguing possibility for the identity of the inward leak current is the development of nonspecific sarcolemmal leak during ischemia. Liu et al. speculated on the occurrence of this phenomenon due to the accumulation of lysophosphatidylcholine during ischemia leading to the formation of nonselective pores in the sarcolemma [125, 126]. While the idea of nonspecific leak is an attractive one, my preliminary results using a nonionic copolymer surfactant, Poloxamer 188 (Sigma-Aldrich), were not promising. Furthermore, an abstract published by Sciuto et al. [127] attempted to detect the occurrence of sarcolemmal permeability during Ischemia using confocal imaging of fluorphores which fluoresce when bound to ribonucleic and nucleic acids but found no evidence of sarcolemmal permeability during ischemia. Overall, it appears that the inward leak current is likely modulated by a $Ca^{++}$ dependent mechanism, which is in agreement with my finding that β-AS promotes electrical failure since the primary action of β-AS is the upregulation of $Ca^{++}$ signaling and cycling. Furthermore, it is known that during ischemia, $[Ca^{++}]_i$ is elevated [103] and hence would activate NCX forward mode producing an inward current. Given the discussion concerning the existence and potential sources of inward leak currents, future work should focus on these mechanisms and determining if and how they contribute to electrical failure during VF-SCA.

### 7.3.2 Additional Projects

Identifying and elucidating the role of the inward leak current is the most obvious next step. Nevertheless, there are several important and exciting projects that can be developed moving forward from this dissertation. In Section 7.2.1, I discussed the potential importance of glycolysis in determining the outcomes of electrical failure in VF-SCA. There are several points of interest. In terms of epidemiology, 1) is there a similar outcome in timing of asystole in the human population and 2) can increased prevalence of metabolic disorders like diabetes mellitus

[128] explain the increased incidence of asystole [36-39]? This work would require a large clinical dataset with a cross-disease investigation into the risk of VF-SCA and survival following the event. On the other hand, projects probing the physiological relationship between glycolysis, glycolytic ATP, and electrical activity can be investigated. For example, the regulation of $I_{KATP}$ through subsarcolemmal ATP derived from glycolysis during ischemia could potentially be investigated using techniques such as total internal reflection fluorescence imaging (TIRF) combined with an ATP sensitive fluorophore in isolated myocytes during simulated ischemia in the presence or absence of pharmacological modulators of glycolysis. In addition to the continued investigation of the pathophysiology of VF-SCA, it is also critical to begin the investigation of electrical recovery during resuscitation whereby based on the physiological understanding of electrical failure in VF-SCA I can begin to design interventions to apply during resuscitation that will significantly improve outcome: in the case of electrical recovery, to specifically reduce postreperfusion arrhythmias. Clearly, there are still years, if not decades, of work ahead in order to understand the physiology of VF-SCA and resuscitation.

## 7.4 Overall Summary and Significance

This dissertation represents the first body of work in which a systematic examination of traditionally accepted hypotheses (hyperkalemia and $I_{KATP}$ activation) for electrical failure in VF-SCA were tested. The result was that neither mechanism individually or combined was sufficient to explain the pattern or degree of electrical failure in VF-SCA. What was discovered was the dependence of electrical failure on both excitation rate and β-AS. While the findings of this dissertation do not provide any direct evidence to change clinical treatment of VF-SCA it does point toward crucial questions that should be studied further in clinically relevant models. First, this dissertation provides direct evidence that β-AS promotes electrical failure. Since in the clinical setting, asystole (i.e., electrical failure) is correlated with much higher mortality, epinephrine treatment may be detrimental. Indeed, the literature on the benefits of epinephrine treatment during resuscitation point towards the same conclusion [42-44, 86]. Second, although more indirect, this dissertation calls into question the use of glucose as a treatment during VF-

SCA. While glucose infusion has been shown to improve cerebrovascular protection during resuscitation [129, 130] evidence presented in this dissertation points towards a potentially detrimental effect on cardiac electrical activity [80]. Furthermore, the potential interplay between outcomes in VF-SCA and metabolic disorders (especially those that raise serum glucose) point toward the necessity for a better understanding of the relationship between diabetes and cardiac arrest. Overall, this dissertation simultaneously provides insight into detailed physiological mechanisms of electrical failure, deepens the need for a system's physiology approach to understand the interplay between electrophysiology and metabolism, and point's toward the need for cross-disease and cross-specialty approaches to the treatment of VF-SCA.

## REFERENCES


1 Bayes de Luna, A., and Elosua, R.: 'Sudden Death,' Rev Esp Cardiol, 2012, 65, (11), pp. 1039-1052

2 Chen, P.S., Wu, T.J., Ting, C.T., Karagueuzian, H.S., Garfinkel, A., Lin, S.F., and Weiss, J.N.: 'A tale of two fibrillations,' Circulation, 2003, 108, (19), pp. 2298-2303

3 Lloyd-Jones, D., Adams, R., Carnethon, M., De Simone, G., Ferguson, T.B., Flegal, K., Ford, E., Furie, K., Go, A., Greenlund, K., Haase, N., Hailpern, S., Ho, M., Howard, V., Kissela, B., Kittner, S., Lackland, D., Lisabeth, L., Marelli, A., McDermott, M., Meigs, J., Mozaffarian, D., Nichol, G., O'Donnell, C., Roger, V., Rosamond, W., Sacco, R., Sorlie, P., Stafford, R., Steinberger, J., Thom, T., Wasserthiel-Smoller, S., Wong, N., Wylie-Rosett, J., and Hong, Y.: 'Heart disease and stroke statistics--2009 update: a report from the American Heart Association Statistics Committee and Stroke Statistics Subcommittee,' Circulation, 2009, 119, (3), pp. e21-181

4 Lloyd-Jones, D., Adams, R.J., Brown, T.M., Carnethon, M., Dai, S., De Simone, G., Ferguson, T.B., Ford, E., Furie, K., Gillespie, C., Go, A., Greenlund, K., Haase, N., Hailpern, S., Ho, P.M., Howard, V., Kissela, B., Kittner, S., Lackland, D., Lisabeth, L., Marelli, A., McDermott, M.M., Meigs, J., Mozaffarian, D., Mussolino, M., Nichol, G., Roger, V.L., Rosamond, W., Sacco, R., Sorlie, P., Thom, T., Wasserthiel-Smoller, S., Wong, N.D., and Wylie-Rosett, J.: 'Heart disease and stroke statistics--2010 update: a report from the American Heart Association,' Circulation, 2010, 121, (7), pp. e46-e215

5 Myerburg, R.J., Halperin, H., Egan, D.A., Boineau, R., Chugh, S.S., Gillis, A.M., Goldhaber, J.I., Lathrop, D.A., Liu, P., Niemann, J.T., Ornato, J.P., Sopko, G., Van Eyk, J.E., Walcott, G.P., Weisfeldt, M.L., Wright, J.D., and Zipes, D.P.: 'Pulseless electric activity: definition, causes, mechanisms, management, and research priorities for the next decade: report from a National Heart, Lung, and Blood Institute workshop,' Circulation, 2013, 128, (23), pp. 2532-2541

6 Kannel, W.B., and McGee, D.L.: 'Epidemiology of sudden death: insights from the Framingham Study,' Cardiovasc Clin, 1985, 15, (3), pp. 93-105

7 Kannel, W.B., and Schatzkin, A.: 'Sudden death: lessons from subsets in population studies,' J Am Coll Cardiol, 1985, 5, (6 Suppl), pp. 141B-149B

8 Gang, U.J., Jons, C., Jorgensen, R.M., Abildstrom, S.Z., Haarbo, J., Messier, M.D., Huikuri, H.V., and Thomsen, P.E.: 'Heart rhythm at the time of death documented by an implantable loop recorder,' Europace, 2010, 12, (2), pp. 254-260

9 Luu, M., Stevenson, W.G., Stevenson, L.W., Baron, K., and Walden, J.: 'Diverse mechanisms of unexpected cardiac arrest in advanced heart failure,' Circulation, 1989, 80, (6), pp. 1675-1680

10 Mitchell, L.B., Pineda, E.A., Titus, J.L., Bartosch, P.M., and Benditt, D.G.: 'Sudden death in patients with implantable cardioverter defibrillators: the importance of post-shock electromechanical dissociation,' J Am Coll Cardiol, 2002, 39, (8), pp. 1323-1328

11 Deakin, C.D., and Nolan, J.P.: 'European Resuscitation Council guidelines for resuscitation 2005. Section 3. Electrical therapies: automated external defibrillators, defibrillation, cardioversion and pacing,' Resuscitation, 2005, 67 Suppl 1, pp. S25-37

12 Valenzuela, T.D., Roe, D.J., Cretin, S., Spaite, D.W., and Larsen, M.P.: 'Estimating effectiveness of cardiac arrest interventions: a logistic regression survival model,' Circulation, 1997, 96, (10), pp. 3308-3313

13 Chan, P.S., Krumholz, H.M., Nichol, G., and Nallamothu, B.K.: 'Delayed time to defibrillation after in-hospital cardiac arrest,' N Engl J Med, 2008, 358, (1), pp. 9-17

14 Berdowski, J., ten Haaf, M., Tijssen, J.G., Chapman, F.W., and Koster, R.W.: 'Time in recurrent ventricular fibrillation and survival after out-of-hospital cardiac arrest,' Circulation, 2010, 122, (11), pp. 1101-1108

15 Mader, T.J., Nathanson, B.H., Millay, S., Coute, R.A., Clapp, M., and McNally, B.: 'Out-of-hospital cardiac arrest outcomes stratified by rhythm analysis,' Resuscitation, 2012, 83, (11), pp. 1358-1362

16 Hallstrom, A., Rea, T.D., Mosesso, V.N., Jr., Cobb, L.A., Anton, A.R., Van Ottingham, L., Sayre, M.R., and Christenson, J.: 'The relationship between shocks and survival in out-of-hospital cardiac arrest patients initially found in PEA or asystole,' Resuscitation, 2007, 74, (3), pp. 418-426

17 Myerburg, R.J., Fenster, J., Velez, M., Rosenberg, D., Lai, S., Kurlansky, P., Newton, S., Knox, M., and Castellanos, A.: 'Impact of community-wide police car deployment of automated external defibrillators on survival from out-of-hospital cardiac arrest,' Circulation, 2002, 106, (9), pp. 1058-1064

18 Neukamm, J., Grasner, J.T., Schewe, J.C., Breil, M., Bahr, J., Heister, U., Wnent, J., Bohn, A., Heller, G., Strickmann, B., Fischer, H., Kill, C., Messelken, M., Bein, B., Lukas, R., Meybohm, P., Scholz, J., and Fischer, M.: 'The impact of response time reliability on CPR incidence and resuscitation success: a benchmark study from the German Resuscitation Registry,' Crit Care, 2011, 15, (6), pp. R282

19 O'Hearn, P.: 'Early defibrillation: lessons learned,' J Cardiovasc Nurs, 1996, 10, (4), pp. 24-36

20 Sladjana, A., Gordana, P., and Ana, S.: 'Emergency response time after out-of-hospital cardiac arrest,' Eur J Intern Med, 2011, 22, (4), pp. 386-393

21 Swor, R.A., Boji, B., Cynar, M., Sadler, E., Basse, E., Dalbec, D.L., Grubb, W., Jacobson, R., Jackson, R.E., and Maher, A.: 'Bystander vs EMS first-responder CPR: initial rhythm and outcome in witnessed nonmonitored out-of-hospital cardiac arrest,' Acad Emerg Med, 1995, 2, (6), pp. 494-498

22 Mollison, W.M.: 'Case of heart failure during an operation for the removal of tonsils and adenoids; heart massage through an abdominal incision; recovery,' Proc R Soc Med, 1917, 10, (Sect Anaesth), pp. 1-7

23 Orr, V.B.: 'Heart Massage in heart failure during anaesthesia,' Proc R Soc Med, 1909, 3, (Anaesth), pp. 1-16

24 Zoll, P.M., and Linenthal, A.J.: 'AC and DC countershock for arrhythmias,' JAMA, 1964, 188, pp. 327

25 Zoll, P.M., Linenthal, A.J., Norman, L.R., Paul, M.H., and Gibson, W.: 'Treatment of unexpected cardiac arrest by external electric stimulation of the heart,' N Engl J Med, 1956, 254, (12), pp. 541-546

26 Jude, J.R., Kouwenhoven, W.B., and Knickerbocker, G.G.: 'Clinical and experimental application of a new treatment for cardiac arrest,' Surg Forum, 1960, 11, pp. 252-254

27 Jude, J.R., Kouwenhoven, W.B., and Knickerbocker, G.G.: 'Cardiac arrest. Report of application of external cardiac massage on 118 patients,' JAMA, 1961, 178, pp. 1063-1070

28 Neumar, R.W., Otto, C.W., Link, M.S., Kronick, S.L., Shuster, M., Callaway, C.W., Kudenchuk, P.J., Ornato, J.P., McNally, B., Silvers, S.M., Passman, R.S., White, R.D., Hess, E.P., Tang, W., Davis, D., Sinz, E., and Morrison, L.J.: 'Part 8: adult advanced cardiovascular life support: 2010 American Heart Association Guidelines for Cardiopulmonary Resuscitation and Emergency Cardiovascular Care,' Circulation, 2010, 122, (18 Suppl 3), pp. S729-767

29 Caffrey, S.: 'Feasibility of public access to defibrillation,' Curr Opin Crit Care, 2002, 8, (3), pp. 195-198

30 Stiell, I.G., Walker, R.G., Nesbitt, L.P., Chapman, F.W., Cousineau, D., Christenson, J., Bradford, P., Sookram, S., Berringer, R., Lank, P., and Wells, G.A.: 'BIPHASIC trial: a randomized comparison of fixed lower versus escalating higher energy levels for defibrillation in out-of-hospital cardiac arrest,' Circulation, 2007, 115, (12), pp. 1511-1517

31 van Alem, A.P., Chapman, F.W., Lank, P., Hart, A.A., and Koster, R.W.: 'A prospective, randomised and blinded comparison of first shock success of monophasic and biphasic waveforms in out-of-hospital cardiac arrest,' Resuscitation, 2003, 58, (1), pp. 17-24

32 Walker, R.G., Koster, R.W., Sun, C., Moffat, G., Barger, J., Dodson, P.P., and Chapman, F.W.: 'Defibrillation probability and impedance change between shocks during resuscitation from out-of-hospital cardiac arrest,' Resuscitation, 2009, 80, (7), pp. 773-777

33 Yao, L., Wang, P., Zhou, L., Chen, M., Liu, Y., Wei, X., and Huang, Z.: 'Compression-only cardiopulmonary resuscitation vs standard cardiopulmonary resuscitation: an updated meta-analysis of observational studies,' Am J Emerg Med, 2014

34 Yeung, J., Chilwan, M., Field, R., Davies, R., Gao, F., and Perkins, G.D.: 'The impact of airway management on quality of cardiopulmonary resuscitation: An observational study in patients during cardiac arrest,' Resuscitation, 2014

35 Yeung, J., Davies, R., Gao, F., and Perkins, G.D.: 'A randomised control trial of prompt and feedback devices and their impact on quality of chest compressions-A simulation study,' Resuscitation, 2014, 85, (4), pp. 553-559

36 Cobb, L.A., Fahrenbruch, C.E., Olsufka, M., and Copass, M.K.: 'Changing incidence of out-of-hospital ventricular fibrillation, 1980-2000,' JAMA, 2002, 288, (23), pp. 3008-3013

37 Herlitz, J., Andersson, E., Bang, A., Engdahl, J., Holmberg, M., lindqvist, J., Karlson, B.W., and Waagstein, L.: 'Experiences from treatment of out-of-hospital cardiac arrest during 17 years in Goteborg,' Eur Heart J, 2000, 21, (15), pp. 1251-1258

38 Polentini, M.S., Pirrallo, R.G., and McGill, W.: 'The changing incidence of ventricular fibrillation in Milwaukee, Wisconsin (1992-2002),' Prehosp Emerg Care, 2006, 10, (1), pp. 52-60

39 Vayrynen, T., Boyd, J., Sorsa, M., Maatta, T., and Kuisma, M.: 'Long-term changes in the incidence of out-of-hospital ventricular fibrillation,' Resuscitation, 2011, 82, (7), pp. 825-829

40 Gilbert, M., Busund, R., Skagseth, A., Nilsen, P.A., and Solbo, J.P.: 'Resuscitation from accidental hypothermia of 13.7 degrees C with circulatory arrest,' Lancet, 2000, 355, (9201), pp. 375-376

41 Nielsen, N., Wetterslev, J., Cronberg, T., Erlinge, D., Gasche, Y., Hassager, C., Horn, J., Hovdenes, J., Kjaergaard, J., Kuiper, M., Pellis, T., Stammet, P., Wanscher, M., Wise, M.P., Aneman, A., Al-Subaie, N., Boesgaard, S., Bro-Jeppesen, J., Brunetti, I., Bugge, J.F., Hingston, C.D., Juffermans, N.P., Koopmans, M., Kober, L., Langorgen, J., Lilja, G., Moller, J.E., Rundgren, M., Rylander, C., Smid, O., Werer, C., Winkel, P., and Friberg, H.: 'Targeted temperature management at 33 degrees C versus 36 degrees C after cardiac arrest,' N Engl J Med, 2013, 369, (23), pp. 2197-2206

42 Arrich, J., Sterz, F., Herkner, H., Testori, C., and Behringer, W.: 'Total epinephrine dose during asystole and pulseless electrical activity cardiac arrests is associated with unfavourable functional outcome and increased in-hospital mortality,' Resuscitation, 2012, 83, (3), pp. 333-337

43 Hagihara, A., Hasegawa, M., Abe, T., Nagata, T., Wakata, Y., and Miyazaki, S.: 'Prehospital epinephrine use and survival among patients with out-of-hospital cardiac arrest,' JAMA, 2012, 307, (11), pp. 1161-1168

44 Wenzel, V., Krismer, A.C., Arntz, H.R., Sitter, H., Stadlbauer, K.H., and Lindner, K.H.: 'A comparison of vasopressin and epinephrine for out-of-hospital cardiopulmonary resuscitation,' N Engl J Med, 2004, 350, (2), pp. 105-113

45 Allison, J.S., Qin, H., Dosdall, D.J., Huang, J., Newton, J.C., Allred, J.D., Smith, W.M., and Ideker, R.E.: 'The transmural activation sequence in porcine and canine left ventricle is markedly different during long-duration ventricular fibrillation,' J Cardiovasc Electrophysiol, 2007, 18, (12), pp. 1306-1312

46 Cha, Y.M., Uchida, T., Wolf, P.L., Peters, B.B., Fishbein, M.C., Karagueuzian, H.S., and Chen, P.S.: 'Effects of chemical subendocardial ablation on activation rate gradient during ventricular fibrillation,' Am J Physiol, 1995, 269, (6 Pt 2), pp. H1998-2009

47 Dosdall, D.J., Tabereaux, P.B., Kim, J.J., Walcott, G.P., Rogers, J.M., Killingsworth, C.R., Huang, J., Robertson, P.G., Smith, W.M., and Ideker, R.E.: 'Chemical ablation of the Purkinje system causes early termination and activation rate slowing of long-duration ventricular fibrillation in dogs,' Am J Physiol Heart Circ Physiol, 2008, 295, (2), pp. H883-889

48 Kong, W., Ideker, R.E., and Fast, V.G.: 'Transmural optical measurements of Vm dynamics during long-duration ventricular fibrillation in canine hearts,' Heart Rhythm, 2009, 6, (6), pp. 796-802

49 Newton, J.C., Smith, W.M., and Ideker, R.E.: 'Estimated global transmural distribution of activation rate and conduction block during porcine and canine ventricular fibrillation,' Circ Res, 2004, 94, (6), pp. 836-842

50 Tabereaux, P.B., Walcott, G.P., Rogers, J.M., Kim, J., Dosdall, D.J., Robertson, P.G., Killingsworth, C.R., Smith, W.M., and Ideker, R.E.: 'Activation patterns of Purkinje fibers during long-duration ventricular fibrillation in an isolated canine heart model,' Circulation, 2007, 116, (10), pp. 1113-1119

51 Venable, P.W., Taylor, T.G., Shibayama, J., Warren, M., and Zaitsev, A.V.: 'Complex structure of electrophysiological gradients emerging during long-duration ventricular fibrillation in the canine heart,' Am J Physiol Heart Circ Physiol, 2010, 299, (5), pp. H1405-1418

52 Worley, S.J., Swain, J.L., Colavita, P.G., Smith, W.M., and Ideker, R.E.: 'Development of an endocardial-epicardial gradient of activation rate during electrically induced, sustained ventricular fibrillation in dogs,' Am J Cardiol, 1985, 55, (6), pp. 813-820

53 Legewie, S., Herzel, H., Westerhoff, H.V., and Bluthgen, N.: 'Recurrent design patterns in the feedback regulation of the mammalian signalling network,' Mol Syst Biol, 2008, 4, pp. 190

54 Luo, C.H., and Rudy, Y.: 'A model of the ventricular cardiac action potential. Depolarization, repolarization, and their interaction,' Circ Res, 1991, 68, (6), pp. 1501-1526

55 Hodgkin, A.L., and Huxley, A.F.: 'Propagation of electrical signals along giant nerve fibers,' Proc R Soc Lond B Biol Sci, 1952, 140, (899), pp. 177-183

56 Hodgkin, A.L., and Huxley, A.F.: 'A quantitative description of membrane current and its application to conduction and excitation in nerve,' J Physiol, 1952, 117, (4), pp. 500-544

57 Hodgkin, A.L., and Huxley, A.F.: 'The dual effect of membrane potential on sodium conductance in the giant axon of Loligo,' J Physiol, 1952, 116, (4), pp. 497-506

58 Hodgkin, A.L., and Huxley, A.F.: 'The components of membrane conductance in the giant axon of Loligo,' J Physiol, 1952, 116, (4), pp. 473-496

59 Hodgkin, A.L., and Huxley, A.F.: 'Currents carried by sodium and potassium ions through the membrane of the giant axon of Loligo,' J Physiol, 1952, 116, (4), pp. 449-472

60 Hodgkin, A.L., and Huxley, A.F.: 'Movement of sodium and potassium ions during nervous activity,' Cold Spring Harb Symp Quant Biol, 1952, 17, pp. 43-52

61 Hodgkin, A.L., Huxley, A.F., and Katz, B.: 'Measurement of current-voltage relations in the membrane of the giant axon of Loligo,' J Physiol, 1952, 116, (4), pp. 424-448

62 Zhang, Z., Zhao, Z., Liu, Y., Wang, W., Wu, Y., and Ding, J.: 'Kinetic model of Nav1.5 channel provides a subtle insight into slow inactivation associated excitability in cardiac cells,' PLoS One, 2013, 8, (5), pp. e64286

63 Alberts, B.: 'Essential cell biology' (Garland Science, 2009, 3rd edn. 2009)

64 Alberts, B., Wilson, J.H., and Hunt, T.: 'Molecular biology of the cell' (Garland Science, 2008, 5th edn. 2008)

65 Hille, B.: 'Ion channels of excitable membranes' (Sinauer, 2001, 3rd edn. 2001)

66 Zipes, D.P., and Jalife, J.: 'Cardiac electrophysiology: from cell to bedside' (Saunders, 2004, 4th edn. 2004)

67 Jalife, J., Delmar, M., Davidenko, J.M., and Anumonwo, J.M.B.: 'Basic cardiac electrophysiology for the clinician' (Futura Publising Company Inc., 1999)

68 Plonsey, R., and Barr, R.C.: 'Bioelectricity: a quantitative approach' (Springer, 2007, 3rd edn. 2007)

69 Miyoshi, S., Miyazaki, T., Asanagi, M., Moritani, K., and Ogawa, S.: 'Differential role of epicardial and endocardial K(ATP) channels in potassium accumulation during regional ischemia induced by embolization of a coronary artery with latex,' J Cardiovasc Electrophysiol, 1998, 9, (3), pp. 292-298

70 Miyoshi, S., Miyazaki, T., Moritani, K., and Ogawa, S.: 'Different responses of epicardium and endocardium to KATP channel modulators during regional ischemia,' Am J Physiol, 1996, 271, (1 Pt 2), pp. H140-147

71 Cordeiro, J.M., Mazza, M., Goodrow, R., Ulahannan, N., Antzelevitch, C., and Di Diego, J.M.: 'Functionally distinct sodium channels in ventricular epicardial and endocardial cells contribute to a greater sensitivity of the epicardium to electrical depression,' Am J Physiol Heart Circ Physiol, 2008, 295, (1), pp. H154-162

72 Billman, G.E.: 'Role of ATP sensitive potassium channel in extracellular potassium accumulation and cardiac arrhythmias during myocardial ischaemia,' Cardiovasc Res, 1994, 28, (6), pp. 762-769

73 Dryer, S.E.: 'Molecular identification of the Na+-activated K+ channel,' Neuron, 2003, 37, (5), pp. 727-728

74 Bhattacharjee, A., Joiner, W.J., Wu, M., Yang, Y., Sigworth, F.J., and Kaczmarek, L.K.: 'Slick (Slo2.1), a rapidly-gating sodium-activated potassium channel inhibited by ATP,' J Neurosci, 2003, 23, (37), pp. 11681-11691

75 Bhattacharjee, A., and Kaczmarek, L.K.: 'For K+ channels, Na+ is the new Ca2+,' Trends Neurosci, 2005, 28, (8), pp. 422-428

76 Berg, A.P., Sen, N., and Bayliss, D.A.: 'TrpC3/C7 and Slo2.1 are molecular targets for metabotropic glutamate receptor signaling in rat striatal cholinergic interneurons,' J Neurosci, 2007, 27, (33), pp. 8845-8856

77 Babenko, A.P., Gonzalez, G., Aguilar-Bryan, L., and Bryan, J.: 'Reconstituted human cardiac KATP channels: functional identity with the native channels from the sarcolemma of human ventricular cells,' Circ Res, 1998, 83, (11), pp. 1132-1143

78 Coetzee, W.A., Amarillo, Y., Chiu, J., Chow, A., Lau, D., McCormack, T., Moreno, H., Nadal, M.S., Ozaita, A., Pountney, D., Saganich, M., Vega-Saenz de Miera, E., and Rudy, B.: 'Molecular diversity of K+ channels,' Ann N Y Acad Sci, 1999, 868, pp. 233-285

79 Shaw, R.M., and Rudy, Y.: 'Electrophysiologic effects of acute myocardial ischemia. A mechanistic investigation of action potential conduction and conduction failure,' Circ Res, 1997, 80, (1), pp. 124-138

80 Shibayama, J., Taylor, T.G., Venable, P.W., Rhodes, N.L., Gil, R.B., Warren, M., Wende, A.R., Abel, E.D., Cox, J., Spitzer, K.W., and Zaitsev, A.V.: 'Metabolic determinants of electrical failure in ex-vivo canine model of cardiac arrest: evidence for the protective role of inorganic pyrophosphate,' PLoS One, 2013, 8, (3), pp. e57821

81 Weiss, J.N., and Lamp, S.T.: 'Glycolysis preferentially inhibits ATP-sensitive K+ channels in isolated guinea pig cardiac myocytes,' Science, 1987, 238, (4823), pp. 67-69

82 Akar, F.G., Aon, M.A., Tomaselli, G.F., and O'Rourke, B.: 'The mitochondrial origin of postischemic arrhythmias,' J Clin Invest, 2005, 115, (12), pp. 3527-3535

83 Akar, F.G., and O'Rourke, B.: 'Mitochondria are sources of metabolic sink and arrhythmias,' Pharmacol Ther, 2011, 131, (3), pp. 287-294

84 Aon, M.A., Cortassa, S., Akar, F.G., Brown, D.A., Zhou, L., and O'Rourke, B.: 'From mitochondrial dynamics to arrhythmias,' Int J Biochem Cell Biol, 2009, 41, (10), pp. 1940-1948

85 Aon, M.A., Cortassa, S., Akar, F.G., and O'Rourke, B.: 'Mitochondrial criticality: a new concept at the turning point of life or death,' Biochim Biophys Acta, 2006, 1762, (2), pp. 232-240

86 Killingsworth, C.R., Wei, C.C., Dell'Italia, L.J., Ardell, J.L., Kingsley, M.A., Smith, W.M., Ideker, R.E., and Walcott, G.P.: 'Short-acting beta-adrenergic antagonist esmolol given at reperfusion improves survival after prolonged ventricular fibrillation,' Circulation, 2004, 109, (20), pp. 2469-2474

87 Omiya, T., Shimizu, A., Ueyama, T., Yoshiga, Y., Doi, M., Hiratsuka, A., Fukuda, M., Yoshida, M., and Matsuzaki, M.: 'Effects of isoproterenol and propranolol on the inducibility and frequency of ventricular fibrillation in patients with Brugada syndrome,' J Cardiol, 2012, 60, (1), pp. 47-54

88 Garcia-Dorado, D., Ruiz-Meana, M., Inserte, J., Rodriguez-Sinovas, A., and Piper, H.M.: 'Calcium-mediated cell death during myocardial reperfusion,' Cardiovasc Res, 2012, 94, (2), pp. 168-180

89 Blake, K., Clusin, W.T., Franz, M.R., and Smith, N.A.: 'Mechanism of depolarization in the ischaemic dog heart: discrepancy between T-Q potentials and potassium accumulation,' J Physiol, 1988, 397, pp. 307-330

90 Rogers, J.M., Melnick, S.B., and Huang, J.: 'Fiberglass needle electrodes for transmural cardiac mapping,' IEEE Trans Biomed Eng, 2002, 49, (12 Pt 2), pp. 1639-1641

91 Johnson, T.A., Engle, C.L., Kusy, R.P., Knisley, S.B., Graebner, C.A., and Gettes, L.S.: 'Fabrication, evaluation, and use of extracellular K+ and H+ ion-selective electrodes,' Am J Physiol, 1990, 258, (4 Pt 2), pp. H1224-1231

92 Taylor, T.G., Venable, P.W., Booth, A., Garg, V., Shibayama, J., and Zaitsev, A.V.: 'Does the combination of hyperkalemia and KATP activation determine excitation rate gradient and electrical failure in the globally ischemic fibrillating heart?' Am J Physiol Heart Circ Physiol, 2013, 305, (6), pp. H903-912

93 Schömig, A., Haass, M., and Richardt, G.: 'Catecholamine release and arrhythmias in acute myocardial ischaemia,' European Heart Journal, 1991, 12, (suppl F), pp. 38-47

94 Priori, S.G., Yamada, K.A., and Corr, P.B.: 'Influence of hypoxia on adrenergic modulation of triggered activity in isolated adult canine myocytes,' Circulation, 1991, 83, (1), pp. 248-259

95 Coetzee, W.A., and Opie, L.H.: 'Effects of components of ischemia and metabolic inhibition on delayed afterdepolarizations in guinea pig papillary muscle,' Circulation Research, 1987, 61, (2), pp. 157-165

96 Cranefield, P.F., Wit, A.L., and Hoffman, B.F.: 'Conduction of the cardiac impulse: III. characteristics of very slow conduction,' The Journal of General Physiology, 1972, 59, (2), pp. 227-246

97 Aupetit, J.F., Frassati, D., Bui-Xuan, B., Freysz, M., Faucon, G., and Timour, Q.: 'Efficacy of a β-adrenergic receptor antagonist, propranolol, in preventing ischaemic ventricular fibrillation: dependence on heart rate and ischaemia duration,' Cardiovascular Research, 1998, 37, (3), pp. 646-655

98 Ng, F.S., Shadi, I.T., Peters, N.S., and Lyon, A.R.: 'Selective heart rate reduction with ivabradine slows ischaemia-induced electrophysiological changes and reduces ischaemia–reperfusion-induced ventricular arrhythmias,' Journal of Molecular and Cellular Cardiology, 2013, 59, (0), pp. 67-75

99 Smith, R.M., Velamakanni, S.S., and Tolkacheva, E.G.: 'Interventricular heterogeneity as a substrate for arrhythmogenesis of decoupled mitochondria during ischemia in the whole heart,' Am J Physiol Heart Circ Physiol, 2012, 303, (2), pp. H224-233

100 Le Grand, B., Coulombe, A., and John, G.W.: 'Late sodium current inhibition in human isolated cardiomyocytes by R 56865,' J Cardiovasc Pharmacol, 1998, 31, (5), pp. 800-804

101 Verdonck, F., Bielen, F.V., and Ver Donck, L.: 'Preferential block of the veratridine-induced, non-inactivating Na+ current by R56865 in single cardiac Purkinje cells,' Eur J Pharmacol, 1991, 203, (3), pp. 371-378

102 Wilhelm, D., Himmel, H., Ravens, U., and Peters, T.: 'Characterization of the interaction of R 56865 with cardiac Na- and L-type Ca channels,' Br J Pharmacol, 1991, 104, (2), pp. 483-489

103 Carmeliet, E.: 'Cardiac ionic currents and acute ischemia: from channels to arrhythmias,' Physiol Rev, 1999, 79, (3), pp. 917-1017

104 Ono, K., Fozzard, H.A., and Hanck, D.A.: 'Mechanism of cAMP-dependent modulation of cardiac sodium channel current kinetics,' Circulation Research, 1993, 72, (4), pp. 807-815

105 Kirstein, M., Kochsiek, K., Langenfeld, H., and Eickhorn, R.: 'Dose-dependent alteration of rat cardiac sodium current by isoproterenol: results from direct measurements on multicellular preparations,' Pflügers Archiv, 1996, 431, (3), pp. 395-401

106 Imredy, J.P., Penniman, J.R., Dech, S.J., Irving, W.D., and Salata, J.J.: 'Modeling of the adrenergic response of the human IKs current (hKCNQ1/hKCNE1) stably expressed in HEK-293 cells,' American Journal of Physiology - Heart and Circulatory Physiology, 2008, 295, (5), pp. H1867-H1881

107 Shaw, R.M., and Rudy, Y.: 'Ionic mechanisms of propagation in cardiac tissue. Roles of the sodium and L-type calcium currents during reduced excitability and decreased gap junction coupling,' Circulation Research, 1997, 81, (5), pp. 727-741

108 Shaw, R.M., and Rudy, Y.: 'Electrophysiologic effects of acute myocardial ischemia: a theoretical study of altered cell excitability and action potential duration,' Cardiovasc Res, 1997, 35, (2), pp. 256-272

109 Warner, M.R., Kroeker, T.S., and Zipes, D.P.: 'Sympathetic stimulation and norepinephrine infusion modulate extracellular potassium concentration during acute myocardial ischemia,' Circulation Research, 1992, 71, (5), pp. 1078-1087

110 Clusin, W.T.: 'Mechanism by which metabolic inhibitors depolarize cultured cardiac cells,' Proc Natl Acad Sci U S A, 1983, 80, (12), pp. 3865-3869

111 Lubbe, W.F., Podzuweit, T., and Opie, L.H.: 'Potential arrhythmogenic role of cyclic adenosine monophosphate (AMP) and cytosolic calcium overload: implications for prophylactic effects of beta-blockers in myocardial infarction and proarrhythmic effects of phosphodiesterase inhibitors,' Journal of the American College of Cardiology, 1992, 19, (7), pp. 1622-1633

112 Shen, M.J., and Zipes, D.P.: 'Role of the autonomic nervous system in modulating cardiac arrhythmias,' Circulation Research, 2014, 114, (6), pp. 1004-1021

113 Bovo, E., Lipsius, S.L., and Zima, A.V.: 'Reactive oxygen species contribute to the development of arrhythmogenic Ca2+ waves during β-adrenergic receptor stimulation in rabbit cardiomyocytes,' The Journal of Physiology, 2012, 590, (14), pp. 3291-3304

114 Gaur, N., Rudy, Y., and Hool, L.: 'Contributions of ion channel currents to ventricular action potential changes and induction of early afterdepolarizations during acute hypoxia,' Circulation Research, 2009, 105, (12), pp. 1196-1203

115 Priori, S.G., and Corr, P.B.: 'Mechanisms underlying early and delayed afterdepolarizations induced by catecholamines,' Am J Physiol, 1990, 258, pp. H1796-H1805

116 Sirenko, S., Maltsev, V.A., Maltseva, L.A., Yang, D., Lukyanenko, Y., Vinogradova, T.M., Jones, L.R., and Lakatta, E.G.: 'Sarcoplasmic reticulum Ca2++ cycling protein phosphorylation in a physiologic Ca2++ milieu unleashes a high-power, rhythmic Ca2++ clock in ventricular myocytes: relevance to arrhythmias and bio-pacemaker design,' Journal of Molecular and Cellular Cardiology, 2014, 66, (0), pp. 106-115

117 Neumar, R.W., Nolan, J.P., Adrie, C., Aibiki, M., Berg, R.A., Bottiger, B.W., Callaway, C., Clark, R.S., Geocadin, R.G., Jauch, E.C., Kern, K.B., Laurent, I., Longstreth, W.T., Jr., Merchant, R.M., Morley, P., Morrison, L.J., Nadkarni, V., Peberdy, M.A., Rivers, E.P., Rodriguez-Nunez, A., Sellke, F.W., Spaulding, C., Sunde, K., and Vanden Hoek, T.: 'Post-cardiac arrest syndrome: epidemiology, pathophysiology, treatment, and prognostication. A consensus statement from the International Liaison Committee on Resuscitation (American Heart Association, Australian and New Zealand Council on Resuscitation, European Resuscitation Council, Heart and Stroke Foundation of Canada, Inter-American Heart Foundation, Resuscitation Council of Asia, and the Resuscitation Council of Southern Africa); the American Heart Association Emergency Cardiovascular Care Committee; the Council on Cardiovascular Surgery and Anesthesia; the Council on Cardiopulmonary, Perioperative, and Critical Care; the Council on Clinical Cardiology; and the Stroke Council,' Circulation, 2008, 118, (23), pp. 2452-2483

118 Taylor, T.G., Venable, P.W., Warren, M., Shibayama, J., and Zaitsev, A.V.: 'Evidence for ATP-sensitive potassium current-mediated polymorphism in the dynamics of long-duration ventricular fibrillation and asystole in isolated canine heart,' Circulation, 2010, 122:A207

119 Taylor, T.G., Venable, P.W., Shibayama, J., Booth, A.E., Rhodes, N.L., Warren, M., and Zaitsev, A.V.: 'Role of hyperkalemia in the transmural activation rate gradient and asystole during long-duration ventricular fibrillation (LDVF) in isolated canine heart,' Circulation, 2011, 124:A9

120 Venable, P.W., Sciuto, K.J., Taylor, T.G., Garg, V., Shibayama, J., Spitzer, K.W., and Zaitsev, A.V.: 'Blebbistatin delays mitochondrial depolarization and asystole during myocardial ischemia, and prevents cell death upon reperfusion,' Biophysical Journal, 2014, 106, (2:Supplement 1), pp. p186a

121 Kleber, A.G.: 'Resting membrane potential, extracellular potassium activity, and intracellular sodium activity during acute global ischemia in isolated perfused guinea pig hearts,' Circ Res, 1983, 52, (4), pp. 442-450

122 Weiss, J., and Shine, K.I.: 'Effects of heart rate on extracellular [K+] accumulation during myocardial ischemia,' Am J Physiol, 1986, 250, (6 Pt 2), pp. H982-991

123 Maier, L.S., and Sossalla, S.: 'The late Na current as a therapeutic target: where are we?' J Mol Cell Cardiol, 2013, 61, pp. 44-50

124 'Guidelines 2000 for cardiopulmonary resuscitation and emergency cardiovascular care. Part 6: advanced cardiovascular life support: section 6: pharmacology II: agents to optimize cardiac output and blood pressure. The American Heart Association in collaboration with the International Liaison Committee on Resuscitation,' Circulation, 2000, 102, (8 Suppl), pp. I129-135

125 Goldhaber, J.I., Deutsch, N., Alexander, L.D., and Weiss, J.N.: 'Lysophosphatidylcholine and cellular potassium loss in isolated rabbit ventricle,' J Cardiovasc Pharmacol Ther, 1998, 3, (1), pp. 37-42

126 Liu, E., Goldhaber, J.I., and Weiss, J.N.: 'Effects of lysophosphatidylcholine on electrophysiological properties and excitation-contraction coupling in isolated guinea pig ventricular myocytes,' J Clin Invest, 1991, 88, (6), pp. 1819-1832

127 Sciuto, K.J., Venable, P.W., Hunter, C., Taylor, T.G., Garg, V., Shibayama, J., Spitzer, K.W., Moreno, A.P., and Zaitsev, A.V.: 'Critical events in myocardial ischemia/reperfusion: mitochondrial depolarization versus sarcolemmal permeability,' Biophysical Journal, 2014, 106, (2:Supplement 1), pp. 186a-187a

128 Cowie, C.C., Rust, K.F., Byrd-Holt, D.D., Eberhardt, M.S., Flegal, K.M., Engelgau, M.M., Saydah, S.H., Williams, D.E., Geiss, L.S., and Gregg, E.W.: 'Prevalence of diabetes and impaired fasting glucose in adults in the U.S. population: National Health And Nutrition Examination Survey 1999-2002,' Diabetes Care, 2006, 29, (6), pp. 1263-1268

129 Nolan, J.P., Soar, J., and Perkins, G.D.: 'Cardiopulmonary resuscitation,' BMJ, 2012, 345, pp. e6122

130 Nolan, J.P., Soar, J., Wenzel, V., and Paal, P.: 'Cardiopulmonary resuscitation and management of cardiac arrest,' Nat Rev Cardiol, 2012, 9, (9), pp. 499-511